Short Papers in Geology Hydrology, and Topography Articles 1–59

GEOLOGICAL SURVEY RESEARCH 1962

GEOLOGICAL SURVEY PROFESSIONAL PAPER 450-B

Scientific notes and summaries of investigations prepared by members of the Geologic, Water Resources, and Topographic Divisions in the fields of geology, hydrology, topography, and allied sciences

UNITED STATES GOVERNMENT PRINTING OFFICE, WASHINGTON : 1962

UNITED STATES DEPARTMENT OF THE INTERIOR

STEWART L. UDALL, *Secretary*

GEOLOGICAL SURVEY

Thomas B. Nolan, *Director*

For sale by the Superintendent of Documents, U.S. Government Printing Office
Washington 25, D.C.

FOREWORD

This collection of 59 short papers on subjects in the fields of geology, hydrology, topography, and related sciences is one of a series to be released during the year as chapters of Professional Paper 450. The papers in this chapter report on the scientific and economic results of current work by members of the Geologic, Topographic, and Water Resources Division of the United States Geological Survey. Some of the papers announce new discoveries or present observations on problems of limited scope; other papers draw conclusions from more extensive or continuing investigations that in large part will be discussed in greater detail in reports to be published in the future.

Chapter A of this series, to be published later in the year, will present a synopsis of results from a wide range of work done during the present fiscal year.

Thomas B. Nolan

THOMAS B. NOLAN,
Director.

CONTENTS

SHORT PAPERS IN GEOLOGY, HYDROLOGY, AND TOPOGRAPHY, ARTICLES 1-59

GEOLOGIC STUDIES

ECONOMIC GEOLOGY

1. STRATIGRAPHIC AND STRUCTURAL CONTROLS OF MINERALIZATION IN THE TAYLOR MINING DISTRICT NEAR ELY, NEVADA

By HARALD DREWES, Denver, Colo.

The Taylor mining district lies on the west flank of the Schell Creek Range 15 miles southeast of Ely and 5 miles northwest of Connors Pass. The district has produced $1 to $2 million worth of silver, and a little gold, copper, lead, zinc, and antimony since 1883, of which about half has been produced since 1935.

The ore occurs sporadically in highly silicified rocks. Stratigraphic and structural controls of the silicified bodies determined through the geologic mapping of the Connors Pass 15-minute quadrangle are reported here. Sulfides (stibnite, galena, sphalerite, and possibly chalcocite) are seen in few hand specimens; no silver was recognized in the field. Spectrographic analysis of 40 samples from 7 pits shows that the silver content generally increases eastward, or stratigraphically upward, and that silver is more closely associated with antimony than with other base metals. The distribution of the ore within the silicified bodies was not further investigated.

The sequence of the rocks and their degree of mineralization are tabulated below; the age of the rocks appears on the map explanation. Silification is restricted to limestone, and preferentially to thin-bedded or shaly limestone beneath thick shale formations. The map (fig. 1.1) illustrates the stratigraphic and structural controls of the main silicified bodies.

Formation	*Degree of mineralization*
Gravel	Barren.
Latite and dacite flows and tuffs.	Do.
Granophyric rhyolitic dikes.	Kaolinized but not mineralized.
Ely Limestone	Barren.
Chainman Shale	Do.
Joana Limestone	Many small lenses of silicified rock near the top of the formation, bearing Sb and Ag.
Pilot Shale	Barren.
Guilmette Formation:	
Member c	Large silicified bodies, especially in the upper half of the unit, bearing Ag, Au, Cu, Pb, and Zn.
Member b	Few, scattered, small silicified bodies.
Member a	Barren.
Simonson Dolomite	Do.
Sevy Dolomite	Do.

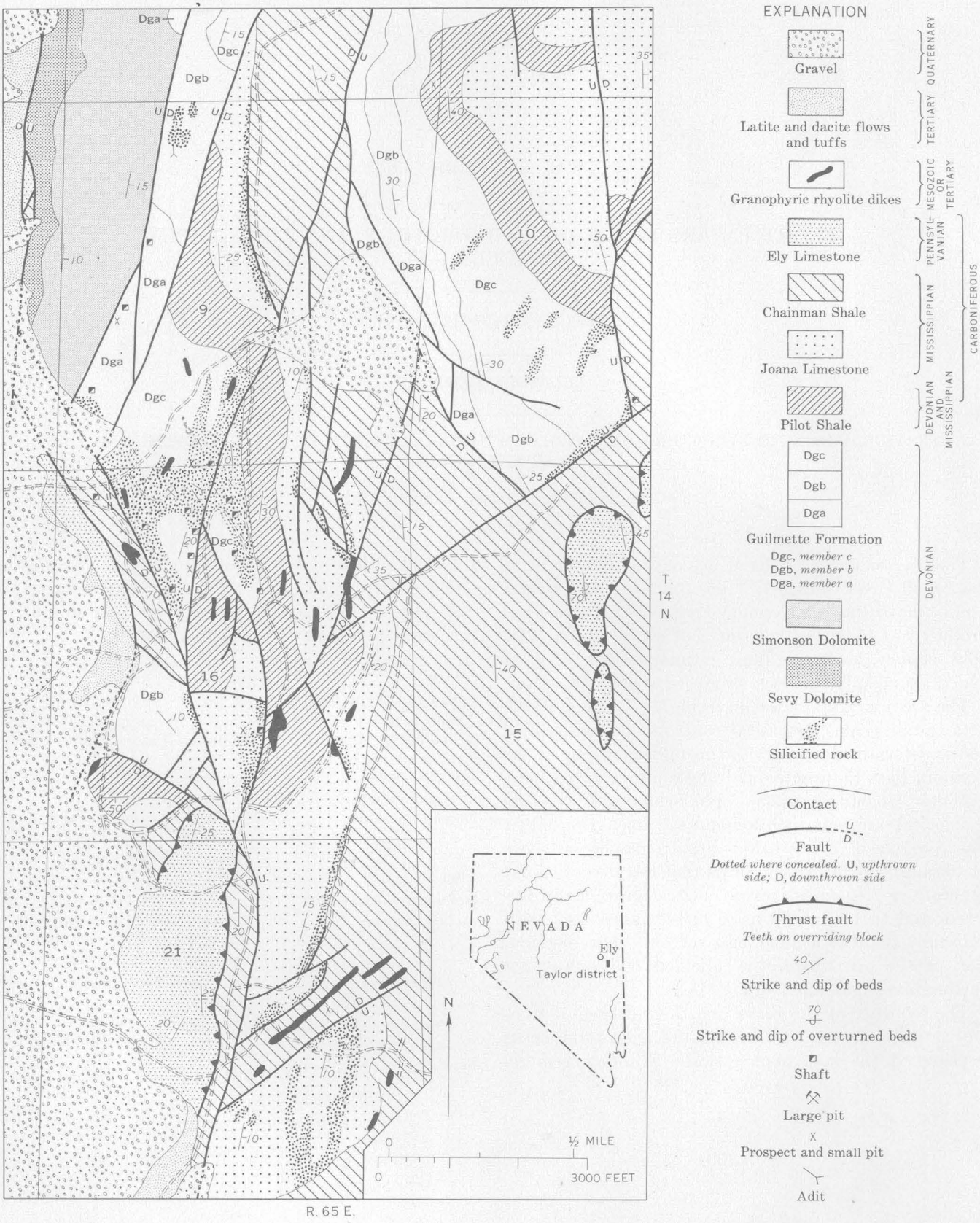

FIGURE 1.1.—Geologic map of the Taylor mining district near Ely, Nev. Silver ore occurs in some silicified bodies.

The silicified limestone is in part localized along normal faults that trend north to northeast and have displacements of a few tens of feet to several hundreds of feet. Silicified rock along these faults is locally sheared. Much smaller silicified bodies are found elsewhere in the quadrangle where normal faults of similar trend cut only the middle or middle and lower plates of the three major thrust plates, and the bodies are probably contemporaneous with the thrusting. A post-mineralization normal fault with many hundreds to possibly several thousands of feet of displacement trends northwest close to the foot of the range and brings young unmineralized rocks down against older mineralized rocks. At least some of the movement on this fault postdates the latite and dacite flows and related sediments, probably of middle Tertiary age, found along the edge of the valley.

Many thick, short rhyolitic dikes with northerly and northeasterly strikes are concentrated in the Taylor district, suggesting that they are related to the mineralization. The feldspars of all the dikes are strongly kaolinized, but none of the dikes are strongly silicified or mineralized. The concentration of dikes near the mineralized bodies and the parallelism between many dikes, older faults, and silicified bodies suggests that the stresses in the rocks were similar during formation of the dikes and mineralized bodies, and that the silicification and the emplacement of the dikes took place at about the same time. The dikes are porphyritic, with phenocrysts of quartz, unlike that of the nearby rhyolitic volcanic rocks. The dikes may be related to other porphyry intrusive bodies accompanied by mineralization in eastern Nevada.

In conclusion, the ore-bearing silicified bodies are localized near the tops of the Guilmette Formation and the Joana Limestone and along normal faults. The same horizons in adjacent downfaulted blocks, and shaly limestone in the middle member and at the base of the lower member of the Guilmette Formation in the mineralized area, should be explored. The rhyolitic dikes are concentrated near the mineralized bodies and are probably related to them temporally, and possibly genetically.

2. SUGGESTIONS FOR PROSPECTING IN THE HUMBOLDT RANGE AND ADJACENT AREAS, NEVADA

By Robert E. Wallace and Donald B. Tatlock, Menlo Park, Calif.

Work done in cooperation with the Nevada Bureau of Mines

During recent geologic investigations in the Humboldt Range, northwestern Nevada, we found that for many of the mineral deposits, a distinctive geologic setting can be defined that should serve as a guide in the search for additional deposits both in the Humboldt Range and in nearby localities of similar geologic setting. In the following suggestions for prospecting, broad geologic areas are primarily defined, and within these areas local structures must be considered.

The geologic structures and lithologic units of the range that are referred to in this article are shown on preliminary geologic maps of the Buffalo Mountain quadrangle (Wallace and others, 1959) and of the Unionville quadrangle (Wallace and others, 1962; Wallace and others, 1960, fig. 133.1, p. B292). These maps are a necessary adjunct to the following discussion.

Silver.—The Weaver Rhyolite and immediately underlying parts of the Rochester Rhyolite are the host rocks for the Rochester and Packard silver districts (Knopf, 1924). In addition, the larger bodies of rhyolite porphyry, which are believed to be feeders for the Weaver Rhyolite, commonly have silver related to them. This type of mineralization is believed to be genetically related to the igneous rocks and thus is of Permian(?) or Early Triassic age.

In prospecting, pay special attention to the Weaver Rhyolite and the rhyolite porphyry stocks that are in a crude line between South American Canyon and Unionville. The silver minerals characteristic of the area are difficult to identify by naked eye and commonly are in rather indistinct silicified zones in the rhyolite. Without thorough testing, such silver-bearing zones may easily be overlooked. Best values are probably within a few hundred feet of the surface.

Silver-scheelite.—A distinctive type of deposit containing conspicuous quartz veins, which in turn contain inconspicuous silver minerals and sparse scheelite, is found in the Prida Formation of Middle Triassic age. This is a limy unit resting on volcanic rocks of the Koipato Group. The Arizona (Cameron, 1939), Rye Patch (Ransome, 1909, p. 43–44) and Relief (Schrader, 1915, p. 362) mines characterize this type of deposit. The possibility exists that the silver in these deposits was remobilized from Permian(?) and Early Triassic deposits by igneous activity in Late Jurassic or Early Cretaceous time.

The entire outcrop band of the Prida Formation warrants prospecting for this type of deposit, but examine particularly the limestone adjacent to or near rhyolite porphyry intrusive bodies of Weaver Rhyolite.

Scheelite-beryl-fluorite.—Scheelite deposits throughout Pershing and Humboldt Counties are related to granitoid rocks generally of granodioritic or quartz monzonitic composition of Late Jurassic or Early Cretaceous age that have intruded limestone bodies. The Little (Oreana) tungsten deposits (Kerr, 1938; Vitaliano, 1944) on the west flank of the Humboldt Range are characteristic and are in veins in limestone near quartz monzonite and related aplite bodies. High-grade pods have formed in limestone immediately below metadiorite sills. Beryl, and in some places fluorite, occupies the same or similar veins in the same setting.

Limestone bodies intruded by granodiorite or quartz monzonite should be examined for scheelite by ultraviolet light. In addition, the combination of beryl, fluorite, and scheelite suggests a similarity to the Mt. Wheeler mine (Stager, 1960; Whitebread and Lee, 1961) where beryl and less conspicuous beryllium minerals such as phenacite have been found. The search for less conspicuous beryllium deposits may require special techniques such as use of a beryllometer.

Lode gold.—Quartz veins containing native gold are related to the swarms of rhyolite porphyry dikes in the headwaters of Limerick, Sacramento, Spring, North American, and South American Canyons (Knopf, 1924, p. 51–52; Schrader, 1915, p. 354). The veins are generally not in the rhyolite porphyry dikes but are in the same host rocks as the rhyolite porphyry dikes.

Any quartz vein cutting the Limerick Greenstone or the Rochester Rhyolite in the general vicinity of rhyolite porphyry intrusive bodies should be considered a potential gold prospect.

Placer gold.—Drainage channels that cross potential lode-gold areas may contain placer gold. For example, Limerick, Spring, and North and South American Canyons (Knopf, 1924, p. 58; Schrader, 1915, p. 368) are known to contain placer gold.

Situations where several stages of concentration might have occurred, for example channels within channels, offer better than average possibilities of successful prospecting.

Cinnabar and stibnite.—Cinnabar and stibnite deposits are believed to be related to late Tertiary and Quaternary basin-range faults that blocked out the range. It is also believed that the main deposits were formed during an early part of this period of faulting, perhaps at about the same time that basaltic and andesitic lavas were extruded. Bailey and Phoenix (1944, p. 29) point out, however, that basalt itself has not proved to be a good host rock and that cinnabar deposits in the more recently active fault zones, commonly accompanied by hot springs, have not proved to be of economic value.

The lower flanks and margins of the range are promising for prospecting, particularly those flanks on which both limy formations and basalt flows are found; the part of the flank basinward from faults of late Tertiary age, such as the Fitting fault, is particularly promising. Within such geologic settings, more detailed prospecting guides, such as rock alteration (Bailey and Phoenix. 1944, p. 29), may be helpful.

Iron.—Magnetite and hematite are clearly related to large altered dioritic bodies and to associated andesitic rocks throughout much of Nevada (Reeves and Kral, 1955). There is growing evidence that these may be of Early Cretaceous or possibly Late Jurassic age. The magnetite and hematite are in veins and in disseminated masses through the diorite. The trends of iron-bearing veins in the Buena Vista Hills area of Pershing County are somewhat random.

Dioritic and andesitic bodies of Mesozoic age should receive attention in prospecting. Within these bodies additional iron deposits might be revealed by magnetic and gravity surveys, both where these bodies crop out, and where these rocks might be concealed by basin fill Gravity anomalies might reveal nonmagnetic hematite bodies.

Limestone.—Analyses of limestone of the Prida and Natchez Pass Formations of Middle and Late Triassic age suggest large limestone bodies of sufficient quality for Portland cement. Samples containing as much as 55 percent CaO, less than 0.2 percent SiO_2, and less than 0.5 percent MgO have been found.

Inasmuch as there appear to be large quantities of limestone of cement quality, the economic considerations of transportation, fuel, and ease of quarrying must receive attention before any part of the limestone is selected for detailed testing.

Perlite.—Numerous bodies of perlite were found in the lower part of the rhyolite flows and tuffs of Tertiary

age. At least one such body is being mined in the Trinity Range.

The contact between Tertiary rhyolite and underlying rocks in the West Humboldt and Trinity Ranges warrants prospecting.

Evaporites.—The basins around the Humboldt Range contain halite and conceivably may contain other evaporites such as borates. Relatively little is known of the buried deposits in the basins, although one hole was drilled in Carson Sink during the search for potash before the first World War (Gale, 1911). D. F. Hewett (oral communication) has found that boron is more abundant in hot springs of western Nevada than in hot springs of eastern Nevada, and this fact together with the relative abundance of boron aluminum silicates such as tourmaline and dumortierite in the Humboldt Range is suggestive of a boron-rich province. Gravity studies by Don Mabey of the U.S. Geological Survey (written communication, 1960) indicate that the basin fill is at least 8,000 feet thick in Buena Vista Valley and more than 4,000 feet thick between the Humboldt River and the west flank of the Humboldt Range in the vicinity of Rye Patch.

Too little is known of the geologic history of the basins to suggest which locality is most favorable for prospecting.

Sand and gravel.—Along the borders of ancient Lake Lahontan, which occupied the basins around the Humboldt Range, many beaches and bars were formed that contain wave-sorted gravel and sand. During low-water levels and after the lake had completely dried up, winds gathered much of the sand into dunes. Such sand and gravel from which the fine particles have been sorted by the action of waves and winds have properties that make them suitable for economic use.

Many beaches and bars of Lake Lahontan, as well as sand dunes, are clearly visible on aerial photographs of the Humboldt Range and surrounding basins. These photographs are available from the U.S. Geological Survey and Army Map Service. Many of these potential sources of sand and gravel are near highways and railroads and thus may have economic value. Examination of aerial photographs may save time in the search for sand and gravel.

REFERENCES

Bailey, E. H., and Phoenix, D. A., 1944, Quicksilver deposits in Nevada: Nevada Univ. Bull., v. 38, no. 5, Geology and Mining ser. 41, 206 p.

Cameron, E. N., 1939, Geology and mineralization of the northeastern Humboldt Range, Nevada: Geol. Soc. America Bull., v. 50, no. 4, p. 563–634.

Gale, H. S., 1911, The search for potash in the United States: U.S. Geol. Survey Bull. 530–A, p. 3–27.

Kerr, P. F., 1938, Tungsten mineralization at Oreana, Nevada: Econ. Geology, v. 33, no. 4, p. 390–427.

Knopf, Adolph, 1924, Geology and ore deposits of the Rochester district, Nevada: U.S. Geol. Survey Bull. 763, p. 1–78.

Ransome, F. L., 1909, Notes on some mining districts in Humboldt County, Nevada: U.S. Geol. Survey Bull. 414, p. 1–75.

Reeves, R. G., and Kral, V. E., 1955, Geology and iron ore deposits of the Buena Vista Hills, Churchill and Pershing Counties, Nevada, pt. A *of* Iron ore deposits of Nevada: Nevada Bur. Mines Bull. 53, p. 1–32.

Schrader, F. C., 1915, The Rochester mining district, Nevada: U.S. Geol. Survey Bull. 580, p. 325–372.

Stager, H. K., 1960, A new beryllium deposit at the Mount Wheeler mine, White Pine County, Nevada: Art. 30 *in* U.S. Geol. Survey Prof. Paper 400–B, p. B70–B71.

Vitaliano, C. J., 1944, Contact metamorphism at Rye Patch, Nevada: Geol. Soc. America Bull., v. 55, no. 8, p. 921–950.

Wallace, R. E., Silberling, N. J., Irwin, W. P., and Tatlock, D. B., 1959, Preliminary geologic map of the Buffalo Mountain quadrangle, Nevada: U.S. Geol. Survey Mineral Inv. Field Studies Map MF–220.

Wallace, R. E., Tatlock, D. B., and Silberling, N. J., 1960, Intrusive rocks of Permian and Triassic age in the Humboldt Range, Nevada: Art. 133 *in* U.S. Geol. Survey Prof. Paper 400–B, p. B291–B293.

Wallace, R. E., Tatlock, D. B., Silberling, N. J., and Irwin, W. P., 1962, Preliminary geologic map of the Unionville quadrangle, Nevada: U.S. Geol. Survey Mineral Inv. Field Studies Map MF–245.

Whitebread, D. H., and Lee, D. E., 1961, Geology of the Mount Wheeler mine area, White Pine County, Nevada: Art. 193 *in* U.S. Geol. Survey Prof. Paper 424–C, p. C120–C122.

STRUCTURAL GEOLOGY

3. POSSIBLE DETACHMENT FAULTS IN THE TEPEE CREEK QUADRANGLE, GALLATIN COUNTY, MONTANA

By Irving J. Witkind, Denver, Colo.

Two folded parallel bedding faults, similar in many respects to the Heart Mountain and South Fork detachment faults of northwestern Wyoming (Pierce, 1957) are exposed in the Tepee Creek quadrangle, Gallatin County, southwestern Montana. The extent of these newly discovered faults is unknown; to date, they have been traced for an outcrop length of about 30 miles (fig. 3.1). Their persistence and continuity suggest that they are of regional extent.

One, and locally both of the faults are well exposed in the northern third of the quadrangle, particularly in the cirque at the head of Bacon Rind Creek (fig. 3.2) and along the flanks of Snowslide (fig. 3.3), Monument, and Red Mountains. Elsewhere they are poorly exposed beneath talus and dense foliage.

These two newly discovered faults, one stratigraphically above the other, bound a segment of the Madison Group (Mississippian) which rests on undifferentiated units tentatively correlated with the Maywood(?) (Devonian) and Red Lion(?) (Cambrian) Formations. The Jefferson Dolomite (Devonian) and Three Forks (Devonian and Mississippian) Formation, which total about 500 feet in thickness, are normally between the Madison and these undifferentiated units in surrounding areas (Hadley, 1960; Robinson, 1959), but they have been cut out by the lower fault, here named the Cone Peak fault.

The similarities between the Cone Peak and Heart Mountain faults are marked, and far exceed the dissimilarities. Thus, both faults cut out Jefferson and Three Forks strata, are at almost the same stratigraphic horizon—the top of the Cambrian, and tend to follow stratigraphic horizons. Further, along both faults, an upper plate of younger rocks rests on older rocks. One great dissimilarity, however, is that the Cone Peak fault has been folded and faulted along with the overlying and underlying strata, whereas, at least locally, the Heart Mountain fault is nearly horizontal and rests on folded rocks. One explanation for this difference is that the bedding faults in the Tepee Creek area began as detachment faults, but have since been modified by one or more orogenic episodes.

The upper plate of the Cone Peak fault is, at a minimum, 12 miles long and about 4 miles wide, but it is only about 550 feet thick. Its shape, therefore, is that of an elongate, broad, extremely thin sheet. This unusual ratio between extent and thickness also marks the upper plate of the Heart Mountain fault, for it is

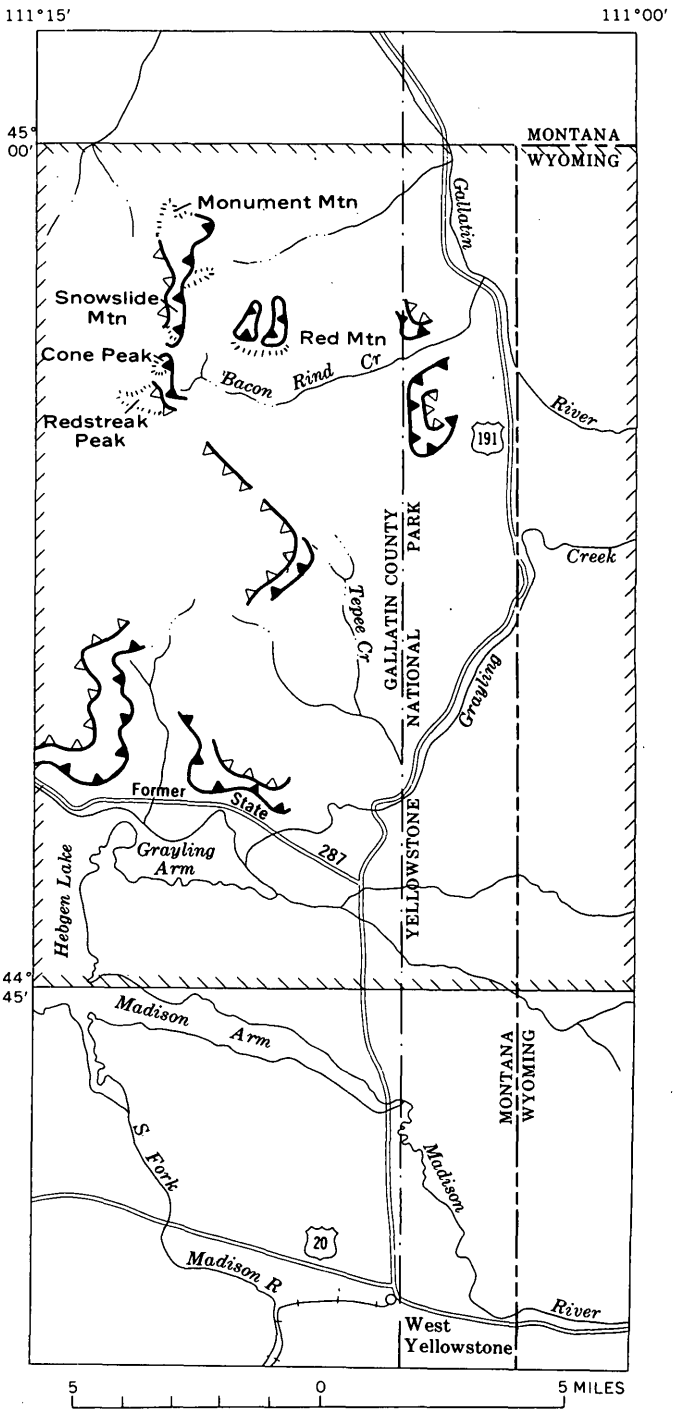

FIGURE 3.1.—Index map of parts of southwestern Montana and northwestern Wyoming. Tepee Creek quadrangle shown by hachures. Barbed lines show approximate outcrop of Cone Peak fault (solid barbs) and Redstreak Peak faults (open barbs). Barbs are on upper plate.

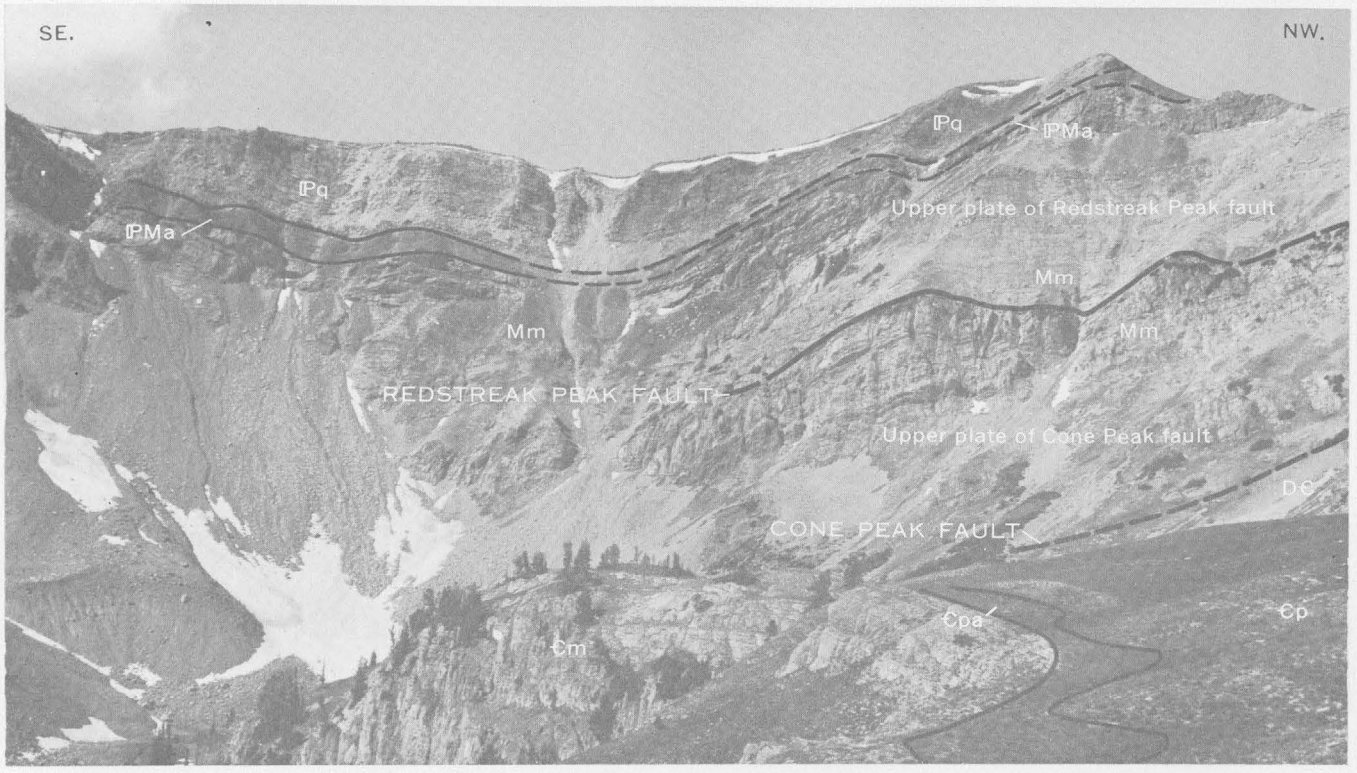

FIGURE 3.2.—View looking southwest into cirque at the head of Bacon Rind Creek showing the general relations between the Cone Peak and Redstreak Peak faults. The upper plate of the Cone Peak fault consists of parts of both the Lodgepole and Mission Canyon Limestones of the Madison Group (Mm) (Mississippian). The lower plate is formed by Cambrian and Devonian (D€) strata (undifferentiated), and the normal Cambrian sequence of this part of southwestern Montana. From the oldest to the youngest these Cambrian strata include the Meagher Limestone (€m), Park Shale (€pa), and Pilgrim Limestone (€p). The upper plate of the Redstreak Peak is composed of the Madison Group (Mm), Amsden Formation (PMa), and Quadrant Formation (Pq).

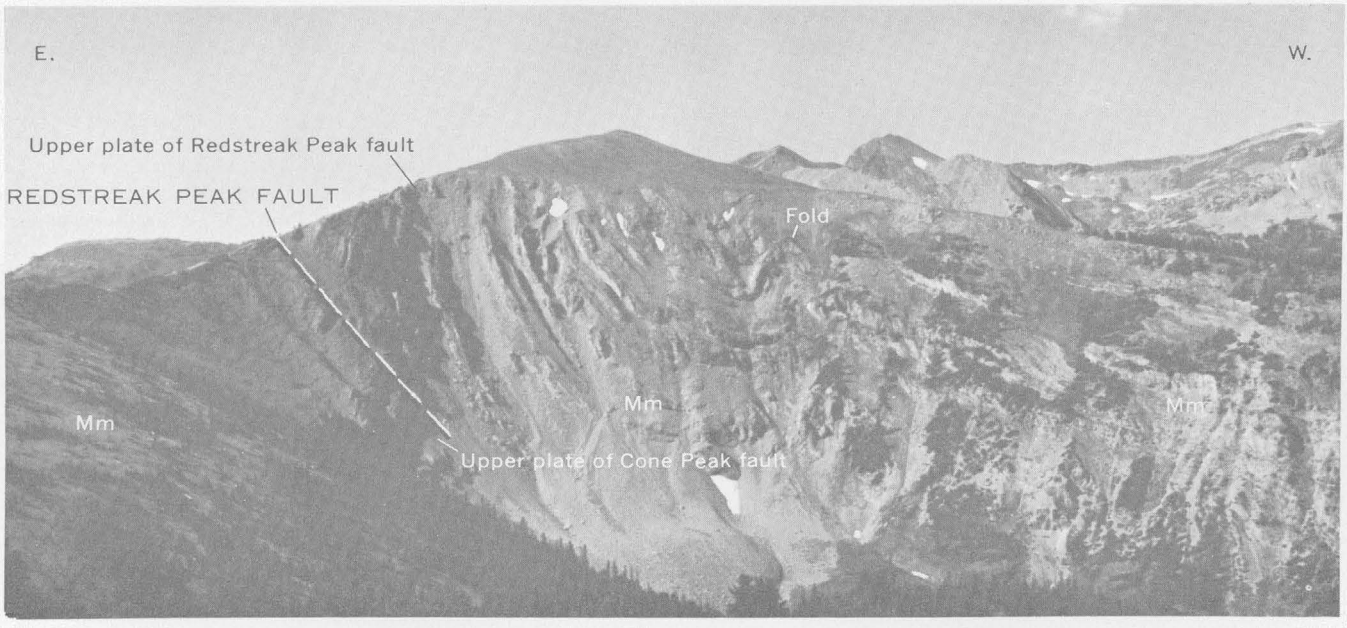

FIGURE 3.3.—View looking south at valley wall near Snowslide Mountain showing tight fold in the Madison (Mm) of the upper plate of the Redstreak Peak fault. Part of the upper plate of the Cone Peak fault (Mm) is exposed below the Redstreak Peak fault.

very thin in comparison to its horizontal extent (Pierce, 1957, p. 593). The upper plate of the Cone Peak fault consists of about 310 feet of thin-bedded cherty fossiliferous limestones tentatively assigned to the upper part of the Lodgepole Limestone of the Madison Group, and 240 feet of thick-bedded to massive oolitic limestones, provisionally assigned to the basal part of the Mission Canyon Limestone of the Madison. The stratigraphic units involved, therefore, are from the middle of the Madison Group.

Normally these beds conform to the attitude of the overlying and underlying strata, but locally they are intensely deformed by folds and small high-angle normal and reverse faults that do not extend into the strata that bound the upper plate. Similar high-angle faults are common in the upper plate of the Heart Mountain fault (Pierce, 1957, p. 593). These folds and faults in the upper plate of the Cone Peak fault suggest that a segment of the Madison Group was detached from the underlying strata and deformed independently, possibly as a result of gravitational gliding, much as proposed for the Heart Mountain fault (Pierce, 1957, p. 615).

The upper fault, here called the Redstreak Peak fault (fig. 3.2), is the top of the upper plate of the Cone Peak fault. Commonly, the Lodgepole Limestone forms the upper plate of the Redstreak Peak fault, although at one locality a thin sliver of the Sappington Sandstone Member of the Three Forks Shale (Devonian and Mississippian) may be between the fault plane and the Lodgepole Limestone. The full Paleozoic and Mesozoic stratigraphic sequence common in southwestern Montana continues unbroken above the Lodgepole Limestone. The beds above the Redstreak Peak fault locally are deformed into tight folds with axial planes that dip west, suggesting that this plate moved eastward (fig. 3.3). The Redstreak Peak fault, like the Cone Peak fault, has been deformed along with the confining strata.

Both faults normally are concealed by debris and foliage. Where exposed, they appear to be smooth and undulatory. Locally, a breccia is below the Cone Peak fault in the uppermost beds of the Maywood(?) Formation.

The two faults seem to have formed essentially as low-angle nearly horizontal bedding-plane faults that here and there cut across the bedding. As yet, neither of these faults has been found to extend across an erosion surface in the manner of the Heart Mountain thrust (Pierce, 1957, p. 598).

Little is known about the direction of movement of the faults but the similarity of these faults to the detachment faults of northwestern Wyoming indicates that the faults in the Tepee Creek area may have formed in the same manner, at about the same time, and from the same upland. If so, the movement on the Tepee Creek faults may have been southwestward from an ancestral high centered near the north edge of Yellowstone National Park. The overturned folds in the beds above the Redstreak Peak fault (fig. 3.3), however, suggest that the sliding was chiefly eastward. Possibly the same direction of movement occurred along the Cone Peak fault.

The age of the faults is known only within rather broad limits, although they probably formed at about the same time. They appear to represent the first major structural event involving consolidated sedimentary strata in the Tepee Creek area. They are almost certainly younger than the youngest strata (Triassic) conformable with the Madison, and are very likely post-Early Cretaceous. As they are folded and faulted along with the overlying and underlying strata, they are older than the regional folding which involves rocks as young as Paleocene or early Eocene. Their age, therefore, is provisionally set as post-Early Cretaceous and pre-early Eocene. By comparison, the age determined for the Wyoming detachment faults is early Eocene (Pierce, 1957, p. 624).

REFERENCES

Hadley, J. B., 1960, Geology of the northern part of the Gravelly Range, Madison County, Montana, *in* Billings Geol. Soc. Guidebook 11th Ann. Field Conf., West Yellowstone-earthquake area, 1960: p. 149–153.

Pierce, W. G., 1957, Heart Mountain and South Fork detachment thrusts of Wyoming: Am. Assoc. Petroleum Geologists Bull., v. 41, no. 4, p. 591–626.

Robinson, G. D., 1959, The disturbed belt in the Sixteenmile area, Montana, *in* Billings Geol. Soc. Guidebook 10th Ann. Field Conf., Sawtooth-disturbed belt area, 1959, p. 34–40.

4. HYDROGEOLOGIC EVIDENCE OF THE EXTENSION OF THE EAST RANGE FAULT, HUMBOLDT AND PERSHING COUNTIES, NEVADA

By PHILIP COHEN, Carson City, Nev.

Work done in cooperation with the Nevada Department of Conservation and Natural Resources

Faults and associated phenomena are known to influence the occurrence and movement of ground water, and apparent hydrologic anomalies commonly are explained on the basis of inferred faults. Less commonly, as in this report, hydrogeologic evidence is used to demonstrate the existence or extension of a fault.

A northward-trending, westward-dipping, high-angle normal fault, herein referred to as the East Range fault (fig. 4.1) borders the western slope of the East Range, Humboldt and Pershing Counties, Nev., where it was mapped by Ferguson, Muller, and Roberts (1951). Evidence of the fault includes fault scarps, displaced strata, slickensides, brecciated zones, and hydrothermal mineralization.

During current hydrologic studies, about 175 test borings were drilled in the unconsolidated deposits of the Humboldt River basin near Winnemucca, Nev. Some of the hydrogeologic data thus collected suggest that the East Range fault extends at least about 2 miles farther northward than previously mapped.

The Krum Hills, the unnamed hills north of the Humboldt River, and that part of the East Range shown in figure 4.1 are composed of dense sedimentary and igneous rocks of Mesozoic age and basaltic lava flows of late Tertiary or Quaternary age. These rocks generally have low permeability and therefore do not transmit appreciable amounts of water, except perhaps through fractured zones.

Most of the ground water of the area is in relatively unconsolidated sedimentary deposits that range in age from Pliocene to Recent. These strata include fanglomerate of Pliocene or Pleistocene age, lacustrine deposits of Pleistocene Lake Lahontan age, and fluviatile and subaerial flood-plain deposits of Recent age.

The fanglomerate ranges from well-sorted moderately permeable sand and gravel to poorly sorted relatively impermeable slope wash. The Lake Lahontan deposits include three stratigraphic units: A so-called lower silt and clay, a medial gravel, and an upper silt and clay; the lower two units are recognized only in the subsurface. The lower silt and clay unit, whose thickness is uncertain, and the upper silt and clay unit, which is about 55 feet thick, consist largely of dense relatively impermeable silt, clayey silt, and clay. The medial gravel, whose maximum thickness is about 150 feet, consists of well-sorted highly permeable sand and gravel. The flood-plain deposits range from highly permeable stringers of sand and gravel to relatively impermeable lenses of silty clay and clay.

The water-level contours of figure 4.1 show the shape of the piezometric surface in December 1960 and suggest that the principal ground-water movement is westward and southwestward, roughly parallel to the course of the Humboldt River.

Streamflow of the Humboldt River tends to increase, especially during periods of low flow, between the east margin of the mapped area shown on figure 4.1 and staff gage *D*. The increase of streamflow, about 5 to 6 cubic feet per second, is largely a result of the discharge of ground-water underflow from Grass Valley into the Humboldt River. Part of the increase, however, may be due to a partial ground-water barrier beneath the channel of the Humboldt River, the barrier being related to the northward extension of the East Range fault.

Other hydrogeologic evidence which suggests that the East Range fault probably extends farther northward than previously mapped includes (a) an area of rising thermal ground water partly indicated by springs 1 and 2, (b) dense siliceous rock exposed in the flood plain about 300 feet north of well 5, (c) thermal water and iron oxide-coated pebbles found in well 5, (d) intense hydrothermal alteration of the material penetrated in well 3, (e) the occurrence of a bedrock high as indicated by the material penetrated in well 4, and (f) the dissolved-solids content of the waters of the area.

A local ground-water mound, as defined by the water levels at springs 1 and 2 and well 3, is about 100 feet above the regional water table. The temperature of the water at springs 1 and 2 and well 3 is 83° F, 82° F, and 82° F respectively, about 20° F to 25° F warmer than the water in all but one of the other wells shown in figure 4.1. The relatively high temperature of the thermal waters presumably is due largely to the contribution of deeply circulating ground water moving through fractured zones associated with the fault and discharging into the alluvium.

Calcareous and siliceous spring sinter is exposed at and near the orifice of spring 1. The previously men-

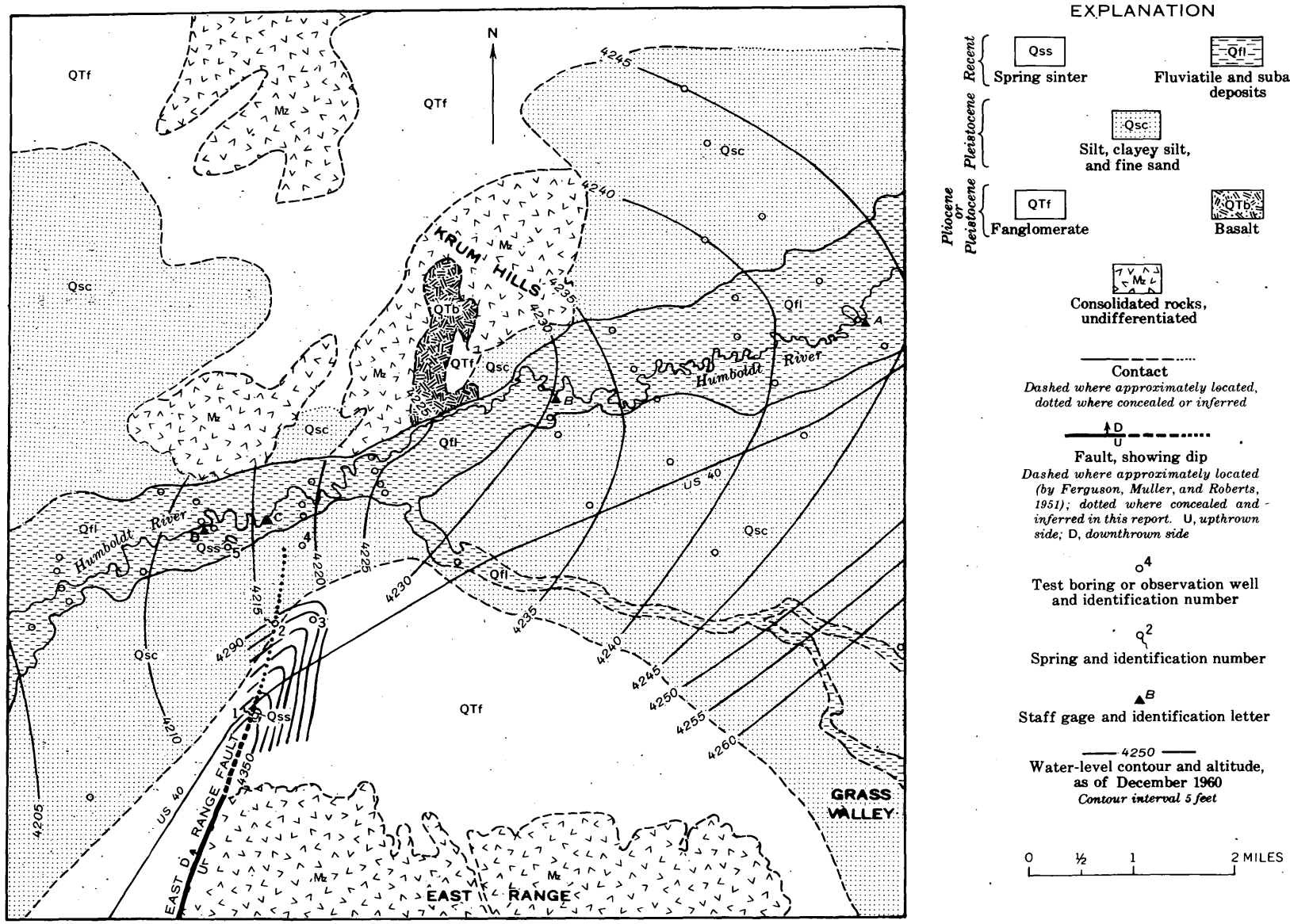

FIGURE 4.1.—Generalized hydrogeologic map of a segment of the Humboldt River valley.

tioned siliceous rock exposed in the flood plain north of well 5 suggests former hot-spring activity at least as far north as that exposure.

The medial gravel unit of Lake Lahontan age was penetrated in well 5 from the land surface to a depth of 83 feet. The pebbles and sand grains are almost completely coated with iron oxide. The temperature of the water in the well is 84° F. This is the only test boring in the flood plain in which thermal water was observed in the medial gravel and in which the particles of the deposit are coated with iron oxide. The iron oxide coatings probably are related to the thermal water, and the thermal water is interpreted as being associated with the fault.

Well 3 penetrated poorly sorted coarse fanglomerate from the land surface to a depth of 32 feet. The stratum beneath the fanglomerate is a dense plastic variegated clay containing small fragments of amorphous silica. The occurrence, texture, and color of the clay, plus the relatively high temperature of the water in the well, also suggest hydrothermal activity—activity that probably is related to the fault.

Well 4 penetrated the upper silt and clay unit of Lake Lahontan age from the land surface to a depth of 42 feet, fanglomerate from 42 to 75 feet, and basalt at a depth of 75 feet. The basalt is believed to be part of the upthrown side of the fault block bounded by the East Range fault, and it is tentatively correlated with the basalt exposed to the northwest across the Humboldt River.

The dissolved-solids content of the waters of springs 1 and 2 and wells 3, 4, and 5 is about 4 to 5 times greater than the dissolved-solids content of the waters of the other wells and of the water of the Humboldt River. Also, the chemical character of the waters of springs 1 and 2 and wells 3 and 4 differs markedly from the chemical character of the other waters in the area. The waters associated with the fault are sodium bicarbonate waters, whereas the other waters of the study area are mixed types.

On the basis of the aforementioned hydrogeologic evidence, it is postulated that the East Range fault extends at least as far northward as shown in figure 4.1. It may extend northward across the Humboldt River, but this is uncertain.

REFERENCE

Ferguson, H. C., Muller, S. W., and Roberts, R. J., 1951, Geology of the Winnemucca quadrangle, Nevada: U.S. Geol. Survey Geol. Quad. Map GQ–11.

STRATIGRAPHY

5. OLD METAVOLCANIC ROCKS OF THE BIG CREEK AREA, CENTRAL IDAHO

By B. F. Leonard, Denver, Colo.

A varied sequence of old metavolcanic rocks is part of a large roof pendant in the Idaho batholith at Big Creek, Valley County, Idaho. Big Creek, at lat 45°07½′ N., long 115°19½′ W., is near the middle of the exposed batholith. The metavolcanics are mainly dark-green amphibole- and mica-rich schists, but elongate-pebble breccias and conglomerates are conspicuous locally. Schistose quartz-feldspar rocks with relict feldspar phenocrysts are exposed in one area. The rocks are interpreted as flows, tuffs, and volcanic breccias that were isoclinally folded and locally disrupted long before the Idaho batholith was emplaced. They were intruded and cut off by the batholith, and were reconstituted by heat and solutions from the cooling granitic mass. The age of the metavolcanic and associated metasedimentary rocks is presumably Precambrian or early Paleozoic. The word "old" is used here to distinguish these metavolcanics from the Casto Volcanics, which are also older than the batholith but are less deformed and of Permian(?) age.

The main belt of old metavolcanic rocks, 5 miles long and 0.5 to 1 mile wide, trends northwest through Big Creek, parallel to a local southeastward projection of the batholith and separated from it by a belt of metasedimentary rocks 0.5 mile wide. The metavolcanics belong mainly to the epidote-amphibolite facies, but rocks of amphibolite facies are exposed where the insulating layer of metasediments pinches out, bringing

629660—62——2

batholithic rocks directly against metavolcanics. To the northwest, the belt of metavolcanics loses its identity in a welter of Tertiary dikes that border the main contact of the batholith at this longitude. To the southeast, the metavolcanics pinch out or pass abruptly into massive metatuffs(?) so poorly exposed that they cannot be distinguished in the field from the neighboring metasiltstones. A small mass of metavolcanic conglomerate in greenschist facies lies in a parallel syncline 3.5 miles northeast of the main belt. The stratigraphic relations of this mass and of remnants farther northeast are uncertain. Fragments of elongate-pebble conglomerate and porphyroblastic amphibole-pyroxene schist resembling rocks of the main belt are found as inclusions in the granitic rocks 20 miles south of Big Creek. Thus the old volcanic rocks may once have extended for at least 20 miles across the present trend of the major fold systems of the metamorphic rocks. Some speculations on the former extent of these rocks are presented at the end of this article.

A stratigraphic section across the best exposures of metavolcanics was measured by miniature theodolite and stadia on the arête west of Placer Lake, 2.6 miles northwest of Big Creek. Three main metavolcanic units were recognized. From the top downward, the inferred sequence and present thickness of units is: metavolcanic breccia and conglomerate, 100–150 feet; hornblende schist and hornfels with relict subophitic fabric, interlayered or interlensed with biotite-rich schist and hornfels, 240–330 feet; and porphyroblastic hornblende schist, 80–260 feet. The total thickness of the partial section is estimated to be 420–740 feet; the bottom of the metavolcanics is not exposed here. Because of isoclinal folding and development of very large boudins, the true sequence may not be the one reported, and the estimates of thickness may be significant only as orders of magnitude.

The upper part of the breccia unit is a strongly lineated rock having a fine gray matrix that contains abundant angular, elongate fragments of blastoporphyritic hornblende-rich hornfels, laminated biotite-rich hornfels, quartz-feldspar hornfels, and perhaps metasiltstone. The fragments range in length from a few millimeters to several centimeters. Some of the smaller ones are rounded. Their outlines are slightly blurred by growth of new biotite. All the fragments except the metasiltstone are of metavolcanic rocks identical with those exposed elsewhere in the belt. The matrix is a mosaic of silt-size quartz and feldspar. It contains scattered euhedral plagioclase relics and rounded quartz grains with authigenic quartz overgrowths, and is partly replaced by biotite and magnetite. The rock is interpreted as a metamorphosed breccia rich in pyroclastic debris but with some fine particles derived from quartz-cemented sandstone ("orthoquartzite"). The lower part of the breccia unit is a light- to dark-green medium-grained massive to schistose amphibole-rich rock containing sporadic elliptical pebbles of fine-grained quartzite and silty limestone. The quartzite and limestone are the same sort as those found in metasediments stratigraphically below the metavolcanics. Rare pebbles of dark-green fine-grained hornblende-rich hornfels are present; probably these represent metamorphosed lava or tuff. The lower part of the breccia unit is interpreted as metamorphosed basaltic tuff, locally conglomeratic, perhaps with some lava.

The middle unit, where hornblende rich, is feldspathic or calcareous. Some of the rock as a relict ophitic fabric, though it now consists of albite-oligoclase laths embedded in porphyroblastic blue-green hornblende and dark-green biotite. Schistose parts contain lenticles of granular sodic plagioclase in masses of hornblende and biotite. Sparse interlayers or lenses of very fine dark-green biotite-rich hornfels and dark-gray silty laminated hornfels are present. Under the microscope, the silty hornfels shows relict euhedral plagioclase, and rounded quartz grains with authigenic quartz overgrowths. Before metamorphism the rocks of this unit were mainly lavas, with subordinate volcanic siltstones.

The lower unit contains little or no clastic debris. It is fine- to medium-grained massive to schistose amphibole-rich rock consisting of dark-green to black hornblende porphyroblasts in a lighter green amphibole matrix. Granular sodic plagioclase is sparingly present. No relict fabric has been seen.

Some epidote and sphene are present in the hornblende-rich rocks of all three units, ilmenite is usually an abundant accessory, and apatite is abundant locally. Blue-green chlorite is sparingly present in some rocks.

A chemical analysis and mode of outwardly homogeneous dark-green hornblende schist from the middle unit are given in the table below. The analyzed sample contained a little vein calcite that is not present in the thin sections or in duplicate hand specimens. The rock was selected for analysis because it was abundant and seemed most nearly representative of the whole metavolcanic sequence. However, the analyzed rock seems to be of slightly higher metamorphic grade—perhaps lowermost amphibolite facies—than rocks in the measured section. The analyzed rock is high in Ti, as are other old mafic igneous rocks of the area. Except for Ti, the minor-element content of the rock does not differ significantly from that of several suites of metasedimentary rock from the various metamorphic zones.

Chemical data on other varieties of old metavolcanic rock are not yet available.

Composition of hornblende schist

[Field No. L/53/617, lab. No. A 73; collected 0.25 mile southwest of Gold Coin copper prospect and 1.8 miles northwest of Big Creek Ranger Station, Big Creek quadrangle, Valley County, Idaho. Lois Trumbull, analyst, 1955]

CHEMICAL ANALYSIS	*Weight percent*
SiO_2	45.00
TiO_2	3.25
Al_2O_3	11.28
Fe_2O_3	3.96
FeO	9.71
MnO	.22
MgO	9.56
CaO	11.77
Na_2O	2.06
K_2O	.57
H_2O+	1.80
H_2O-	.07
P_2O_5	.43
CO_2	.43
Cl	.01
F	.11
S	.05
Total	100.28
Less O	.07
Total (corrected)	100.21

MODE[1]	*Volume percent*
Quartz[2]	≈2.7
Plagioclase[2]	≈15.1
Epidote	1.0
Hornblende	62.1
Biotite	10.0
Sphene	1.4
Apatite	.4
Opaque minerals[3]	5.0
Zircon	Tr.
Chlorite	2.3
Total	100.0

[1] Average of 5 thin sections; 7,442 points counted.

[2] Quartz plus plagioclase 17.8 percent in thin sections. Proportions estimated from grain counts in oils. Plagioclase, seldom twinned, has refractive indices indicating a composition of An_{15-35}, averaging An_{25}.

[3] Examined in 2 polished sections. Mostly ilmenite; some martitized magnetite; a few specks of oxidized pyrite.

The rock is interpreted as a metamorphosed basaltic lava or tuff; the analyzed rock, apparently homogeneous, is similar to the matrix of neighboring rocks that contain several percent of quartzite and silty limestone pebbles. However, the analyzed rock is low in SiO_2 and Al_2O_3 relative to CaO, or has relatively more CaO than known basaltic rocks of corresponding SiO_2/Al_2O_3 ratio. Unmetamorphosed lavas or basaltic intrusive rocks of similar composition are indeed known, but they seem to be rather rare. Accordingly, an orthomagmatic process leading to enrichment in CaO seems unlikely for the hornblende schist. The difference in composition might be accounted for by several other processes, metamorphic or premetamorphic.

Intense metamorphic differentiation in rocks of this grade is not an attractive hypothesis: neighboring rocks retain many primary features of igneous, pyroclastic, or epiclastic fabric; quartz veins along the margins of the belt of metavolcanics, and thus interpretable as venitic, show little evidence of the deformation that has affected several silicified zones younger than the Idaho batholith; and metasedimentary rocks flanking the belt are not enriched in Al_2O_3.

If SiO_2 and Al_2O_3 did not leave the hornblende schist, CaO may have entered as calcite, possibly during diagenesis of the tuffaceous rocks, or possibly during the earliest stage of metasomatic metamorphism, a change that was probably accompanied by introduction of H_2O and other volatiles. As the rock advanced through the greenschist facies to the epidote-amphibolite or lowermost amphibolite facies, CO_2 may have been expelled preferentially, leaving a homogenized rock relatively enriched in CaO, H_2O, F, Cl, and perhaps TiO_2 and P_2O_5.

The metavolcanics near Big Creek are the uppermost unit of a thick sequence of fine-grained, clastic, shallow-water rocks. This whole assemblage was mapped by Shenon and Ross (1936, fig. 2) as the Yellowjacket Formation, which Ross (1934, p. 15 and pl. 1) had assigned to the Belt Series (Precambrian). Identifiable fossils have not yet been found in this formation. Most of its least metamorphosed rocks are very similar to the Belt rocks of northern and eastern Idaho, and the inference of a Precambrian age is reasonable. However, lower Paleozoic rocks of similar composition and appearance are found southeast of Big Creek, in the Bayhorse region described by Ross (1937). In the central part of the Big Creek quadrangle, the metavolcanics overlie a carbonate unit which, where least metamorphosed, is fine-grained, thinly cross laminated quartzose limestone. Contacts between the carbonate unit and metavolcanics are now conformable, but this relation may be due to deformation, not to primary deposition.

The metavolcanics are overlain—again with apparent local conformity—by a generally clean, dominantly white quartzite mapped by Shenon and Ross (1936) as the Hoodoo Quartzite, which Ross (1934, p. 15, 18–20; pl. 1) regarded as Precambrian. This quartzite has also failed to yield identifiable fossils. The evidence for a Precambrian age of the white quartzite in the Big Creek area is inconclusive; the quartzite may be Precambrian, Cambrian, or Ordovician, deposited unconformably on various units of the Yellowjacket or thrust over them.

Both the Yellowjacket and Hoodoo of Shenon and Ross (1936) are cut by narrow mafic dikes of several sorts. These dikes, emplaced after isoclinal folding of the host rocks but before their reconstitution, have not been recognized within the metavolcanics, possibly because all the reconstituted mafic rocks look much alike in the field.

The old metavolcanics are not to be confused with a younger assemblage of pre-batholith volcanic rocks in the area. The younger assemblage comprises flows, breccias, tuffs, welded tuffs, and volcanic grits that be-

long to the Casto Volcanics, a formation first described by Ross (1934, p. 28–35). In the Big Creek quadrangle, the Casto Volcanics lie unconformably on the Hoodoo Quartzite of Shenon and Ross. The old metavolcanics are isoclinally folded and show greater internal deformation than the Casto. However, parts of the Casto have been intruded and thermally metamorphosed by the Idaho batholith to form hornfelses that resemble some of the old metavolcanics. The two sets of volcanics, as well as the post-batholith Challis Volcanics of Tertiary age, can be distinguished only by careful mapping.

Old metavolcanic rocks of the sort described here have not been reported from central Idaho, though Ross (1934, p. 27) mentioned tuffaceous rocks as one of several possible antecedents for "black schist" of indeterminate age near Woodtick Creek, Casto quadrangle. Lava flows are present in Belt rocks in northern Idaho and neighboring areas, but pyroclastic or epiclastic volcanics seem to be rare: Johns (1961, p. 26) mentions one occurrence of basalt-pebble "agglomerate" overlying a flow of Purcell Basalt in northern Lincoln County, Mont.; Leech (1958, p. 8) notes that tuff is associated with andesitic lava at the top of the Kitchener-Siyeh Formation of the Purcell Series in the Fernie area, southeastern British Columbia. Far to the northwest and southeast of the Big Creek area, along the trend of regional structures in the old rocks, sequences that include both old metavolcanic rocks and coarse clastic deposits are found in northeastern Washington and in the Pocatello area, southeastern Idaho.

In the Metaline district, Washington, Park and Cannon (1943, p. 7–15) found that the thick, virtually unsorted, generally nonvolcanic(?) Shedroof Conglomerate graded upward into greenstone and green schist of the Leola Volcanics. Relict ophitic, diabasic, and amygdular(?) textures, rare pillow structures, and tuffaceous fabric are preserved in some of the volcanics. Park and Cannon tentatively assigned both formations to the top of the Precambrian sequence in that area. The two units, each more than 5,000 feet thick, are unconformably(?) overlain by fine-grained phyllites with subordinate carbonate rocks, quartzite, and grit (Monk Formation, tentatively placed at the base of the Cambrian) and by the thick Gypsy Quartzite of Cambrian age. A similar sequence of conglomerate and overlying volcanics of Precambrian age, succeeded by quartzite of Cambrian age, has been recognized some distance south of the Metaline district by Bennett (1941), Campbell and Loofbourow (1957), Weis (1959), and others. The correlatives of these rocks in Canada have been discussed by Reesor (1957, p. 158–162; 175), who interpreted part of the Precambrian sequence as eugeosynclinal.

The metavolcanics near Pocatello are also greenstones. These metamorphosed lavas, tuffs, and volcanic breccias constitute the Bannock Volcanic Formation of Ludlum (1942). According to Ludlum, a minimum thickness of 400 feet of Bannock is overlain by a thick sequence of mainly clastic rocks (Pocatello Formation) whose lower part contains coarse conglomerates that he interpreted as tillites. According to Ludlum the Bannock, Pocatello, and overlying Blackrock Limestone are Precambrian, overlain unconformably by the very thick Brigham Quartzite of Cambrian age. Earlier workers assigned younger ages to some of these rocks. Others dispute the assignment of the nonfossiliferous lower strata of the Brigham to the Cambrian.

In northeastern Utah, coarse clastic rocks of Precambrian and Cambrian age, locally overlain by quartzite of Cambrian age, have been interpreted as tillites by Blackwelder (1932) and others. Mafic volcanic rocks seem to be sparse or absent from the scattered exposures of these coarse clastic rocks. Dott (1961, fig. 4 and p. 1301–1303) recently reexamined some of the Utah "tillites" and concluded that their origin was uncertain.

Precise correlation of metavolcanics at Big Creek with those to the northwest or southeast is not possible, and none should be inferred from this brief account. However, there is a "family resemblance" in the association of greenstones and coarse clastic deposits of relatively great age, overlain by thick, rather clean quartzites. The coarse clastic deposits are somewhat enigmatic in origin; they underlie the greenstone at Metaline but overlie it at Big Creek and Pocatello. The overlying quartzite is not conformable with the assemblage of greenstone and conglomerate. Possibly the quartzite is late Precambrian in places; the upper parts are Cambrian near Metaline and Pocatello; conceivably the quartzite is as young as Ordovician in central Idaho, if it is the correlative of the Kinnikinic.

The Metaline and Big Creek areas of metavolcanics and coarse clastics coincide with the southwest margin of the Belt sea inferred by C. P. Ross (1961, personal communication) from his compilation of regional data. (Because he regards the age assignment of the greenstone and conglomerate near Pocatello as uncertain, Ross does not include those rocks in the Belt.) It is easy to speculate that the eugeosyncline of Belt age postulated near the Canadian border by Reesor (1957) and others extended southward and southeastward, passing into a miogeosyncline that contained relatively thin deposits of volcanic and epiclastic volcanic rocks in the Big Creek area, and relatively thin volcanics

locally overlain by "tillite" in the Pocatello area. Such speculation is scarcely supported by the meager data on distribution of rocks having the family resemblance noted above. However, recognition of the resemblance may be useful in attacking some other problems of central Idaho geology.

REFERENCES

Bennett, W. A. G., 1941, Preliminary report on magnesite deposits of Stevens County, Washington: Washington State Dept. Conserv. and Devel., Div. Geology, Rept. Inv. 5, 25 p.

Blackwelder, Eliot, 1932, An ancient glacial formation in Utah: Jour. Geology, v. 40, p. 289–304.

Campbell, Ian, and Loofbourow, J. S., Jr., 1957, Preliminary geologic map and sections of the magnesite belt, Stevens County, Washington: U.S. Geol. Survey Mineral Inv. Field Studies Map MF–117.

Dott, R. H., Jr., 1961, Squantum "tillite," Massachusetts—evidence of glaciation or subaqueous mass movements?: Geol. Soc. America Bull., v. 72, p. 1289–1305.

Johns, W. M., 1961, Progress report on geologic investigations in the Kootenai-Flathead area, northwest Montana, pt. 3, Northern Lincoln County: Montana Bur. Mines and Geology Bull. 23, 57 p.

Leech, G. B., 1958, Fernie map-area, west half, British Columbia: Canada Geol. Survey Paper 58–10, 40 p.

Ludlum, J. C., 1942, Pre-Cambrian formations at Pocatello, Idaho: Jour. Geology, v. 50, p. 85–95.

Park, C. F., Jr., and Cannon, R. S., Jr., 1943, Geology and ore deposits of the Metaline quadrangle, Washington: U.S. Geol. Survey Prof. Paper 202, 81 p.

Reesor, J. E., 1957, The Proterozoic of the Cordillera in southeastern British Columbia and southwestern Alberta, *in* Gill, J. E., ed., The Proterozoic in Canada. Royal Soc. Canada Special Pub. 2, p. 150–177.

Ross, C. P., 1934, Geology and ore deposits of the Casto quadrangle, Idaho: U.S. Geol. Survey Bull. 854, 135 p.

——— 1937, Geology and ore deposits of the Bayhorse region, Custer County, Idaho: U.S. Geol. Survey Bull. 877, 161 p.

Shenon, P. J., and Ross, C. P., 1936, Geology and ore deposits near Edwardsburg and Thunder Mountain, Idaho: Idaho Bur. Mines and Geology Pamph. 44, 45 p.

Weis, P. L., 1959, Lower Cambrian and Precambrian rocks in northeastern Washington [abs.]: Geol. Soc. America Bull., v. 70, p. 1790.

6. ANGULAR UNCONFORMITY BETWEEN MESOZOIC AND PALEOZOIC ROCKS IN THE NORTHERN SIERRA NEVADA, CALIFORNIA

By L. D. Clark, R. W. Imlay, V. E. McMath, and N. J. Silberling, Menlo Park, Calif., Washington, D.C., Univ. of Oregon, Eugene, Oreg., Menlo Park, Calif.

Work done in cooperation with the California Division of Mines and Geology

In the canyon of the North Fork of the American River about 5 miles south of Cisco in the northern Sierra Nevada, Calif., rocks of probable Silurian age are overlain with pronounced angular unconformity by rocks of Mesozoic age. The truncated Paleozoic strata are overlain by a sedimentary chert breccia which in turn is overlain conformably by limestone of Late Triassic(?) age in the northern part of the area studied. Lower Jurassic beds of the Sailor Canyon Formation unconformably overlie the limestone in the northern part of the area and the chert breccia in the southern part. The Paleozoic rocks are complexly folded and have a well-developed slaty cleavage; the Mesozoic rocks dip steeply but are little folded, and cleavage in them is obscure. The sharp contact between the Paleozoic rocks and the chert breccia is well exposed and is not faulted. The dihedral angle between the bedding of the Paleozoic and Mesozoic rocks ranges from 0° to 90°.

These relations provide evidence that the rocks of probable Silurian age were strongly folded, regionally metamorphosed to a low grade, and deeply eroded during later Paleozoic or Triassic time and that little folding occurred during latest Triassic(?) and earliest Jurassic time. Relations are much less clear elsewhere in northern California and westernmost Nevada, and proof of pre-Jurassic regional metamorphism and folding sufficient to cause vertical dips has been lacking. The unconformity separating Paleozoic and Mesozoic rocks was first recognized by Lindgren (1900), but new stratigraphic and structural information requires that his description of the relations be expanded and modified.

CORRELATION AND AGE OF ROCKS BENEATH THE UNCONFORMITY

Paleozoic strata beneath the unconformity, exposed in the western part of the area (fig. 6.1), were included with the Blue Canyon Formation by Lindgren (1900).

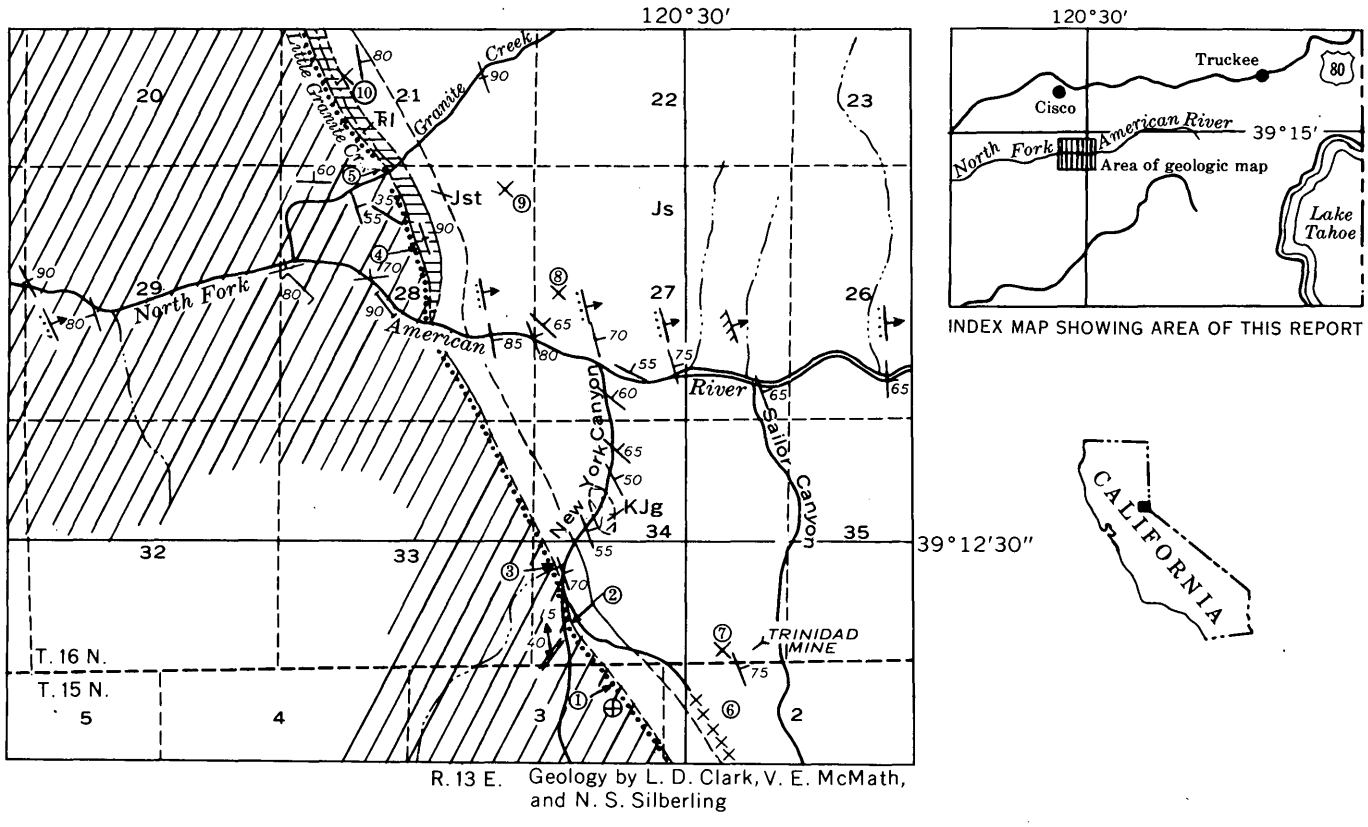

EXPLANATION

KJg — Granitic rocks

Js / Jst — Sailor Canyon Formation
Js, *siltstone, graywacke, subordinate conglomerate, and limestone*
Jst, *basal tuff unit*

Tl — Limestone

Chert breccia

Shoo Fly Formation

JURASSIC-CRETACEOUS

JURASSIC

TRIASSIC(?)

SILURIAN(?)

Contact
Dashed where approximately located

Strike and dip of beds

Strike of vertical beds

Horizontal beds

Strike and dip of cleavage

Strike of vertical cleavage

Direction of tops of beds
Determination based on (a) graded bedding, and (b) crossbedding. Plotted on strike with structure reading taken at point of observation

Minor fold
Showing strike and dip of axial surface, and bearing and plunge of axis

Fossil locality

Locality referred to in text

FIGURE 6.1.—Geologic map of an area including New York Canyon, Placer County, Calif.

The Blue Canyon Formation constitutes but one segment of a belt more than 100 miles long that is marked throughout by a distinctive and unusual assemblage of rocks. Of the three names that were used to designate various segments of this belt the name Shoo Fly Formation, applied by Diller (1892, p. 375; 1908, p. 28) to the northern part, has priority and is here used for the entire belt (fig. 6.2). The name Blue Canyon Formation, which has been applied to rocks only in the Colfax quadrangle (Lindgren, 1900), is here abandoned, and the name Calaveras Formation is restricted from the area shown as Shoo Fly Formation on figure 6.1.

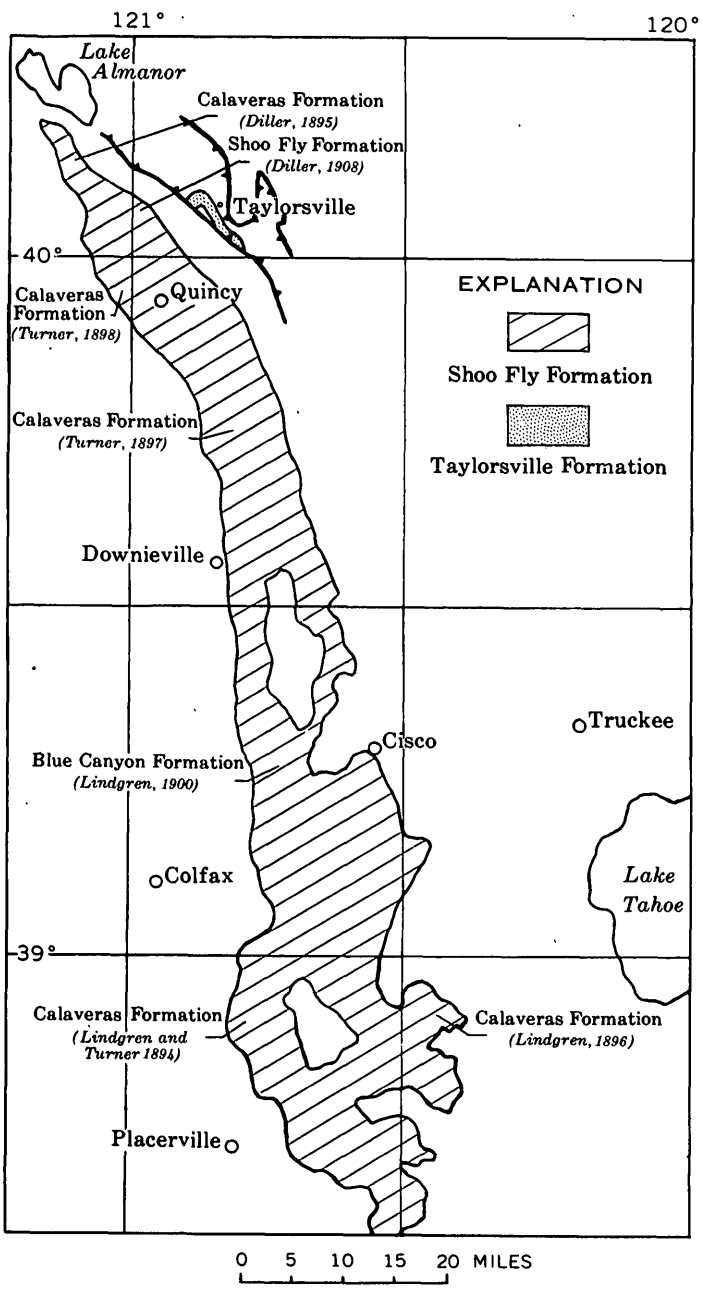

FIGURE 6.2.—Map showing distribution of the Shoo Fly and Taylorsville Formations. Other names applied to rocks of the Shoo Fly Formation in earlier studies of various 30-minute quadrangles are shown also.

The Shoo Fly Formation is composed mostly of thin- to thick-bedded light-colored graywacke or tuff or both, and grayish-green slate. Interbedded with these are subordinate dark-gray slate, orthoquartzite, arkose, thin-bedded chert, andesitic(?) pyroclastic rocks, thin limestone beds, conglomerate containing very well rounded pebbles of quartzite, and other rocks mentioned below in descriptions of local areas. The graywacke or tuff beds are commonly graded and consist of roundish quartz grains, and less commonly plagioclase and K-feldspar, in a sericite matrix.

Of four fossil localities previously reported to be in the Shoo Fly Formation, one (Lindgren, 1900, p. 2) is in the Late Triassic(?) limestone of this report, and fossils at another (Lindgren, 1900, p. 2) suggest only Paleozoic age. A fusulinid locality (Diller, 1908, p. 23) is almost certainly separated from the Shoo Fly Formation by a fault, according to McMath[1]. Stromatoporoids suggesting Devonian or Mississippian age were found near the contact between the Shoo Fly Formation and an overlying volcanic sequence, about midway between Taylorsville and the North Fork of the American River by Clark[2]. Clark's description does not permit unequivocal assignment of the fossiliferous rocks to either the Shoo Fly Formation or the volcanic sequence.

A Silurian age for at least part of the Shoo Fly Formation, exposed west of Taylorsville (fig. 6.2) in the lower plate of a thrust fault, is suggested by correlating it with the fossiliferous Taylorsville Formation of Silurian age (Diller, 1908, p. 16), which is in the upper plate of the thrust[3]. Both the Shoo Fly and Taylorsville Formations are overlain with angular unconformity by a volcanic sequence having as its lowest three units an unnamed rhyolite, the Taylor Meta-Andesite of Mississippian age (Diller, 1908, p. 84), and the Peale Formation, also of Mississippian age. A similar relation between rocks here included with the Shoo Fly Formation and an overlying volcanic sequence is found about 25 miles southeast of Taylorsville (Durrell and Proctor, 1948, p. 171).

West of Taylorsville, the lower and much the greater part of the Shoo Fly Formation consists of the quartzose sandstones or tuffs and slates that characterize the formation elsewhere. An overlying unit of the Shoo Fly Formation, and the equivalent Taylorsville Forma-

[1] McMath, V. E., 1958, Geology of the Taylorsville, Plumas County, California: California Univ., Los Angeles, Ph. D. thesis, p. 38.
[2] Clark, S. G., 1930, The Milton Formation of the Sierra Nevada of California: California Univ., Berkeley, Ph. D. thesis, p. 72.
[3] McMath, ibid., p. 27, 167.

tion above a fault that truncates its lower part, are each about 2,000 feet thick. They consist largely of black or greenish-gray obscurely laminated phyllite and slate, and thin beds, commonly graded, of feldspathic, possibly tuffaceous, graywacke. In the Shoo Fly Formation this unit is overlain by about 3,000 feet of andesitic greenstone, mostly derived from lava, and subordinate interlayered chert.

DESCRIPTION OF AREA

Within the area studied (fig. 6.1), the most abundant rocks in the Shoo Fly Formation are thin-bedded dark-gray slate and siltstone that is in part pyritic and in part quartzose, thin-bedded chert, and fine-grained thin-bedded quartz-rich graywacke or rhyolitic tuff. Medium-grained arkose containing both plagioclase and K-feldspar is exposed on the North Fork of the American River. Conglomerate consisting of well-rounded quartz and quartzite pebbles is sparse. Some beds of coarse sandstone and fine conglomerate composed of angular fragments of chert are interbedded with siltstone and chert on the ridge north of map locality 4 (fig. 6.1). Slaty cleavage is prominent in the originally argillaceous rocks, but original textures in the rocks of sand size and larger are well preserved, and in most places the rocks are little sheared. Because rocks of the Shoo Fly Formation within the area of figure 6.1 have not been correlated with a specific part of the section in the Taylorsville area, they are designated Silurian(?).

The Shoo Fly Formation is unconformably overlain by a coarse, nonbedded, poorly sorted chert breccia that locally attains a thickness of 75 feet or more. The breccia separates the Shoo Fly Formation to the southwest from fossiliferous Mesozoic rocks to the northeast, is structurally concordant with the Mesozoic rocks, and is considered Mesozoic in age. The composition and texture of the breccia vary along strike, but chert pebbles of various colors are everywhere the most abundant. Fragments of thin-bedded dark-gray slate and fine-grained graywacke or silicic tuff derived from the Shoo Fly Formation are common locally. Fine-grained dioritic or quartz monzonitic rocks are common in the breccia near the north side of the map area. Sparse pebbles of mica schist were found at locality 4. The matrix consists of sand- and granule-sized grains of chert. Commonly the largest pebbles in the breccia are about 4 inches in diameter, but near the north edge of the area, scattered blocks as much as 20 inches long occur in the breccia. At locality 4 and on the crest of the ridge to the north, outcrop areas of the Shoo Fly Formation more than 20 feet long and 5 feet wide are surrounded by chert breccia. Such a pattern could result either from deposition of the breccia on a very irregular erosion surface or from incorporation of detached blocks of the Shoo Fly in the breccia.

The contact between the chert breccia and the underlying Shoo Fly Formation is a nearly straight line at map scale, but in outcrops the contact surface has a relief of several feet. Where well exposed at localities 2 and 4, the contact alternately follows bedding of the Shoo Fly Formation and fracture surfaces that cut across the bedding. Rocks of the Shoo Fly Formation in contact with the chert breccia are: At locality 1, thin-bedded chert; at 2 and 4, thin-bedded black slate; and at 3 and 5, medium- and fine-grained graywacke or silicic tuff.

North of the North Fork of the American River the chert breccia is conformably overlain by limestone of Late Triassic(?) age. In New York Canyon the breccia is overlain by the Sailor Canyon Formation of late Early Jurassic age. The chert breccia is of probable Triassic age.

The limestone that overlies the chert breccia is about 400 feet thick at the crest of the spur north of locality 4. It is absent in New York Canyon, but is possibly concealed on the south side of the canyon of the North Fork of the American River. The lower part of the limestone unit consists of alternating layers of thin-bedded argillaceous gray limestone that weathers reddish brown, and thin- to medium-bedded gray limestone that weathers very light gray. Well-rounded granules or angular fragments of chert characterize some of these beds. The middle part consists of less argillaceous limestone beds that form bold cliffs, and the upper part consists of thin interbeds of light-gray limestone and light-greenish-gray very fine grained pyritic sandstone probably derived from silicic tuff.

A Late Triassic(?) age for the limestone is based mainly on the occurrence at locality 10 (USGS Mes. loc. M1167) of numerous spherical objects with the surficial and internal structure of *Heterastridium*, a supposed hydrozoan coelenterate that is widely distributed in deposits of Norian (late Late Triassic) age. However, in view of the doubtful biologic affinities and unknown evolutionary history of this organism, the age must be considered provisional. A post-Paleozoic age for the limestone is corroborated by the presence of poorly preserved scleractinian corals, large cidarid echinoid spines, and *Pentacrinus*-like crinoid columnals with petaloid crenulations on the articulating surfaces.

The Sailor Canyon Formation, occupying the eastern part of the map area, overlies the limestone unit in the northern part of the area and the chert breccia in the southern part. It is at least 10,000 feet thick and consists largely of graywacke, tuff of intermediate compo-

sition, and dark-gray siltstone. The lowermost unit here included in the Sailor Canyon Formation consists of sparsely bedded, probably andesitic, tuff about 500 to 700 feet thick. It weathers light gray green and ranges in texture from very fine grained tuff to lapilli tuff.

The base of the Sailor Canyon Formation is well exposed in New York Canyon (fig. 6.1, loc. 2), where the tuff unit rests on the chert breccia along an irregular surface having a local relief of about 10 feet. Here the tuff unit contains a 4-foot layer of chert breccia about 20 feet above its base. The absence of the Upper Triassic(?) limestone and the relief of the upper breccia surface are interpreted as evidence of an erosional unconformity at the base of the Sailor Canyon Formation, although very little Jurassic time can be represented by the unconformity.

The age of the Sailor Canyon Formation, determined by ammonites, includes most of the Early Jurassic and some of the Middle Jurassic. About 1,000 feet above its base (fig. 6.1, loc. 6; USGS Mes. loc. 28403) *Crucilobiceras* of middle Early Jurassic (late Sinemurian to early Pliensbachian) age was found. About 2,000 feet above the base of the formation (fig. 6.1, locs. 7, 8, and 9; USGS Mes. locs. 28396, 28391, 28395, respectively) *Zugodactylioceras*, *Dactylioceras*, *Orthildaites*, *Hildaites*, and *Protogrammoceras?* of late Early Jurassic (early Toarcian) age were found.

STRUCTURE

The Shoo Fly Formation is complexly folded, but near the North Fork of the American River the gross strike is easterly and the gross dip is northerly. Open to tightly compressed folds range in amplitude from a few feet to many hundreds of feet. Slaty cleavage that is especially marked in the thin-bedded siltstones of the Shoo Fly Formation strikes northwest and dips steeply southwest or is vertical. The Mesozoic rocks are much less intricately folded; the trace of bedding on well-exposed canyon walls is nearly straight, and beds strike about N. 25° W. and dip northeast or are vertical. Cleavage is weakly developed in the Sailor Canyon Formation. The angle between bedding in the Shoo Fly and bedding in the Mesozoic rocks ranges from a few degrees to nearly 90°, owing to the earlier folding of the Shoo Fly Formation. Large dihedral angles are formed both where bedding in the Shoo Fly Formation is nearly horizontal and where it is nearly vertical.

REFERENCES

Diller, J. S., 1892, Geology of the Taylorsville region of California: Geol. Soc. America Bull., v. 3, p. 370–394.

——— 1895, Description of the Lassen Peak sheet [California]: U.S. Geol. Survey Geol. Atlas, Folio 15.

——— 1908, Geology of the Taylorsville region, California: U.S. Geol. Survey Bull. 353, 128 p.

Durrell, Cordell, and Proctor, P. D., 1948, Iron-ore deposits near Lake Hawley and Spencer Lakes, Sierra County, California, *in* Iron resources of California: California Div. Mines Bull. 129, pt. L, p. 165–192.

Lindgren, Waldemar, 1896, Description of the gold belt; description of the Pyramid Peak quadrangle [California]: U.S. Geol. Survey Geol. Atlas, Folio 31, 8 p.

——— 1900, Description of the Colfax quadrangle [California]: U.S. Geol. Survey Geol. Atlas, Folio 66, 10 p.

Lindgren, Waldemar, and Turner, H. W., 1894, Description of the gold belt; description of the Placerville sheet [California]: U.S. Geol. Survey Geol. Atlas, Folio 3.

Turner, H. W., 1897, Description of the gold belt; description of the Downieville quadrangle [California]: U.S. Geol. Survey Geol. Atlas, Folio 37, 8 p.

——— 1898, Description of the gold belt; description of the Bidwell Bar quadrangle [California]: U.S. Geol. Survey Geol. Atlas, Folio 53, 6 p.

7. MESOZOIC AGE OF METAMORPHIC ROCKS IN THE KINGS RIVER AREA, SOUTHERN SIERRA NEVADA, CALIFORNIA

By James G. Moore and Franklin C. Dodge, Menlo Park, Calif.

Fossils of Triassic or Jurassic age have been found in a large pendant near the confluence of the Middle and South Forks of the Kings River, in the southern Sierra Nevada, Calif. This pendant, here called the Boyden Cave pendant after the cave of that name, consists chiefly of metamorphosed sedimentary strata. It is one of a group of metamorphic remnants of similar lithology that are strung out through the dominantly granitic terrane of the Sierra Nevada for a distance of more than 70 miles. They extend from near Shaver Lake (Krauskopf, 1953) in the San Joaquin drainage to Mineral King in the Kaweah and Kern River drain-

ages (Ross, 1958; Knopf and Thelen, 1905) and are composed of arkosic sandstone, argillite, marble (in part dolomitic), and only minor volcanic material. Figure 7.1 is a geologic reconnaissance map of part of the Boyden Cave pendant.

The Boyden Cave pendant is well exposed along State Highway 180, 67 road miles east of Fresno. It trends about N. 20° W. and is 3 miles wide and more than 6 miles long. Neither end has been mapped; northward it may be continuous with a pendant mapped by Krauskopf (1953), 3 miles north of the junction of the forks of the Kings River. The intervening terrain on the 7,000-foot-high north wall of the Middle Fork canyon has not been mapped.

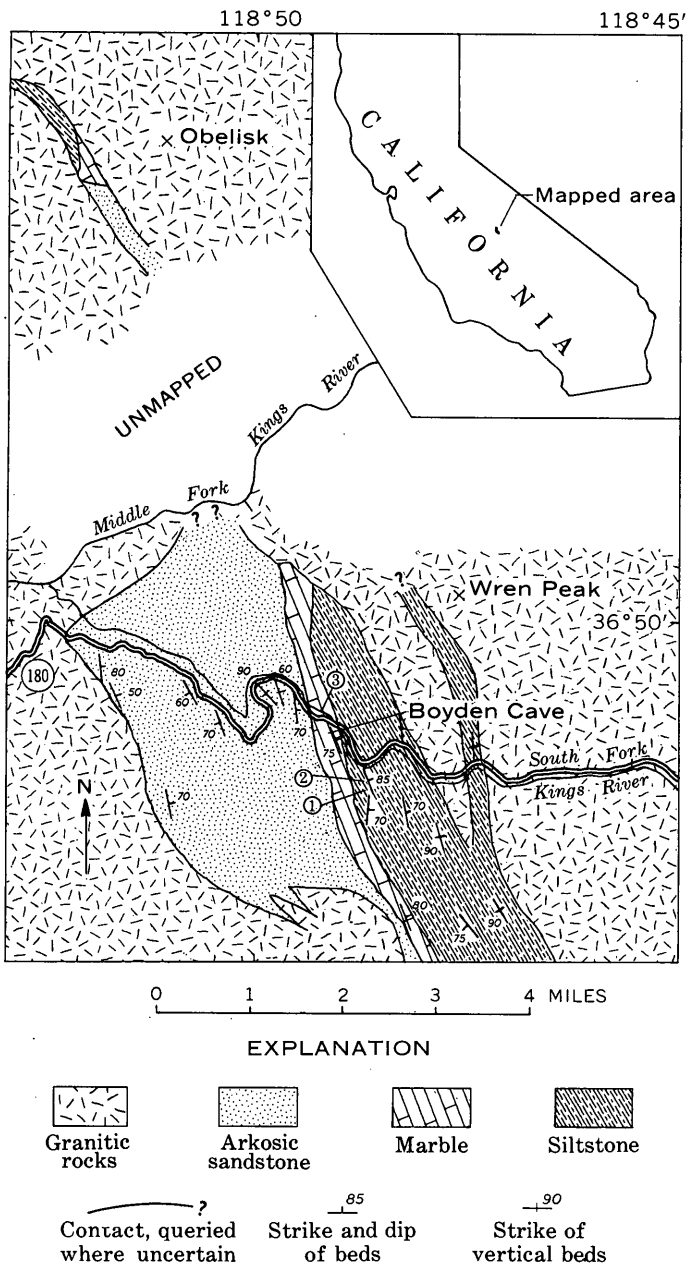

FIGURE 7.1.—Reconnaissance geologic map of an area near the junction of the Middle and South Forks of the Kings River, southern Sierra Nevada, Calif. Circled numbers are fossil localities described in the table. Most of the map west of long. 118°51.5′ W. is after Krauskopf (1953).

The bedding is steep or vertical in most places; therefore the horizontal width of the lithologic units represents their approximate thickness. Accurate measurement of stratigraphic thickness is not practicable because the rocks are metamorphosed and strongly deformed. The average maximum width of the pendant is 14,000 feet. The major units from west to east are: an arkosic sandstone unit, a marble unit, and a siltstone unit.

Arkosic sandstone unit.—The westernmost unit in the pendant forms a band about 9,000 feet wide and is composed of white or gray metamorphosed arkosic sandstone. Except for quartz, the most abundant mineral of the sandstone is K-feldspar, which averages about 13 percent by volume of the rock. The western part of the sandstone unit is argillaceous and contains limy layers, but the middle and eastern parts lack these impurities. Where the sandstone is rather pure, it is commonly thick bedded and contains cross-bedded laminations. In places these individual laminations, which are about 1 inch thick, show graded bedding. Both the crossbeds and graded beds suggest that the top of this unit is to the west, and hence, that it is the youngest unit of the pendant. A zone of shaly and limy sandstone about a thousand feet wide forms the eastern part of the unit.

Marble unit.—East of the sandstone unit is a band of coarsely crystalline marble slightly more than 1,000 feet wide. Most of the carbonate rock is dolomite marble and contains less than 10 percent calcite, but Boyden Cave and many other small caves in the eastern side of this unit are in calcite marble containing only a little dolomite.

Siltstone unit.—East of the marble is 4,000 feet of thin-bedded siltstone, shale, and fine sandstone, much of which is metamorphosed to hornfels, slate, and phyllite. The eastern part contains thin-bedded layers of limestone. On the western side, about a quarter mile south of the highway, is a discontinuous layer several hundred feet thick of sedimentary breccia composed of fragments of thin-bedded sandstone, siltstone, and shale in an argillaceous matrix. Small-scale intricate folding is common in the siltstone unit, probably because it is composed of thin alternating competent and incompetent layers. In contrast, the other thicker bedded units show only broad open folds. The siltstone unit contains some volcanic rocks. Metamorphosed rhyolitic

material is present in a thin strip of metamorphic rock projecting northward from the east side of the pendant and also near the south margin of the map (fig. 7.1).

Fossils have been collected from three localities in the siltstone unit of the Boyden Cave pendant. These fossils (see table below) indicate a Mesozoic age, Triassic or Jurassic, for the siltstone unit and probably for all the rocks of the Boyden Cave pendant.

Fossils from the Boyden Cave pendant, southern Sierra Nevada, Calif.

No. on fig. 7.1	Locality	Fossils	Age	Identified by—
1	East side of Boulder Creek, 100 yards upstream from trail bridge; near center of sec. 10, T. 13 S., R. 29 E.	Shell impression	Post-Precambrian	R. J. Ross, Jr. (written commun., May 23, 1961).
2	Near ridge crest, 100 yards east of Boulder Creek; close to center of sec. 10, T. 13 S., R. 29 E.	*Pentacrinus* sp	Early Triassic to Late Jurassic.	Porter M. Kier (written commun., July 14, 1961).
3	200-pound boulder in bed of South Fork of Kings River, 200 feet downstream from highway bridge across river; SW¼ sec. 3, T. 13 S., R. 29 E. Lithology of boulder indicates it originated less than ½ mile upstream.	Ammonite (?)	Mesozoic (?)	N. J. Silberling (written commun., Aug. 15, 1961).

The fossils of Triassic or Jurassic age found in the Boyden Cave pendant suggest that the rocks in the 70-mile-long belt of lithologically similar roof pendants are all of pre-Cretaceous Mesozoic rather than Paleozoic age. Fossils of Late Triassic age previously reported from the Mineral King pendant at the south end of the belt (Durrell, 1940, p. 17) strongly support this view. East of this belt of pendants of sedimentary rocks is a more extensive belt characterized by predominantly volcanic material which has yielded Early Jurassic fossils (Rinehart, Ross, and Huber, 1959). The stratigraphic relationship between the rocks of these two belts of pendants is unknown; the two lithologies may be of different age or different facies of the same age.

REFERENCES

Durrell, Cordell, 1940, Metamorphism in the southern Sierra Nevada, northeast of Visalia, California: California Univ. Pub. Geol. Sci., v. 25, no. 1, p. 1–118.

Knopf, A., and Thelen, P., 1905, Sketch of the geology of the Mineral King District: California Univ. Pub., Dept. Geology, v. 4, p. 227–262.

Krauskopf, K. B., 1953, Tungsten deposits of Madera, Fresno, and Tulare Counties, California: California Div. Mines Spec. Rept. 35, 83 p.

Rinehart, C. D., Ross, D. C., and Huber, N. K., 1959, Paleozoic and Mesozoic fossils in a thick stratigraphic section in the eastern Sierra Nevada, California: Geol. Soc. America Bull., v. 70, p. 941–946.

Ross, D. C., 1958, Igneous and metamorphic rocks of parts of Sequoia and Kings Canyon National Parks, California: California Div. Mines Spec. Rept. 53, 24 p.

8. RED BIRD SILTY MEMBER OF THE PIERRE SHALE, A NEW STRATIGRAPHIC UNIT

By James R. Gill and William A. Cobban, Denver, Colo.

The name Red Bird Silty Member of the Pierre Shale is given herein to a 200- to 725-foot unit of gray marine silty shale that crops out along the flanks of the Black Hills uplift in eastern Wyoming, southeastern Montana, and western South Dakota. The name is derived from the Red Bird store in the NE¼ sec. 27, T. 38 N., R. 62 W., Niobrara County, Wyo. (fig. 8.1).

The Red Bird Member was recorded originally as a "sandy shale member" (Cobban, 1951, p. 817). Later the outcrops on the north flank of the Black Hills uplift were briefly described as 200 feet of gray silty to sandy shale that contains iron-stained calcareous septarian concretions (Cobban, 1952, p. 87). In subsequent papers the unit has been referred to as the "un-

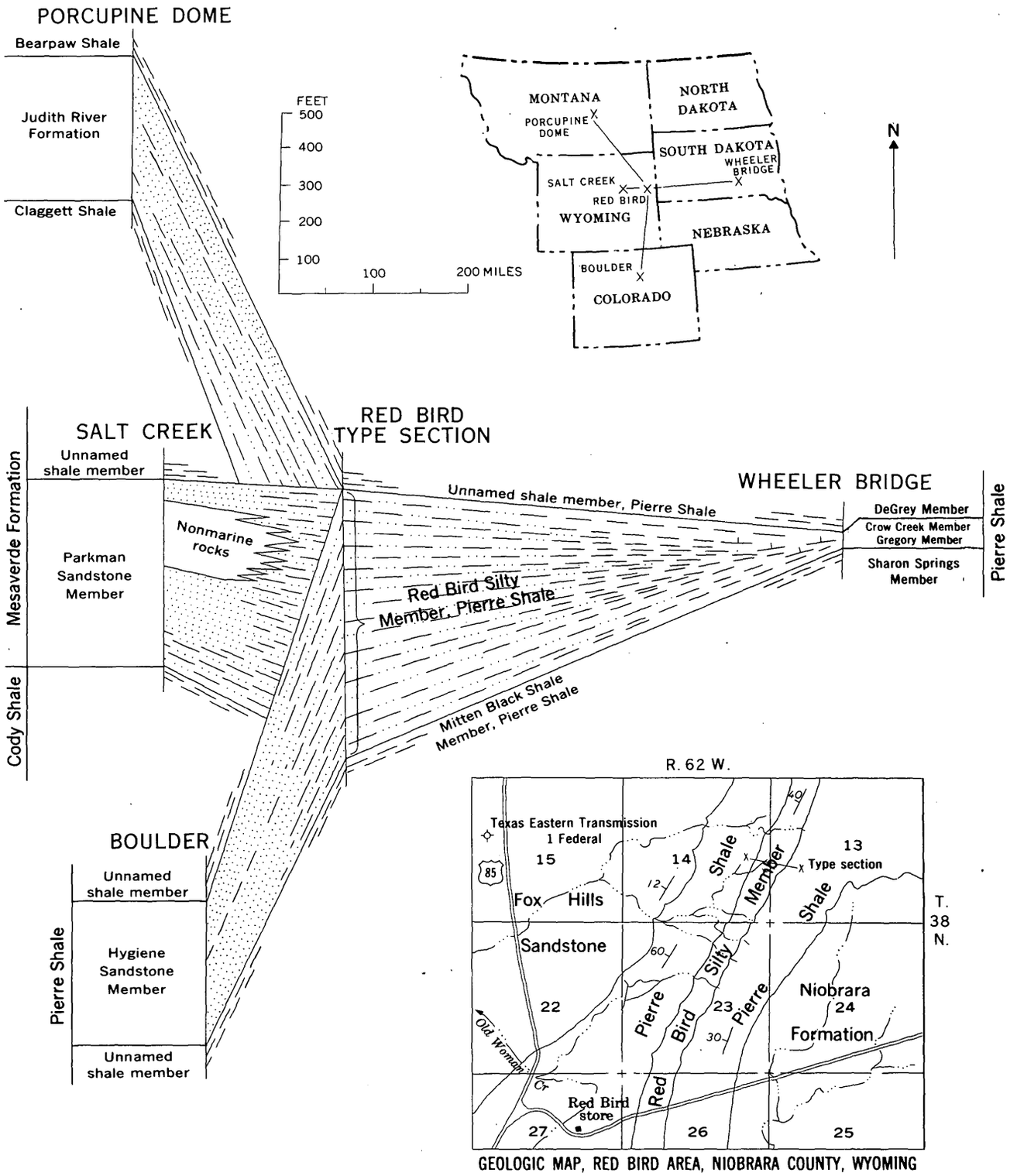

FIGURE 8.1.—Location of the type section of the Red Bird Silty Member, Pierre Shale, Niobrara County, Wyo., and correlation with equivalent rocks in Wyoming, Montana, South Dakota, and Colorado.

named silty member" (Cobban, 1958a, p. 663, 1958b, p. 116; Robinson, Mapel, and Cobban, 1959, p. 108; Scott and Cobban, 1959, p. 129; Tourtelot, Schultz, and Gill, 1960, p. B447, B448; Gill and Cobban, 1961, p. D190).

The Red Bird Member consists of soft silty shale that weathers light to medium gray and contains numerous limestone concretions that weather light gray, yellowish gray, grayish orange, dark yellowish orange, and light brown to moderate yellowish brown and orange brown. The concretions are ordinarily 1 to 2 feet in diameter and 6 to 12 inches thick. Some are septarian, with thin veins of pale-yellow calcite. Very closely spaced concretions form conspicuous ridges in places.

The Red Bird rests conformably on the very dark colored Mitten Black Shale Member and is conformably overlain by an unnamed dark-gray shale member. The Red Bird commonly forms a light to medium gray grass-covered outcrop belt between the adjoining darker and more poorly vegetated members of the Pierre Shale.

Fossil mollusks are common throughout the Red Bird Member. In the type section near Red Bird the lower 322 feet of the member is characterized by an undescribed species of *Baculites* that has a strongly ribbed venter. The next 343 feet is featured by *Baculites gregoryensis* Cobban, and the upper 60 feet is marked by *Baculites scotti* Cobban.

The Red Bird Member was deposited marginal to nearshore marine sandstones that form the eastern edges of the Judith River Formation of Montana and the Parkman Sandstone Member of the Mesaverde Formation of Wyoming (fig. 8.1). East of the Black Hills the Red Bird becomes less silty and is replaced by the calcareous Crow Creek and partly calcareous Gregory Members of the Pierre Shale. The name Red Bird Silty Member can be applied to a 150-mile-wide north-trending belt of rocks that lies east of the recognizable limits of the Hygiene Sandstone Member of the Pierre Shale in Colorado, the Parkman Sandstone Member of the Mesaverde Formation in Wyoming, and the Judith River Formation in Montana, and west of the recognized limits of the Crow Creek and Gregory Members of the Pierre Shale in central South Dakota (Gill and Cobban, 1961, fig. 352.3B).

The Red Bird ranges from 690 to 745 feet in thickness in the type area and is 725 feet thick in the type section. The following section, measured with a Jacob staff in the NW¼SW¼ sec. 13 and NE¼SE¼ sec. 14, T. 38 N., R. 62 W., Niobrara County, Wyo., is designated the type section. At this locality all of the Red Bird Member is silty. Bed 1 rests on the Mitten Black Shale Member and bed 15 is overlain by an unnamed dark shale member of the Pierre Shale. The Red Bird dips 45°–60° NW. off the Old Woman anticline.

Pierre Shale:
Red Bird Silty Member:

		Feet
15.	Shale; weathers light gray; contains small limestone concretions at top and larger very closely spaced limestone concretions at base that form a conspicuous yellowish-brown ridge	4
14.	Shale; weathers light gray	47
13.	Shale; weathers medium gray; contains at base and top conspicuous beds of limestone concretions that weather gray to yellowish brown	9
12.	Shale; weathers medium to light gray; contains very few limestone concretions	47
11.	Shale; contains closely spaced limestone concretions at base and top	3
10.	Shale; weathers light gray; contains inconspicuous light-brown limestone concretions	140
9.	Shale; contains closely spaced limestone concretions that weather orange and brown	1
8.	Shale; weathers light to medium gray; contains inconspicuous limestone concretions	53
7.	Shale; contains very closely spaced limestone concretions that weather yellowish gray and form a ridge	1
6.	Shale; weathers medium gray; contains scattered gray-weathering limestone concretions	86
5.	Shale; weathers light gray; contains highly fossiliferous limestone concretions that weather medium gray to yellowish brown	30
4.	Shale; weathers light gray; contains inconspicuous beds of limestone concretions that weather yellowish gray to yellowish brown	136
3.	Shale; weathers light gray; beds of brown-weathering limestone concretions at base and top, and 56 and 82 ft below top, form ridges	121
2.	Shale; lower 2 ft and upper 4.5 ft weather light gray, remainder weathers brown	21
1.	Shale; weathers medium gray; contains a conspicuous bed of brown-weathering limestone concretions at top and a few concretions lower in the unit	26
	Total thickness Red Bird Member	725

Texas Eastern Transmission 1 Federal oil and gas test well located in the center SW¼NW¼ sec. 15, T. 38 N., R. 62 W., Niobrara County, Wyo. (figs. 8.1, 8.2) started in essentially horizontal rocks of the Fox Hills Sandstone and reached the top of the Red Bird Silty Member of the Pierre Shale at a depth of about 1,790 feet and the base of the unit at about 2,390 feet. A thickness of 600 feet is assigned to the unit in the subsurface.

The Red Bird Member is characterized on the electric log by a sharp but variable increase in the resistivity

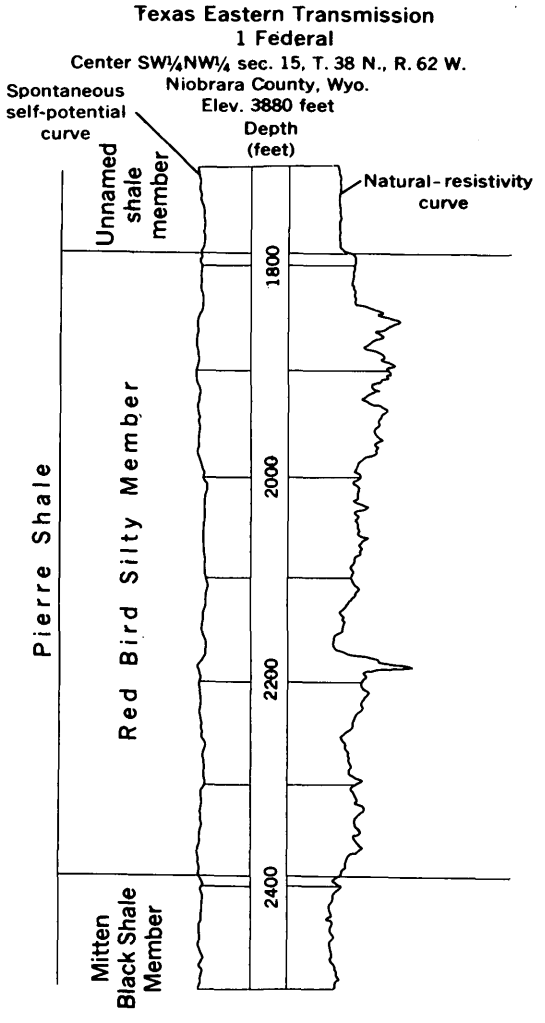

FIGURE 8.2.—Electric log of the Red Bird Silty Member, Pierre Shale, from well near type locality, Niobrara County, Wyo.

curve which contrasts markedly with the uniformly low resistivity curves for the overlying and underlying shale units (fig. 8.2). The spontaneous self-potential curve shows noticeable but less well defined changes. The unit can be recognized easily on electric logs throughout the Powder River basin, eastern Montana, and part of North Dakota, but it is difficult to trace the unit in the area to the east.

REFERENCES

Cobban, W. A., 1951, New species of *Baculites* from the Upper Cretaceous of Montana and South Dakota: Jour. Paleontology, v. 25, no. 6, p. 817–821.

——— 1952, Cretaceous rocks on the north flank of the Black Hills uplift, *in* Billings Geol. Soc. Guidebook 3d Ann. Field Conf., Black Hills-Williston basin, 1952: p. 86–88.

——— 1958a, Two new species of *Baculites* from the western interior region: Jour. Paleontology, v. 32, no. 4, p. 660–665.

——— 1958b, Late Cretaceous fossil zones of the Powder River basin, Wyoming and Montana, *in* Wyoming Geol. Assoc. Guidebook 13th Ann. Field Conf., Powder River basin, 1958: p. 114–119.

Gill, J. R., and Cobban, W. A., 1961, Stratigraphy of the lower and middle parts of the Pierre Shale in the northern Great Plains States: Art. 352 *in* U.S. Geol. Survey Prof. Paper 424–D, p. D185–D191.

Robinson, C. S., Mapel, W. J., and Cobban, W. A., 1959, Pierre Shale along western and northern flanks of Black Hills, Wyoming and Montana: Am. Assoc. Petroleum Geologists Bull., v. 43, no. 1, p. 101–123.

Scott, G. R., and Cobban, W. A., 1959, So-called Hygiene Group of northeastern Colorado, *in* Rocky Mtn. Assoc. Geologists Guidebook 11th Ann. Field Conf., Washakie, Sand Wash, and Piceance Basins, 1959: p. 124–131.

Tourtelot, H. A., Schultz, L. G., and Gill, J. R., 1960, Stratigraphic variations in mineralogy and chemical composition of the Pierre shale in South Dakota and adjacent parts of North Dakota, Nebraska, Wyoming, and Montana: Art. 205 *in* U.S. Geol. Survey Prof. Paper 400–B, p. B447–B452.

9. NOTE ON POST-RUSTLER RED BEDS OF PERMIAN AGE OF SOUTHEAST NEW MEXICO AND WEST TEXAS

By JAMES B. COOPER, Albuquerque, N. Mex.

Work done in cooperation with U.S. Atomic Energy Commission

Red beds in southeast New Mexico and west Texas generally range in thickness from 200 to 500 feet and directly overlie the Rustler Formation of Permian age.

The age of the red beds has been in question since about 1935. Red beds directly overlying the Rustler Formation in the subsurface of Loving County, Tex., were described by Lang (1935, p. 264) and were named the Pierce Canyon Redbeds, of Permian age. Later Lang (1937, p. 876) placed them in the Triassic System. Adams (1935, p. 1021) also considered the red

beds directly overlying the Rustler farther east in Texas to be of Permian age, but Page and Adams (1938, p. 1709) redefined the Triassic-Permian boundary and placed it at the top of the red-bed unit which they named Dewey Lake Redbeds. A description of the Dewey Lake Redbeds, from a subsurface section in Glasscock County, Tex., is contained in Page and Adams (1940, p. 63).

The writer became aware of the disputed age of the red-bed unit during the preparation of subsurface sections relative to ground-water investigations at the Project Gnome site in Eddy County, N. Mex., on behalf of the U.S. Atomic Energy Commission. Cuttings from test wells were examined to determine if the red-bed unit correlated with the "Pierce Canyon" of Triassic age or with the Dewey Lake of Permian age.

Figure 9.1 shows the relations of the red beds directly above the Rustler Formation in Eddy County, N. Mex., to those in Loving County, Tex., and eastward into Glasscock County, Tex., and to the overlying and underlying rocks. Data used were obtained by examination of cuttings from each well shown on the cross section. Well 7 is the type section of the "Pierce Canyon Redbeds" and well 11 is the type section of the Dewey Lake Redbeds.

The red beds are composed of pale-reddish-brown fine sandy siltstone and a few thin beds of reddish-orange fine sandstone. The composition is remarkably uniform in texture and color. The beds generally are dotted with small round to subround green to gray reduction spots. Gypsum is the common cementing agent; light-colored mica is a common accessory mineral.

The basal contact of the red beds with the underlying Rustler is nowhere exposed at the surface, but the contact is clear and distinct in the subsurface. The change from red siltstone to the light-colored anhydrite and gypsum of the Permian evaporite sequence cannot be overlooked in an examination of sample cuttings, or mistaken by drillers. The top of the anhydrite is marked on radioactivity logs by a sharp decrease in natural radioactivity.

The contact of the red beds with overlying formations of Triassic or younger age is difficult to determine. It

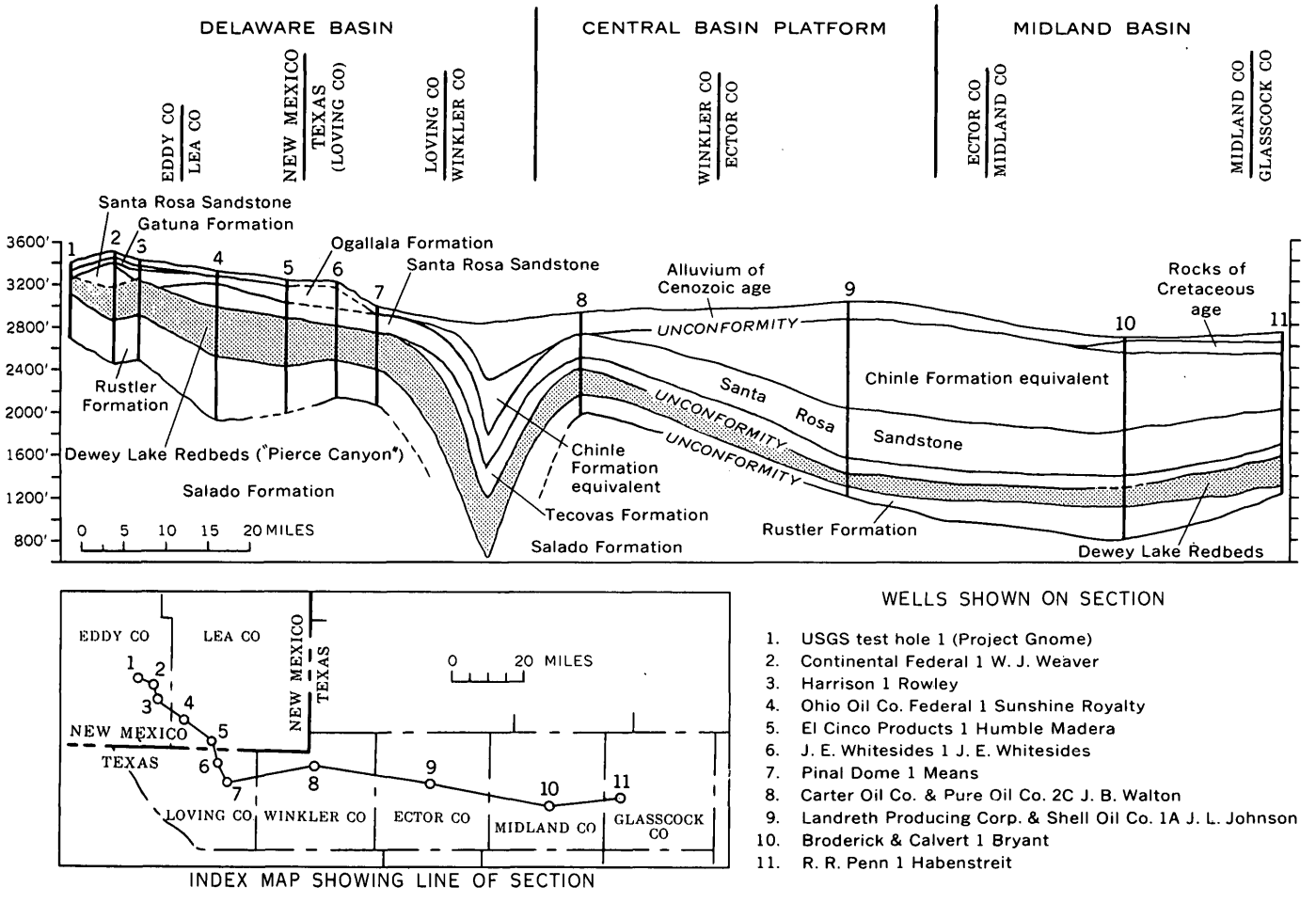

FIGURE 9.1.—Geologic section showing relation of Dewey Lake Redbeds to "Pierce Canyon Redbeds," southeast New Mexico and west Texas.

is not usually recognized by drillers. The contact is not always apparent from an examination of sample cuttings, although it is generally recognizable if the samples have been properly collected and prepared. As shown on figure 9.1, the red beds are overlain by the Tecovas Formation as far west as eastern Loving County, Tex.; northwest of these the red beds are overlain by the Santa Rosa Sandstone of Triassic age and the Ogallala Formation (Pliocene).

The change from rocks of known Triassic age to red beds of Permian or Triassic age is generally marked by a change from a dark purplish color to a dull reddish brown. Rocks of Triassic age generally contain fine angular sand grains and much dark mica, which are uncommon in the red beds. Reduction spots are useful, in a general way, as a stratigraphic marker, although they are not limited to the red beds but are found also in the overlying beds of Triassic age. However, the reduction spots are more abundant in the red beds, and when the spots are present in quantity the observer can search more closely for other diagnostic features of the red beds.

Garza and Wesselman (1959, p. 18) report that in Winkler County, Tex., the top of the red beds generally is recognizable on gamma-ray and electric logs. The structural trough in Winkler County, shown on the cross section, was outlined by them from electric-log data. This trough was formed by subsidence during removal by ground water of soluble salts in the underlying Permian rocks. The east edge of the trough approximately overlies the buried Capitan reef, and the axis of the trough trends generally south, extending from Lea County, N. Mex., through the western part of Winkler County and southward into Ward County.

The purpose of this paper is to point out that the red beds overlying the Rustler Formation in southeast New Mexico and the Dewey Lake Redbeds overlying the Rustler in west Texas appear to be a single lithologic and stratigraphic unit, and that, to the writer, the lithology, color, and apparently conformable relation with the Rustler Formation suggest that the red beds are of Permian age. In view of these relationships, only one name should be used for this unit. The name Dewey Lake Redbeds is well established in the literature and is used by industry for this unit in New Mexico as well as Texas, and no question has been raised as to its validity or age designation. Also, the age designations of Permian, Triassic, and Permian or Triassic given the red beds called "Pierce Canyon" in geologic literature have been confusing. Accordingly the name Dewey Lake Redbeds is used herein for the post-Rustler red-bed-unit.

REFERENCES

Adams, J. E., 1935, Upper Permian stratigraphy of West Texas Permian Basin: Am. Assoc. Petroleum Geologists Bull., v. 19, no. 7, p. 1010–1022, 2 figs.

Garza, S., and Wesselman, J. B., 1959, Geology and groundwater resources of Winkler County, Texas: Texas Board of Water Engineers Bull. 5916, 200 p., 8 pls., 15 figs.

Lang, W. B., 1935, Upper Permian formations of Delaware basin of Texas and New Mexico: Am. Assoc. Petroleum Geologists Bull., v. 19, no. 2, p. 262–270, 7 figs.

———1937, The Permian formations of the Pecos Valley of New Mexico and Texas: Am. Assoc. Petroleum Geologists Bull., v. 21, no. 7, p. 833–898, 29 figs.

Page, L. R., and Adams, J. E., 1938, Stratigraphy, Eastern Midland Basin, Texas [abs.]: Am. Assoc. Petroleum Geologists Bull., v. 22, no. 12, p. 1709.

———1940, Stratigraphy, Eastern Midland Basin, Texas: Am. Assoc. Petroleum Geologists Bull., v. 24, no. 1, p. 52–64, 2 figs.

10. VOLCANIC ROCKS OF OLIGOCENE AGE IN THE SOUTHERN PART OF THE MADISON RANGE, MONTANA AND IDAHO

By Warren Hamilton and Estella B. Leopold, Denver, Colo.

The south end of the Madison Range is composed of Oligocene tuffs and flows that overlie rocks ranging from middle (?) Precambrian to Early Cretaceous in age and that are overlapped by Pliocene(?) and Pleistocene rhyolite tuffs of the surrounding Yellowstone-Snake River volcanic province (fig. 10.1). This article is based upon reconnaissance made as part of the geologic study of the region of the Hebgen Lake earthquake of 1959. A summary of the volcanic geology has been published (Hamilton, 1960).

The Oligocene rocks, exposed in the mountains south of Targhee Pass, make a bedded sequence about 1,000 feet thick of rhyolite welded tuff and mafic alkaline lava. This part of the Madison Range is a fault block

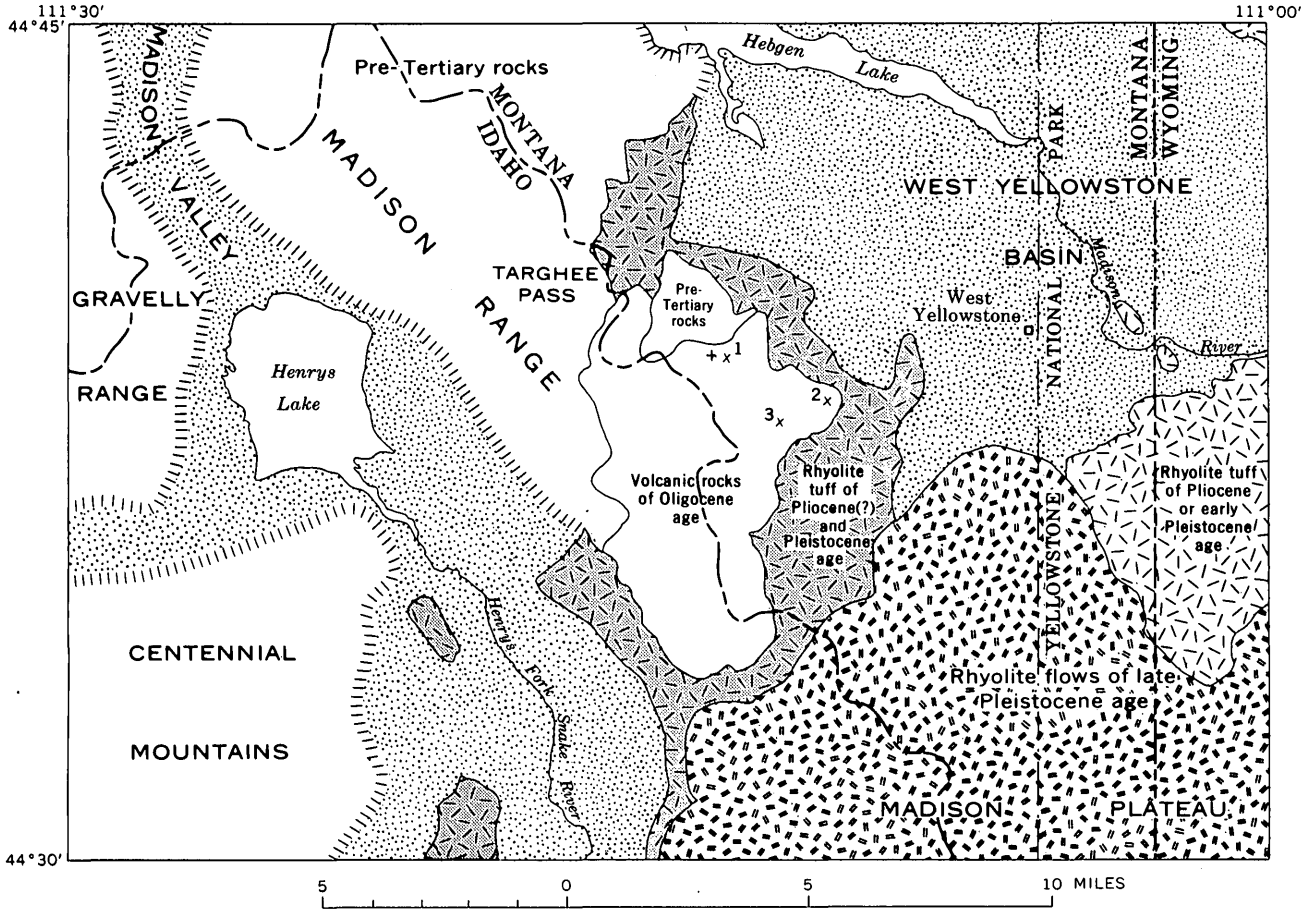

FIGURE 10.1.—Geologic outline map of the south end of the Madison Range and vicinity, Idaho, Montana, and Wyoming, showing distribution of volcanic rocks of Cenozoic age. Oligocene fossil flora were collected at locality marked by +, and chemically analyzed rock samples were collected at localities marked by ×. Volcanic rocks of Cenozoic age are not shown in the Gravelly Range, Centennial Mountains, or Madison Valley. Stippled pattern indicates alluvium.

in which the Oligocene volcanic rocks dip gently east-southeastward, complicated by minor faults and local folds. Exposures are poor owing to thick colluvium and dense forest.

Welded rhyolite tuff forms about half the sequence. The tuff varies from glassy to thoroughly devitrified and contains abundant small phenocrysts of clear sanidine and a few phenocrysts of quartz and oligoclase; no biotite or hornblende was seen. Welding is generally dense and secondary flowage apparent. The specimen analyzed chemically (see table, No. 3) is silicic, moderately aluminous, and has a molecular ratio of K_2O to Na_2O of 3 : 2, a little lower than that of Nockolds' (1954, p. 1012) average calc-alkaline rhyolite. Relative to Nockolds' average, this rhyolite tuff is low in both calcium and magnesium. Relative to the amounts of some minor elements in rhyolite and dacite glass from many areas in the Western States (Coats, 1956), this sample is intermediate in content of fluorine, lanthanum, lead, niobium, and tin; moderately high in zirconium; low in beryllium; and very low in boron. The chlorine content is high.

Flows of mafic alkaline rocks are interbedded with the rhyolite tuff. Near the top of the sequence, a distinctive flow of trachyandesite and another of leucite basanite, each about 150 feet thick, can be traced for several miles. Flows with the appearance of open-textured basalt are present but were not studied petrographically. No intermediate rock of andesitic or dacitic composition was recognized.

629660—62——3

Chemical analyses of volcanic rocks of Oligocene age in the southern part of the Madison Range, Mont.

[Major oxides determined by rapid colorimetric methods by Paul Elmore, Ivan Barlow, Samuel Botts, and Gillison Chloe, Washington, D.C., 1961. Fluorine and chlorine determined by Vertie C. Smith, Denver, Colo., 1961. Other minor elements determined by semiquantitative spectrographic methods by Paul R. Barnett, Denver, Colo., 1961; values reported as midpoints of logarithmic-third divisions. All determinations are given in weight percent]

MAJOR OXIDES

	1	2	3
SiO_2	48. 6	52. 6	75. 6
Al_2O_3	10. 2	13. 9	12. 6
Fe_2O_3	3. 4	6. 6	1. 0
FeO	5. 4	2. 0	. 76
MgO	12. 4	5. 8	. 07
CaO	7. 8	7. 9	. 59
Na_2O	2. 6	2. 3	3. 6
K_2O	2. 0	4. 4	5. 1
H_2O	5. 9	2. 7	. 36
TiO_2	. 70	. 76	. 12
P_2O_5	. 76	. 62	. 02
MnO	. 16	. 14	. 04
Total	99. 9	99. 7	99. 9

MINOR ELEMENTS

	1	2	3
B	0. 003	<0. 001	<0. 001
Ba	. 15	. 15	. 07
Be	. 00015	. 00015	. 0003
Ce	<. 01	<. 01	. 015
Cl	. 02	. 01	. 13
Co	. 003	. 003	<. 0002
Cr	. 07	. 03	. 00015
Cu	. 007	. 015	. 0007
F	. 05	. 10	. 08
Ga	. 0007	. 0007	. 0015
La	<. 002	<. 002	. 007
Mo	<. 0002	<. 0002	. 0003

	1	2	3
Nb	<0. 0005	<0. 0005	0. 003
Nd	<. 005	<. 005	. 007
Ni	. 015	. 003	<. 0002
Pb	. 0007	. 0007	. 0015
Sc	. 003	. 003	<. 0005
Sn	<. 0002	<. 0002	. 0007
Sr	. 15	. 15	. 003
V	. 015	. 03	<. 0005
Y	. 0015	. 0015	. 007
Yb	. 00015	. 00015	. 0007
Zr	. 007	. 007	. 03

1. Leucite basanite. Euhedral phenocrysts of leucite, augite, and subordinate olivine comprise about half the rock, and are set in glass that is dark gray in hand specimen and pale green in thin section. Leucite occurs as 1-mm trapezohedra. Stubby prisms of augite ($+2V \approx 65°$) as long as 5 mm are greenish black in hand specimen and light green in thin section. Colorless olivine has $2V = 90°$. No phenocrysts are altered or embayed. Magnetite is sparse. The glass is clear and nondevitrified, except for small brown radially structured amygdules of an unidentified low-birefringent material with or without isotropic cores. Collected by forest road on west slope of hill 7890, SW¼ sec. 3, T. 14 S., R. 4 E. Field No. YS–17; lab. Nos. 158053 and H3308.
2. Iddingsite-augite trachyandesite. Grayish-red holocrystalline groundmass, consisting of andesine (An_{40}) laths, granules of alkali feldspar, augite, iddingsite, and magnetite, and interstitial clay(?), is studded with euhedral prisms, 2–7 mm long, of greenish-black augite. There are fewer phenocrysts of normally zoned labradorite, and abundant pseudomorphs of red iddingsite after small phenocrysts and granules of olivine. Collected from bluffs above forest road, SE¼ sec. 1, T. 14 S., R. 4 E. Field No. YS–12; lab. Nos. 158051 and H3306.
3. Rhyolite welded tuff (dark-gray pitchstone in hand specimen). Abundant small phenocrysts of clear sanidine, and subordinate ones of oligoclase and high quartz, lie in brown glass formed of mashed shards that show conspicuous secondary flowage. The glass contains microlite needles of pyroxene(?) and rare granules of magnetite. The glass shows no devitrification except for sparse incipient spherulites. By forest road at altitude of 7,000 feet, SE¼ sec. 2, T. 14 S., R. 4 E. Field No. YS–14; lab. Nos. 158052 and H3307.

The trachyandesite has a distinctive grayish-red holocrystalline groundmass of andesine and alkali feldspar, with subordinate augite and iddingsite, and is conspicuously studded with phenocrysts of greenish-black augite. Iddings (1895) coined the name "shoshonite" for similar rocks in the Oligocene volcanic sequence of the Absaroka Range. There is no disseminated hematite; the red color is due to iddingsite, as is shown in the analysis (table, No. 2) by a high Fe_2O_3:FeO ratio.

The leucite basanite is a dark-gray rock studded densely with large phenocrysts of augite and olivine and smaller ones of leucite, set in a matrix of dark glass. The glass weathers to a brownish-yellow surface, against which the phenocrysts are conspicuous, but in fresh rock the glass is not devitrified. The phenocrysts are fresh, sharply euhedral, and show no embayment, corrosion, or reaction rims. This rock is identified as basanite, although no plagioclase is present, because of its chemical composition (table, No. 1); calculations suggest that plagioclase would have formed had the glass crystallized. Relative to most leucite-bearing rocks, however, this specimen is low in aluminum and potassium. It is chemically similar to some of the lavas of Vesuvius.

Like many mafic-alkaline rocks, the trachyandesite and the basanite have relatively large amounts of barium and strontium. They have a rather high fluorine content, but the amounts of other minor elements are comparable to those in most basaltic rocks.

Soft tuffaceous siltstone and a little gray to buff sandstone and mudstone are interbedded with rhyolite tuff in the lower part of the sequence near its north boundary. The sediments have an aggregate thickness of about 200 feet. Tuffaceous siltstone collected from a cut along a logging road 6 miles west of West Yellowstone, Mont. (fig. 10.1), in the SE¼ sec. 34, T. 13 S., R. 4 E., at USGS Paleobotany Locality D–1430, yielded pollen as listed below according to genus and USGS code species:

Gymnospermae
- Podocarpaceae
  - cf. *Podocarpus;* V2S/sm–8, V2L/sm–12 (podocarpus)
- Pinaceae
  - *Abies* cf. *A. lasiocarpa* Nuttall; V2L/p–1 (fir)
  - cf. *A. concolor* (Gordon) Coopes; V2S/sm–4
  - *Picea,* cf. *P. engelmanni* Engelmann; V2S/sm–5 (Engelmann? spruce)

Pinus V2S/sm–10 (pine)
Tsuga cf. *T. mertensiana* (Bongard) Sargent; Tsng–1 (hemlock)
Taxodiaceae
cf. *Sequoia affinis* Lesquereaux; Tax–p–1 (sequoia?)
Gnetaceae
Ephedra cf. *E. nevadensis* Watson; Gn–7 (ephedra)
Angiospermae
Gramineae, undetermined (grass)
Salicaceae
cf. *Salix;* C3–rt–13 (willow)
Juglandaceae
Carya; P3–sm–40, P3–sm–14a (hickory)
Pterocarya; P5–sm–5, P6–sm–2 (lingnut)
Betulaceae
Betula; P3-sm-12 (birch)
Alnus; P5-sm-1, P4-sm-3 (alder)
cf. *Ostrya;* P3-sm-43 (hornbeam)
Ulmaceae
Ulmus or *Zelkova;* P4-foss-1, P5-foss-1 (elm)
Aquifoliaceae
Ilex; C3P3-p-4 (holly)
Rosaceae; C3-st-2
Family and generic affinities not certain:
cf. *Eucommia;* C3-sm-18
cf. *Platanus;* C3-r-21 (sycamore?)
cf. *Liquidambar;* P3-sm-42
cf. *Tilia;* BCP3-r-7 (linden?)
Stephanoporopollenites; P5-sm-4 (a pollen-form genus)

Four of the certainly identified genera (*Carya*, *Pterocarya*, *Ulmus* or *Zelkova*, and *Ilex*) do not now live in the region. The pollen species of *Salix*(?), *Platanus*(?), *Tilia* (?), and *Stephanoporopollenites* have been found in the Western States only in sediments of Oligocene age, including the Florissant Lake Beds of Colorado and the White River Group of Wyoming. Most of the other plants are known from strata of both Oligocene and Miocene ages in the region, although several have not been found previously in the region in rocks of either age. An Oligocene age is probable, and a moist-temperate climate is indicated.

Lapping onto the Oligocene and pre-Tertiary rocks of the southern part of the Madison Range are rhyolite tuffs of the Snake River-Yellowstone volcanic province (fig. 10.1) of Pliocene and Quaternary volcanism. The young rhyolite is generally on low ground about the base of the mountains—porous Pleistocene rhyolite laps across the Madison Range frontal fault from the basin of Henrys Fork of the Snake River—although Pliocene(?) rhyolite has been considerably uplifted north of Targhee Pass. Constructional surfaces are preserved on large areas of these young rhyolites, whereas they are lacking on the Oligocene rocks. Alkaline mafic rocks are limited to the Oligocene sequence, but as some of the rhyolite of that sequence is similar to welded tuff of the Yellowstone volcanic province the two assemblages may have been confused in part.

REFERENCES

Coats, R. R., 1956, Relationship of uranium and other trace elements to post-Cretaceous vulcanism: U.S. Geol. Survey TEI-159, 66 p., issued by U.S. Atomic Energy Comm. Tech. Inf. Service, Oak Ridge, Tenn.

Hamilton, Warren, 1960, Late Cenozoic tectonics and volcanism of the Yellowstone region, Wyoming, Montana, and Idaho, *in* Billings Geol. Soc. Guidebook 11th Ann. Field Conf., West Yellowstone-earthquake area, 1960: p. 92–105.

Iddings, J. P., 1895, Absarokite-shoshonite-banakite series: Jour. Geology, v. 3, p. 935–959.

Nockolds, S. R., 1954, Average chemical compositions of some igneous rocks: Geol. Soc. America Bull., v. 65, p. 1007–1032.

11. RADIOCARBON DATES RELATING TO A WIDESPREAD VOLCANIC ASH DEPOSIT, EASTERN ALASKA

By Arthur T. Fernald, Washington, D.C.

A conspicuous blanket of volcanic ash, first described by Schwatka (1885, p. 196) and Dawson (1889, p. 43b–46b), covers a wide area in eastern Alaska and southern Yukon Territory. It generally occurs at or near the surface of the ground, but in certain localities it has been buried by several feet of loess and organic material. The distribution and thickness of the ash have been mapped in detail by Bostock (1952, fig. 1).

Capps (1916, p. 69–75, 81–83) estimated the age of the ash to be 1,400 years in the White River valley, where it is overlain by 7 feet of peat. He based this estimate on a calculated accumulation rate of 1 foot of peat in 200 years determined from the ages of trees, as shown by their annual rings, growing on a constantly thickening moss mat. He had observed that the trees send out successively higher root branches as the permafrost table, which is related to the thickness of moss, rises.

The 1,400-year age is remarkably close to radiocarbon-dated peat samples that indicate the ash fell between

1,750 and 1,520 B.P. (Before Present). The samples were collected from layered peat that overlies and underlies the ash in an exposure in the upper Tanana River valley. A pit dug in an interdune hollow within a stabilized dune field exposes, from top to bottom, (a) 16 inches of peat with admixtures of silt, (b) 6 inches of white ash, (c) 2 inches of peat, and (d) gray-brown dune sand. The sample (I–276) [1] from the bottom 2 inches of the upper peat bed is dated at 1,520±100 B.P. The sample (I–275) [1] from the lower bed has a date of 1,750±110 B.P.

Another radiocarbon-dated peat sample, collected from within the flood-plain deposits of the upper Tanana River, gives a maximum age of 2,000±250 years B.P. for the ash fall. The cut bank exposes, from top to bottom, (a) 12 inches of layered peat, (b) 42 inches of bedded silt and fine sand with organic debris, (c) 30 inches of white ash with thin beds of gray silt, and (d) 6 inches of layered peat. The sample (W–978) [2] was collected from the middle part of the lower peat bed.

The age of the ash provides an important reference point in the interpretation of the surficial geology of the upper Tanana River valley, particularly the flood-plain deposits. The ash is not present on or within the deposits of the slip-off slopes of the Tanana River, but it is present on all low terraces. It has been reworked into the deposits of parts of the flood plain that are intermediate between the slip-off slopes and the low terraces, as in the cut bank described above.

REFERENCES

Bostock, H. S., 1952, Geology of northwest Shakwak valley, Yukon Territory: Canada Geol. Survey Mem. 267, 54 p.

Capps, S. R., 1916, The Chisana-White River District, Alaska: U.S. Geol. Survey Bull. 630, 130 p.

Dawson, G. M., 1889, Report on an exploration in the Yukon District, N. W. T., and adjacent northern portion of British Columbia: Canada Geol. Survey Ann. Rept., v. 3, pt. 1, rept. B (1887–88), 277 p.

Schwatka, Frederick, 1885, Along Alaska's great river: New York, Cassell & Co., 360 p.

[1] Dated by Isotopes, Inc., Westwood, N.J.
[2] Dated by U.S. Geological Survey Radiocarbon Laboratory.

SEDIMENTATION AND SEDIMENTARY PETROLOGY

12. ORIGIN OF SPHERULITIC PHOSPHATE NODULES IN BASAL COLORADO SHALE, BEARPAW MOUNTAINS, MONTANA

By W. T. Pecora, B. C. Hearn, Jr., and Charles Milton, Washington, D.C.

STRATIGRAPHY

Spherulitic phosphate nodules occur in the Fall River Sandstone Member at the base of the marine Colorado Shale in the Bearpaw Mountains, north-central Montana. Virtually only the basal 30 feet of black fissile shale contains these nodules, and none have been found elsewhere in the stratigraphic section in this region. Interbedded with the black shale are thin beds of very fine grained thinly laminated sandstone that contain surficial casts of worm trails and similar "spaghetti" markings. In the upper, more sandy part of the member, which is some 300 feet thick, molds and prints of mollusks collected by W. T. Pecora and Joe H. Kerr in 1952 were identified by W.A. Cobban, of the U.S. Geological Survey, as *Inoceramus bellevuensis* Reeside, *Ostrea larimerensis* Reeside, and *Ostrea noctuensis* Reeside, which are indicative of Albian age.

In an easterly distance of 30 miles along the Bearpaw Mountains structural arch, spherulitic nodules have been found wherever the contact between the Kootenai Formation and overlying Colorado Shale is well exposed. In the eastern part of the mountains, near Cleveland, several domes in an area of about 60 square miles afford excellent exposures, whereas in the western part, metamorphism has somewhat inhibited liberation of the nodules from enclosing rock.

Black shale enclosing the phosphatic nodules is nonfossiliferous and free of other nodules or concretions, such as those of carbonate, pyrite, or barite that occur in shale at other stratigraphic horizons in the region. The shale is laminated and composed of the typical ultra fine grained platy minerals (clay and mica) and angular to subrounded grains of quartz. Chemical analyses of unweathered basal shale that was free of

phosphatic nodules and sandstone (tables 12.1 and 12.2) show very little phosphorus; the samples were collected along a trench 30 feet long. A pyrite content of 0.04 percent is indicated by assigning all the S in the analysis to FeS_2. The amounts of organic matter (1.91 percent) and sulfur (0.02 percent) are substantially less than those reported by Rubey (1930, p. 8) for black shales higher in the Colorado Shale equivalents in the Black Hills region. Poverty in CO_2 characterizes all these black shales.

TABLE 12.1.—*Chemical analyses of basal 30 feet of Colorado Shale and composite samples of fragments of phosphatic silt rind and internal spherulites of phosphatic nodules, Suction Creek, Bearpaw Mountains, Mont.*

[Analysts, with exceptions noted in footnotes: Black shale, P. L. D. Elmore and K. E. White; black rind and spherulites, L. M. Kehl]

	Black shale	*Black rind*	*Spherulites*
SiO_2	61. 4	19. 46	4. 46
Al_2O_3	19. 1	5. 13	1. 10
Fe_2O_3	2. 5	. 99	7. 02
FeO	3. 1	. 83	. 47
MgO	1. 4	. 50	. 30
CaO	. 54	37. 81	46. 22
Na_2O	. 53	. 35	. 16
K_2O	2. 4	. 67	. 04
H_2O^-	6. 2	. 46	. 35
H_2O^+		1. 78	1. 65
TiO_2	1. 1	. 41	. 07
P_2O_5	. 16	27. 71	33. 92
F	--------	[1] [2] 1. 93	[1] [3] 2. 25
S	[4] <. 02	. 03	. 04
MnO	--------	. 09	. 08
BaO	. 12	. 08	. 00
C	[4] 1. 91	[1] . 80	[1] . 49
CO_2	. 05	[1] 1. 22	[1] . 90
	100. 53	100. 25	99. 52
Less O for F	--------	. 81	. 95
		99. 44	98. 57

[1] Analyzed by E. J. Tomasi.
[2] Replicate, 1.89.
[3] Replicate, 2.15.
[4] Analyzed by J. J. Fahey.

TABLE 12.2.—*Semiquantitative spectrographic analysis of 10 phosphate nodules and enclosing black shale, Suction Creek, Bearpaw Mountains, Mont.*

[Analyst: Harry Bastron]

	10 nodules	*Shale*
0.X	Mn, Ti	Ti
.0X	Ba, Sr, Zr, Y, La	Mn, V, Sr, Zr, La
.00X	Cu, Zn, Co, Ni, Cr, V	Cu, Zn, Co, Ni, Ga
.000X	Ag, Sc	Sc

NOTE.—Equivalent uranium (by B. A. McCall) 0.001 in nodules, 0.002 in shale.

SPHERULITIC PHOSPHATE NODULES

The phosphatic nodules are typically "bumpy" and "warty" (fig. 12.1) and have a maximum diameter of 4 inches. Most of them range from ½ to 2 inches in size and are globular to spheric in form. The nodules are conspicuously strewn on weathered surfaces or nested in soft shale, but trenching below grass-roots level reveals their isolated, random distribution in the shale, without preferential orientation. Nodules are easily removed intact from their original sites in unweathered shale. Laminae in the shale abut sharply against each nodule at its equatorial region and arch over and under at the polar regions. Laminae or bedded structures are absent in the nodules themselves. The spherulitic character of the nodules is observed only in broken specimens. Even in their densest concentration the nodules make up less than 2 percent of the black shale.

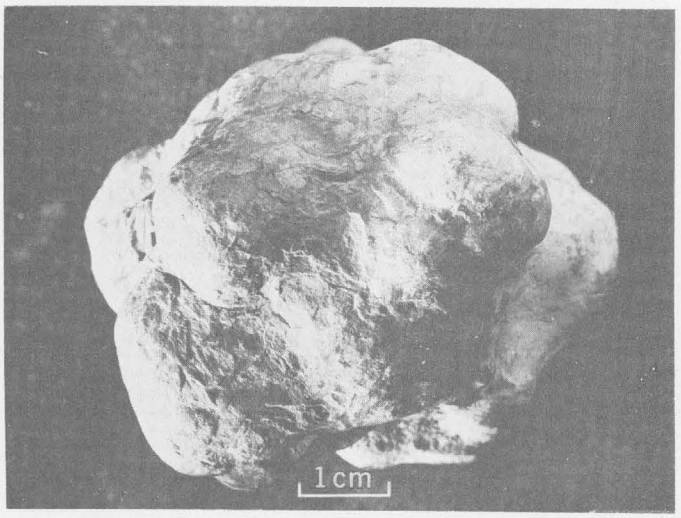

FIGURE 12.1.—Globular phosphate nodule from basal Colorado shale, Suction Creek, Bearpaw Mountains, Mont.

INTERNAL STRUCTURE

Sawed or broken nodules show two principal lithologic features—a homogeneous, black, phosphatic silt that forms a peripheral zone or "rind," and one or more internal phosphatic spherulites (fig. 12.2). Some nodules, particularly those of simple, spheric form and of small size, contain but one spherulite; most, however, contain several that are imbedded in phosphatic silt. The warty and bumpy nodules contain many spherulites, with each protuberance indicative of a spherulite. As many as 20 to 30 have been counted in single specimens. No direct relation exists between size of nodule and proportion of phosphatic silt to spherulite. Every one of hundreds of nodules examined shows spherulitic development. In many well-weathered specimens, the black envelope is absent and the surface of the nodules is pitted. In aggregate spherulites, the black matrix is like the rind in appearance and composition. The contact between spherulite and black rind within the nodules (fig. 12.2) is commonly marked by yellow-white veins. The central part of a spherulite either is a void that is lined with a botryoidal crust or it is filled with other minerals.

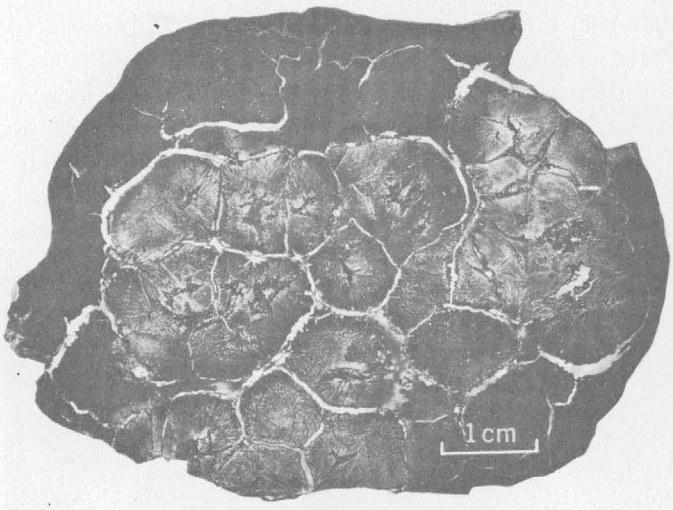

FIGURE 12.2.—Polished slab of a phosphate nodule showing phosphatic rind, spherulites, and veins.

COMPOSITION

A grab sample of 13 nodules, analyzed by H. F. Phillips and P. W. Scott, of the U.S. Geological Survey, contains 33 percent P_2O_5.

The matrix phosphatic silt enveloping the spherulites within each nodule is nonfossiliferous, structureless, and homogeneous, and it is composed of very fine grained angular quartz grains and mica in an opaque matrix. Locally, coarser quartz grains are abundant. A chemical analysis of selected fragments of this silt (table 12.1) reveals less SiO_2 than the shale, but more CaO, P_2O_5, F, and CO_2. Supplementary X-ray examination by J. M. Axelrod and Z. S. Altschuler of the U.S. Geological Survey establishes the presence of carbonate-fluorapatite. The fact that apatite is the only identified phosphate mineral to account for the peculiar chemical composition of the silt suggests that it must exist as a microcrystalline cement in the black silt of the nodules.

The spherulites, on the other hand, are composed of well-crystallized carbonate-fluorapatite in three habits: (1) Prismatic, elongate, and radially developed to form the spherulite itself; (2) veins and patches of microbotryoidal apatite parallel to or traversing the spherulitic fibers; and (3) mammillary, botryoidal crusts that line cavities and cracks in the spherulites. A chemical analysis of selected fragments of spherulites (table 12.1) shows high P_2O_5 and F contents.

Among the veins in the nodules, those that are typically curvilinear septa between the spherulites and black rind are composed of chlorite, apatite, quartz, and pyrite. The apatite normally forms a crust along both borders of these veins. Similar veins occur in, or project from the septa into, both the rind and spherulites. Some are composed only of apatite or of apatite and one or more vein minerals.

Quartz diminishes in amount in phosphatic silt that is but partly spherulitized. Petrographic relations at the termini of spherulitic fibers (fig. 12.3) against the

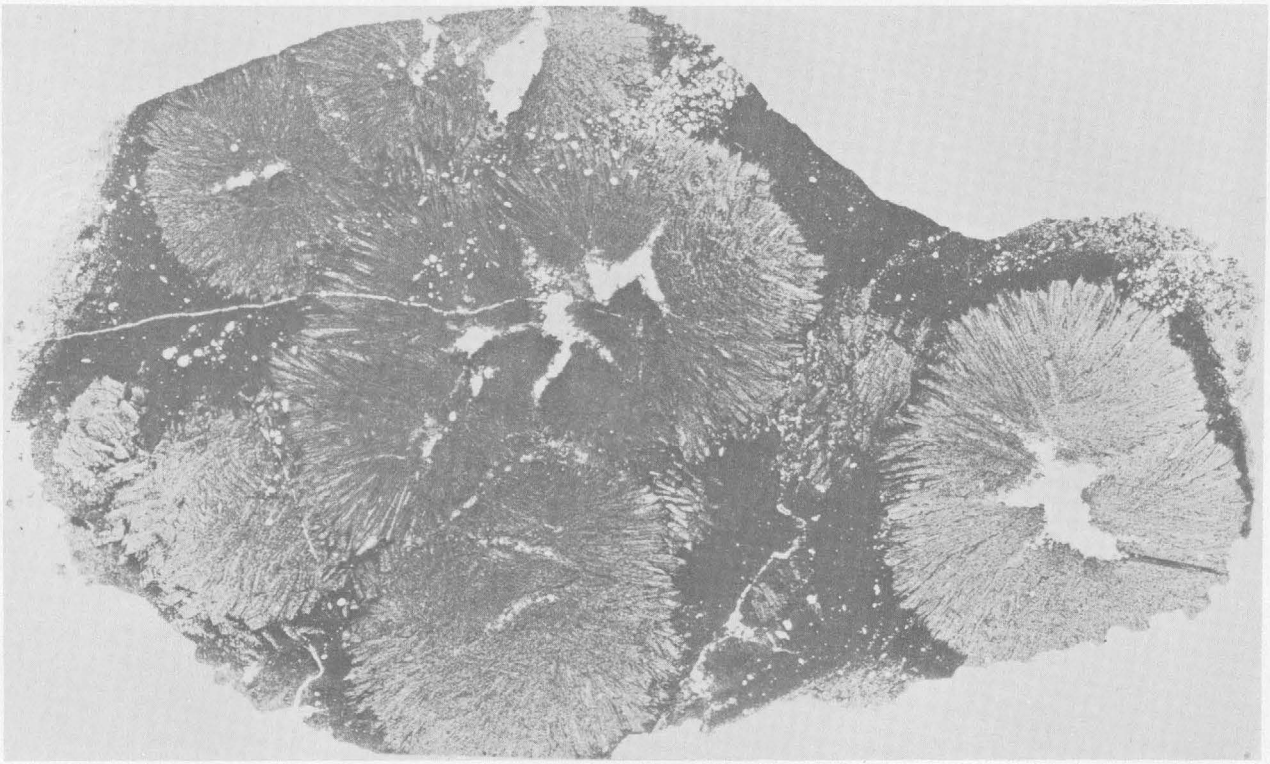

FIGURE 12.3.—Photomicrograph showing spherulitic growth of fibers in phosphatic silt of nodule (3.5 × 2 cm).

black silt in the envelope or interior part of nodules strongly suggest in situ growth of the fiber by replacement or by recrystallization of the homogeneous phosphatic silt.

The cavities in the central part of a spherulite are lined, like the veins, with a thin layer of botryoidal apatite with or without chlorite, pyrite, and quartz. Some cavities are filled or partly filled with pyrite, which alters to limonite. Rarely, barite is the cavity-filling mineral, instead of pyrite. Both pyrite and barite have not been seen in the same cavity.

EFFECT OF METAMORPHISM

Thermal metamorphism of shale to hornfels in some places within the mountains has effected changes in the phosphatic nodules. Secondary quartz-chlorite veins are more abundant. Pyrite and limonite are rarely preserved although vestiges remain in some places. Better crystallization of the apatite characterizes heat-altered nodules, for well-terminated, gemmy crystals of apatite occur in many cavities in association with tablets of chlorite but are unknown in the unmetamorphosed spherulites. The phosphatic siltstone rind and matrix of the spherulites is "blacker" and carbonaceous bands and areas are locally accentuated.

ORIGIN OF SPHERULITIC STRUCTURE

We believe that the nodules were originally homogeneous phosphatic silty concretions in "blue mud" (=black shale). The carbonate-fluorapatite in the matrix later recrystallized to form spherulites resulting in a net loss of volume that permitted veins and cavity-filling mineralization. Quartz and chlorite in veins can well be a product of internal recrystallization, but locally abundant pyrite requires derivation of sulfur from an external source.

Field relations show that the spherulitic structure developed prior to the thermal metamorphism and deformation that accompanied igneous intrusions in middle Tertiary time; but early transformation of originally homogeneous phosphatic silt to spherulites by some process of static metamorphism (diagenesis) is all that can be concluded from our information.

OTHER OCCURRENCES OF PHOSPHATIC SPHERULITES

Phosphatic spherulites are well known in the basal part of the Thermopolis Shale (=basal Colorado Shale) in Park County, Wyo. (Pierce and Andrews, 1940, p. 121) and were described as dahllite by McConnell (1935). M. R. Klepper (written communication, 1955) has provided spherulitic apatite nodules from basal black shale (=Skull Creek(?) of the Colorado sequence) about 50 feet above a basal sandstone member (=Fall River(?)) that overlies the Kootenai Formation in Broadwater County, southwestern Montana. The existence of phosphatic nodules in basal black shale of the Lower Cretaceous sequence over several hundred square miles thus provides a well-defined stratigraphic datum and poses a regional problem in sedimentology.

Spherulitic phosphate nodules in Silurian shale in the Dneister River basin of the Podolia Province, Russia, reported by Schwackhöfer (1871) and O'Reilly (1882) and described as a new mineral "podolite" by Tschirwinski (1907) were shown by Schaller (1912) to be structurally identical with dahllite. A sample (No. 103116) provided to us by the U.S. National Museum is identified as carbonate-fluorapatite (=francolite) and is virtually identical with the Wyoming spherulites. Spherulitic phosphate nodules in Cretaceous and younger formations in the eastern part of the Donetz basin are reported by Orekhov (1958). Spherulitic nodules may be more widespread than heretofore reported in the geological literature.

ORIGIN

The occurrence of spherulitic phosphate nodules poses a dual problem: (1) Origin of the original homogeneous discrete nodules, and (2) development of the spherulitic structure. We believe that abundant information exists in the geologic literature to suggest that these nodules formed as concretions at numerous nucleation loci in unconsolidated mud on the sea floor by precipitation of microcrystalline carbonate-fluorapatite from sea water. We seek some hydrogeochemical process by which this phenomenon can form discrete concretions randomly distributed within "blue mud" over hundreds of square miles, and conclude that geologic relations provide the best clues.

Marine shale of Cretaceous age, stratigraphically higher than the spherulitic phosphate horizon in the Bearpaw Mountains, contains calcareous concretions with varying proportions of Ca, Mg, Fe, and Mn. Many of these concretions, septarian or homogeneous, contain unbroken delicate fossil shells, like *Baculites*, and were probably formed before compaction of the shale was completed (Clifton, 1957). An analogy in authigenic process for origin of the calcareous and phosphatic concretions at different horizons in the Colorado Shale is likely, although carbonate and phosphate concretions are not formed at the same horizon. Mutual exclusion has also been noted by Abele and McGowran (1959, p. 311) for Lower Cambrian phosphate nodules in South Australia.

GEOLOGIC CONSIDERATIONS

Phosphorites are widely distributed in the geologic column. Most of them, however, are phosphatic shales interbedded with sandstone, limestone, chert, or glauconitic greensand and are characterized by phosphatized fossil fragments, oolitic pellets, or smooth pebble-like units with rock, mineral, or fossil nuclei. Fossil fragments commonly are entirely replaced by phosphate or are armored by pelletal colloform apatite.

Phosphatic nodules dredged from the sea floor (Murray and Renard, 1891; Dietz and others, 1942; Emery and others, 1952) at depths up to 11,000 feet are slabby to rounded and composed of rock, mineral, bone, and foram fragments cemented and coated by microcrystalline phosphate. The nodules are most abundant on shelves and banks near continental borders where cold and warm water currents meet. One nodule from the Coronado Bank, provided to us by F. R. Shepard, is composed of a heterogeneous mixture of subangular detrital fragments (quartz, plagioclase, hypersthene, hornblende, tourmaline, sphene, biotite, and porphyritic andesite) in a matrix of dark submicroscopic carbonate fluorapatite containing irregularly distributed thread-like areas of greenish chlorite. Neither spherulitic structure nor carbonate is present in the nodule.

SOURCE OF PHOSPHORUS

Phosphate to form concretions in the Colorado Shale was most likely derived from sea water transgressing a broad shelf area in Early Cretaceous time rather than from alteration of excreta or calculi of marine animals.

Many investigators have recorded a systematic variation of the phosphoric acid content of sea water as a function of temperature, depth, pH, and season (Matthews, 1917; Atkins, 1928). Surface oceanic waters, through the activity of organisms, become impoverished in plant nutrients such as phosphate and nitrate, and deeper waters become enriched by "mineralized" organic matter falling to the sea bottom. Thomsen (1931, 1937) reported about 100 to 200 mg per m^3 P_2O_5 at depths of about 3,000 m in several oceans, and Atkins (1925, 1928) reports an increase from 8 mg per m^3 P_2O_5 at 100 m depth (T=15.1°C) to 88 mg per m^3 P_2O_5 at 3,000 m depth (T=3.1° C) in the Atlantic Ocean between the Canary Islands and Lisboa.

Kazakov (1938, 1950) stated that his experimental studies of the equilibrium system $CaO–P_2O_5–H_2O$ and $CaO–P_2O_5–HF–H_2O–CO_2$ suggested that precipitation of phosphate probably does not occur in the phytoplankton zone on oceanic shelf areas, and that all the phosphate precipitated below that zone would be apatite in association with calcium carbonate. We do not support Kazakov's conclusion, however, that precipitation of calcium carbonate must precede that of apatite in sea water. CO_2 in apatite analyses, normally assigned to $CaCO_3$ as a separate phase mixed with apatite (Kazakov, 1938), is currently interpreted (Altschuler and others, 1952) to be a component of a single structural phase. Bottom muds containing organic matter, apatite, and sulfide would require, with reference to the Eh-pH diagram of Krumbein and Garrels (1952), a hydrogeochemical environment of pH above 7 but less than 7.8, and of Eh in the negative region (Swanson, 1961). Higher pH and positive Eh would favor precipitation of carbonate and sulfate. In the mud-bottom habitat represented by the basal Colorado black shale, any preexisting $CaCO_3$ phase would not be in equilibrium and would be dissolved, replaced, or armored by an apatite aureole, according to our interpretation. As indicated by the Cretaceous system in Montana and Wyoming, and as earlier noted by McKelvey and others (1953) for part of the Phosphoria Formation of Permian age, first carbonate-fluorapatite, and later $CaCO_3$, were precipitated as the transgressive sea ascended the shelf.

CONCLUSIONS

Phosphate nodules in basal marine Colorado Shale in the northern Great Plains of Montana and Wyoming record a special situation of a widespread transgressive shelf sea where bottom muds were accumulating beyond the influence of nearshore turbulent conditions and at a depth greater than the base of the zone of photosynthesis. Environmental hydrochemical conditions of the bottom slimes and water are low pH, reducing conditions, high partial pressure of CO_2, and high concentration of Ca, P, F, and H_2S. Only soft-bodied animals were present. Precipitation of carbonate-fluorapatite occurred first as a concretionary microcrystalline cement in silt prior to final compaction of the bottom mud shale. The phenomenon is most likely a result of saturation in P_2O_5 caused by a rise in pH and temperature to disturb the apatite solution equilibrium in upwelling ocean water. These concretions later recrystallized diagenetically and developed apatite spherulites and secondary veins.

REFERENCES

Abele, C., and McGowran, B., 1959, The geology of the Cambrian south of Adelaide: Royal Soc. South Australia Trans., v. 82, p. 301–320.

Altschuler, Z. S., Cisney, E. A, and Barlow, I. H., 1952, X-ray evidence of the nature of carbonate-apatite [abs.]: Geol. Soc. America Bull., v. 63, p. 1230–1231.

Atkins, W. R. G., 1925, The phosphate content of fresh and salt waters in its relationship to the growth of algal plankton: Marine Biol. Assoc. Jour., [United Kingdom], v. 13, p. 119–150.

——— 1928, Seasonal variations in the phosphate and silicate content of sea water: Marine Biol. Assoc. Jour., v. 15, p. 191–205.

Clifton, H. E., 1957, Carbonate concretions of the Ohio shale: Ohio Jour. Sci., v. 57, p. 114–129.

Dietz, R. S., Emery, K. O., and Shepard, F. P., 1942, Phosphorite deposits on the sea floor off southern California: Geol. Soc. America Bull., v. 53, p. 815–847.

Emery, K. O., Butcher, W. S., Gould, H. R., and Shepard, F. P., 1952, Submarine geology off San Diego, California: Jour. Geology, v. 60, p. 511–549.

Kazakov, A. V., 1938, The phosphorite facies and the genesis of phosphorites, *in* Geological investigations of agricultural ores U.S.S.R.: Sci. Inst. Fertilizers and Insectofungicides Trans. (U.S.S.R.), no. 142, p. 95–113. (Special issue in English published for 17th Internat. Geol. Cong.)

——— 1950, Fluorapatite system equilibria under conditions of formation of sedimentary rocks: Akad. Nauk SSSR Inst. Geol. Nauk Trudy, Vyp. 114, Geol. Ser. no. 40, p. 1–21.

Krumbein, W. C. and Garrels, R. M., 1952, Origin and classification of chemical sediments in terms of pH and oxidation-reduction potentials: Jour. Geology, v. 60, p. 1–33.

Matthews, D. J., 1917, On the amount of phosphoric acid in the sea water off Plymouth Sound: Marine Biol. Assoc. Jour., v. 11, p. 251–257.

McConnell, Duncan, 1935, Spherulitic concretions of dahllite from Ishawooa, Wyoming: Am. Mineralogist, v. 20, p. 693–698.

McKelvey, V. E., Swanson, R. W., and Sheldon, R. P., 1953, The Permian phosphorite deposits of western United States *in* Giulham, P. L. R., ed., Paper XI *in* Origine des Gisements de phosphates de chaux: Internat. Geol. Cong., 19th, Algiers, 1952, Comptes rendus, sec. 11, pt. 11, p. 45–64.

Murray, J., and Renard, A. F., 1891, Report on the scientific results of the exploring voyage of H.M.S. *Challenger*, 1873–76, Deep sea deposits, p. 396–400.

O'Reilly, J. P., 1882, The phosphorite nodules of Podolia: Royal Soc. Dublin Proc., v. 4, p. 215–222.

Orekhov, S., 1958, Mineralogy and structural types of phosphorites of the Rostov region [translation of abstract]: Uchenye Zapiski Rostov—na Donu Gosudarst Univ., v. 53, p. 273–287.

Pierce, W. G., and Andrews, D. A., 1940, Geology and coal resources of the region south of Cody, Park County, Wyoming; U.S. Geol. Survey Bull. 941–B, p. 99–175.

Rubey, W. W., 1930, Lithologic studies of fine-grained Upper Cretaceous sedimentary rocks of the Black Hills region: U.S. Geol. Survey Prof. Paper 165–A, 54 p.

Schaller, W. T., 1912, The probable identity of podolite with dahllite *in* Mineralogic notes, series 2: U.S. Geol. Survey Bull. 509, p. 96–97.

Schwackhöfer, Fr., 1871, Ueber die Phosphorit-Einlagerungen an den Ufern des Dniester in russich und osterreichisch Podolien und in der Bukowina: K. K. Geol. Reichsanstalt Jahrb., v. 21, p. 211–230.

Swanson, V. E., 1961, Geology and geochemistry of uranium in marine black shales, a review: U.S. Geological Survey Prof. Paper 356–C, p. 67–112.

Thomsen, H., 1931, Nitrate and phosphate contents of Mediterranean water: Danish Oceanographic Expedition Rept., 1908–10, v. 3, misc. papers, no. 6, 14 p.

——— 1937, Hydrographical observations made during the Dana Expedition 1928–1930: Dana Repts., no. 12, 46 p.

Tschirwinski, W., 1907, Über Podolite, ein Neues Mineral: Centralbl. Mineralogie, p. 279–283.

13. STREAM DIRECTIONS IN THE LAKOTA FORMATION (CRETACEOUS) IN THE NORTHERN BLACK HILLS, WYOMING AND SOUTH DAKOTA

By William J. Mapel and Charles L. Pillmore, Denver, Colo.

The Lakota Formation of Early Cretaceous age is 100 to 250 feet thick in the northern Black Hills. It consists largely of sandstone, siltstone, and claystone deposited on the flood plains of streams. The formation and its regional stratigraphic relations in the Black Hills have been described by Waagé (1959), Mapel and Gott (1959), and Post and Bell (1961).

Sandstone beds in much of the Lakota Formation are conspicuously crossbedded in sets a few inches to about 3 feet thick. At places the crossbeds dip as steeply as 30°. The crossbedded sandstones are mostly medium to coarse grained and at many places contain lenses of granules and small pebbles.

The dip directions of the crossbeds were determined at 65 localities between Devils Tower and Newcastle on the west side of the Black Hills and at 20 localities near Aladdin at the north end of the Black Hills (fig. 13.1) to establish the direction of flow of streams that deposited the sediments. Dip directions of from 10 to 20 sets of crossbeds were averaged to find the dip direction at each locality. Directions from place to place are greatly diverse, but fairly definite trends become apparent if the dip directions are averaged for localities grouped according to geographic location, stratigraphic position, or both. Four such groupings are shown on figure 13.1 and a statistical analysis of the results is

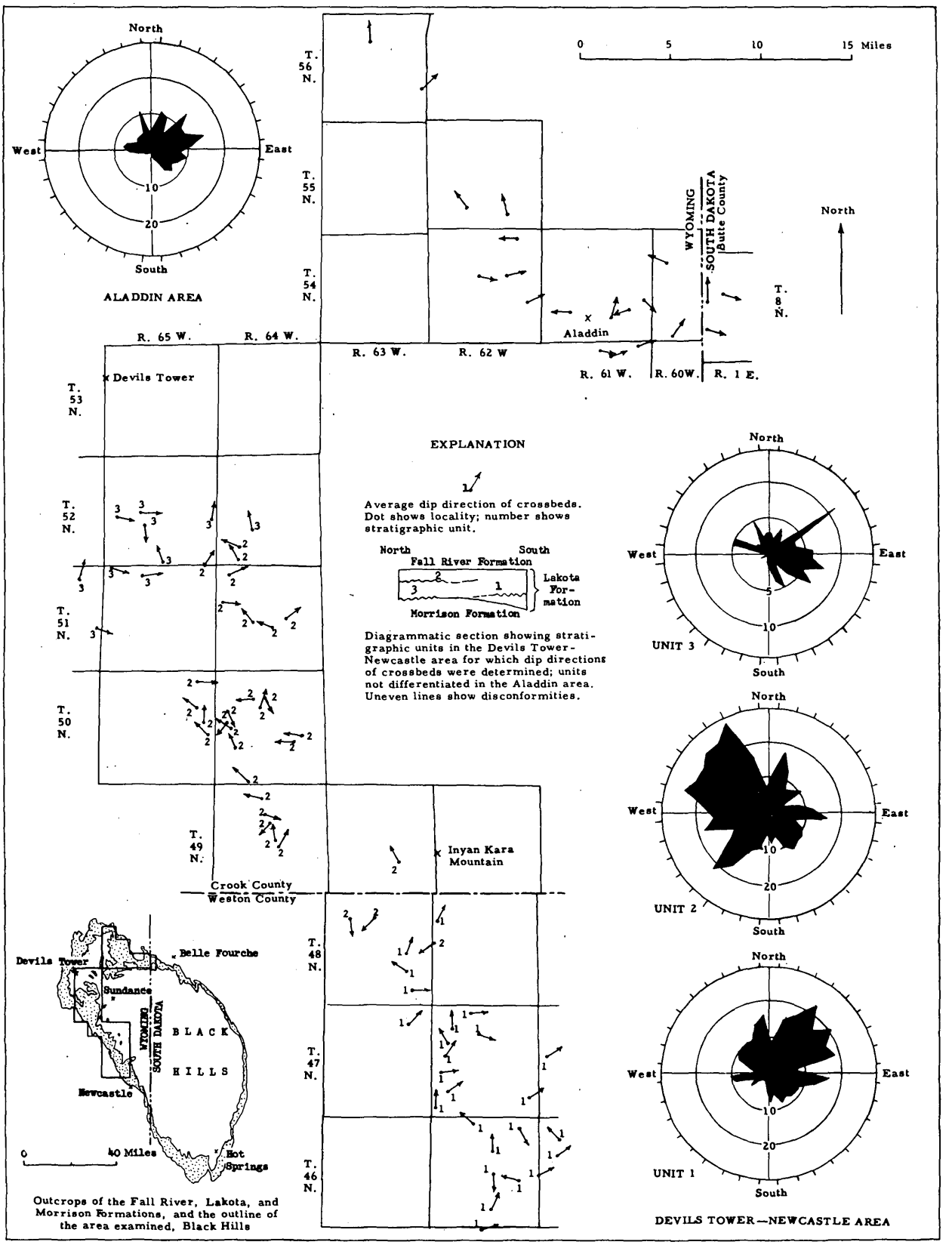

FIGURE 13.1.—Dip directions of crossbeds, northern Black Hills. Map and diagrams summarize dip directions of 1,184 sets of crossbeds at 85 localities.

given in the table below. A resultant dip direction of about N. 60° W. was found in an area south of Devils Tower in and near Tps. 49 to 51 N., Rs. 64 and 65 W. (stratigraphic unit 2). In the other three areas analyzed, resultant dip directions vary from N. 40° E. to N. 75° E. and average about N. 60° E. Trends to the northwest and to the northeast or east also can be read from figure 13.2, where all the measured dip directions are plotted.

Statistical analysis of data

Group	Number of measurements	Resultant dip direction	95-percent confidence interval (degrees)	Standard deviation (degrees)	Consistency ratio[1]
Devils Tower–Newcastle area:					
Unit 1	359	N.40° E.	±9	84	0. 34
Unit 2	492	N.60° W.	±9	100	. 22
Unit 3	112	N.75° E.	±15	82	. 37
Aladdin area	221	N.45° E.	±12	94	. 27

[1] Obtained by dividing the length of the resultant direction vector by the number of measurements.

The data indicate a complicated local pattern of stream flow such as would result from meandering streams that flowed generally northward. Similar conclusions regarding the direction of stream flow have been made for areas in the southern Black Hills by Russell (1928, p. 135), who reports a dominant northwestward dip of crossbeds in the Lakota near Hot Springs, and by Brobst (1956), who reports a northwestward alinement of stream channels south of Newcastle.

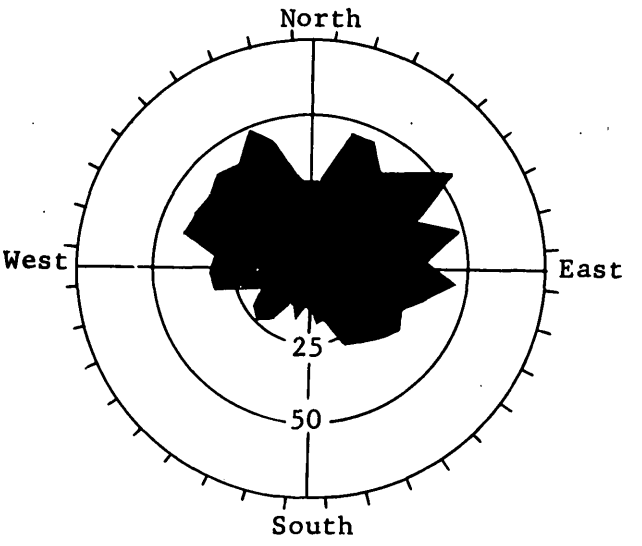

FIGURE 13.2.—Summation of dip directions of all crossbeds measured, northern Black Hills.

REFERENCES

Brobst, D. A., 1956, Channel sandstones, southern Black Hills, *in* Geologic investigations of radioactive deposits—Semiannual progress report, June 1 to Nov. 30, 1956: U.S. Geol. Survey TEI–640, p. 102–108, issued by the U.S. Atomic Energy Comm. Tech. Inf. Service, Oak Ridge, Tenn.

Mapel, W. J., and Gott, G. B., 1959, Diagrammatic restored section of the Inyan Kara group, Morrison formation, and Unkpapa sandstone on the western side of the Black Hills, Wyoming and South Dakota: U.S. Geol. Survey Mineral Inv. Field Studies Map MF–218.

Post, E. V., and Bell, Henry, III, 1961, Chilson member of the Lakota formation in the Black Hills, South Dakota and Wyoming: Art. 349 *in* U.S. Geol. Survey Prof. Paper 424–D, p. D173–D178.

Russell, W. L., 1928, The origin of artesian pressure: Econ. Geology, v. 23, no. 2, p. 132–157.

Waagé, K. M., 1959, Stratigraphy of the Inyan Kara group in the Black Hills: U.S. Geol. Survey Bull. 1083–B, p. 11–90.

14. FORMATION AND DEPOSITION OF CLAY BALLS, RIO PUERCO, NEW MEXICO

By CARL F. NORDIN, JR., and WILLIAM F. CURTIS, Albuquerque, N. Mex.

The environment of the Rio Puerco in New Mexico is ideally suited to the formation of clay balls. The stream is characterized by ephemeral runoff from local storms of short duration and high intensity. Clays derived from weathered shales, primarily the Chinle Formation of Triassic age and the Mancos Shale of Cretaceous age, are readily available on the denuded watershed. Flows carry extremely high concentrations of fine materials in suspension.

Deposits of clay balls were observed at a reach of the Rio Puerco near Bernardo in 1961 (fig. 14.1). During the summer, the sand bed of the channel was impregnated with clay to a depth of about 0.5 foot (fig. 14.2*A*). By early fall, a headcut had moved upstream through

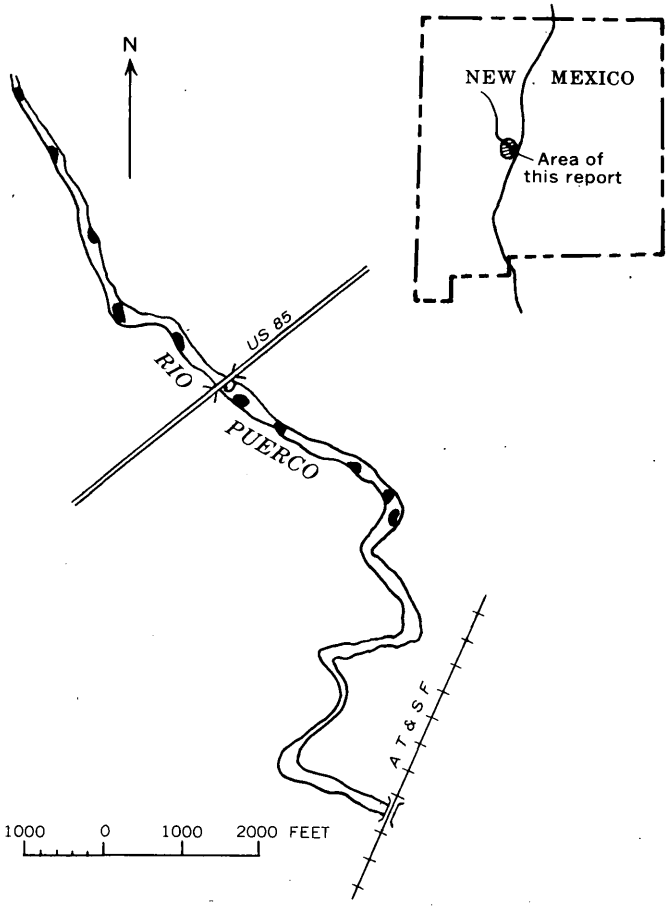

FIGURE 14.1.—Sketch map of study reach, showing deposition pattern of clay balls.

the study reach, cutting a trench about 3 feet deep and 30 feet wide in the channel (fig. 14.2*B*). The cut exposed numerous deposits of clay balls.

The clay balls are of two types—armored and unarmored. Those that formed on and moved over the clay-impregnated bed are not armored (fig. 14.2*C*) and contain negligible amounts of sand and pebbles. Those that formed on and moved over the sand bed are armored with sand and pebbles in a clay matrix (fig. 14.2*D*, *E*). Armor comprises 15 to 75 percent of the weight of the balls. Bell (1940) found a close relation between surface area and weight of armor for mud balls observed in Las Posas Barranca, Ventura County, Calif. A similar relation was found for the armored clay balls of the Rio Puerco, although the weight of the armoring for a given surface area was about 1½ times as great as that found by Bell.

Some of the balls have no perceivable internal structure, some have concentric structure, and some have laminated structure. Some of the clay balls have a composite structure; for example, a structureless core with concentric layers of clay or armor or both (fig. 14.2*E*) or a laminated core (fig. 14.2*F*) surrounded by concentric layers.

Most of the balls show no core structure. There is no evidence to suggest that the cores remained dry during formation and transportation, as was found by Bell (1940). Rather, the lack of structure suggests that the core material may have been damp at the time of formation and that the plastic material was deformed sufficiently during transportation to destroy all vestiges of structure. Conversely, cores that have definite structure (fig. 14.2*F*) certainly must have remained dry on the interior during the period of formation and transportation, otherwise these structural features would have been distorted or destroyed by plastic deformation.

Curve *A* on figure 14.3 is the size distribution of core material of the clay balls. Curve *B* shows the size distribution of typical suspended-sediment samples collected in flow over the clay-impregnated bed. Curves *A* and *B* are similar. They indicate that the cores of the balls are formed from clay that was carried in suspension during flow and was deposited in depressions of the bed. Curve *C* shows the size distribution of the clay-impregnated layer of the bed and is very close to the size distribution of the sediment forming the banks. Curve *C* indicates that the material comprising the clay balls is not derived primarily from bank sloughing or from headcutting through the clay-impregnated bed. The cores of the balls contain about 65 percent clay, whereas the material from bank sloughing and from headcutting through the clay-impregnated bed contains less than 30 percent clay. Curve *D* shows the average size distribution of bed material that is not impregnated with clay. Curve *E* shows the average size distribution of the armor from the clay balls. Two points of interest are notable in curve E: The armor contains about 40 percent silt and clay as binding material, and more than 15 percent of the armor consists of material coarser than 1 mm. However, sieve analysis indicates that material coarser than 1 mm forms less than 0.2 percent of the bed material.

Clay balls selectively accrete the coarser portion of the bed material probably because angular, coarse particles penetrate farther into the ball and adhere to the clay more firmly than do the smaller, well-rounded sand grains.

The size distribution of the clay balls was determined in the field by measuring the diameter of 406 of the balls selected at random from 3 separate deposits. The maximum size observed was 400 mm (about 16 inches). The size distribution, shown in figure 14.4, is almost precisely log-normal. The slight tendency for a distri-

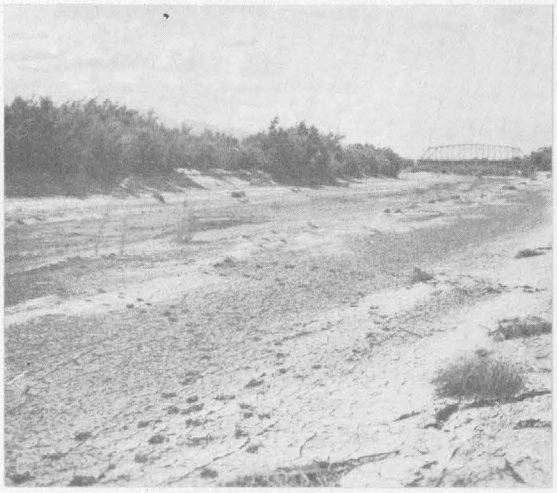

A

D

B

E

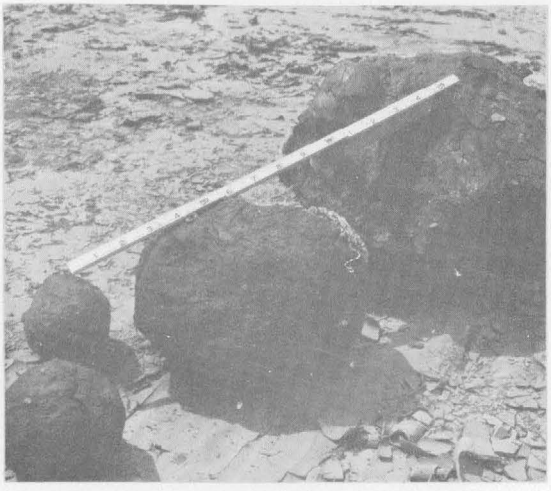

C

F

FIGURE 14.2.—Study reach and clay balls, Rio Puerco near Bernardo, N. Mex. *A*, Study reach, view upstream, summer. *B*, Study reach showing trenching, fall. *C*, Typical unarmored clay balls. *D*, Deposit of armored clay balls. *E*, Concentric structure, armored clay ball. *F*, Laminated structure, core of clay ball.

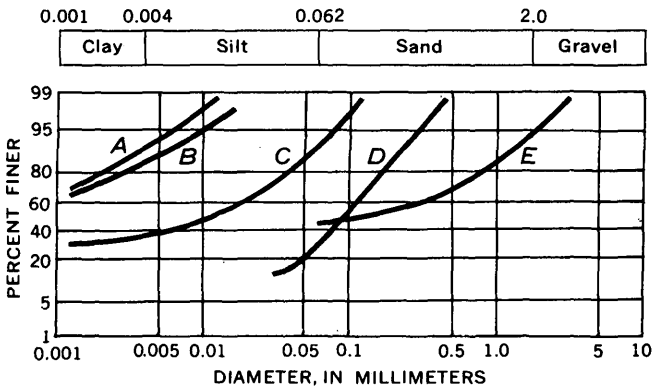

FIGURE 14.3.—Typical particle-size distributions.

bution skewed toward the smaller sizes probably reflects the difficulty of accurately measuring the smallest sizes. The median diameter is 50 mm, and there was no difference in the size distribution of the three deposits. All of the balls exhibited a high degree of sphericity.

In the reach studied, the clay balls were deposited with remarkable regularity (fig. 14.1) in groups or bars, roughly parallel to the channel. The distance between deposits ranges from 4 to 8 times the channel width. This pattern of deposition corresponds closely to the pattern of meanders or riffles given by Leopold and Wolman (1960), who show that the meander wavelength or twice the distance between successive riffles is approximately 10 times the channel width.

Clay balls probably will be formed if the following three conditions are satisfied:

1. A source of clay material is available.
2. Fragments of source material possess sufficient strength to maintain their identity.
3. The flow is strong enough to move the fragments and to maintain motion until they are rounded to form clay balls.

After every flow, clay is deposited in depressions of the bed. When dried, this material cracks and curls, and the fragments formed may range in size and shape from paper-thin flakes to polygonal chunks several feet thick. Thus, flakes formed by surface cracking are available in sizes that will be moved by flows of almost any intensity.

The deciding factor for the formation of clay balls is the requirement that the source material possess sufficient strength to maintain its identity for the duration of the flow. The strength of the clays of the Rio Puerco depends mainly on the water content. The material may range in moisture conditions from dry sheets, which develop maximum strength through an

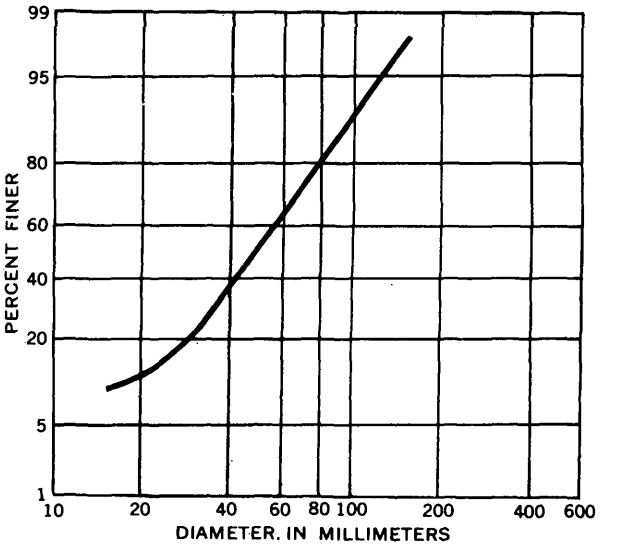

FIGURE 14.4.—Size distribution of clay balls.

entire range of plastic material to a liquid slurry. Clay balls do not form after prolonged periods of flow, under which conditions source material either is not available or is saturated and does not meet the strength requirements.

REFERENCES

Bell, H. S., 1940, Armored mud balls—their origin, properties, and role in sedimentation: Jour. Geology, v. 48, no. 1, p. 1–31.

Leopold, L. B., and Wolman, M. G., 1960, River meanders: Geol. Soc. America Bull., v. 71, p. 769–793.

15. ESTIMATING POROSITY FROM SPECIFIC GRAVITY

By PHILIP COHEN, Carson City, Nev.

Work done in cooperation with the Nevada Department of Conservation and Natural Resources

As a part of a hydrologic study, 115 samples of the unconsolidated deposits of a 40-mile segment of the flood plain and terraces of the Humboldt River, Humboldt County, Nev., were collected in the summer of 1960. Eighty-two undisturbed samples were collected by means of a 2-inch-diameter Pomona core barrel; 33 disturbed samples also were collected. All of the samples were collected from a depth less than 20 feet below land surface.

For all samples the dry unit weight (apparent specific gravity) and the average unit weight of the particles comprising each sample (absolute specific gravity), were determined at the Hydrologic Laboratory of the Ground Water Branch of the Survey at Denver, Colo. From these data, porosity was determined by the following formula:

$$n = 100\frac{(\gamma_s - \gamma_d)}{\gamma_d}$$

where n = porosity, in percent by volume;
γ_s = average unit weight of the particles comprising the sample in grams per cubic centimeter (absolute specific gravity);
γ_d = dry unit weight of the dry undisturbed or repacked sample, in grams per cubic centimeter (apparent specific gravity).

The absolute specific gravity of the samples was determined by the pycnometer method (Krumbein and Pettijohn, 1938, p. 501). The dry unit weight of the undisturbed cores was determined by measuring the volume and weighing the oven-dried cores; the dry unit weight of the disturbed samples was determined by measuring the volume and oven-dried weight of samples that were repacked in the laboratory.

It is apparent from the above equation that a graph with porosity as the abscissa and dry unit weight as the ordinate will plot as a straight line for samples having the same absolute specific gravity (average unit weight of particles). This relationship is true irrespective of other factors such as particle size, particle shape, degree of assortment, sedimentary structures, or degree of compaction. For mineralogically or lithologically heterogeneous deposits, the points will tend to be scattered—the degree of scattering being related to differences in the absolute specific gravity of the samples.

Figure 15.1 is a graph showing the relation of porosity and dry unit weight of the samples of the Humboldt River valley. The points on the graph tend to define a straight line and fall in a very narrow band, indicating that the absolute specific gravity of the samples does not vary substantially. The deposits of the flood plain of the Humboldt River contain many different minerals and rock types derived largely from the erosion of Quaternary and Tertiary alluvial fans and Pleistocene lake deposits. It appears from the graph that the older deposits were thoroughly reworked and mixed by the Humboldt River, causing the resulting flood-plain deposits to have a fairly constant absolute specific gravity.

Dry unit weight is equal to the average unit weight when porosity is equal to zero (see equation), and the approximate average unit weight of the particles comprising all the samples can be obtained by extending the line shown in figure 15.1 so that it intersects the ordinate. Thus, the average unit weight of particles of the samples plotted is about 2.67.

The aforementioned relations between porosity and dry unit weight can be useful in future hydrogeologic studies in the Humboldt River valley. In the present area of study, it is possible to use figure 15.1 to estimate porosity from dry unit weight with an approximate accuracy of ± 1.5 percent. This degree of accuracy is adequate for the present study. In order to estimate porosity from dry unit weight in other areas it will be necessary to determine dry unit weight, absolute specific gravity, and porosity of a sufficient number of samples to define the relation between these parameters. Once this relation is defined, it is necessary only to determine dry unit weight in order to estimate porosity.

The relation between porosity and dry unit weight also may be useful in other areas where lithologic and stratigraphic control permits an accurate estimate of average unit weight of particles. If this value alone is known for any deposit, a straight-line graph similar to figure 15.1 can be drawn showing the relation between the dry unit weight and the porosity of the deposit. From the equation, it is apparent that the line must

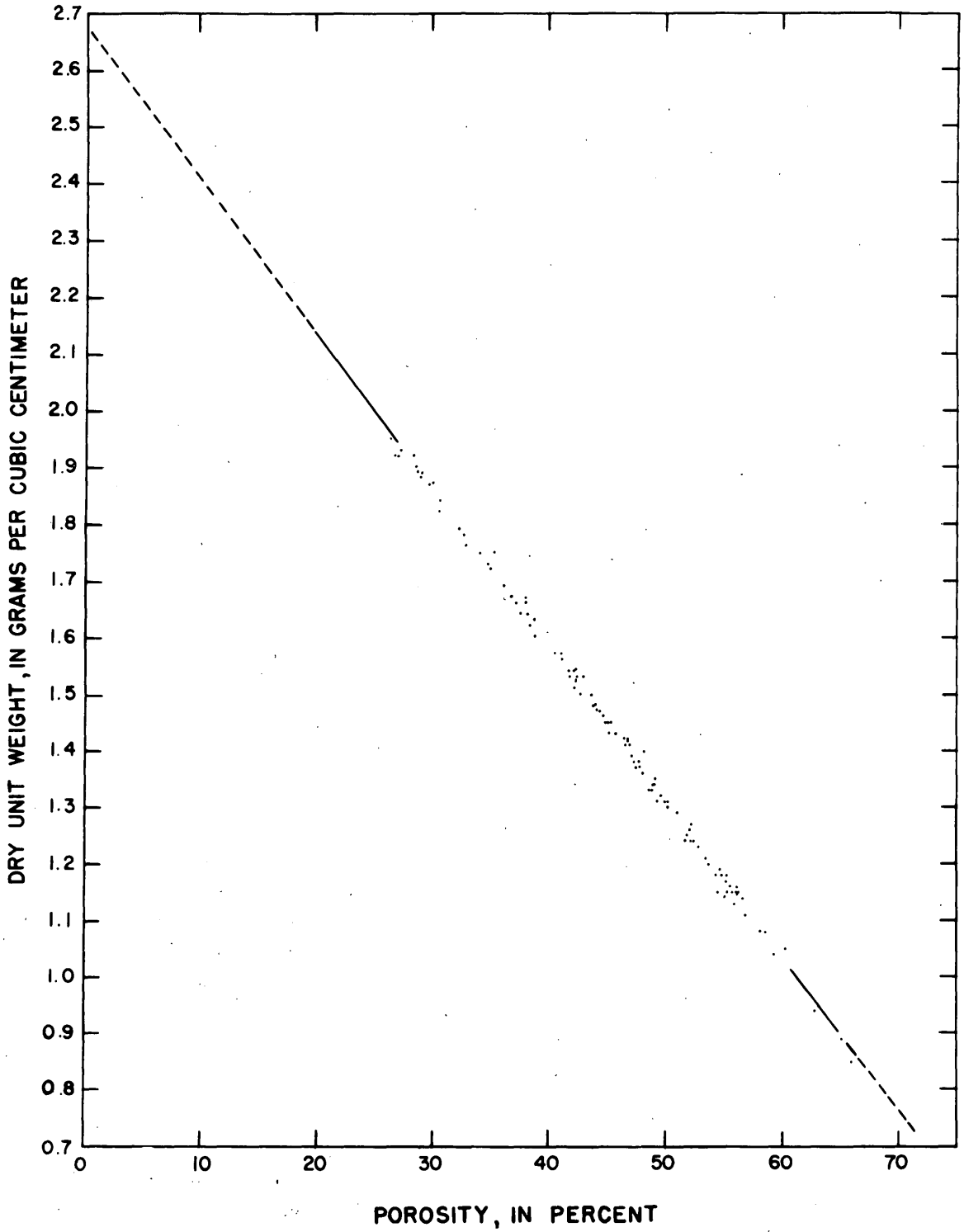

FIGURE 15.1.—Relation between porosity and dry unit weight in the Humboldt River Valley, Humboldt County, Nev.

intersect the abscissa, or zero dry unit weight line, where porosity equals 100 percent, and the line must intersect the ordinate, or zero porosity line, at the value of the average unit weight of particles (absolute specific gravity) for the deposit.

At present, dry-unit-weight data are being collected by means of the nuclear density meter in many areas. A few determinations of dry unit weight (apparent specific gravity) then may make it possible to obtain a fairly accurate estimate of the porosity and the absolute specific gravity of all the materials tested with the meter by use of a plot similar to that described. The absolute specific gravity of any sample represented by a point plotted on a graph similar to figure 15.1 could be ascertained by drawing a straight line from the 100-percent porosity value on the abscissa through the point to the ordinate. The dry-unit-weight value at the point of intersection of the line and the ordinate is equal to the absolute specific gravity of the sample.

REFERENCE

Krumbein, W. C., and Pettijohn, F. J., 1938, Manual of sedimentary petrography: New York, Appleton-Century-Crofts, 549 p.

16. RELATION OF VOLUMETRIC SHRINKAGE TO CLAY CONTENT OF SEDIMENTS FROM THE SAN JOAQUIN VALLEY, CALIFORNIA

By A. I. Johnson and D. A. Morris, Denver, Colo.

More than 300 "undisturbed" samples taken from depths as great as 2,000 feet from 3 core holes in the Los Banos–Kettleman City area, California, were analyzed in the Hydrologic Laboratory of the Geological Survey as part of an investigation of the physical character of sediments in an area subject to land subsidence in the San Joaquin Valley (Inter-Agency Committee on Land Subsidence in the San Joaquin Valley, 1958).

Atterberg (1911) and Goldschmidt (1926) found that plasticity is a function of the finer particles in a sediment mass. Therefore, the consistency limits and indices should vary according to the clay content. The relation of the liquid and plastic limits and of the pasticity index to clay content has been shown (Atterberg, 1911; Terzaghi, 1926; Russell and Wehr, 1928; and Baver, 1948). This paper shows the close relationship between clay content and volumetric shrinkage.

When fine-grained sediments are deposited in water, the mass has the appearance of a dense fluid. If the water content of this mass is progressively reduced, the sediment mass will pass from the liquid state, through a plastic state and a semisolid state, to a solid state. The water content, in percent of dry weight, at the transition between the liquid and plastic states is called the liquid limit, at the transition between the plastic and semisolid states is called the plastic limit, and at the transition between the semisolid and solid states is called the shrinkage limit. A decrease in volume of the sediments takes place continuously as the water content decreases to the shrinkage limit, which is the maximum water content, in percent of dry weight, at which a reduction in water content produces no further decrease in volume of the sediment mass. Volumetric shrinkage is the decrease in volume, in percent of dry volume, of the sediment mass when the water content is reduced from the liquid limit to the shrinkage limit. Volumetric shrinkage is computed by the equation

$$V_s = (w_L - w_s)R,$$

where V_s = volumetric shrinkage, in percent of dry volume;
w_L = liquid limit, in percent of dry weight;
w_s = shrinkage limit, in percent of dry weight;
R = shrinkage ratio, in grams per cubic centimeter.

The shrinkage ratio is defined as the ratio of a given change in volume, expressed as percent of the dry volume, to the corresponding change in water content above the shrinkage limit, expressed as percent of the weight of the oven-dried soil.

The clay content (particles smaller than 0.0004 mm) was determined by the hydrometer method. Clay content and volumetric shrinkage are plotted against depth (fig. 16.1) for one of the three core holes. A close comparison between clay content and volumetric shrinkage was also noted for the other two core holes. The relation of clay content to volumetric shrinkage for samples from all three core holes in the Los Banos-

629660—62——4

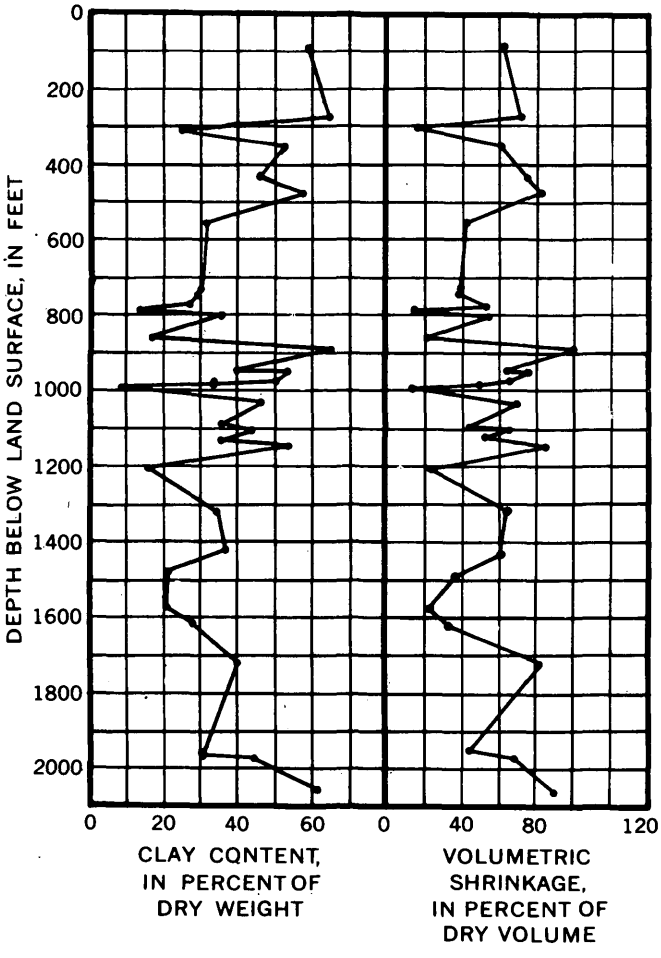

FIGURE 16.1.—Clay content and volumetric shrinkage of samples from core hole 19/17–22J1,2.

Kettleman City area is plotted in figure 16.2, which shows that the decrease in volume in a sediment mass is proportional to the percentage of clay. A 10-percent increase in clay content causes an approximate increase of 20 percent in volumetric shrinkage. The relationship indicated by the trend line in figure 16.2 may be represented by the equation

$$V_s = 2.1(C - 10),$$

where V_s = volumetric shrinkage, in percent of dry volume;

C = clay content, in percent of dry weight.

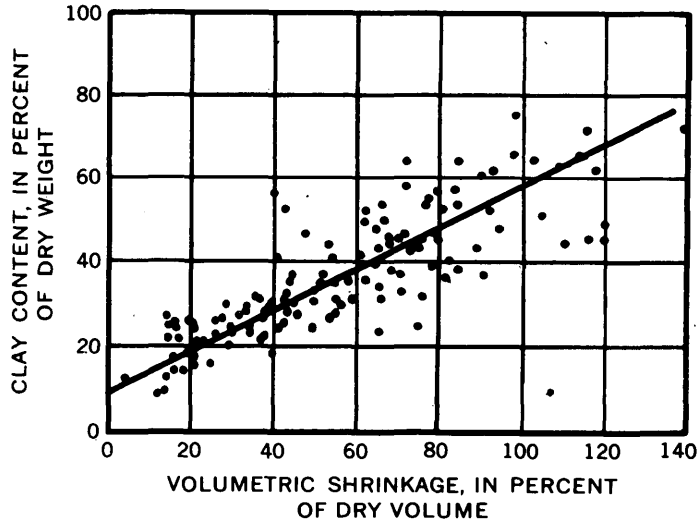

FIGURE 16.2.—Relation of volumetric shrinkage to clay content for samples from three core holes in the Los Banos-Kettleman City area, California.

This relationship thus makes it possible to estimate the volumetric shrinkage by determining the clay content of samples of the sediments.

REFERENCES

Atterberg, A., 1911, Über die physikalische Bodenuntersuchung, und Über die Plastizitat der Tone: Internat. Mitteilungen für Bodenkunde, Band 1, Heft 1, p. 7–9, p. 10–43.

Baver, L. D., 1948, Soil physics: 2d ed., New York, John Wiley and Sons, Inc., p. 101–124.

Goldschmidt, V. M., 1926, Undersöekser over Lersedimenter: Beretning om Nordiske Jordbrugs forskeres Kongress i Osla: Nordisk Jordsbrugsforskning, 4–7, p. 434–445.

Inter-Agency Committee on Land Subsidence in the San Joaquin Valley, 1958, Progress report on land subsidence investigations in the San Joaquin Valley, California, through 1957: Sacramento, Calif., 160 p., 45 pls.

Poland, J. F., and Davis, G. H., 1956, Subsidence of the land surface in the Tulare-Wasco (Delano) and Los Banos-Kettleman City area, San Joaquin Valley, California: Am. Geophys. Union Trans., v. 37, no. 3, p. 287–296.

Russell, J. C., and Wehr, F. M., 1928, The Atterberg consistency constants: Am. Soc. Agronomy Jour., v. 20, p. 354–372.

Terzaghi, Karl, 1926, Simplified soil tests for subgrades and their physical significance: Public Roads, v. 7, p. 153–162.

GEOMORPHOLOGY

17. LOWER PLEISTOCENE PRAIRIE DIVIDE TILL, LARIMER COUNTY, COLORADO

By D. V. Harris and R. K. Fahnestock, Fort Collins, Colo.

Work done in cooperation with the Colorado State University Geology Department

A large glacial deposit forms the divide between the North Fork of Rabbit Creek and the upper drainage of the North Fork of Cache la Poudre River in the Front Range of northern Colorado. It is located on the borders of the Livermore and Home quadrangles in secs. 5, 12, and 17, T. 10 N, R. 72 W, 30 miles northwest of Fort Collins (fig. 17.1). The deposit was first described by Ray (1938,[1] 1940) and by Bryan and Ray (1940). Other features probably of glacial origin are the Red Feather and Creedmore Lakes (fig. 17.1).

[1] Ray, L. L., 1938, Geomorphology and Quaternary chronology of northeastern Colorado: Harvard Univ. Ph. D. thesis.

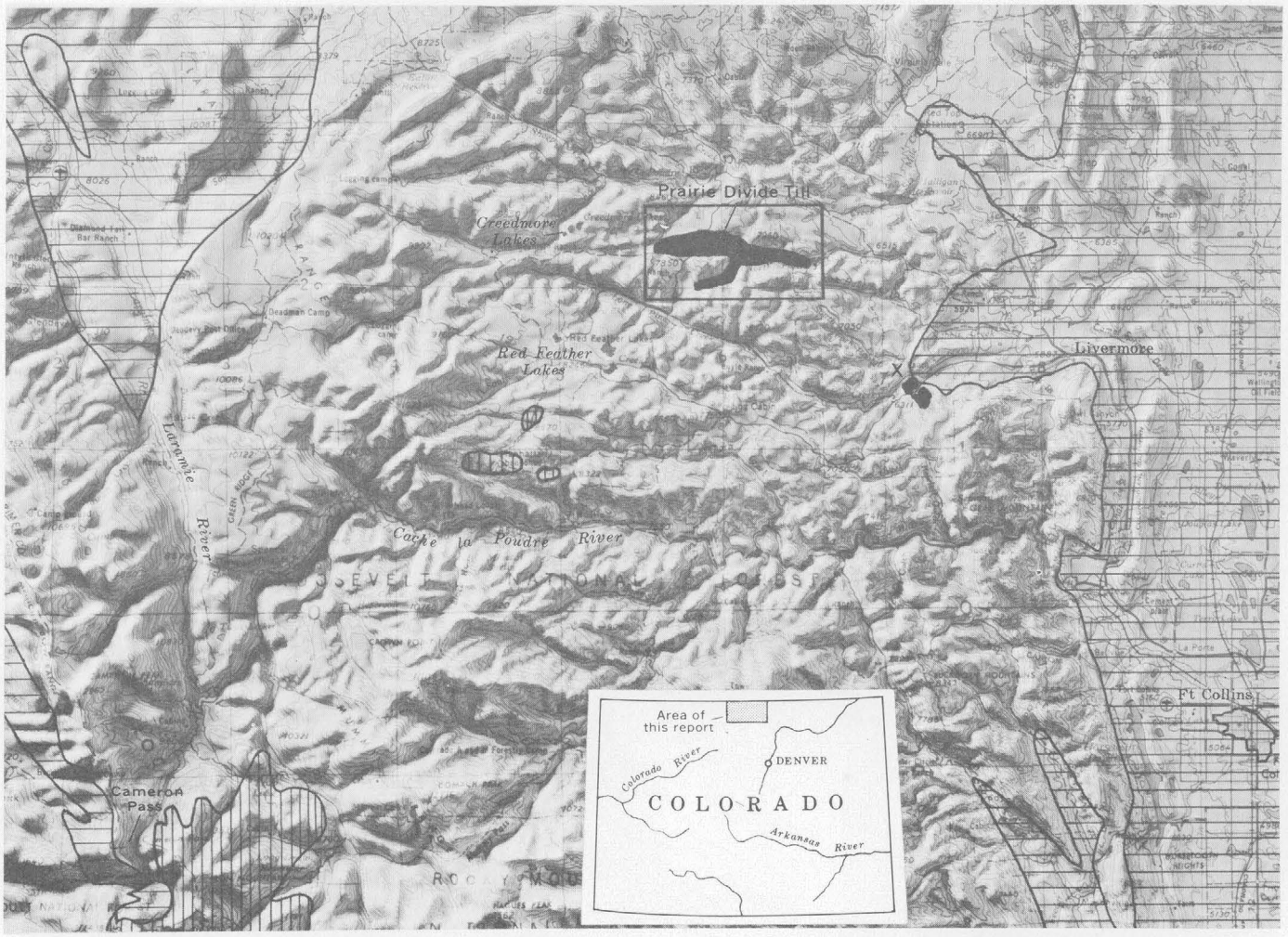

FIGURE 17.1.—Relief map showing location and geologic setting of the Prairie Divide Till of Ray (1938) and a similar glacial deposit (X). Horizontal lines delineate areas of sedimentary rocks; vertical lines indicate possible source areas of igneous marker rocks; unlined areas are underlain by granite and schist of Precambrian age (after Lovering and Goddard, 1950). The rectangle marks the area covered by figure 17.2. The major canyons cut since Prairie Divide time are those of the Cache la Poudre River and the Laramie River.

The surface of the main body of this deposit is a high, flat, treeless prairie lying at an altitude of 7,900 to 8,000 feet. A ridge extends 3 miles downvalley from the dissected east edge of the main body of till (fig. 17.2). The ridge was formed by streams that cut their valleys along the contact between the till and granite, leaving a ridge of till. In the broad preglacial valley shown in figures 17.2 and 17.3, small patches of drift remain on the valley sides at an altitude as low as 6,700 feet. Another large deposit occupies the tributary valley to the south.

Figure 17.3 shows profiles of the Prairie Divide deposit and the North and Middle Fork valleys of Rabbit Creek. Location of these profiles is shown on figure 17.2. Longitudinal profile *A* shows the high treeless prairie and the long ridge. *B* extends across the main valley and the till ridge. At *C*, downvalley from the till deposits, the valley is broad in distinct contrast with the narrow, V-shaped valley of the Middle Fork of Rabbit Creek to the south, shown in profile *D*.

Boulder till is exposed in road cuts and gully banks within the deposit. Many of the boulders are deeply weathered, but other boulders, apparently of the same rock type, are essentially unweathered. A few cobbles are altered to green plastic clay. The upper 8 to 18 inches of the till is noncalcareous, but at many places a caliche zone is developed 2 to 3 feet below the surface.

Most of the material in the deposit comes from areas of Precambrian rocks (mainly granitic and metamorphic rocks) shown in figure 17.1. However, two rock types, felsite and red sandstone, indicate that the ice moved from the Cameron Pass area (fig. 17.1) 35 miles northeast to Prairie Divide. According to John A. Campbell (oral communication) the only outcrops of the red sandstone (Chugwater) at higher elevations than the till occur about 2 miles north of Cameron Pass. The volcanic area near Cameron Pass is a possible source of the felsite, but more probably it was derived from small bodies of Tertiary intrusive rocks south of Red Feather Lakes, in direct line from Cameron Pass to Pairie Divide.

The topography over which the ice traveled must have been radically different from the present topography (fig. 17.1) or from that of Wisconsin time when the canyons directed ice movement. If the canyon of the Cache la Poudre River, which is as much as 2,000 feet deep, had existed at the time of the Prairie Divide deposition, it would have directed the flow of the ice to the east. In addition, the form of the present canyon would be similar to the valley of Lake Chelan (Willis, 1903) because of extensive erosion by through-flowing ice. Prairie Divide would then be unlikely to contain thick, extensive glacial deposits.

Prairie Divide Till fills a broad valley (fig. 17.3, profiles *B* and *C*) cut below the Rocky Mountain surface formed during the Pliocene prior to the main canyon-cutting cycle (fig. 17.3, profile *D*). From work elsewhere in the Southern Rocky Mountains, Van Tuyl and Lovering (1935), Atwood (1937), Wahlstrom

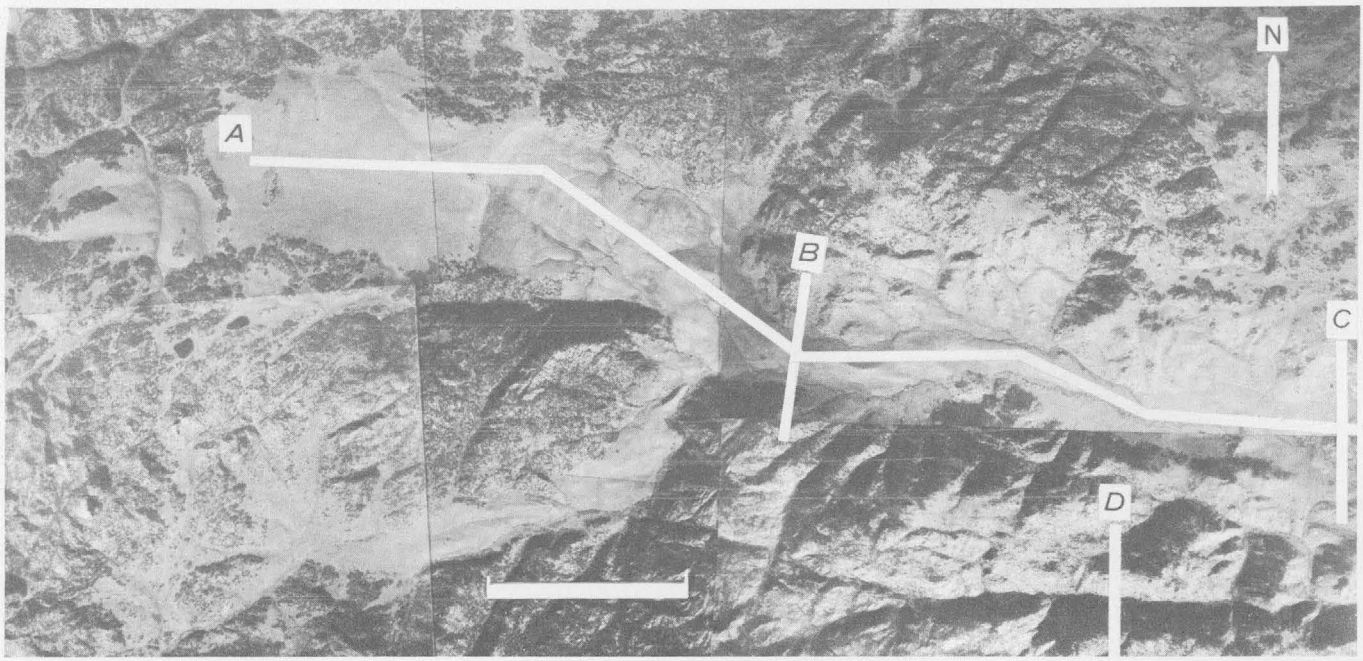

FIGURE 17.2.—Aerial mosaic of the Prairie Divide deposit. Most of the treeless areas are covered by till. Letters refer to the sections shown on figure 17.3. Bar in center foreground represents a distance of about 1 mile.

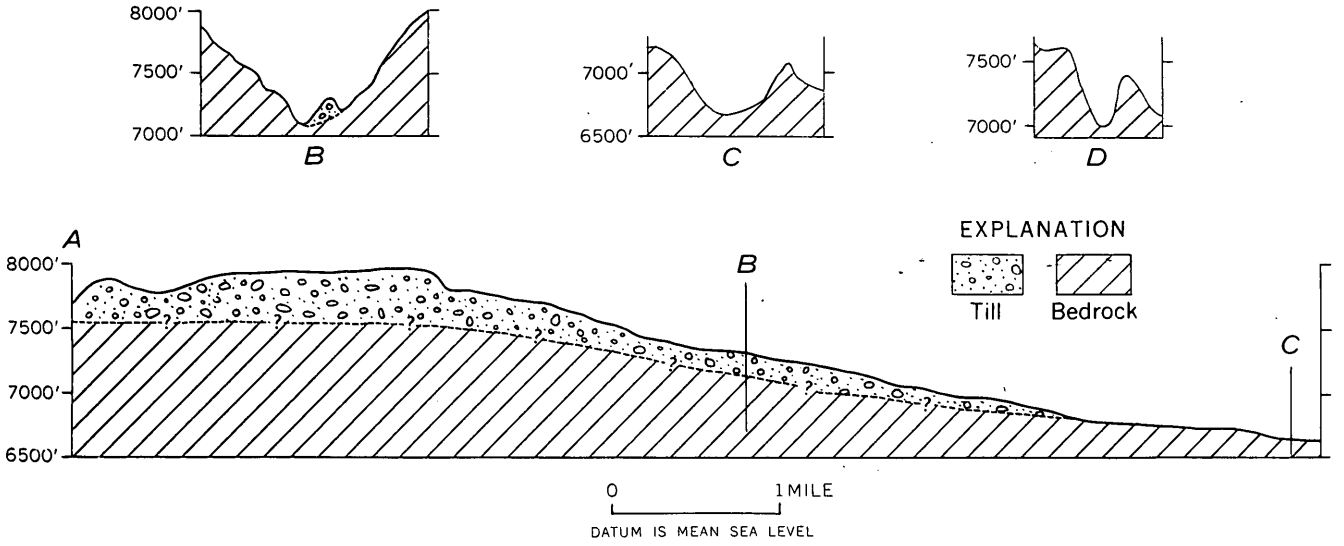

FIGURE 17.3.—Longitudinal and transverse profiles of the Prairie Divide deposit and the North and Middle Fork Valleys of Rabbit Creek. Location of sections is shown on figure 17.2.

(1947), Ives (1953), and Richmond (1957) concluded that lower Pleistocene glaciers were icecaps rather than valley glaciers. The position of Prairie Divide Till with respect to its source area substantiates this interpretation.

A deposit of bouldery material at least a square mile in area, and closely resembling the Prairie Divide Till, lies about 8 miles southeast of Prairie Divide at the edge of the Colorado Piedmont (fig. 17.1, X). This deposit, located on Lone Pine Creek, is tentatively correlated with the Prairie Divide deposit. If these 2 deposits are contemporaneous, this lobe of the ice sheet covered a large area and moved downslope to altitudes as low as 6,300 feet.

Future work may establish age relationships between the Prairie Divide Till, the till at Lone Pine Creek, and the high pediment in the Colorado Piedmont. The fact that the Prairie Divide ice traveled at least 35 miles suggests that farther south, where the high country lies within 20 miles of the mountain front, deposits of this ice sheet should be sought as far east as the mountain front and, in selected areas, even beyond.

REFERENCES

Atwood, W. W., Jr., 1937, Records of Pleistocene glaciers in the Medicine Bow and Park Ranges (Wyoming and Colorado): Jour. Geology, v. 45, no. 2, p. 113–140.

Bryan, Kirk, and Ray, L. L., 1940, Geologic antiquity of the Lindenmeier site in Colorado: Smithsonian Misc. Colln., v. 99, no. 2, pub. 3554, 76 p.

Ives, R. L., 1953, Anomalous glacial deposits in the Colorado Front Range area, Colorado: Am. Geophys. Union Trans., v. 34, no. 2, p. 220–226.

Lovering, T. S., and Goddard, E. N., 1950, Geology and ore deposits of the Front Range, Colorado: U.S. Geol. Survey Prof. Paper 223, 319 p.

Ray, L. L., 1940, Glacial chronology of the southern Rocky Mountains: Geol. Soc. America Bull., v. 51, no. 12, p. 1851–1917.

Richmond, G. M., 1957, Three pre-Wisconsin glacial stages in the Rocky Mountain region: Geol. Soc. America Bull, v. 68, no. 2, p. 239–262.

Van Tuyl, F. M., and Lovering, T. S., 1935, Physiographic development of the Front Range: Geol. Soc. America Bull., v. 46, no. 9, p. 1291–1350.

Wahlstrom, E. E., 1947, Cenozoic physiographic history of the Front Range, Colorado: Geol. Soc. America Bull., v. 58, no. 7, p. 551–572.

Willis, Bailey, 1903, Contributions to the geology of Washington: U.S. Geol. Survey Prof. Paper 19, p. 58–63, 81–83.

18. LATE PLEISTOCENE AND RECENT EROSION AND ALLUVIATION IN PARTS OF THE COLORADO RIVER SYSTEM, ARIZONA AND UTAH

By MAURICE E. COOLEY, Tucson, Ariz.

Work done in cooperation with the Bureau of Indian Affairs

Most valleys and canyons on the Colorado Plateau contain alluvium which ranges in thickness from 25 to 200 feet. At least five cycles of downcutting and alluviation of Pleistocene age record the entrenchment of the streams in the Colorado River basin. The total cutting that occurred during Quaternary time was between 800 and 1,500 feet and that during late Pleistocene and Recent time was between 100 and 300 feet. The Quaternary events are listed on figure 18.1.

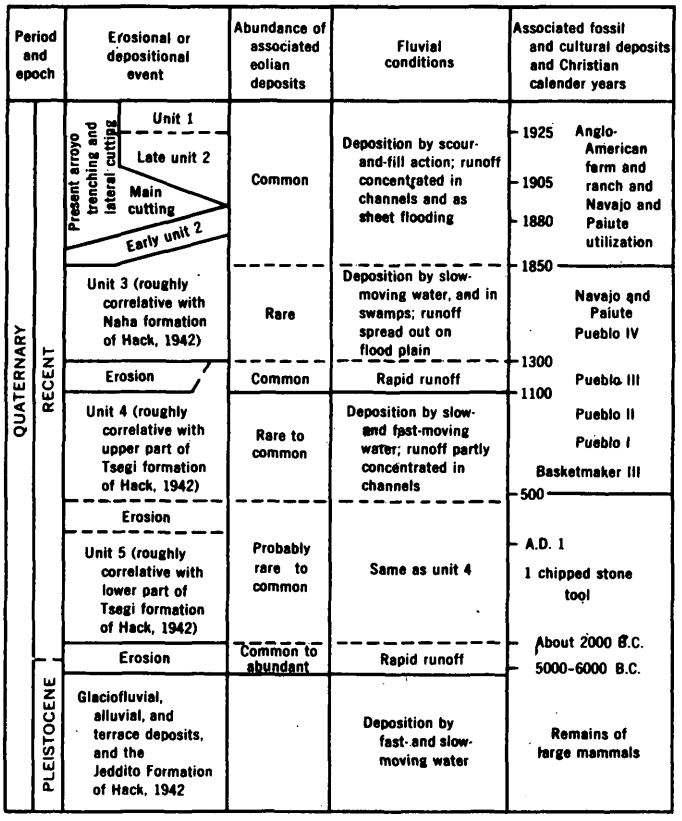

FIGURE 18.1.—Chart showing late Pleistocene and Recent erosional and depositional events in parts of the Colorado River system.

Most alluvial sediments in the valleys and canyons are indicated to be of late Pleistocene age by the presence of fossils of large mammals near the Little Colorado River (Reiche, 1937; Hack, 1942; Lance, 1960) and by the relations of the deposits and stream terraces to the glaciofluvial deposits in the nearby mountains. The fossils were found only in the Jeddito Formation and in the terrace deposits along the Little Colorado River. Geologic mapping indicates that glaciofluvial sediments described by Sharp (1942) on San Francisco Mountain extend downstream and grade into terrace deposits along Deadman Wash and the Little Colorado River. The lower gravel terraces along the San Juan and Animas Rivers can be traced into the glacial-outwash deposits in the San Juan Mountains (Atwood and Mather, 1932, p. 131).

Most deposits of late Pleistocene age in the Colorado River system consist predominantly of sand and gravel, although muddy and sandy deposits were laid down by some streams. The type of deposit is related to the stream regimen and to periglacial and glacial activity within the drainage area. Streams that have a sizeable part of their headwater areas above 7,500 feet, such as the Colorado, San Juan, Little Colorado, and Escalante Rivers, and Deadman Wash, tended in Pleistocene time to deposit gravelly sediments much coarser than those laid down in Recent time. Streams that head below 7,500 feet, such as Jeddito Wash and Castle Creek, deposited a relatively small amount of gravel, and the gravel, at least locally, is finer than that in the Recent alluvium.

The Pleistocene deposits form terraces, and possibly are preserved beneath Recent alluvium, along the Colorado, Little Colorado, and San Juan Rivers and along the lower parts of the larger tributary streams (figs. 18.2*A*, *B*). In the upstream reaches of the tributaries, post-Pleistocene cutting exposed only the upper part of the Pleistocene deposits (figs. 18.2*C*, *D*).

Recent time is represented by 5 alluvial units and by 2 prominent and 2 secondary cycles of erosion and arroyo formation (fig. 18.1).

The age of Recent events has been interpreted from associated cultural material, which ranges from Basketmaker III to the present land utilization, or since about A.D. 500 (R. H. Thompson, oral communication, 1961). However, nearly all the cultural deposits that can be used for dating are related to or are embedded within unit 4 and are only indirectly related to the other depositional and erosional events of Recent time. Unit 4 forms the bulk of the Recent alluvium in the arroyo walls of most washes of the Colorado Plateau. The lower parts of the exposures usually contain cross-bedded sand and gravel beds which intertongue laterally with and grade upward into sandy silt and silty sand layers. Buried soils containing carbona-

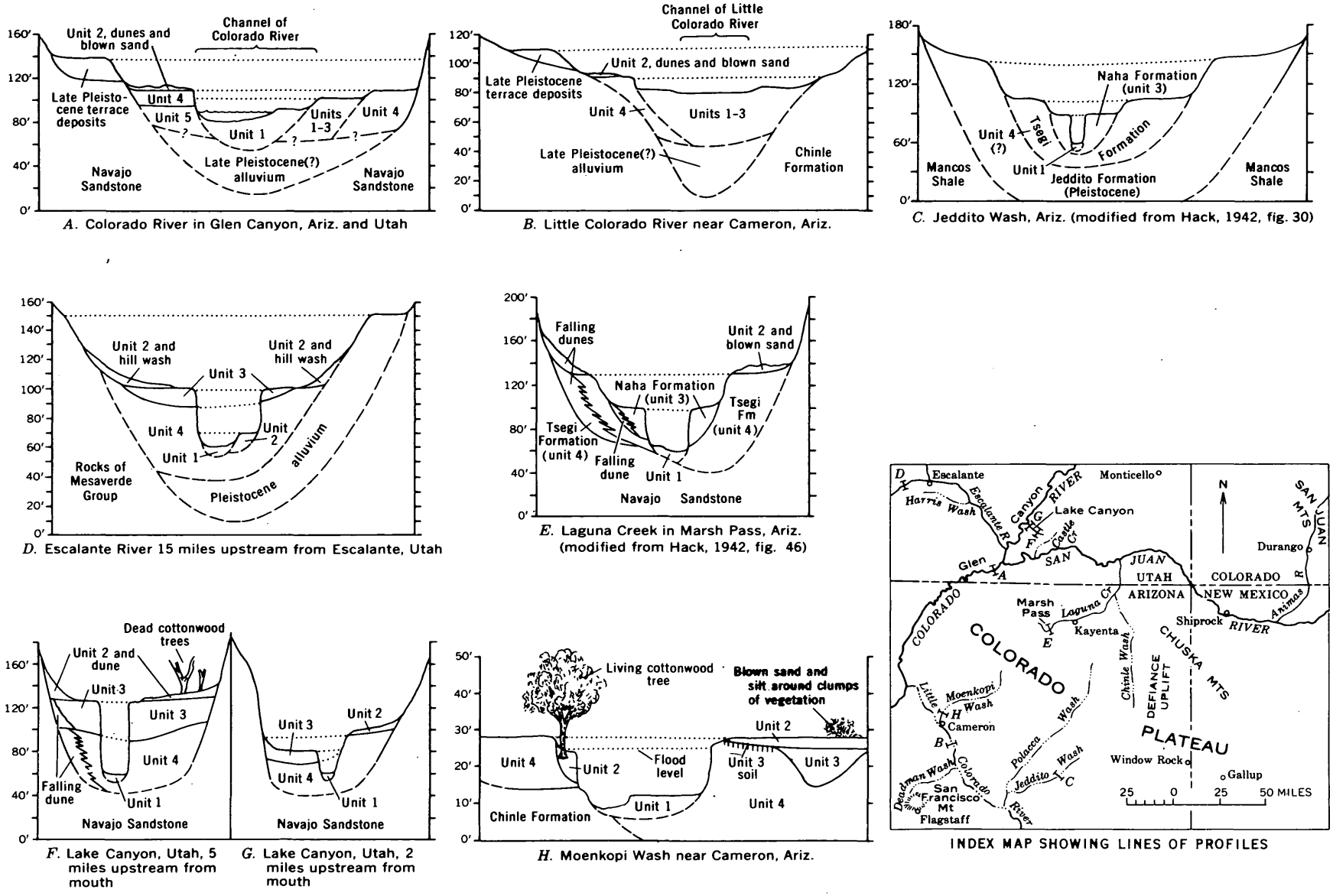

FIGURE 18.2.—Profiles showing late Pleistocene and Recent alluvial and terrace deposits in parts of the Colorado River drainage system, Arizona and Utah. The sediments of Recent age consist in descending order of units 1, 2, 3 (Naha Formation of Hack, 1942), and units 4 and 5 (Tsegi Formation of Hack, 1942). The sediments of late Pleistocene age consist of glaciofluvial, alluvial, and terrace deposits, and the Jeddito Formation of Hack, 1942.

ceous material and very thin mud beds are scattered throughout the unit. The upper few feet of the unit usually contains considerable interbedded eolian material.

Unit 5 (fig. 18.2*A*), the oldest alluvial unit of Recent age, is beneath unit 4 in small exposures in Glen Canyon and possibly in other areas. It is lithologically similar to unit 4, although it is more firmly cemented. In some places a channeled erosion surface separates units 5 and 4, and in others their contact appears to be gradational. Evidence is insufficient at present to determine whether the channeled surfaces represent a regional or a local event.

Deposition of unit 4 was terminated by an erosional episode which may have started as early as A.D. 1100; erosion seems to have predominated during the A.D. 1200's, although in a few drainages no evidence of erosion during this time span was found. Stripping seems to have predominated during the earlier part of this erosional cycle, and deep channeling and arroyo cutting were restricted to the later part. In areas away from the deep channels, the erosion surface had slight relief; the channels were cut from 10 to 20 feet below the general level of this surface and are about two-thirds as deep and one-fifth as wide as the present arroyos formed in the same area.

Terraces were formed on unit 4 deposits during erosion in the A.D. 1100's and 1200's along the Colorado River along most reaches of the Little Colorado and San Juan Rivers and along parts of tributary drainages, such as Harris Wash, Jeddito Wash, Laguna Creek, and Lake Canyon (fig. 18.2*A*, *B*, *C*, *E*, and *G*). In most places along the tributary streams the overlying sediments of unit 3 were deposited over the entire valley floor (fig. 18.2*F*, *H*).

Unit 3 contains a relatively large amount of carbonaceous material. It is composed mainly of very thin to thin-bedded sediments ranging from mud to silty sand. Gravel, prominent crossbedding features, and wind-deposited material are uncommon. The unit contains buried soils, and usually a prominent soil is the uppermost bed. In many exposures unit 3 is represented only by this soil zone.

Units 5, 4, and 3 are probably roughly correlative with the Tsegi and Naha Formations defined by Hack (1942) (fig. 18.2*C*, *E*). Hack (1942, p. 51) noted that locally in Jeddito Valley, the Tsegi is separated by an erosion surface into a lower part and an upper part, which probably correlate with units 5 and 4, respectively. The Naha probably correlates with unit 3. However, the correlations are tentative and the names Naha and Tsegi have not been extended beyond the areas where they were originally defined.

Events associated with the present episode of arroyo cutting abruptly terminated the deposition of unit 3. The earliest event was deposition of a thin mantle of sand and gravel (early unit 2). This was followed by the main cutting of the arroyos which occurred generally between about A.D. 1850 and 1900 (Bryan, 1925; Gregory and Moore, 1931, p. 143). Locally, deposits of late unit 2 were laid down within the confines of the arroyo, partly burying living cottonwood trees (figs. 18.2*D*, *H*). These deposits form low alluvial terraces whose heights approximate those of high floods (fig. 18.2*H*). Most arroyos have widened since the main cutting, and at the present time some may be aggrading in a few places in the Defiance uplift-Chuska Mountains area.

The alluvial units were deposited under different fluvial conditions. Sediments of unit 3 were laid down by sluggish streams, and gravels in units 1, 2, and 4 by more vigorous streams (fig 18.1). The division of late Quaternary time into three broad periods of alluviation separated by periods of erosion (Bryan, 1940) can be recognized in many canyons and valleys, although the number, magnitude, and duration of the erosional and depositional events differ from drainage to drainage and along reaches of the same drainage.

REFERENCES

Atwood, W. W., and Mather, K. F., 1932, Physiography and Quaternary geology of the San Juan Mountains, Colorado: U.S. Geol. Survey Prof. Paper 146.

Bryan, Kirk, 1925, Date of channel trenching in the arid Southwest: Science, v. 62, p. 338–344.

——— 1940, Erosion in the valleys of Southwest: New Mexico Quart., v. 10, p. 227–232.

Gregory, H. E., and Moore, R. C., 1931, The Kaiparowits region, a geographic and geologic reconnaissance in parts of Utah and Arizona: U.S. Geol. Survey Prof. Paper 164.

Hack, J. T., 1942, The changing physical environment of the Hopi Indians of Arizona: Peabody Museum Papers, v. 35, no. 1.

Lance, J. F., 1960, Stratigraphic and structural position of Cenozoic fossil localities in Arizona: Arizona Geol. Soc. Digest, v. 3, p. 155–160.

Reiche, Parry, 1937, Quaternary deformation in the Cameron district of the Plateau province: Am. Jour. Sci., 5th ser., v. 24, p. 128–138.

Sharp, R. P., 1942, Multiple Pleistocene glaciation on San Francisco Mountain, Arizona: Jour. Geology, v. 50, p. 481–503.

19. RELATIONS OF ALLUVIAL-FAN SIZE AND SLOPE TO DRAINAGE-BASIN SIZE AND LITHOLOGY IN WESTERN FRESNO COUNTY, CALIFORNIA

By WILLIAM B. BULL, Sacramento, Calif.

Work done in cooperation with the California Department of Water Resources

Along the western border of the San Joaquin Valley in western Fresno County, Calif., the relations of the area and slope of alluvial fans to the area and lithology of their drainage basins have basic and applied significance. The relations illustrate some fundamental concepts of fan morphology, and they demonstrate the effect of drainage-basin lithology on the areal extent and thickness of deposits susceptible to near-surface subsidence when wetted. Near-surface subsidence is a phenomenon that seriously hinders engineering and agricultural operations on certain alluvial fans.

The fan slope used in computing quantitative relations is the average overall slope from the apex of the fan to the outer margin, where the fan coalesces with another fan or with the deposits of rivers in the trough of the San Joaquin Valley. Radial profiles drawn near the middle of the fans from apex to foot were used to help determine the lower end of the slope to be measured. The fan boundaries were determined by contour maps, aerial photographs, and tests of the gypsum content of 400 core-hole samples. The gypsum content of fan deposits whose drainage basins are underlain predominantly by clay-rich rocks is about five times that of fan deposits whose drainage basins are underlain predominantly by sandstone. Lithology of the bedrock in the drainage basins of the area has been described in detail by the writer (Bull, 1961a).

The fans studied range in size from 0.4 to 260 square miles. Figure 19.1*A* shows that all the fans derived from drainage basins underlain mainly by mudstone and shale and half of the fans derived from drainage basins underlain mainly by sandstone are larger than their drainage basins. The plotted points scatter moderately about straight lines described by the equations shown on the figure. On the logarithmic graph the slopes of the lines (0.88) are equal, showing that fan area increases in about the same exponential manner as drainage-basin area increases, despite appreciable differences in lithology. The coefficients of the equations (1.3 and 2.4) show that, on the average, fans derived from drainage basins characterized mainly by mudstone and shale are roughly twice as large as the fans derived from drainage basins of comparable size characterized mainly by sandstone.

The fans studied range in overall slope from 0.0035 (0° 12′) to 0.029 (1° 40′). Figure 19.1*B* shows that the overall fan slope decreases with an increase in drainage-basin size. In drainage basins of comparable size, all but the smallest fans of mudstone and shale drainage basins slope more steeply than fans of sandstone basins. The apexes of fans of mudstone and shale drainage basins are, on the average, 520 feet above the trough of the San Joaquin Valley, whereas the apexes of fans of sandstone drainage basins have an average height of 400 feet above the valley trough. These relations indicate that, for drainage areas of comparable size, fans derived from mudstone and shale are not only larger, as shown by figure 19.1*A*, but also thicker than fans derived from sandstone. Presumably, these differences may be attributed largely to the greater erodibility of the mudstone and shale.

The relation of fan area to fan slope for the fans studied is shown in figure 19.1*C*. In general, fan slope decreases with increasing fan area. The fans derived from mudstone and shale drainage basins are: (1) steeper than fans of similar area that are derived from sandstone drainage basins, and (2) larger than fans of similar slope from sandstone basins.

Irrigation has produced more than 10 feet of near-surface subsidence on certain alluvial fans in western Fresno County and about 125 square miles has subsided or probably would subside if irrigated. This settling of the land surface is caused by the compaction of moisture-deficient clay-rich deposits by the overburden load as the clay bond supporting the voids is weakened by water percolating through the deposits for the first time (Bull, 1961b). The magnitude of the subsidence is controlled by the thickness of the moisture-deficient deposits and by such factors as overburden load and amount and type of clay.

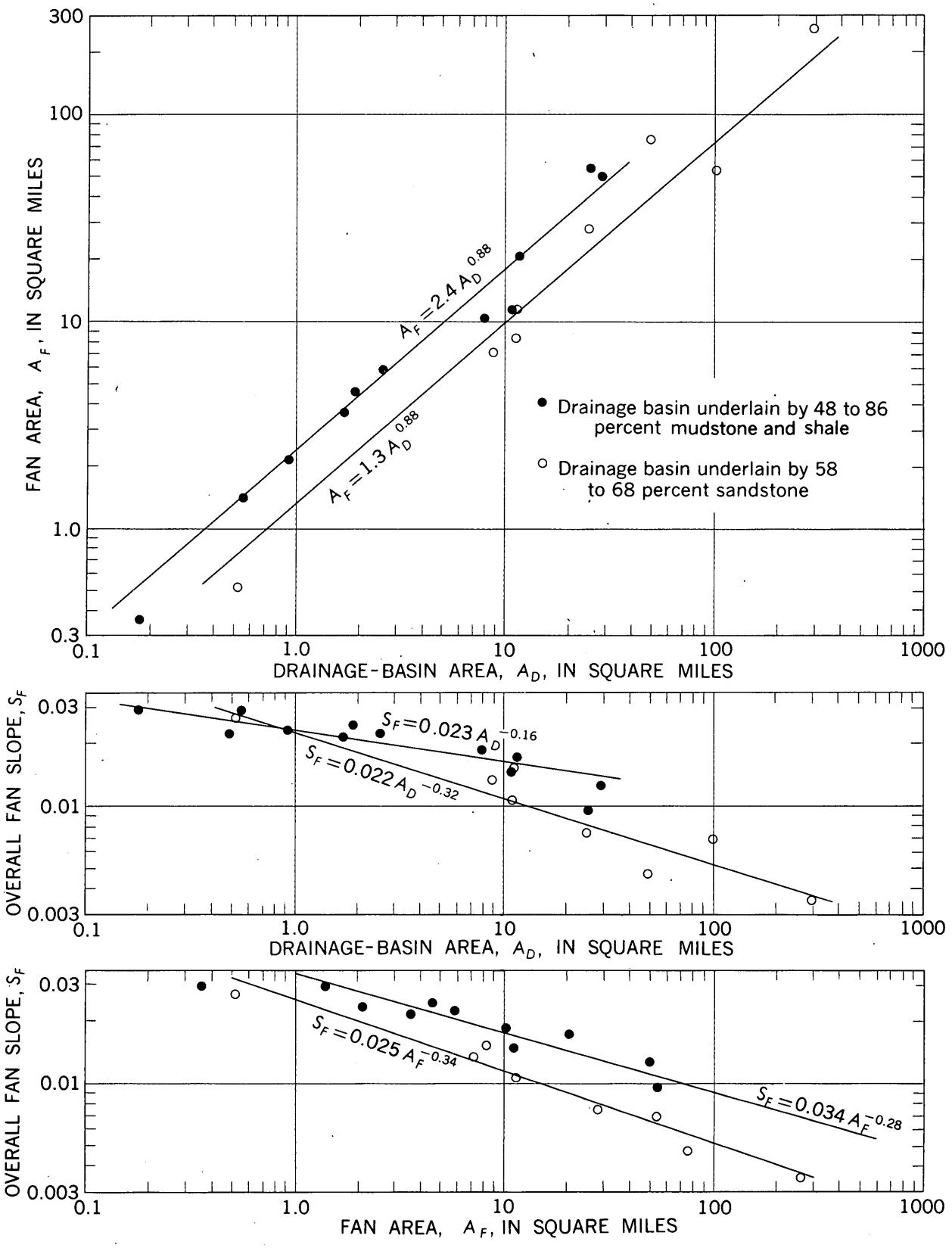

FIGURE 19.1.—Relations of fan area and slope to drainage-basin area and lithology in western Fresno County.

The subsiding fans are associated with drainage basins that are underlain mainly by mudstone and shale. Subsiding fans are thicker and almost twice as large as nonsubsiding fans derived from basins of comparable size. Thus the drainage-basin lithology directly affects both the potential areal extent and the potential amount of near-surface subsidence.

REFERENCES

Bull, W. B., 1961a, Alluvial fans and near-surface subsidence in western Fresno County, California: U.S. Geol. Survey open-file report, 264 p.

——— 1961b, Causes and mechanics of near-surface subsidence in western Fresno County, California: Art. 77 *in* U.S. Geol. Survey Prof. Paper 424–B, p. B187–B189.

20. RECENT GROWTH OF HALEMAUMAU, KILAUEA VOLCANO, HAWAII

By Donald H. Richter, James G. Moore, and Robert T. Haugen, Hawaiian Volcano Observatory, Hawaii, and National Park Service, Washington, D.C.

Work done in cooperation with the U.S. National Park Service

Halemaumau is a nearly circular crater indenting the relatively flat floor of the summit caldera of Kilauea Volcano on the island of Hawaii (fig. 20.1). In historic time Halemaumau, or the general southwest area of the caldera it presently occupies, has been the principal site of Kilauea's summit activity and is generally regarded as overlying the main magma conduit leading to the summit. Presently 550 feet deep and averaging 3,400 feet in diameter, Halemaumau continues to enlarge year after year by slides and rockfall off its precipitous and highly fractured walls. This paper, based on mapping and measurement of cracks around Halemaumau's rim, is a study of the crater's growth through the period 1928 to 1961.

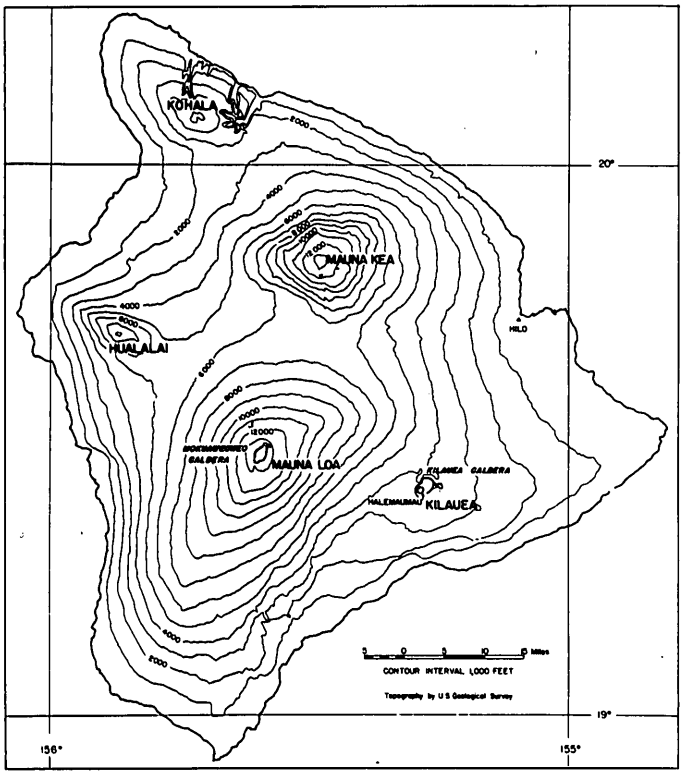

FIGURE 20.1.—Map of the island of Hawaii showing the Kilauea caldera and the inner crater of Halemaumau.

In the 140 years that has elapsed since Kilauea was first visited, Halemaumau has had a complex history. Between 1823 and 1890, a period marked by four great collapses involving almost the entire caldera floor, the general area of present-day Halemaumau contained a number of active lakes of lava that intermittently filled, overflowed, and drained away. About 1905, Halemaumau became identifiable as a single crater—the famous "fire-pit" of Kilauea—and for almost 20 years there was a dazzling display as liquid lava circulated in a lake 1,500 feet in diameter. In 1924 the lava lake suddenly drained away, and a series of violent steam eruptions, resulting from the penetration of ground water into the heated conduits beneath the caldera, blasted from Halemaumau. These eruptions and concurrent collapse left Halemaumau more than 1,300 feet deep and over 3,000 feet in diameter, essentially its present width. Since 1924, 11 separate eruptions (the last in July 1961) have added to the fill in the bottom of the crater.

During the enlargement of Halemaumau in 1924 a number of peripheral cracks developed around the crater, leaving the rim unstable and subject to landslides. The subsequent gradual enlargement of the crater has been largely controlled by these cracks, which bound the successive slide blocks. The cracks are nearly

vertical at the surface, but they probably dip steeply toward the crater at depth. On the northwest rim, where the crater outline is chordlike, rather than arcuate, the cracks continue far back of the edge and tend to complete the pit's circular outline.

Figure 20.2, an outline map of Halemaumau, shows the progressive enlargement of the crater during 3 consecutive intervals (1928–45, 1945–52, 1952–61) in the 33-year period between 1928 and 1961. The 1928 outline is based on a topographic survey made by R. M. Wilson (Jaggar, 1930); the 1945 outline on an aerial photomosaic; and the 1952 and 1961 outlines on planetable mapping and triangulation by G. A. Macdonald, W. E. Benson, and the authors. The precision of matching each successively older outline with the 1961 outline decreases because of the removal of recogniz-

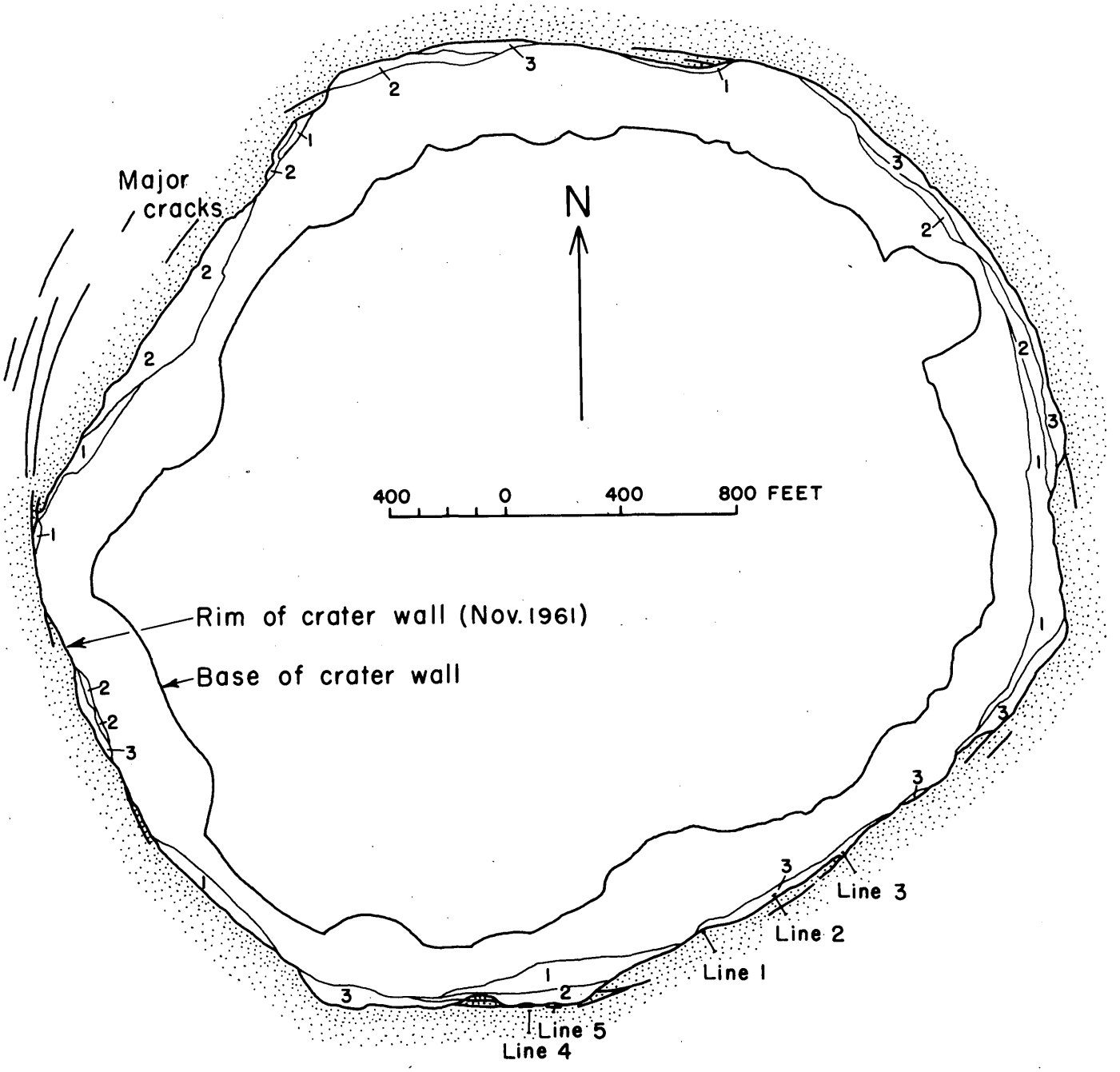

FIGURE 20.2.—Outline map of Halemaumau showing major peripheral cracks and rim recession due to landsliding between 1928 and 1961. Recession is divided into three periods: 1, 1928–45; 2, 1945–52; and 3, 1952–61. Positions of measured lines plotted on figure 20.3 is shown by lines 1–5.

able features by sliding. Since 1928 the crater opening on the caldera floor has grown in area from 942,000 to 998,000 square yards, an increase of 56,000 square yards or almost 6 percent (see table below). The average annual growth for the 3 time intervals varies from 1,300 to 2,200 square yards per year. Average annual growth throughout the entire 33-year period is 1,700 square yards per year, equivalent to a rate of rim recession averaging 1.5 feet per year. However, as is shown in figure 20.2, the growth pattern has been neither consistent nor regular, and some 15 percent of the original 1928 rim still remains standing. Greatest attrition has occurred on the east, northeast, south, and northwest parts of the crater, where the rim has retreated as much as 150 feet in the last 33 years.

Increase in area of Halemaumau during the period 1928–61.

Year	Area (square yards)	Increase (square yards)	Rate (square yards per year)	Rate of rim recession (feet per year)
1928	942, 000			
		22, 000	1, 300	1. 1
1945	964, 000			
		14, 000	2, 000	1. 7
1952	978, 000			
		20, 000	2, 200	2. 0
1961	998, 000			
33-year average			1, 700	1. 5

For many years the width of individual cracks around Halemaumau has been periodically measured in an attempt to correlate the opening of cracks with volcanic activity and, in the interest of public safety, to ascertain which areas along the crater rim are likely to collapse. The pattern of crack development determined from these individual measurements, however, is not consistent. Most of the cracks, if they are not lost in collapse, have opened irregularly since the measurements began, with unaccountable periods of no change and even of measurable closing. Moreover, some cracks have shown a marked increase in opening preceding an eruption (Macdonald, 1955) while others have shown an increase following eruption (Jaggar, 1930).

In the belief that measurements along lines perpendicular to the crater rim and spanning a number of peripheral cracks might be more definitive, measurements were begun in the fall of 1959 along three lines normal to the rim (fig. 20.2, lines 1, 2, 3). The 3 lines, which average about 80 feet in length were measured from before the 1959 summit eruption until after the 1960 flank eruption. In May 1960 the rim-end pins of two lines fell into the crater on large slides. The dramatic increase in the length of all lines, culminating in the slides of May, is shown graphically in figure 20.3. Plotted on the same base are the eruption periods and the east-west component of ground tilting at Uwekahuna, 1 mile northwest of the center of Halemaumau. The tilt plot is a measure of the slight deformation, measured in radians, of the earth's surface in the Kilauea summit region caused by the accumulation and movement of magma within the volcano from April 1959 to November 1961. In response to the gradual accumulation of magma, preceding and during periods of summit activity, the summit region tumesces. Detumescence occurs when magma from within the volcano drains away into the rift zones, often producing a flank eruption (Eaton and Murata, 1960). Clearly, the accelerated rate of crack growth (fig. 20.3), began with the great detumescence of the dome in January 1960; there was no measurable effect on the length of the lines during the tumescence in October, November, and December 1959. Additional measurements along two new lines (fig. 20.2, lines 4, 5) during the 1960–61 period of tumescence and detumescence of Kilauea's dome are also shown on figure 20.3. As during the earlier observations, the relatively rapid tumescence, from the end of 1960 to September 1961, was not accompanied by a marked change in the length of the lines, but during the brief detumescence, in September 1961, the length of the lines increased measurably as rim cracks enlarged.

Although slides and rockfalls off the wall of Halemaumau are almost daily phenomena, the long-line measurements on the crater's rim reported here indicate that the opening of peripheral cracks, and hence growth of the crater, accelerates during detumescence of the volcanic dome. The reason for this correlation of accelerated crack opening with beginning of detumescence is not fully understood. Quite likely the withdrawal of magma from beneath the summit area, resulting in the removal of vertical support, may also substantially reduce the lateral support at the base of the crater and initiate crack opening. This appeared to be the case in the detumescence of January–March 1960 when almost the entire floor of Halemaumau dropped 100 to 350 feet. In the detumescence of September 1961, however, there was no evident physical change in the bottom of the crater. Strong, local earthquake activity accompanying detumescence is another factor that may play an important role in the development of new cracks and the widening of existent cracks.

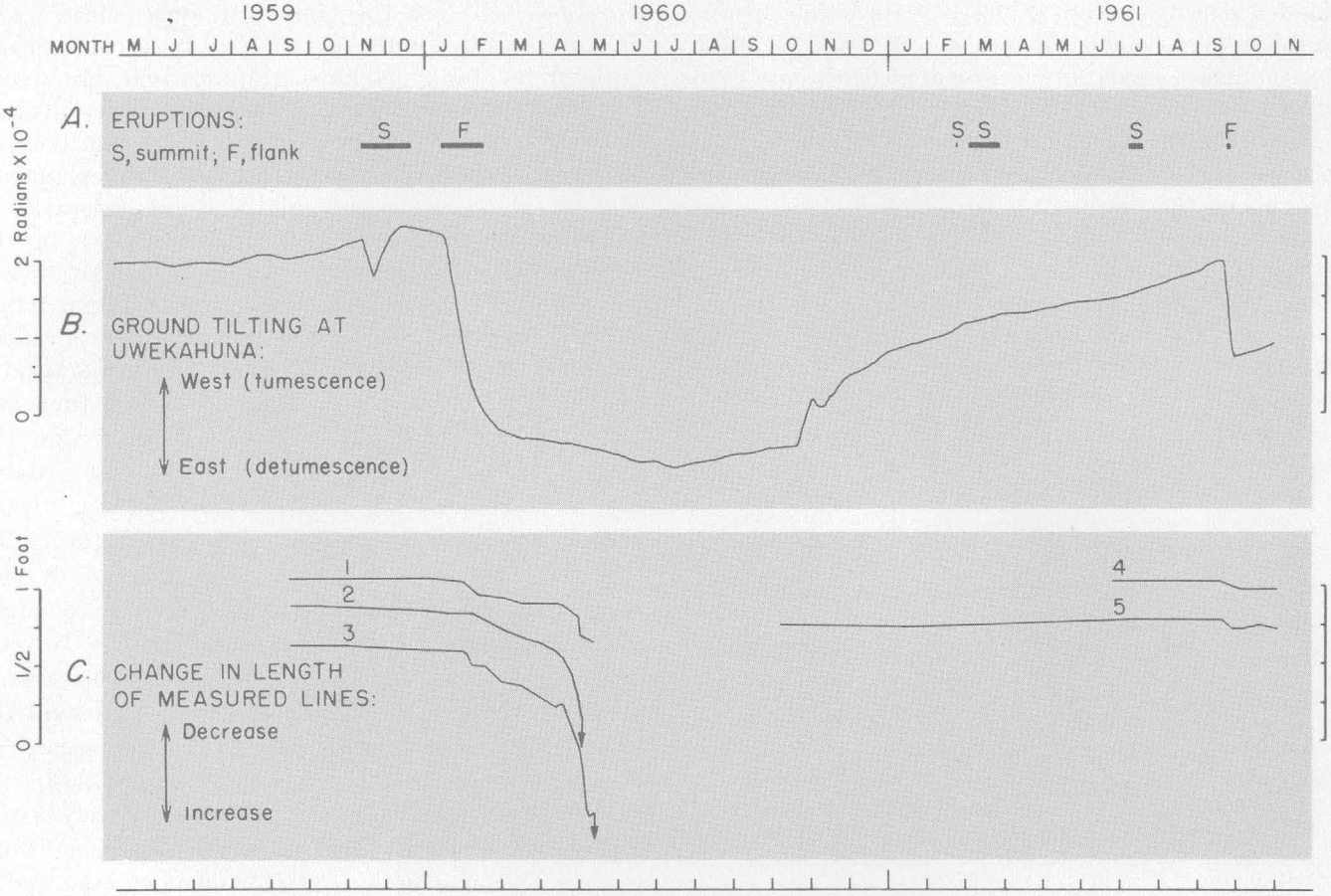

FIGURE 20.3.—Graph showing relations during period May 1959–November 1961 of: *A*, Kilauea eruptions; *B*, ground tilt at Uwekahuna in the Kilauea caldera area; and *C*, changes in the length of lines normal to the rim of Halemaumau.

REFERENCES

Eaton, J.P., and Murata, K. J., 1960, How volcanoes grow: Science, v. 132, p. 925–928.

Jaggar, T. A. 1930, Rim cracks and crater slides: Volcano Letter 283, p. 1–3.

Macdonald, G. A., 1955, Hawaiian volcanoes during 1952: U.S. Geol. Survey Bull. 1021–B, p. 1–108.

PALEONTOLOGY

21. MARGINAL SEA OF MIDDLE EOCENE AGE IN NEW JERSEY

By STEPHEN M. HERRICK, Atlanta, Ga.[1]

Perfectly preserved specimens of *Marginulina vacavillensis* (Hanna) and associated small Foraminifera in a test well in Camden County, N.J., suggest the presence of a sea in New Jersey in middle Eocene time similar to that of the Gulf coast. The nearest previously reported occurrence of this species was in a well in Liberty County, Ga. (Herrick, 1961a, p. 260). Previous to this, *Marginulina vacavillensis* had been

[1] Ruth Todd, U.S. Geological Survey, furnished the following significant identifications: *Pseudouvigerina wilcoxensis* and *Chiloguembelina martini* at a depth of 360 to 362 feet; *Globigerina bowerí* at 370 to 372 feet; and *Globorotalia bullbrooki* and *Truncatulinoides roheri* at 380 to 382 feet.

reported from western Florida (Herrick, 1961b, p. D239.) As this fossil was originally described from California (Hanna, 1923) its discovery in New Jersey (fig. 21.1) proves the distribution of this species in all the coastal plains of North America.

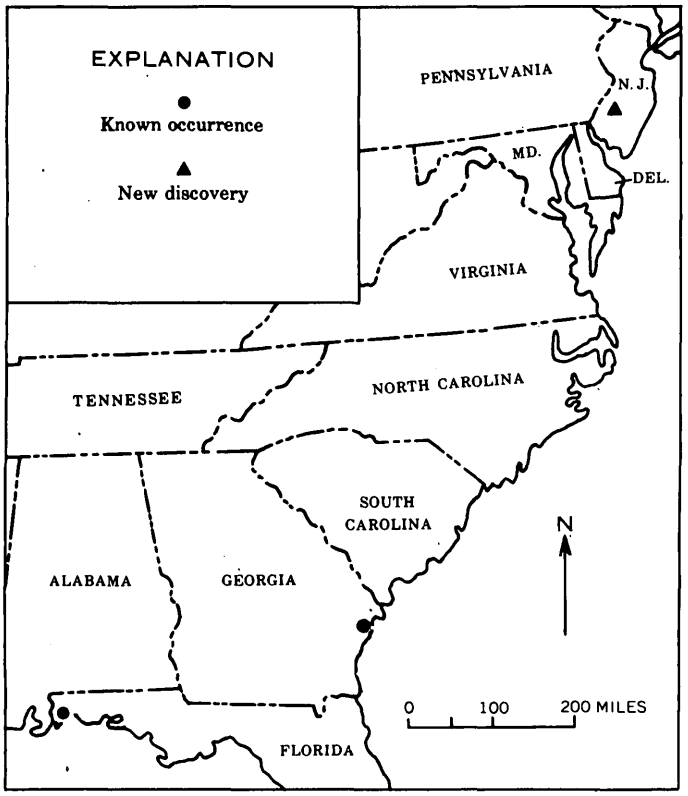

FIGURE 21.1.—Geographic distribution of *Marginulina vacavillensis* along the Atlantic and eastern Gulf coasts. New discovery is in U.S. Geological Survey New Brooklyn Park 2 well, Camden County, N.J.

Sediments containing the Foraminifera found in New Jersey were probably deposited in a marginal moderately deep sea—on the order of 80 fathoms (Wermund, 1961, p. 1682—which fluctuated at intervals during middle Eocene time. In spite of these fluctuations the sea persisted in New Jersey long enough for the deposition of approximately 140 feet of abundantly glauconitic sands, sandy clays, and marls, all of which are here regarded as the Manasquan Formation. These deposits bear a strong lithologic and faunal similarity to the Weches Greensand Member of the Mount Selman Formation of Texas and a strong faunal similarity to the Cook Mountain Formation of Louisiana (Howe, 1939). In addition to *Marginulina vacavillensis*, many foraminiferal species previously reported from the Cook Mountain Formation also are present in this microfauna (fig. 21.2).

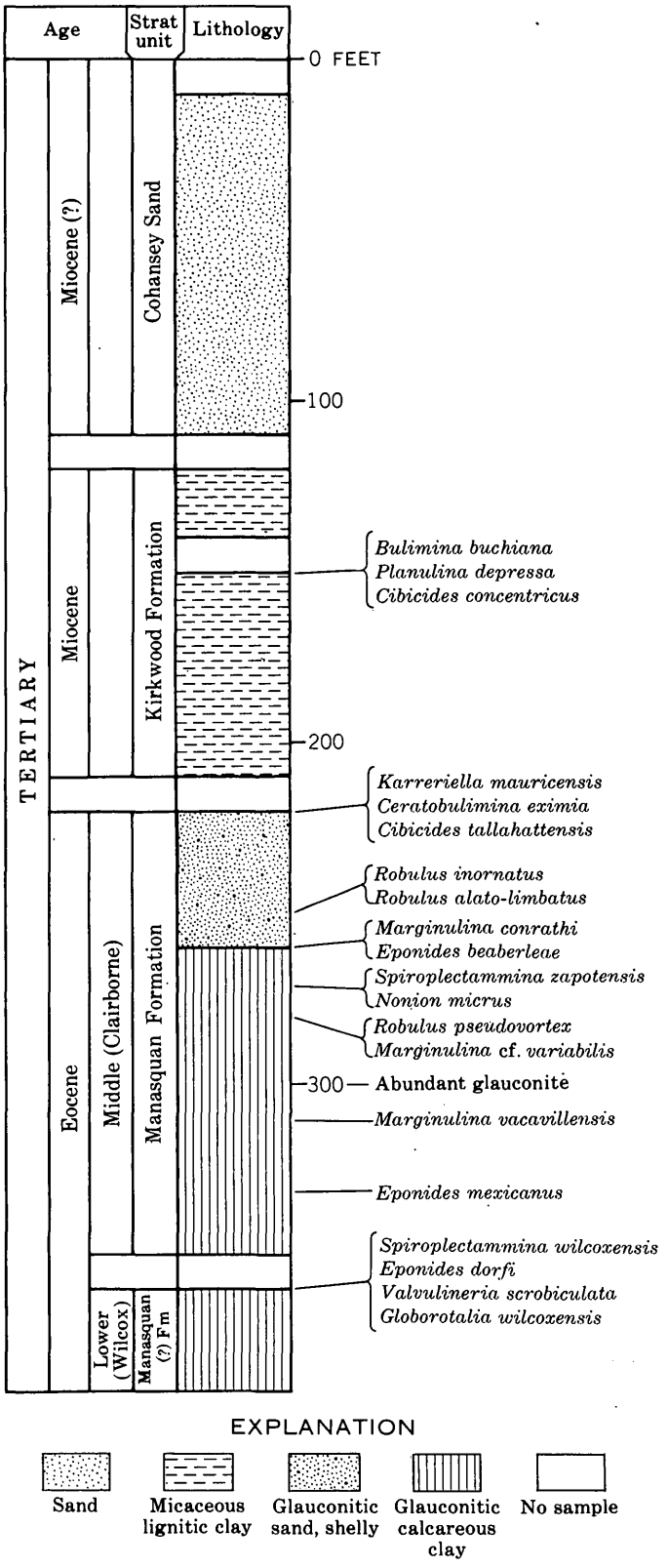

FIGURE 21.2—Log prepared from samples from the upper part of U.S. Geological Survey New Brooklyn Park 2 well, Camden County, N.J.

Ecologic studies of living organisms suggest that similar fossil species lived under similar environmental conditions. One may conclude from the evidence at hand, therefore, that a sea, similar to that known to have occupied the Gulf coast during middle Eocene time, also existed in coastal Georgia and New Jersey and probably in unreported intervening areas (the Carolinas and Virginia).

As far as the writer is aware this paper constitutes the first recognition of middle Eocene Foraminifera this far north in the Atlantic Coastal Plain. Spangler and Peterson (1950, p. 61) in a paper on the geology of the coastal plain in the central Atlantic States, consider the Manasquan Formation to be early Eocene (Wilcox) in age. On the basis of a few molluscan fossils, a vertebrate fossil, and a crab's claw, Miller (1956, p. 733) concludes that "the Manasquan Formation is mid-Eocene Claiborne in age." The age of the Manasquan has been considered by Loeblich and Tappan (1957, p. 1113) to be earliest Eocene (Ypresian). On the basis of previous work and information presented in this article, the age of the Manasquan is considered to be early and middle Eocene.

REFERENCES

Hanna, G. D., 1923, Some Eocene Foraminifera near Vacaville, California: California Univ. Dept. Geol. Sci. Bull., v. 14, no. 9, p. 319–328.

Herrick, S. M., 1961a, Well Logs of the Coastal Plain of Georgia: Georgia Dept. Mines, Mining, and Geology Bull. 70, 462 p.

——— 1961b, A stratigraphically significant association of smaller Foraminifera from western Florida: Art. 376 *in* U.S. Geol. Survey Prof. Paper 424–D, P. D239.

Howe, H. V., 1939, Louisana Cook Mountain Eocene Foraminifera: Louisiana State Dept. Conserv., Geol. Bull. 14, 122 p.

Loeblich, A. R., Jr., and Tappan, Helen, 1957, Correlation of the Gulf and Atlantic Coastal Plain, Paleocene and lower Eocene formations by means of planktonic Foraminifera: Jour. Paleontology, v. 31, no. 6, p. 1109–1137.

Miller, H. W., Jr., 1956, Correlation of Paleocene and Eocene formations and Cretaceous-Paleocene boundary in New Jersey: Am. Assoc. Petroleum Geologists Bull., v. 40, no. 4, p. 722–736.

Spangler, W. G., and Peterson, J. J., 1950, Geology of Atlantic Coastal Plain in New Jersey, Delaware, Maryland, and Virginia: Am. Assoc. Petroleum Geologists Bull., v. 34, no. 1, 99 p.

Wermund, E. G., 1961, Glauconite in early Tertiary sediments of Gulf Coastal Province: Am. Assoc. Petroleum Geologists Bull., v. 45, no. 10, p. 1667–1696.

22. RECENT DISCOVERIES OF THE CRETACEOUS AMMONITE *HARESICERAS* AND THEIR STRATIGRAPHIC SIGNIFICANCE

By William A. Cobban, Glenn R. Scott, and James R. Gill, Denver, Colo.

The Late Cretaceous ammonite *Haresiceras* was found in the Niobrara Formation near Pueblo, Colo., in October 1961. Owing to its association with the well known *Scaphites hippocrepis* (DeKay) of early Campanian age, *Haresiceras* has been considered a guide fossil to that Cretaceous stage (Cobban and Reeside, 1952, p. 1019, and correlation chart). The discovery of *Haresiceras* near Pueblo thus provides evidence of a long-suspected early Campanian age for the upper part of the Niobrara of the central Great Plains (Jeletzky, 1955). The purpose of this paper is to discuss the stratigraphic implications of this discovery and to bring up to date the known records of occurrences of *Haresiceras*.

Haresiceras was proposed by Reeside (1927, p. 17) to include ammonites that have compressed whorls, narrow umbilicus, flat venter bordered by two rows of very small nodes, and subparallel flanks crossed by weak sigmoidal ribs. Reeside described three species: *H. placentiforme* from the Telegraph Creek Formation of Park County, Wyo., *H. natronense* from the Cody Shale of Natrona County, Wyo., and *H. fisheri* from the Mancos Shale of Emery County, Utah.

Haresiceras was first found by C. J. Hares in 1916. The genus is now known from 23 Geological Survey Mesozoic localities in the western interior of the conterminous United States, 18 of which have been recorded in earlier reports. Reeside (1927, distribution table) listed 13 occurrences in Utah, Colorado, Wyoming, South Dakota, and Montana from rocks now assigned to the Mancos Shale, Cody Shale, Telegraph Creek Formation, and Gammon Ferruginous Member of the Pierre Shale. Five other occurrences in the Cody Shale of central Wyoming have been recorded by Yenne and Pipiringos (1954), Hose (1955, p. 96), and Keefer and Troyer (1956).

New occurrences of *Haresiceras* are listed below with their Geological Survey Mesozoic catalog numbers:

23477. NE¼NE¼ sec. 13, T. 9 S., R. 61 E., Carter County, Mont. From gray limestone concretions in Gammon Ferruginous Member of Pierre Shale about 130 feet below Groat Sandstone Bed and 460 feet above top of Niobrara Formation. *Haresiceras placentiforme.*

D1847. Three miles north of Bear Butte in the NE¼NE¼ sec. 6, T. 6 N., R. 6 E., Meade County, S. Dak. From marlstone lens in lower part of Gammon Ferruginous Member of Pierre Shale. *Haresiceras natronense.*

D1849. About 3.5 miles south of Alkali Creek in the NW¼ sec. 9, T. 4 N., R. 8 E., Meade County, S. Dak. From marlstone lens 50 feet above base of Gammon Ferruginous Member of Pierre Shale. *Haresiceras natronense.*

D2827. Four miles north of Boulder in the SW¼SE¼ sec. 1, T. 1 N., R. 71 W., Boulder County, Colo. From 28 feet below top of Niobrara Formation (base of upper yellowish-orange chalky limestone unit of Smoky Hill Shale Member). *Haresiceras natronense*(?)

D3266. One mile east of Apishapa River on small spur at base of mesa in the NE¼SW¼NW¼ sec. 23, T. 23 S., R. 59 W., Otero County, Colo. From 84 feet below top of Niobrara Formation (platy yellowish-gray chalky limestone about 70 feet below upper yellowish-orange chalky limestone unit of Smoky Hill Shale Member). *Haresiceras placentiforme.*

The last four localities are of exceptional interest in that they are the first records of *Haresiceras* in South Dakota east of the Black Hills and in Colorado east of the Front Range. The two collections from east of the Black Hills were made by Gill from grayish-orange-weathering marlstone in a partly calcareous shale unit assigned by the writers to the Gammon Ferruginous Member of the Pierre Shale but clearly transitional into Niobrara lithology. The fossils are chiefly impressions but include a few well-preserved uncrushed septate coils. *Scaphites aquilaensis* Reeside and a fine-ribbed form of *Scaphites hippocrepis* (DeKay) are associated with the *Haresiceras* at the Bear Butte locality (D1847). The two collections from the Front Range area in Colorado were made by Scott from rocks of unquestioned Niobrara lithology. The collection from locality D2827 near Boulder consists of an impression of part of a very large specimen that does not show the venter. The strongly ribbed flanks suggest assignment to *H. natronense.* The collection from Otero County (D3266) consists of rather poor impressions of 15 weakly ribbed specimens assigned to *H. placentiforme.* These are associated with impressions of fragments of scaphites that could be *S. hippocrepis.*

Haresiceras placentiforme and *H. natronense* have not been found together. The holotype of *H. placentiforme* came from the Elk Basin Sandstone Member of the Telegraph Creek Formation in the Elk Basin oil field along the boundary of Montana and Wyoming where it was associated with coarse-ribbed forms of *Scaphites hippocrepis.* The type of *H. natronense* came from the Cody Shale 200 feet below the Shannon Sandstone Member in the Salt Creek oil field in Natrona County, Wyo. Fossil collections made subsequently by Gill at that locality show that a level 200 feet below the Shannon Sandstone Member is near the top of the range of *S. hippocrepis* and that the late form of this scaphite is characterized by fine ribbing. The Eagle Sandstone of central and south-central Montana contains this type of scaphite. A preliminary study of the collections of *Haresiceras* from all localities in the western interior region shows that *H. placentiforme* is older than *H. natronense* and is associated with a coarser form of *S. hippocrepis.* Both coarse- and fine-ribbed forms of *S. hippocrepis* were figured by Grossouvre (1893, pl. 32, figs. 2, 3a, 3b; pl. 35, figs. 6a-c; pl. 37, figs. 3a, 3b) and assigned to the Campanian.

The Telegraph Creek Formation at Elk Basin overlies undifferentiated "Niobrara and Carlile Shales" (Dobbin and others, 1945). Farther east on the northwest flank of the Powder River Basin the Telegraph Creek is treated as a member of the Cody Shale and overlies the Niobrara Shale Member of the Cody which is in part calcareous (Richards, 1955, p. 55). The occurrence of *Haresiceras placentiforme* in the Telegraph Creek Formation at Elk Basin and in the Niobrara Formation near Pueblo, Colo., shows that the top of the Niobrara rises in time in a southeasterly direction. That the Eagle Sandstone, which overlies the Telegraph Creek Formation, is also a time equivalent to the upper part of the Niobrara Formation is suggested by the occurrence of *H. natronense* associated with fine-ribbed forms of *Scaphites hippocrepis* in Niobrara and Pierre transition rocks on the east side of the Black Hills uplift and by the presence of what appears to be *H. natronense* within the Niobrara Formation in Colorado.

629660—62——5

REFERENCES

Cobban, W. A., and Reeside, J. B., Jr., 1952, Correlation of the Cretaceous formations of the Western Interior of the United States: Geol. Soc. America Bull., v. 63, no. 10, p. 1011–1044.

Dobbin, C. E., and others, 1945, Geologic and structure map of the Elk Basin oil and gas field and vicinity, Park County,

Wyoming, and Carbon County, Montana: U.S. Geol. Survey General Mineral Resources Map.

Grossouvre, A. de, 1893, Recherches sur la Craie Supérieure, pt. 2, Paléontologie, Les ammonites de la Craie Supérieure: Mém. Carte géol. France, 264 p. [1894].

Hose, R. K., 1955, Geology of the Crazy Woman Creek area, Johnson County, Wyoming: U.S. Geol. Survey Bull. 1027–B, p. 33–118.

Jeletzky, J. A., 1955, *Belemnitella praecursor*, probably from the Niobrara of Kansas, and some stratigraphic implications: Jour. Paleontology, v. 29, no. 5, p. 876–885.

Keefer, W. R., and Troyer, M. L., 1956, Stratigraphy of the Upper Cretaceous and lower Tertiary rocks of the Shotgun Butte area, Fremont County, Wyoming: U.S. Geol. Survey Oil and Gas Inv. Chart OC–56.

Reeside, J. B., Jr., 1927, The cephalopods of the Eagle Sandstone and related formations in the Western Interior of the United States: U.S. Geol. Survey Prof. Paper 151, p. 1–87.

Richards, P. W., 1955, Geology of the Bighorn Canyon-Hardin area, Montana and Wyoming: U.S. Geol. Survey Bull. 1062, p. 1–93.

Yenne, K. A., and Pipiringos, G. N., 1954, Stratigraphic sections of Cody Shale and younger Cretaceous and Paleocene rocks in the Wind River Basin, Fremont County, Wyoming: U.S. Geol. Survey Oil and Gas Inv. Chart OC–49.

23. TRIASSIC FOSSILS FROM THE SOUTHERN KLAMATH MOUNTAINS, CALIFORNIA

By N. J. Silberling and W. P. Irwin, Menlo Park, Calif.

Fossils recently collected near the mutual boundary of Tehama, Trinity, and Shasta Counties in northwestern California confirm the Late Triassic age of some of the eugeosynclinal rocks included by Irwin (1960, fig. 3, p. 20–26) in the "Western Paleozoic and Triassic Belt" of the Klamath Mountains. Heretofore, the presence of Triassic rocks in this belt was indicated by its continuance northward into exposures of the Applegate Group, which was assigned a Late(?) Triassic age by Wells, Hotz, and Cater(1949, p. 3, 4), and by several small, poorly preserved specimens of the Triassic ammonite *Arcestes* in one of several collections made by Diller (1903, p. 344–356) in the southern Klamath Mountains. The new collection of fossils described here provides a relatively precise age determination for one locality in this large structurally and stratigraphically complex belt, and it demonstrates that well-preserved biologically and stratigraphically useful faunas can be found in these rocks, which for the most part have not yet received detailed study.

In May and October 1961, the writers attempted to relocate Diller's ammonite locality near White Rock, a prominent limestone outcrop on the divide between the drainages of the Sacramento and Trinity Rivers about 5 miles northwest of North Yolla Bolly Mountain. At the approximate location given by Diller a concentration of fossiliferous limestone float was found in an area underlain mostly by mafic volcanic rocks and thin-bedded radiolarian chert. Its localized occurrence near the crest of the drainage divide and its proximity to outcrops of limestone interstratified with volcanic rocks and chert indicates that this fossiliferous float was derived more or less in place from a small limestone lens which may have been only several inches thick and a few feet long.

The fauna obtained from this locality (USGS Mesozoic locality M1140; see locality list at end of paper) is surprisingly diverse and well preserved, although the cephalopods are mainly small immature specimens which cannot be identified positively as to species. Of foremost age significance are the ammonites, which include:

Clionitites cf. *C. angulosus* (Mojsisovics)
Lecanites sp.
Styrites cf. *S. vermetus* (Dittmar)
Juvavites sp.
Arcestes sp.
Cladiscites cf. *C. pusillus* (Mojsisovics)
Megaphyllites cf. *M. jarbas* (Munster)
Placites cf. *P. placoides* (Mojsisovics)
Mojsvarites cf. *M. eugyrus* (Mojsisovics)

Also present are shell fragments of the pelecypod *Halobia* with ribbing like that of *H. austriaca* Mojsisovics; pectenid, pteriid, nuculid, and other pelecypods; indeterminate gastropods; orthoconic nautiloids; rhynchonellid, spiriferid, terebratulid, and lingulid brachiopods; and crinoid columnals. The ammonites for the most part belong to long-ranging genera including some that first appear in the upper Middle Triassic and others that range through the Upper Triassic. The association of ammonite genera, however, is distinctive and unlike that of any other known fauna from the

Triassic of North America. The genera and species of ammonites represented are most like those of the middle Karnian fauna of the *Trachyceras aonoides* zone, described by Mojsisovics (1893, p. 796–798; 1902, p. 336–337) from the Hallstatt region of Austria. The ammonites from near White Rock thus represent a somewhat older part of the Karnian than the rich late Karnian ammonite fauna, monographed by J. P. Smith (1927), from the so-called Hosselkus Limestone about 60 miles to the northeast in the easternmost Klamath Mountains.

The fauna from the limestone float at locality M1140 is markedly different from that of nearby larger masses of limestone, some of which have an outcrop area of several acres or more. These large limestone bodies, such as White Rock (USGS Mesozoic localities M1217 and M1218) and a conspicuous limestone about 5 miles to the northwest on the divide between Hayfork and Prospect Creeks (USGS Mesozoic locality M1216), consist of massive pure somewhat recrystallized organic detrital limestone bounded on all sides by volcanic rocks. Recognizable fossils are scarce, though fragmentary scleractinian corals, hydrozoans, bryozoa, and calcareous algae were found in both limestone bodies. Some of these fossils are indicative of an early Mesozoic age, but they provide no basis for detailed age assignment.

LOCALITIES CITED

[All localities in southern Klamath Mountains, Calif.]

USGS Mesozoic loc. M1140. Near boundary between Trinity and Tehama Counties about ½ mile west of White Rock limestone. Float blocks of limestone found together on south side of Sacramento Valley–Trinity River drainage divide just downhill from low saddle on crest. Center of E½ sec. 19, T. 28 N., R. 10 W., Dubakella Mt. 15-min. quad. Collected by N. J. Silberling, D. L. Jones, and W. P. Irwin, May 1961. [Possibly the same as loc. 705 of Diller (1903, p. 344).]

USGS Mesozoic loc. M1216. Trinity County. Conspicuous limestone mass on north side near crest of ridge between Hayfork and Prospect Creeks. NE¼NE¼ sec. 4, T. 28 N., R. 11 W. Dubakella Mt. 15-min. quad. Collected by N. J. Silberling and W. P. Irwin, October 1961. [Approximately the same as locs. 703 and 706 of Diller (1903, p. 346).]

USGS Mesozoic loc. M1217. Near boundary between Trinity and Tehama Counties. Isolated limestone mass about 1/10 mile north of main White Rock limestone outcrop area. On north side near crest of Sacramento Valley-Trinity River drainage divide. Center of W¼ sec. 20, T. 28 N., R. 10 W. Dubakella Mt. 15–min, quad. Collected by N. J. Silberling and W. P. Irwin, October 1961.

USGS Mesozoic loc. M1218. Near boundary between Trinity and Tehama Counties. Northeast end of main White Rock limestone outcrop area. On south side near crest of Sacramento Valley-Trinity River drainage divide. Center of W½ sec. 20, T. 28 N., R. 10 W. Dubakella Mt. 15-min. quad. Collected by N. J. Silberling and W. P. Irwin, October 1961. [Approximately the same as loc. 704 of Diller (1903, p. 344).]

REFERENCES

Diller, J. S., 1903, Klamath Moutain section. Am. Jour. Sci., ser. 4, v. 15, p. 342–362.

Irwin, W. P., 1960, Geologic reconnaissance of the northern Coast Ranges and Klamath Mountains, California: California Div. Mines Bull. 179, 80 p.

Mojsisovics, Edmund von, 1893, Die Cephalopoden der Hallstätter Kalke: Abh. geol. Reichsanst. Wien, Band 6, Hälfte 2, 835 p., pls. 71–200.

——— 1902, Die Cephalopoden der Halstätter Kalke. Suppl.-Heft: Abh. Geol. Reichsanst. Wien, Band 6, Hälfte 1, p. 175–356, 23 pls.

Smith, J. P., 1927, Upper Triassic marine invertebrate faunas of North America; U.S. Geol. Survey Prof. Paper 141, 262 p., 121 pls.

Wells, F. G., Hotz, P. E., and Cater, F. W., Jr., 1949, Preliminary description of the geology of the Kerby quadrangle, Oregon; Oregon Dept. Geology and Mineral Industries Bull. 40, 23 p.

GEOPHYSICS

24. THERMAL REGIME IN THE RAISED DELTA OF CENTRUM SØ, NORTHEAST GREENLAND

By Daniel B. Krinsley, Washington, D.C.

Work done in cooperation with Air Force Cambridge Research Laboratories

Centrum Sø (lake), lat 80° 10′ N. and long 22° W., occupies a northeast-oriented glacial valley that has been cut 2,300 feet below an extensive plateau. The lake is 12 miles long and 2.5 miles wide near its midpoint (fig. 24.1); the surface of the lake is 328 feet above sea level. The principal tributaries, Saefaxi Elv and Graeselven [1] (rivers), originate at the margin of the Greenland Ice Cap 25 miles west and southwest of the lake. The outlet into Lower Saefaxi Elv, at the east end of the lake, is 20 miles from the sea at Hekla Sund.

[1] Provisional name.

The bedrock surrounding the western two-thirds of the lake is part of a thick series of banded dark limestones and lighter dolomitic beds of Ordovician and Silurian age (Centrum Limestone). The beds dip gently eastward but are tightly folded locally. East of the Centrum Limestone along an approximately north strike, older dolomitic rocks, most of which are of Precambrian age, have been thrust over the Silurian limestones (Fränkl, E., 1954).

Glacial and glaciolacustrine deposits of variable thickness mantle the lower slopes and the high plateau above the lake. Recessional moraines on the plateau are

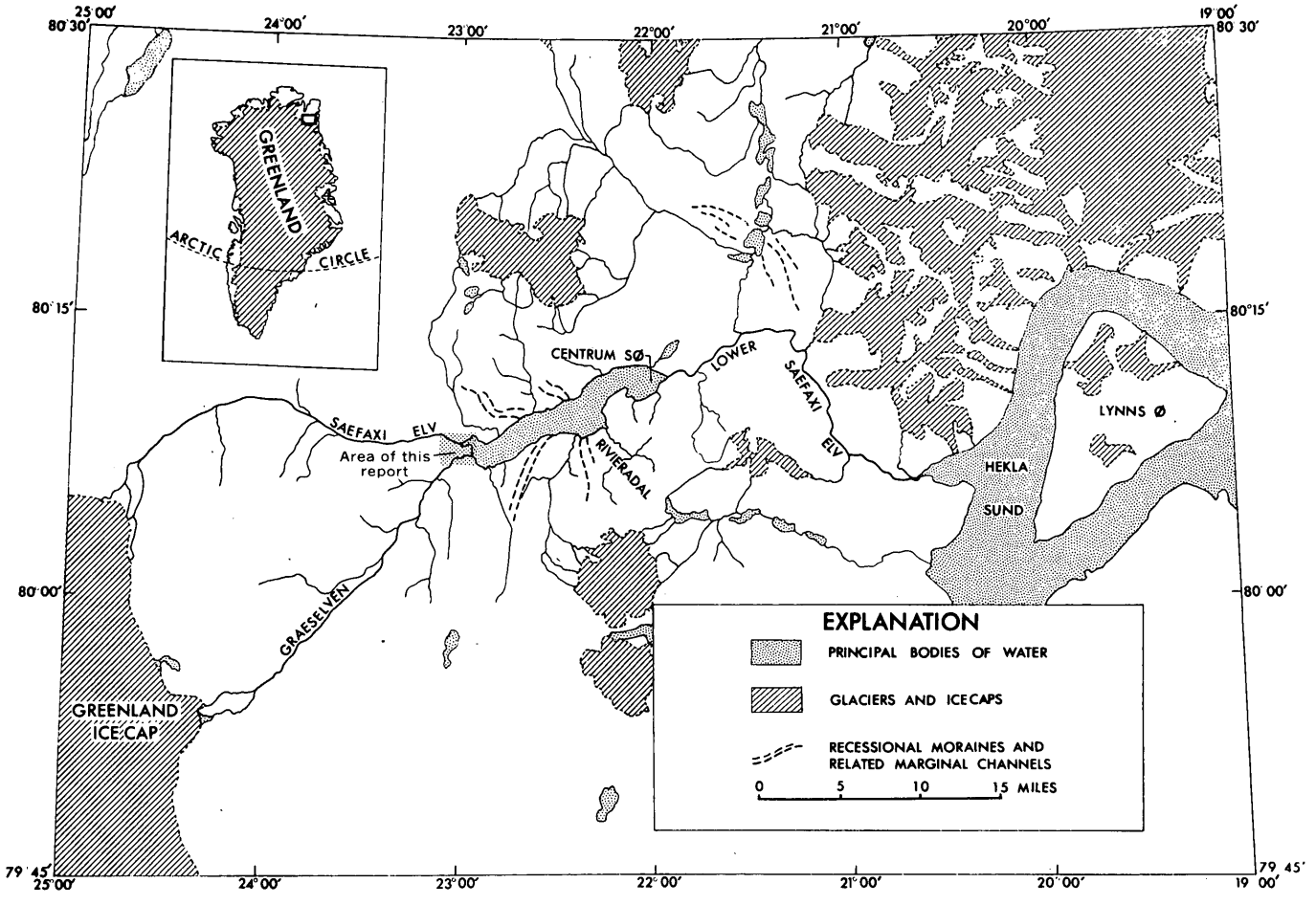

FIGURE 24.1.—Map of the Centrum Sø area.

convex downvalley and, along with associated marginal channels which have been cut in the steep valley slopes, have been traced westward to the margin of the Greenland Ice Cap (Krinsley, 1961). Well-preserved lake terraces, as much as 256 feet above the present lake surface, overlie coarse morainal materials and grade into extensive lacustrine deposits of fine sandy red silt and coarser ice-rafted materials at the outlet of the lake. Random shallow corings along the lake bottom consist uniformly of fine red silt.

Centrum Sø freezes over in late September, and the ice breaks up in June; the lake is generally ice free by late July. There are no meteorological records for the winter months; the nearest weather station at Nord, 127 miles northeast, has a considerably wetter climate so that extrapolation is not reliable. Meteorological data collected during the field season of 1960, together with the reports of previous summer and winter visitors, suggest that the Centrum Sø area is an arctic desert with a total annual precipitation of 4 to 6 inches. In 1960, mean daily air temperatures ranged from −20.0°C to 5.0°C in May; −6°C to 13.0°C in June, and from 12.0°C to 14.0°C in July. The prevailing wind was from the west in May and June and from the southwest in July. Mean wind speed was about 8 miles per hour from May through July. On June 9, a windstorm from the north produced gusts of as much as 42 miles per hour.

A deltaic deposit formed by the coalescence of Saefaxi Elv and Graeselven, when the lake level was 24 feet higher than at present, now occupies a triangular area between the tributaries at the west end of the lake (fig. 24.2). This raised delta, the apex of which is oriented toward the east, is 1.2 miles long, and 1,500 feet wide at its midpoint. Near the east end of the delta, the foreset beds dip 28° NE.; at the center the dip is 4° NE. The delta is composed of alternating layers of sand and sand with pebbles and granules of limestone and crystalline materials. The composition and structure of the delta indicate that it was constructed primarily from crystalline and sedimentary rocks carried by Graeselven from areas near the margin of the icecap (fig. 24.1).

The deltaic deposits are covered with as much as 4 inches of silty (eolian) sand containing dreikanter pebbles and granules. Neither clay sizes nor particles larger than a pebble have been observed in the delta. Low-center polygons ranging from 3 to 22 feet in diam-

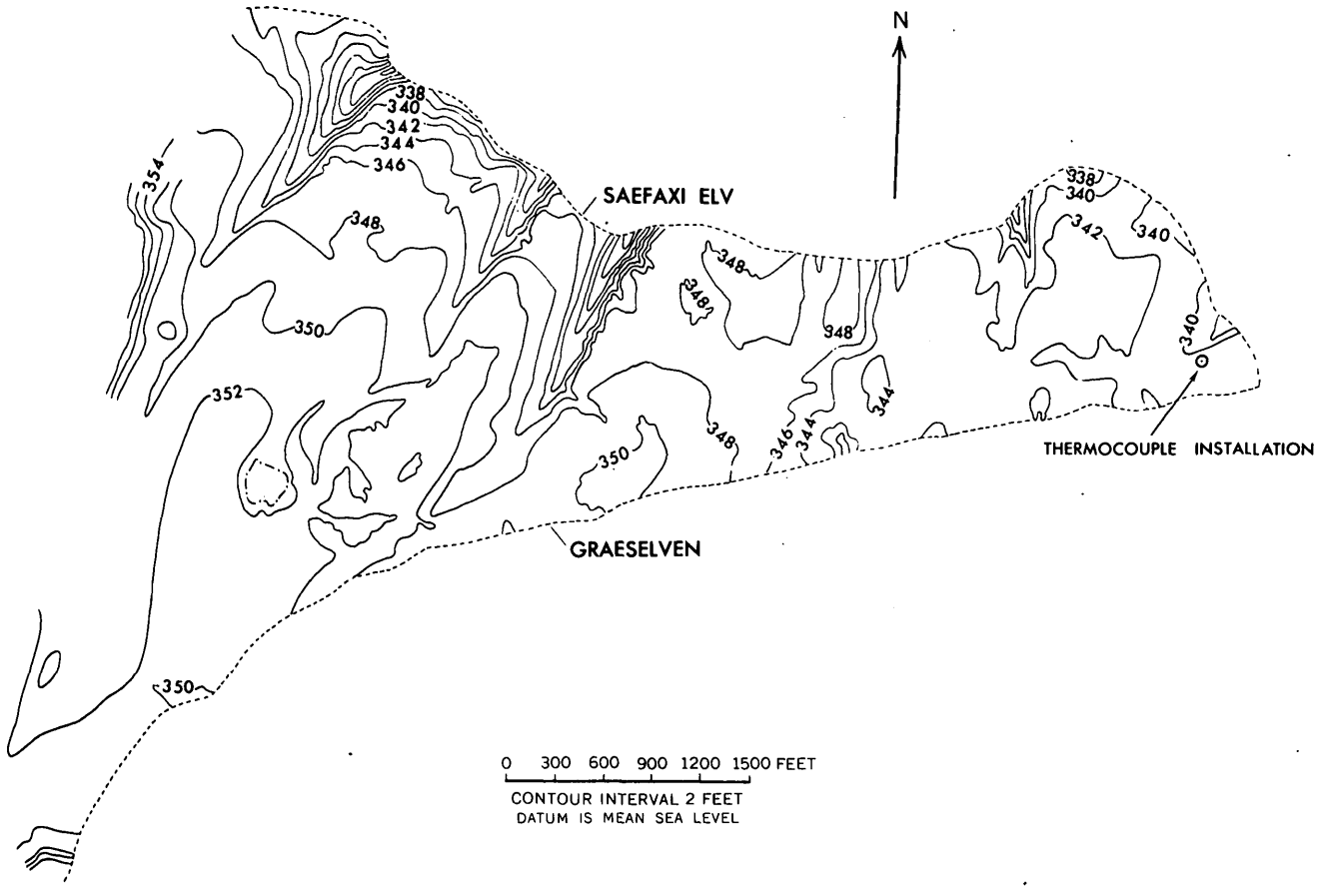

FIGURE 24.2.—Generalized map of the raised delta of Centrum Sø.

eter with borders rising as much as 4.7 inches are best developed in the east half of the delta. The west half is characterized by blowouts as much as 30 inches deep, sand mounds 1 foot high, covered with low arctic plants, and wide gullies, most of which drain into Saefaxi Elv. Some blowouts are filled with water during the June thaw.

Currently the delta is eroded by gullying during the snowmelt period (June 1–15) and by lateral stream cutting from Saefaxi Elv and Graeselven. Deflation during the snow-free period (June 15 to September 15) is an important mechanism for surficial erosion.

In May, the frost table was approximately 12 inches below the surface at the center of the delta and dipped gently to 16 inches below the surface at the northeast edge of the delta. On May 19, a hole 60 inches deep was drilled in the center of a polygon which was located 300 feet from the east end of the delta (fig. 24.2). A thermocouple cable was lowered into the hole and thermocouples were placed 60, 36, 22.5, 20.5, and 2 inches below the surface; one thermocouple was installed 4 inches above the surface. At the time of the installation, the frost table was approximately 12 inches below the surface, but the thermal regime was disrupted by the drilling and the frost table was lowered locally as much as 4 inches within a 2-day period. The disruption of the thermal regime abated during the second week in June, approximately 3 weeks after the installation (fig. 24.3).

The following general characteristics of the thermal regime may be inferred from the observed data, although the period of observation was relatively short and the disturbed ground did not have sufficient time for complete thermal stabilization. Ground temperatures start to rise as soon as the insulating snow cover has been removed (about May 15). Sublimation appears to be far more important in snow removal than melting, consequently there is little downward trans-

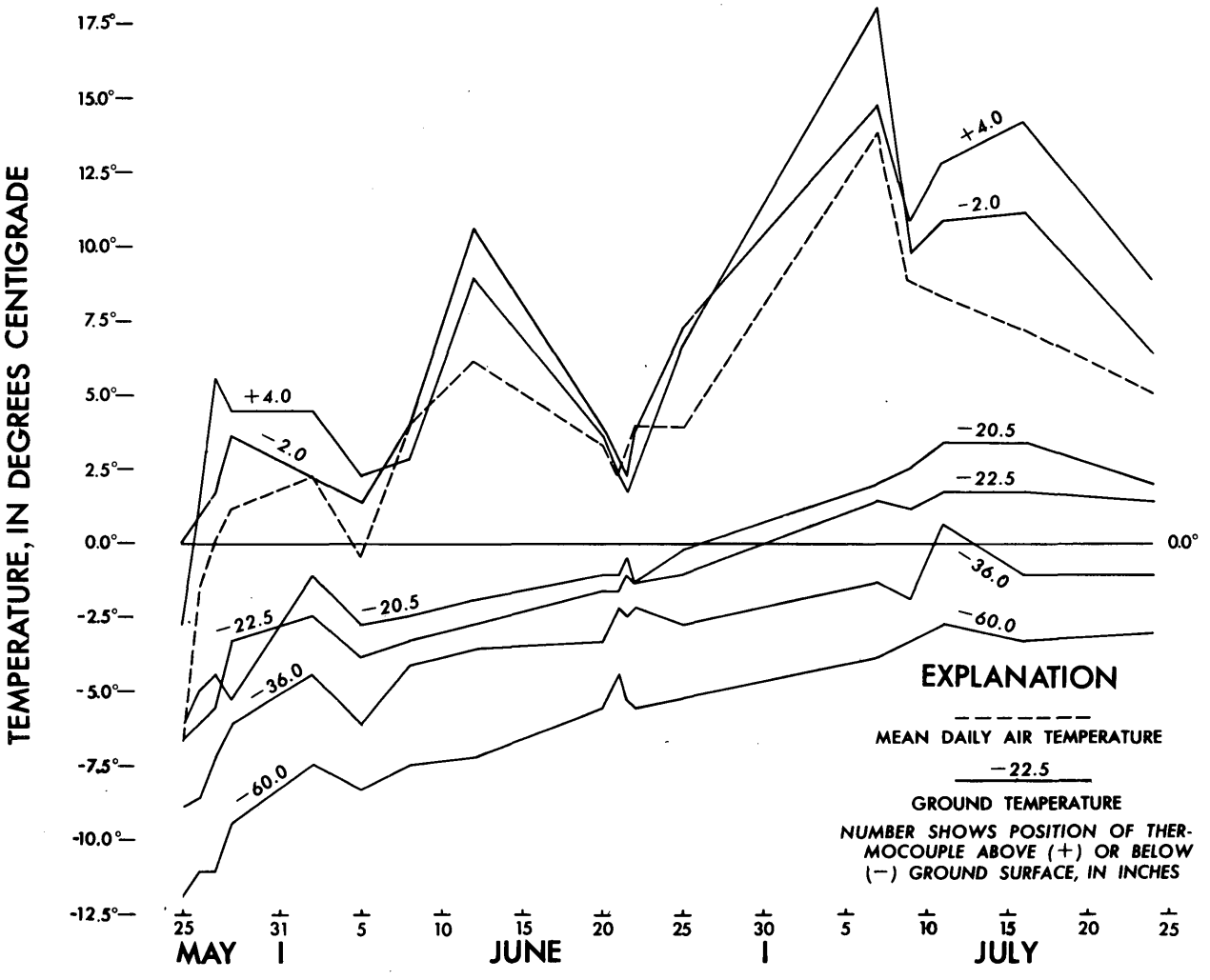

FIGURE 24.3.—Air and ground temperatures in the raised delta of Centrum Sø.

mission of heat from melt water during this period. The maximum increase in ground temperatures occurs between the last week in May and the second week in July. After mid-July the ground temperatures continue to rise slowly even though the air temperatures fall sharply. The frost table on July 25 was 30 inches below the surface at the thermocouple cable site. The flattening of the ground-temperature curves during late July (fig. 24.3) suggests that the permafrost table is probably at a depth of 40 inches. Consequently, the active layer is approximately 40 inches thick.

REFERENCES

Fränkl, E., 1954, Vorlaufige Mitteilung uber die Geologie von Kronprins Christians Land: Meddelelser om Grønland, bd. 116, nr. 2.

Krinsley, D. B., 1961, Late Pleistocene glaciation in Northeast Greenland; Geology of the Arctic: Toronto, Toronto Univ. Press, v. 2, p. 747–751.

25. MAGNETIC ANOMALIES AND ULTRAMAFIC ROCK IN NORTHERN CALIFORNIA

By WILLIAM P. IRWIN and GORDON D. BATH, Menlo Park, Calif.

Work done in cooperation with the California Division of Mines and Geology

Large positive magnetic anomalies are shown by aerial traverses across the northern Coast Ranges, Great Valley, and Klamath Mountains of California. Seven reconnaissance aeromagnetic traverses shown as line *B–B′* through *H–H′* (fig. 25.1) were flown by R. W. Bromery in 1954 in conjunction with a geologic reconnaissance (Irwin, 1960). Line *A–A′* is the western part of a traverse flown from Denver, Colo., to Pt. Reyes, Calif. (Balsley, 1953). The area of contoured anomalies in the Great Valley (fig. 25.1) was flown during the period 1951 to 1954 (Grantz and Zietz, 1960).

In both the northern Coast Ranges and Klamath Mountains the large positive anomalies are chiefly over areas of ultramafic rock (fig. 25.1), and nearly all samples of ultramafic rock that were collected are strongly magnetic. Thus, the ultramafic rocks are thought to cause the principal anomalies.

In the southern part of the Klamath Mountains the linear bodies of ultramafic rocks generally reflect the prevailing northwesterly lithic and structural grain. The largest exposure of ultramafic rock, however, is an irregular area in the east-central part of the province, crossed at its south end by traverse line *F–F′* and slightly beyond its north end by line *G–G′*. This large irregular area is interpreted to be the exposed crest of a great, broadly arched, sheetlike mass of ultramafic and gabbroic rock. Positive magnetic anomalies along traverse lines *F–F′* and *G–G′* are greatest in the general vicinity of this ultramafic mass. Along line *E–E′*, the maximum high of the broad anomaly lies well east of the easternmost linear mass of ultramafic rock in the southern part of the Klamath Mountains. However, this seeming departure from the general pattern of positional correlation of magnetic anomalies and ultramafic rocks might be explained by the fact that this ultramafic mass is a sill that dips eastward, and thus the magnetic anomaly may reflect a sheetlike extension of the sill at depth.

The principal body of ultramafic rock in the northern Coast Ranges, exposed along the western border of the Great Valley, separates rocks of the shelf and slope facies of late Mesozoic age on the east from chiefly eugeosynclinal rocks of late Mesozoic age on the west. It has a total length of more than 110 miles from where it is crossed by traverse line *A–A′* to beyond line *C–C′*, although in the southern part it is discontinuous at many places owing to faulting. Large positive magnetic anomalies are shown along traverse lines *A–A′*, *B–B′*, and *C–C′* where the lines cross this body of ultramafic rocks. These anomalies are on the west limb of the broad and generally stronger Great Valley anomaly.

The Great Valley anomaly trends along nearly the entire length of the Great Valley for more than 300 miles. Jenny (1932) reported that it extended along the valley from Red Bluff in the north through Stockton to Bakersfield in the south. Only the northern part of the Great Valley anomaly is shown on figure 25.1, indicated by the contoured area (Grantz and Zietz, 1960) and by the profiles along lines *A–A′* and *B–B′*.

The Great Valley is underlain by a thick section of mildly deformed strata of late Mesozoic and Cenozoic age, and along the anomaly the depth to the basement

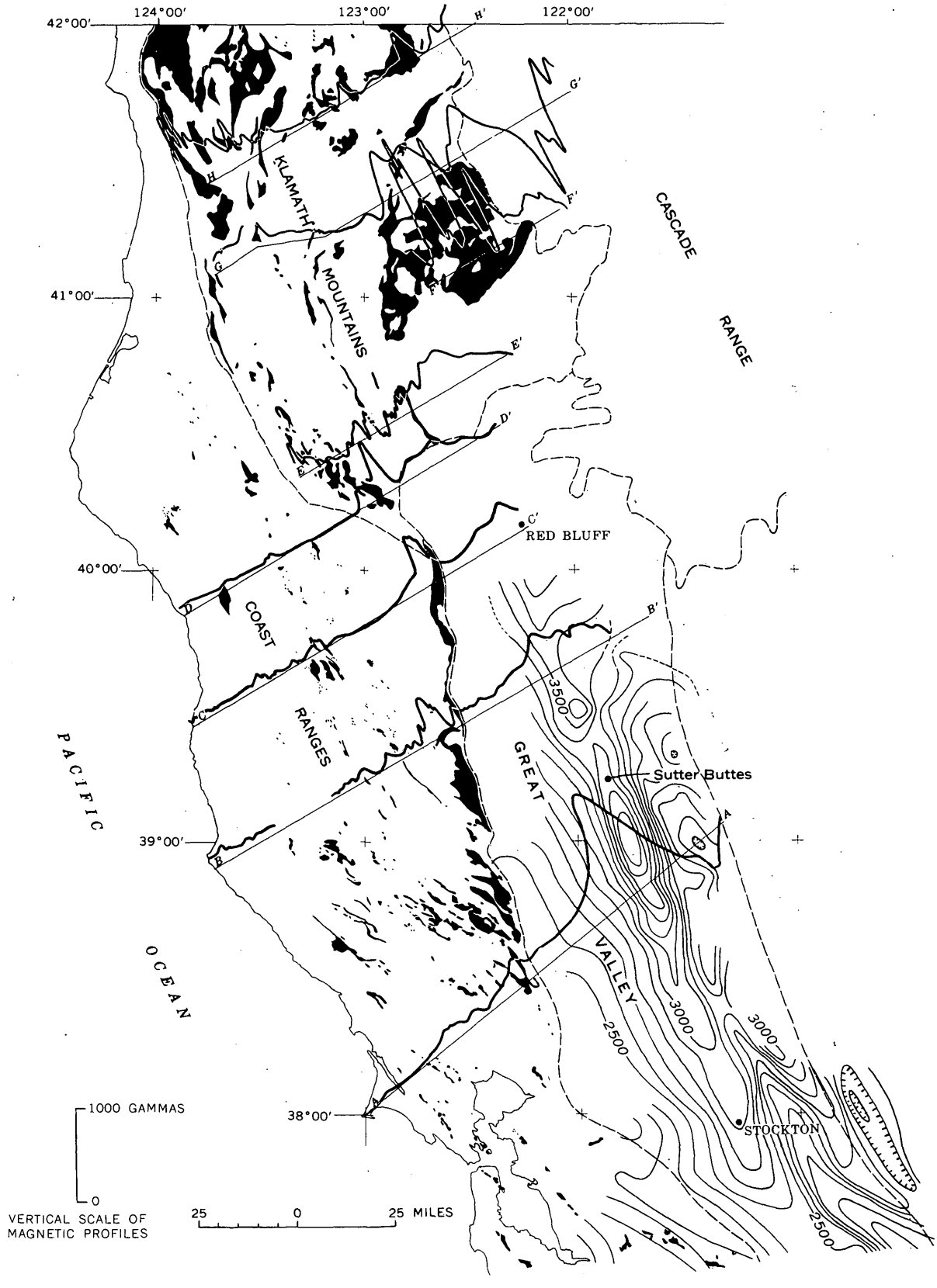

FIGURE 25.1.—Map of northern California showing aerial traverse lines *A–A′* through *H–H′*, and outline of geologic provinces. Ultramafic rocks are shown as black areas. Aeromagnetic profiles, with regional gradient (U.S. Coast and Geodetic Survey, 1955) removed, are plotted along the traverse lines. Line *A–A′* after Balsley (1953). Lines *B–B′* through *H–H′* observed and prepared under supervision of R. W. Bromery and J. R. Henderson. Contoured anomalies from Grantz and Zietz (1960). Traverse lines are not shown for the area of contoured anomalies. Contour interval 100 gammas.

complex has been established by drilling to range from approximately 1 to 3 miles. Little is known regarding the kind of basement rock cored by drilling. Data available for 10 holes drilled along or near the crest of the anomaly, chiefly near Sutter Buttes, show the cored basement rock to be chiefly intrusive rocks of intermediate composition; 1 core was gabbro, and 1 about 50 miles south of Sutter Buttes was ultramafic.

Ultramafic rock buried at considerable depth along the length of the valley may be the cause of the Great Valley anomaly. This relation is suggested chiefly by the fact that the large anomalies are principally over areas of ultramafic rock where the causative rocks are exposed. According to Grantz and Zietz (1960),

> the rocks producing the Great Valley anomaly are buried about 5 to 10 miles, but sharper, superimposed anomalies yield depths that approximate the base of the Mesozoic and Tertiary sedimentary rocks. Because they are magnetic and very large, the rock masses which produce the broad magnetic highs are thought to be igneous.

The ultramafic rock, assuming that to be the cause of the Great Valley anomaly, must lie chiefly below a considerable thickness of basement rock in addition to the late Mesozoic and Cenozoic strata, judging from the difference between the known depth to basement and the depth to the anomaly-producing rock estimated by Grantz and Zietz (1960). Locally, however, the ultramafic rock is part of the basement complex at or near the interface of the basement and overlying strata, as shown by at least one well core, and thus might also account for the sharp local anomalies superimposed on the broad Great Valley anomaly.

REFERENCES

Balsley, J. R., 1953, Total-intensity aeromagnetic profile from Denver, Colo. to Point Reyes, Calif.: U.S. Geol. Survey open-file report.

Grantz, Arthur, and Zietz, Isidore, 1960, Possible significance of broad magnetic highs over belts of moderately deformed sedimentary rocks in Alaska and California: Art. 158 *in* U.S. Geol. Survey Prof. Paper 400–B, p. B342–B347.

Irwin, W. P., 1960, Geologic reconnaissance of the northern Coast Ranges and Klamath Mountains, California: California Div. Mines Bull. 179, 80 p.

Jenny, W. P., 1932, Magnetic vector study of regional and local geologic structure in principal oil states: Am. Assoc. Petroleum Geologists Bull., v. 16, p. 1171–1203.

U.S. Coast and Geodetic Survey, 1955, Total intensity chart of the United States: U.S. Coast and Geod. Survey, chart no. 3077.

MINERALOGY, GEOCHEMISTRY, AND PETROLOGY

26. VANADIUM-RICH GARNET FROM LAGUNA, NEW MEXICO

By Robert H. Moench, Denver, Colo.

Work done on behalf of the U.S. Atomic Energy Commission

Vanadium-rich garnet has been identified as a constituent of a metamorphosed uranium-vanadium deposit in the Laguna mining district, about 45 miles west of Albuquerque, N. Mex. The garnet occurs in one of several small deposits in the Sandy uranium mine, about 4 miles southeast of the village of Laguna.

The presence of vanadium in garnet was previously reported by Doelter (1916), who classed V_2O_3 as a rare component of calcium garnet and reported 0.09 and 0.24 percent V_2O_3 in 2 chemical analyses. According to his formula ($Ca_3V_2Si_3O_{12}$) trivalent vanadium substitutes for aluminum and trivalent iron in the calcium garnet series. More recently, Badalov (1951) described a vanadium-rich grossularite that contains 4.52 percent V_2O_3, the highest vanadium content reported in garnet to date. This garnet is associated with vanadium-bearing tourmaline in the contact zone between quartz veins and vanadiferous graphitic hornfels.

This paper presents preliminary data that establish the existence of the vanadium-rich garnet (an unnamed new mineral) and describes its occurrence and geologic significance. The garnet is fine grained and can be separated in pure form only with great difficulty. Spectrographic analyses reported here were made by Nancy M. Conklin, of the U.S. Geological Survey, on a small quantity of the purified mineral. Complete chemical

and mineralogic data will be presented at a later date after a quantity sufficient for complete chemical analysis has been separated.

The Laguna district forms the east end of the southern San Juan Basin mineral belt (Hilpert and Moench, 1960), one of the world's most productive uranium regions. The largest uranium-vanadium deposits in the belt are in sandstones of the Morrison Formation, many smaller deposits are in the Todilto Limestone, and a few small deposits are in the Entrada Sandstone, all of Jurassic age. The sedimentary strata and some of the uranium-vanadium deposits of the district are cut by diabase sills and dikes, which metamorphosed the rocks and ore deposits for distances of a few feet from the contacts. The vanadium-rich garnet described here is one of the products of this metamorphism.

The Sandy mine is in an area where small uranium-vanadium deposits are found in the Todilto Limestone and Entrada Sandstone (Hilpert and Moench, 1960, p. 457–460). These deposits, the largest of which has yielded about 3,000 tons of uranium ore, contain about equal amounts of uranium and vanadium. Where unoxidized, the uranium is largely in coffinite and uraninite, and the vanadium is largely in vanadium clay, which is composed of interstratified mica (probably roscoelite) and montmorillonite mixed with some chlorite (identifications by John C. Hathaway, U.S. Geological Survey). Quantitative and semiquantitative spectrographic analyses show that the vanadium clay contains 7 or 8 percent vanadium. The clay is interstitial to sand grains of the Entrada Sandstone and embays the calcite cement; it occurs also in thin laminae in the Todilto Limestone and along boundaries between the calcite grains. It is concentrated along small folds that formed while the limestone was being deposited.

The sedimentary strata at the mine are nearly horizontal and have been intruded by many vertical diabase dikes, most less than 5 feet wide, and by sills that range from 1 to 75 feet in thickness. Metamorphic effects are conspicuous for several feet above and below sills more than about 15 feet thick. The metamorphic envelopes are best developed in the calcareous parts of the Entrada Sandstone and the Todilto Limestone and are marked by the presence of garnet, idocrase, diopside, biotite, plagioclase, epidote, and wollastonite.

Garnet is the most widespread and abundant metamorphic mineral. Two types of garnet have been distinguished—andradite-grossularite and vanadium-rich garnet. The andradite-grossularite forms pale-green to reddish-brown dodecahedral crystals, occurs as granular aggregates in barren sandstone and limestone, and encrusts joints in barren sandstone and in ore. The garnet on joints does not contain much vanadium and gives X-ray powder patterns similar to standard andradite-grossularite patterns (Mary E. Mrose, written communication, 1959).

Vanadium-rich garnet was discovered in the prospect pit in a small uranium-vanadium deposit (fig. 26.1) on the contact between the Entrada Sandstone and the Todilto Limestone. The deposit is separated by 2 or 3 feet of limestone from an overlying sill. The sill, largerly eroded in the vicinity of the prospect pit, was originally about 20 feet thick; garnet is present in a zone at least 5 feet thick below the base of the sill. In the pit, barren light-tan sandstone is sharply mottled and banded with uranium- and vanadium-bearing dark-gray to black sandstone. The dark color is caused by vanadium clay.

In thin sections of banded ore, garnet embedded in vanadium clay is distinctly darker than that in barren sandstone. This relationship was observed within the space of a single thin section. Preliminary tests made on a small separate (10 milligrams) of the darker garnet indicated a vanadium content of 21 percent (see table, sample G–2a). On the theory that this high vanadium content might be caused by impurities, a second and larger sample (25 milligrams) was separated and proved to contain 14 percent vanadium (table, sample G–2b). Though colored deep greenish brown to brownish green, the analyzed material was clear, free from inclusions, and contained no visible impurities. It yielded an X-ray powder pattern (9-hour exposure) that shows only garnet lines similar in spacing and intensity to an andradite standard.

Quantitative and semiquantitative spectrographic analyses of vanadium-rich garnet

[M, major constituent. Nancy M. Conklin, analyst]

Laboratory serial No.	Field No.	V	Al	Fe	Mg	Ca	Ti	Mn	Ba	Cr	Cu
256540	G-2a	[1] 21	7.	[1] 4.2	0.15	M	0.3	0.3	0	0.003	0
289952	G-2b	[1] 14	7.	7.	.3	M	.15	.3	.007	.03	.007

[1] Quantitative spectrographic determinations; all others are semiquantitative.

The high calcium content of both samples indicates that the garnet is a member of the calcium-rich series. In this garnet, vanadium, iron, and aluminum probably proxy for one another according to the formula $Ca_3(V,Fe,Al)_2 Si_3O_{12}$.

As the garnet formed in a uranium-vanadium deposit, one might expect it to contain uranium as well as vanadium, but none was detected. The detection limit of uranium by spectrographic analysis is about 0.05 percent, but as a dilution technique was used, a uranium content of somewhat more than 0.1 percent might have escaped detection.

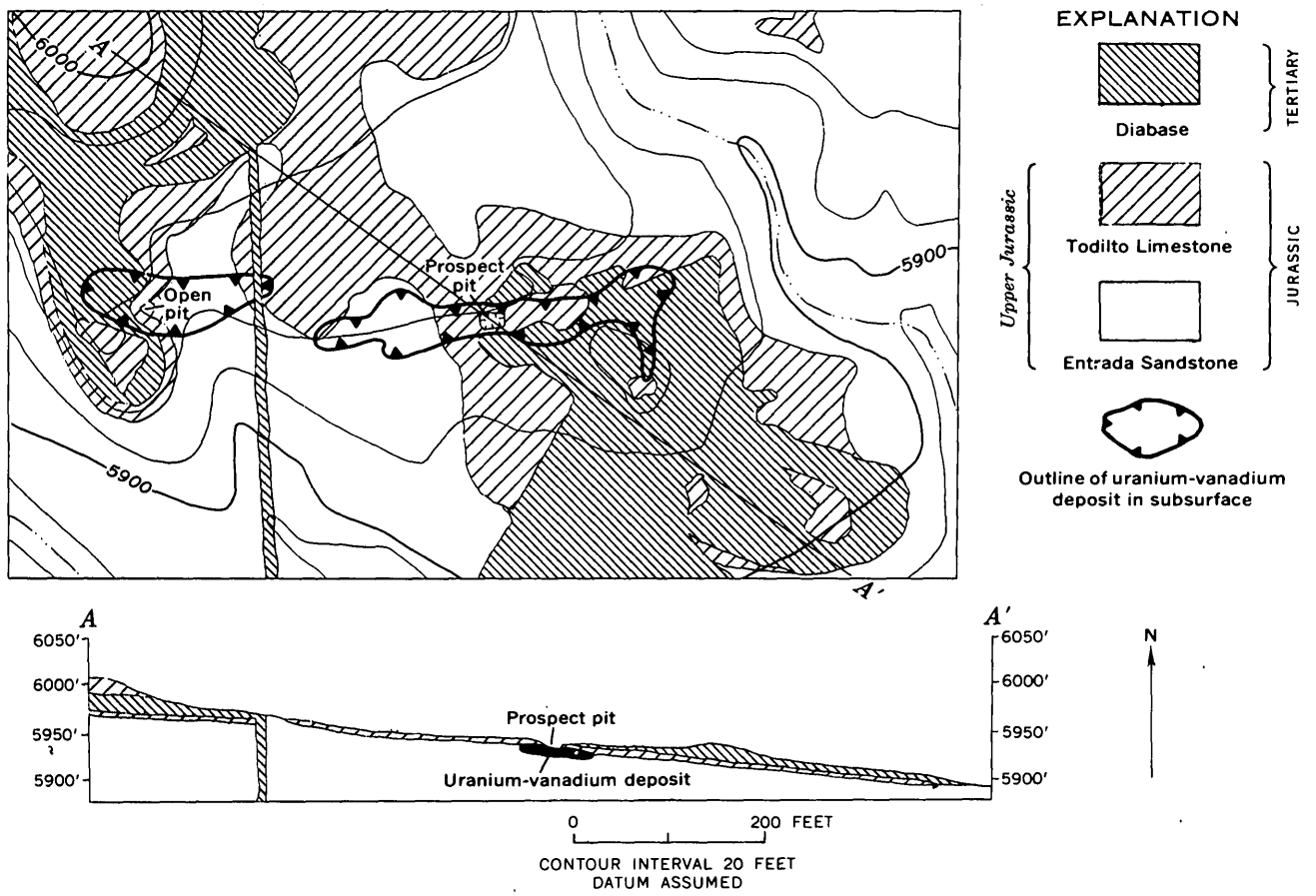

FIGURE 26.1.—Geologic map and section of part of the Sandy mine, Valencia County, N. Mex.

The vanadium-rich garnet is embedded in the darkest sandstone of the prospect pit and forms less than 10 percent of the rock. It forms tiny grains (0.1 mm or less in diameter) many of which exhibit sharply defined dodecahedral faces. Viewed with a hand lens, the garnet is clear and dark greenish brown to brownish green. In thin section it is deep brownish green, is not visibly zoned, and is weakly birefringent. It occurs together with brown vanadium clay in granular aggregates in the interstices between detrital grains. Zoned garnets with deep-brownish-green cores and colorless rims have been found in other parts of the Sandy mine, but the presence of vanadium in these garnets has not yet been verified.

The diabase dikes and sills have been inferred from structural evidence to be younger than the uranium-vanadium deposits (Hilpert and Moench, 1960, figs. 11, 17). The presence of vanadium-rich garnet in the contact metamorphic envelope further substantiates this age relationship, for the garnet must have formed at the expense of vanadium-bearing minerals in the ore. Vanadium clay is the only vanadium-bearing substance identified in the unoxidized ores of the district, and vanadium-rich garnet probably was a product of a complex reaction involving vanadium clay, calcite, and probably quartz. Other minerals may have acquired vanadium during the metamorphic reactions, but they have not been investigated.

REFERENCES

Badalov, S. T., 1951, Vanadium-bearing tourmaline and garnet: *in* Zapiski Vsesoyuz. Mineral. Obshchestva (Mém. soc. russe minéral), v. 80, p. 212–213.

Doelter, C., 1916, Granatgruppe, *in* Handbuch der Mineralchemie: Bd. II, 1915–17, p. 878–915.

Hilpert, L. S., and Moench, R. H., 1960, Uranium deposits of the southern part of the San Juan Basin, New Mexico: Econ. Geology, v. 55, no. 3, p. 429–464.

27. THORIUM AND URANIUM IN SOME ALKALIC IGNEOUS ROCKS FROM VIRGINIA AND TEXAS

By David Gottfried, Roosevelt Moore, and Alice Caemmerer, Washington, D.C.

Certain types of alkalic igneous rocks contain greater amounts of thorium and uranium than the ordinary calc-alkalic igneous rocks. Within the broad category of alkalic rocks, however, more systematic studies are needed to enable us to correlate the chemical characteristics of contrasting suites with their thorium and uranium content. As part of a broad study concerned with the geochemistry of thorium and uranium in igneous rocks, analyses for these elements in 51 samples of a variety of alkalic igneous rocks from Virginia and Texas are presented in this article.

Thorium was determined by the chemical method of Levine and Grimaldi (1958) and uranium by the fluorimetric method of Grimaldi and others (1952). The thorium and uranium results given in this report are believed to be accurate to about ±10 percent.

AUGUSTA COUNTY, VA.

Three types of alkalic igneous rocks are predominant in the dike complex of Augusta County, Va.—nepheline (natrolite) syenite, teschenite, and picrite. These rocks are being studied by R. W. Johnson, Jr., and Charles Milton, of the U.S. Geological Survey, who provided the samples, chemical analyses, and information on the petrographic characteristics of the samples. An earlier description of the dike complex was published by Watson and Cline (1913).

Table 27.1.—*Partial analyses of alkalic igneous rocks from Augusta County, Va.*

Sample	Rock type	SiO_2 (percent)	CaO / Na_2O+K_2O	Th (ppm)	U (ppm)	Th/U
D-4a	Nepheline syenite	57.9	0.02	87	10.4	8.4
D-48	do	58.0	.03	53	14.0	3.8
D-42	Nepheline (natrolite) syenite.[1]	57.8	.05	60	20.0	3.0
D-12a	Nepheline syenite	57.7	.05	40	12.5	3.2
9	Nepheline (natrolite) syenite.	57.7	.05	51	14.8	3.4
D-2	Nepheline syenite	58.3	.09	38	10.6	3.6
D-38b	Nepheline (natrolite) syenite.	58.1	.02	49	14.1	3.5
D-70	do	59.0	.01	42	12.1	3.5
D-31	Nepheline syenite [1]	57.4	.03	42	12.8	3.3
D-22c	do	56.9	.02	40	10.3	3.9
D-18	do [1]	58.7	.07	30	22.0	1.4
D-6-St. 26	Teschenite	51.2	1.4	20	4.5	4.4
D-14	do	59.8	.10	33	8.3	4.0
D-22b	do	57.1	.51	39	11.5	3.4
D-24b	do	55.1	.36	18	4.4	4.1
D-17-St. 23	do	52.2	.60	13.4	4.4	4.0
D-1-St. 11	do	51.8	1.4	21.0	5.4	3.9
D-7	do	62.9	.29	13.9	3.9	3.6
D-69	do	51.1	.93	11.1	3.2	3.5
D-8	do	48.4	1.1	7.1	2.8	2.5
D-14b	Picrite	46.7	1.7	12.5	3.4	3.7
D-26	do	44.7	2.2	14.1	3.0	4.7
B	do	45.7	2.1	9.9	2.6	3.8
D-12	do	45.6	3.4	7.8	2.0	3.9

[1] Float material.

The syenites and teschenites are closely related spatially and genetically. The nepheline (natrolite) syenites consist essentially of potassic feldspar–nepheline–natrolite aggregates, with acmitic pyroxene and little hornblende or biotite. The teschenites contain plagioclase, diopsidic pyroxene, abundant brown hornblende and biotite, and analcite. The few picrite instrusives consist mainly of olivine, pyroxene and biotite.

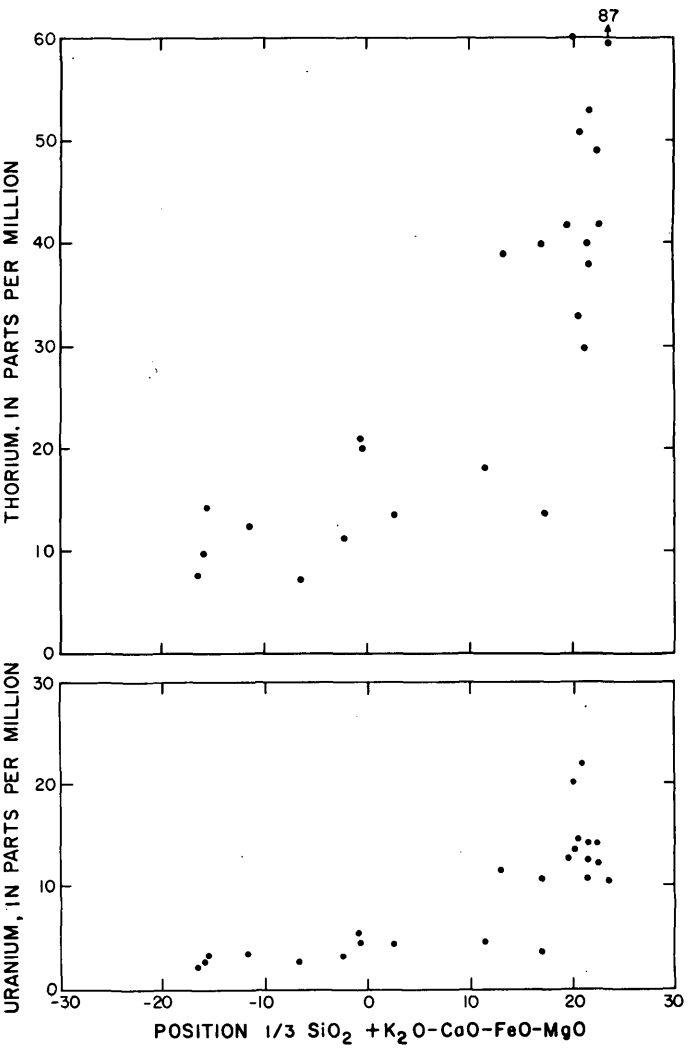

Figure 27.1.—Variation diagrams showing distribution of thorium and uranium in alkalic igneous rocks from Virginia.

Table 27.1 gives the silica content, the $\frac{CaO}{Na_2O+K_2O}$ ratio, and the thorium and uranium content of 24 samples. These data show a clear trend toward increasing

thorium and uranium in the more siliceous rocks, which contain 57 to 59 percent SiO_2 and have a $\frac{CaO}{Na_2O+K_2O}$ ratio of less than 0.1. The syenites average about 48 ppm of thorium and 14 ppm of uranium. The most mafic rocks, the picrites, average 11 ppm of thorium and 2.8 ppm of uranium. Figure 27.1 shows a plot of the thorium and uranium data on a variation diagram of the type proposed by Larsen (1938). Figure 27.3 shows the relation between the Th/U ratios of the rocks and their chemical composition. There appears to be no systematic variation of thorium relative to uranium between any of the rock types.

BIG BEND NATIONAL PARK, TEX.

The igneous rocks from the Big Bend National Park, Tex., area range from alkalic basalt containing about 44 percent SiO_2 to riebeckite rhyolite and granite with about 76 percent SiO_2. The suite of rocks constitutes one of several alkalic subprovinces along the front of the Rocky Mountains extending from Montana to Texas. Brief discussions of the petrology and geologic setting of these rocks are given by Lonsdale and Maxwell (1949) and Maxwell and Lonsdale (1949). Igneous rocks from the Terlingua-Solitario region (Lonsdale, 1940) are very similar to most of the rocks of the Big Bend area. Table 27.2 lists the SiO_2 content, the $\frac{CaO}{Na_2O+K_2O}$ ratio, and the thorium and uranium content for 27 samples. The samples and chemical data were provided by the late Prof. J. T. Lonsdale, of the University of Texas. The siliceous rocks in the range from about 70 to 77 percent SiO_2 have $\frac{CaO}{Na_2O+K_2O}$ ratios ranging from about 0.03 to about 0.1, indicating they are extremely lime poor. In these rocks the thorium content ranges from about 25 to 45 ppm and the uranium content from 9 to 45 ppm. Nearly all the rocks contain greater amounts of thorium and uranium than corresponding rocks of the calc-alkalic suites studied by Larsen and Gottfried (1960). Figure 27.2 shows the relation between the thorium and uranium content of the rocks and their chemical composition on a variation diagram. Both thorium and uranium show

TABLE 27.2.—*Partial analyses of alkalic igneous rocks from Big Bend National Park, Texas*

Sample	Rock type	SiO_2 (percent)	$\frac{CaO}{Na_2O+K_2O}$	Th (ppm)	U (ppm)	Th/U
Ch689F-2	Quartz sanidine porphyry, intrusive.	76.78	0.03	32	9.4	3.4
Ch234	Riebeckite granophyre, intrusive.	77.47	.08	45	16.4	2.7
Ch203	Riebeckite microgranite porphyry.	76.62	.03	26	9.8	2.7
Ch232D	Riebeckite granophyre, intrusive.	75.94	.04	26	9.0	2.9
Ch162B	Riebeckite granite, intrusive	75.76	.08	45	42	1.1
Ch746F	Riebeckite rhyolite	75.09	.04	41	16.4	2.5
Ch767A-3	Pyroxene microgranite, intrusive.	70.00	.14	24	7.0	3.4
Ch668F	Reibeckite trachyte, extrusive.	69.14	.04	40	19.5	2.1
Ch340B	Aegerine augite trachyte, intrusive.	66.49	.12	11.3	1.9	5.9
Ch61B	Augite soda trachyte, intrusive.	65.40	.11	11.6	3.4	3.4
Ch747C	Trachyandesite porphyry	64.26	.23	14.1	6.2	2.3
Ch577B	do	63.97	.57	11.3	3.3	3.4
Ch47B	Analcite-syenite	62.76	.10	10.9	3.4	3.2
Ch726F	Trachyandesite	58.60	.70	9.5	4.3	2.2
Ch258	Olivine syenodiorite	55.36	.83	11.0	4.4	2.5
Ch727D	Basalt porphyry, extrusive	55.64	.96	8.3	3.3	2.5
Ch176A	Analcite-andesine syenite	53.70	.76	7.5	2.5	3.0
Ch47A	Syenogabbro	53.40	.83	4.2	1.6	2.6
Ch724	Porphyritic olivine basalt, intrusive.	52.35	1.4	3.8	1.6	2.4
Ch179	Analcite syenogabbro	51.04	1.1	5.0	1.6	3.1
Ch148	Olivine basalt intrusive	49.90	1.5	3.4	1.2	2.8
Ch386	do	48.40	2.2	3.4	1.1	3.1
Ch69D	Analcite labradorite syenite	48.51	1.1	4.7	1.7	2.8
Ch589	Olivine basalt porphyry, extrusive.	47.69	2.0	2.6	1.2	2.2
Ch840B	Basalt, intrusive	45.89	2.3	4.7	1.9	2.5
Ch243D	Nepheline basalt, intrusive	43.75	3.1	5.4	2.2	2.5
Ch1	Porphyritic olivine basalt	46.19	1.8	3.9	1.9	2.1

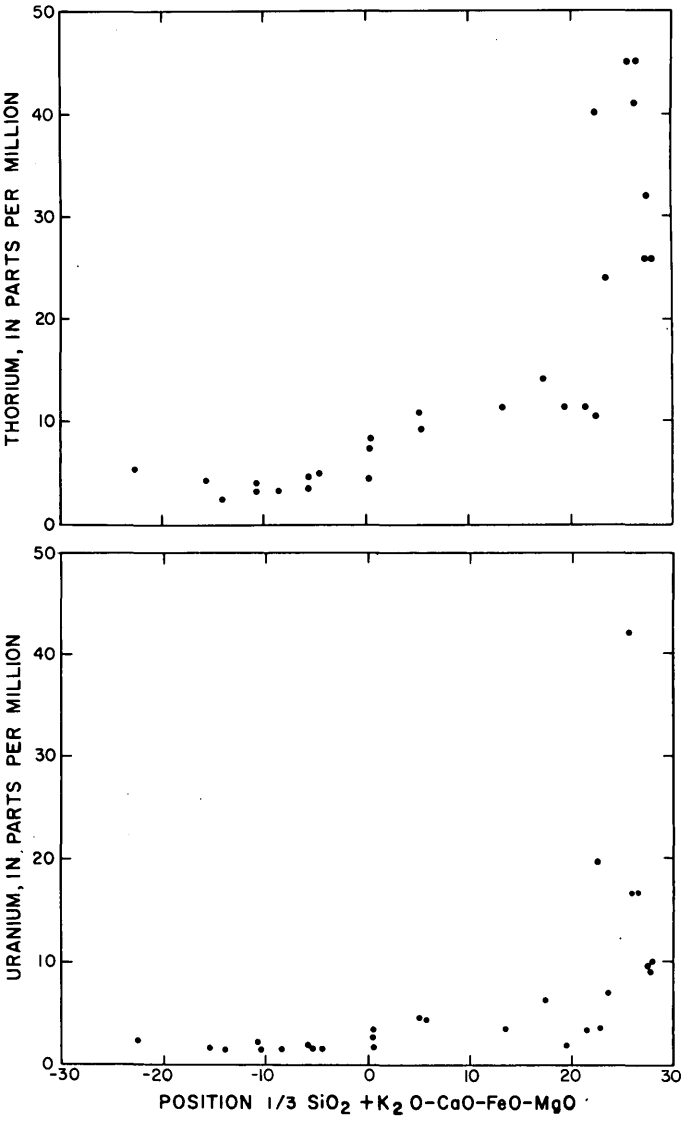

FIGURE 27.2.—Variation diagrams showing the distribution of thorium and uranium in alkalic igneous rocks from Big Bend National Park, Tex.

a rather systematic increase from the mafic to the siliceous rocks. The thorium to uranium ratio is nearly the same over the range of composition (fig. 27.3). Except for two samples, all the Th/U ratios fall between 2 and 3½.

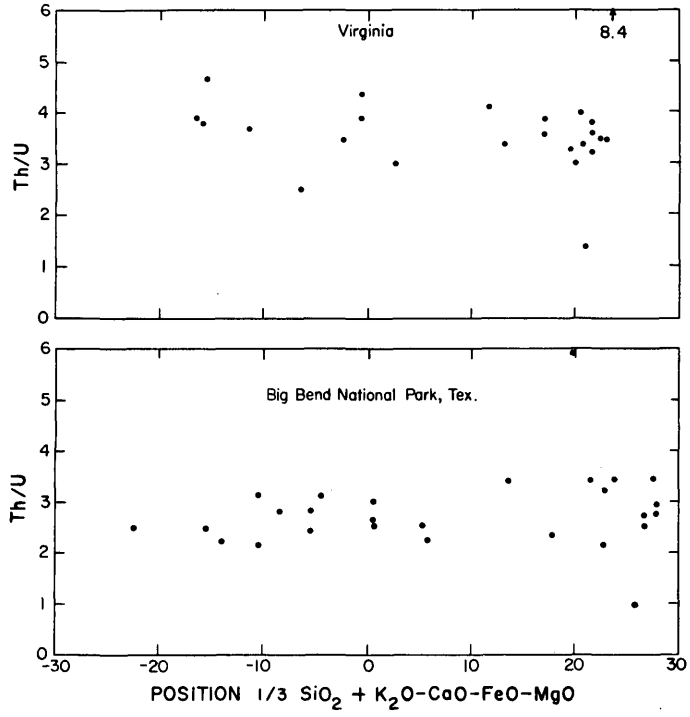

FIGURE 27.3.—Variation diagrams showing the thorium to uranium ratios in alkalic igneous rocks from Texas and Virginia.

DISCUSSION

Although the two alkalic suites of igneous rocks discussed here have significant differences in their mineralogic composition and in some chemical features, they have similarities with respect to their low $\frac{CaO}{Na_2O+K_2O}$ ratio and relatively high thorium and uranium content. The late differentiates of each suite contain about 2 to 3 times the amount of thorium and uranium found in the highly siliceous rocks of calc-alkalic provinces (Larsen and Gottfried, 1960).

It is of interest to compare the data given in this report with those obtained on the subsilicic-alkalic igneous rocks of the Bearpaw Mountains of Montana. Chemically the rocks of the Bearpaw Mountains are characterized by a low SiO_2 content and a high K_2O and CaO content. The late differentiates of this province are syenites which average 14.3 and 4.1 ppm of thorium and uranium respectively (Larsen and Gottfried, 1960). Their thorium and uranium contents are somewhat similar to the amounts found in late differentiates of calc-alkalic suites and significantly lower than the amounts found in the lime-poor alkalic rocks discussed here.

The data presented here and the previous studies by Phair (1952) and Larsen and others (1955) indicate that the distinguishing characteristic of alkalic igneous rocks enriched in thorium and uranium is their extremely low CaO content. Hence these studies provide a chemical guide for possibly delineating certain areas of alkalic igneous rocks that would be significantly enriched in thorium and uranium.

REFERENCES

Grimaldi, F. S., May, Irving, and Fletcher, M. H., 1952, U.S. Geological Survey fluorimetric methods of uranium analysis: U.S. Geol. Survey Circ. 199, 20 p.

Larsen, E. S., Jr., 1938, Some new variation diagrams for groups of igneous rocks: Jour. Geology, v. 46, p. 505–520.

Larsen, E. S., Jr., Phair, George, Gottfried, David, Smith, W. L., 1956, Uranium in magmatic differentiation: U.S. Geol. Survey Prof. Paper 300, p. 65–74.

Larsen, E. S., 3rd, and Gottfried, David, 1960, Uranium and thorium in selected suites of igneous rocks: Am. Jour. Sci., v. 258–A, p. 151–169.

Levine, Harry, and Grimaldi, F. S., 1958, Determination of thorium in the parts per million range in rocks: Geochim. et Cosmochim. Acta, v. 14, p. 93–97.

Lonsdale, J. T., 1940, Igneous rocks of the Terlingua-Solitario region, Texas: Geol. Soc. America Bull., v. 51, p. 1539–1626.

Lonsdale, J. T., and Maxwell, R. A., 1949, Petrology of Big Bend National Park, Texas [abs.], Geol. Soc. America Bull., v. 60, no. 12, pt. 2, p. 1906.

Maxwell, R. A., and Lonsdale, John T., 1949, General geology of Big Bend National Park, Texas [abs.]: Geol. Soc. America Bull., v. 60, no. 12, pt. 2, p. 1908.

Phair, George, 1952, Radioactive Tertiary porphyries in the Central City district, Colorado, and their bearing upon pitchblende deposition: U.S. Geol. Survey TEI–247, 53 p., issued by U.S. Atomic Energy Comm. Tech. Inf. Service Ext., Oak Ridge, Tenn.

Watson, T. L., and Cline, J. H., 1913, Petrology of a series of igneous dikes in central western Virginia: Geol. Soc. America Bull., v. 24, p. 301–334.

28. SALINE FEATURES OF A SMALL ICE PLATFORM IN TAYLOR VALLEY, ANTARCTICA

By WARREN HAMILTON, IRVING C. FROST, and PHILIP T. HAYES, Denver, Colo.

Work supported by the National Science Foundation

In Taylor Valley, at approximate lat. 77°43′ S. and long. 162°15′ E. in South Victoria Land, the snout of the large Taylor Glacier rests against Bonney Lake (fig. 28.1). The lake is thickly frozen during most of the year, although in late December and January the ice melts in a band a few yards wide around the lake. Air temperatures are below freezing except on occasional warm summer days, but ground-surface temperatures are above freezing more frequently.

The glacier lies directly against the ice of the lake across most of its width (Hamilton and Hayes, 1961, fig. 2). At the north side of the snout, however, a sloping, gently rolling platform of ice separates glacier and lake (fig. 28.1). The platform is triangular in plan, 400 by 600 feet, with the obtuse angle at the junction of glacier and lake ice; the platform rises gently toward the Recent till of the valley side, and even more gently up the valley. The platform is probably an ice

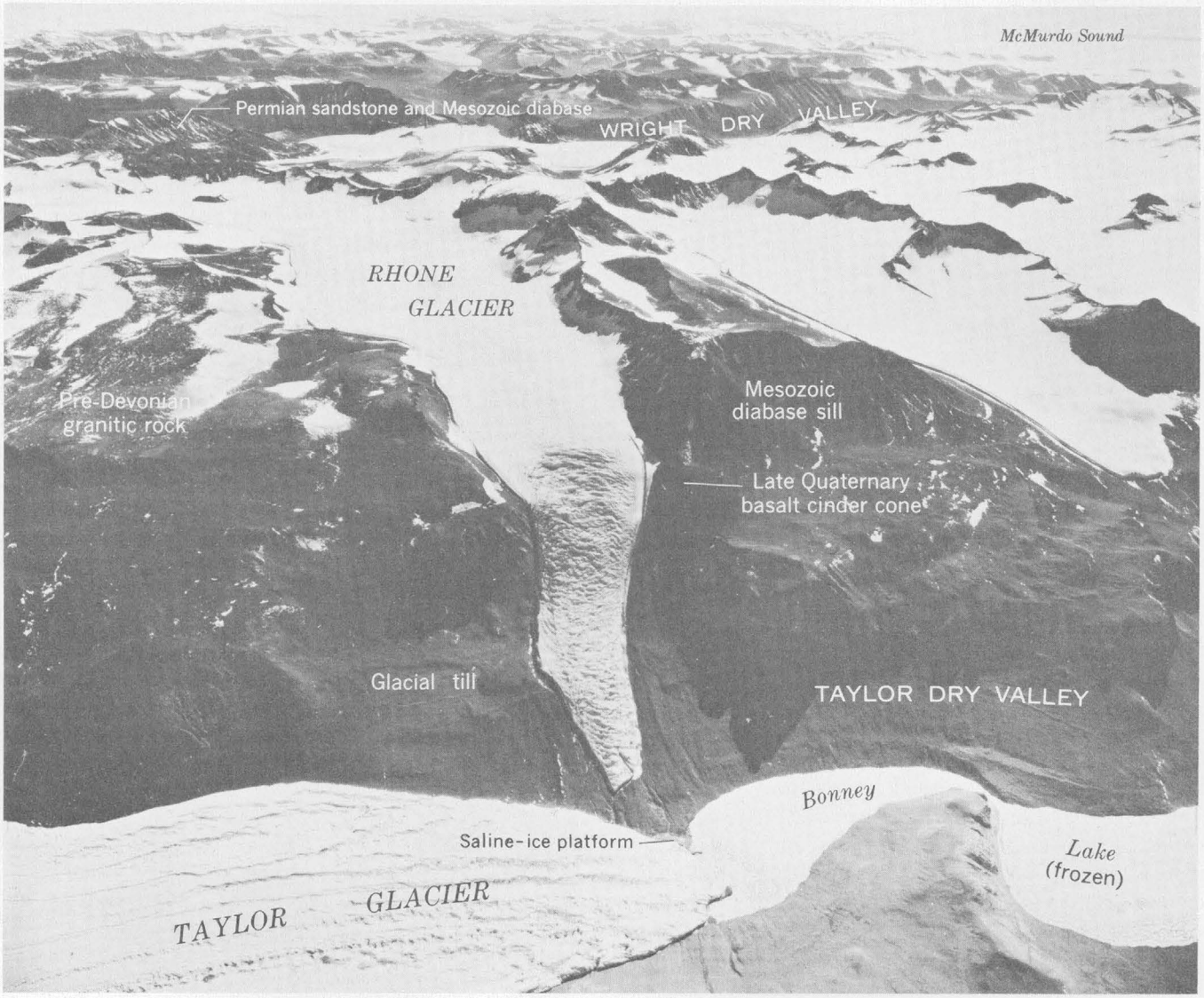

FIGURE 28.1.—View north across the end of Taylor Glacier, showing location of the saline ice platform. The pictured area is 4½ miles wide along Taylor Glacier and Bonney Lake. (U.S. Navy photograph.)

delta, formed by refreezing of melt-water streams from the small Rhone Glacier and, to a lesser extent, from Taylor Glacier. Total relief of the platform is about 6 feet. This ice platform has a fretted surface due to the accumulation of saline waters on its surface, has numerous small saline pools upon it, and the till at its edge is thickly encrusted by halite. The field study of the platform was made by Hamilton and Hayes on December 15, 1958, before there was appreciable melting of the margin of Bonney Lake, at a time when the air temperature was perhaps 30°F. This article was largely prepared by Hamilton; chemical analyses are by Frost.

Melt-water streams from Taylor and Rhone Glaciers are entrenched in gullies as deep as 3 feet in the ice platform. The surface of the platform is stained yellowish brown by minute granules of iron oxide, in striking contrast to the clean white ice of lake and glacier. The surface is covered throughout by pinnacles of ice one to several inches high, with sulfatic water in the intervening depressions; numerous small pools several feet in diameter and a few inches deep lie upon the ice (fig. 28.2). The pools are moderately

FIGURE 28.2.—Sulfate-water pool, with dark precipitate of iron oxide and calcite, on platform of salt-pitted ice.

dilute solutions of sodium sulfate and are floored by a loose, slimy precipitate of calcite and iron oxide.

Water and sediment from one of these pools were collected in a single small container and after several months were studied in the laboratory. The relative composition of solution and precipitate may have changed during the intervening months due to the uncontrolled temperatures. The filtered and dried solid has the appearance of yellowish orange silt. It consists of about 98 percent calcite in crystals 0.002 to 0.01 mm long, mostly aggregated in ragged clusters near 0.1 mm in diameter. Most crystals are anhedral, but some are bluntly terminated prisms and a few are rhombohedra and other forms. Gypsum forms rare tablets 0.05 mm long. Reddish-brown aggregates 0.005 mm in diameter of 0.001–mm particles of limonite constitute about 2 percent of the sample. The sediment is completely soluble, with effervescence, in cold dilute HCl, and abundant $Fe(OH)_3$ is precipitated from this solution when alkalized with NH_4OH. A dry, untreated sample was analyzed by X-ray diffractometer by Theodore Botinelly, who found the only peaks rising above background levels to be of calcite.

The sample solution was filtered from the sediment and analyzed by standard quality-of-water methods. It was found to contain:

ANIONS			CATIONS		
	Weight percent	*Equivalent parts per liter*		*Weight percent*	*Equivalent parts per liter*
CO_3^{-2}	0.054	18	Na^{+1}	0.41	178
HCO_3^{-1}	.061	10	K^{+1}	.003	0.8
CL^{-1}	.060	17			
SO_4^{-2}	.79	165	Sum		179
			Deficiency		31
Sum		210	Sum		210

The solute is primarily sodium sulfate. The sample was too small (12 ml) for determination of calcium and magnesium; the indicated cation deficiency would be balanced if 0.060 weight percent Ca^{+2} or 0.037 percent Mg^{+2}, or an equivalent combination, were present. Total salinity is about 1.4 percent by weight.

The edge of the ice platform is pitted by insolation holes, containing saline water, around boulders (fig. 28.3). Evaporites, mostly halite, as thick as 1 inch en-

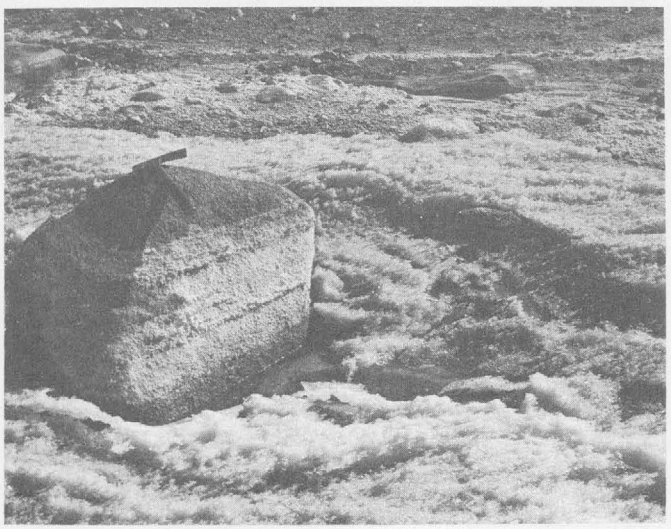

FIGURE 28.3.—Salt crust at margin of ice platform. An insolation hole about the boulder contains a saline pool. The boulder and the lower part of the till in the background are encrusted with halite and subordinate amounts of other salts.

crust the boulders and also form a surface crust and subsurface caliche in the till at the edge of the ice. The upper limit of salt deposition—the white line near the top of figure 28.3—rises upvalley (left) with a 2° slope, parallel to the surface of the ice platform; this line was about 1 foot vertically below the limit of water-saturated till when studied.

The salt crust disintegrates into firm fragments of sand and granule size when disturbed. Charles B. Hunt examined a sample petrographically and found about 95 percent of it to be halite (NaCl) in rough 0.1-mm cubes clouded by abundant rectangular holes. He also recognized calcite ($CaCO_3$); a polysynthetically twinned sulfate, probably polyhalite ($K_2SO_4 \cdot MgSO_4 \cdot 2CaSO_4 \cdot 2H_2O$); gypsum ($CaSO_4 \cdot 7H_2O$), forming the largest crystals in the material; and an orthorhombic sulfate, perhaps epsomite ($MgSO_4 \cdot 7H_2O$). Hydration states of some of the salts may of course have changed between times of collection and study. Sylvite (KCl) is possibly present as cubelets within halite cubes. No sodium sulfate was recognized. A rapid colorimetric test for nitrate by Hunt indicated a probable content of about 0.1 percent NO_3^{-2}. The assemblage is much like salt crusts in Death Valley except that no polyhalite occurs there, according to Hunt.

The same salt sample was analyzed chemically. About 18 percent of it is insoluble, largely windblown silt. The portion soluble after heating repeatedly on a steam bath was analyzed with the following results:

ANIONS			CATIONS		
	Weight percent of total solute	*Molecular percent*		*Weight percent of total solute*	*Molecular percent*
CO_3^{-2}	0.25	0.2	Na^{+1}	39.7	50
HCO_3^{-1}	.52	.2	K^{+1}	.13	0.1
Cl^{-1}	55.2	45	Ca^{+2}	.77	1.1
SO_4^{-2}	3.1	1.9	Mg^{+2}	.36	.9
Sum		47	Sum		52
			Excess		5

The cation excess is probably due to the determined values being too high for sodium or too low for chlorine. The soluble salt is about 95 molecular percent NaCl, 1.8 percent $MgSO_4$, 1.5 percent $CaSO_4$, 0.5 percent each of $CaCO_3$, $NaHCO_3$, and Na_2SO_4, and 0.2 percent K_2SO_4. This agrees reasonably well with the mineralogic observations.

An inconspicuous salt crust is developed around much of Bonney Lake and along melt-water streams from Taylor Glacier and other glaciers. Although salts must be more concentrated in the small proportion of liquid water than in the ice, no water elsewhere about the lake or in other melt water was found to have the slightest saline taste.[1]

The composition and concentration of the solutions of the ice platform must fluctuate during the year to maintain equilibrium with the adjacent ice, as air temperatures vary from perhaps −50° to +40°F. The solutions must have been near maximum dilution when studied.

The restriction of the saline solutions to the sloping ice platform is puzzling. The platform appears to be an ice delta, formed largely by refreezing of melt water from Rhone Glacier, but nothing comparable to its saline features was seen elsewhere in the region. The bright yellow-brown coloration of the ice by ferric iron is so conspicuous as seen from either the air or the ground that similar features could not have been overlooked in the region visited.

A preliminary concentration of the solution as a saline residuum after freezing is likely, the solutes remaining in the last-freezing portion. Evaporation must control the subsequent precipitation of calcite, iron, and salts. Dry winds are nearly constant. Rhone Glacier drains an area of granitic rocks, sandstone, diabase, basalt, and surficial materials (fig. 28.1); the exceptionally large quantities of dissolved matter apparently present in its melt water suggest that mineralized ground, perhaps pyritic, may underlie some part of that glacier. Windblown salt from the sea presumably adds sodium chloride in particular to the waters.

REFERENCES

Angino, E. E., and Armitage, K. B., 1962, Geochemical study of Lakes Bonney and Vanda, Victoria Land, Antarctica: Geol. Soc. America Abs. for 1961, Spec. Rept. 68, p. 129.

[1] Water as warm as 8°C was found in a layer at a depth of 40 feet in Lake Bonney, at an unspecified distance below the ice, by Angino and Armitage (1962) in December 1960. Although their analytical data have not yet been published, they report "highly saline bottom waters" (at a depth of about 100 feet?) having a Cl/SO_4 ratio of about 70:1 and a Mg/Ca ration of 16:1, and they conclude that this "indicates a probable sea-water origin for the deeper waters." As the respective ratios in sea water are only 7:1 and 3:1 (Clarke, 1924, p. 127), the basis for the conclusion is unclear; further, the sea has not entered Taylor Dry Valley during late Quaternary time (Péwé, 1960; see also Ball and Nichols, 1960, p. 1704). The warm-temperature layer was attributed by Angino and Armitage to a high geothermal gradient or to warm springs in the lakebed; however, no warm springs are known in the region, and some other explanation is more likely.

Ball and Nichols (1960) found efflorescent salt on unconsolidated materials near McMurdo Sound a short distance northeast of the mouth of Taylor Dry Valley to consist of subequal amounts of NaCl and Na_2SO_4. They considered the chloride to have come in spray from the nearby sea, and the sulfate to have formed from sulfuric acid produced by the oxidation of pyrite.

629660—62——6

Ball, D. G., and Nichols, R. L., 1960, Saline lakes and drill-hole brines, McMurdo Sound, Antarctica: Geol. Soc. America Bull., v. 71, p. 1703–1708.

Clarke, F. W., 1924, The data of geochemistry: U.S. Geol. Survey Bull. 770, 841 p.

Hamilton, Warren, and Hayes, P. T., 1961, Structure of lower Taylor Glacier, South Victoria Land, Antarctica: Art. 224 *in* U.S. Geol. Survey Prof. Paper 424–C, p. C206–C209.

Péwé, T. L., 1960, Multiple glaciation in the McMurdo Sound region, Antarctica—a progress report: Jour. Geology, v. 68, p. 498–514.

ANALYTICAL AND PETROGRAPHIC METHODS

29. INDEX OF REFRACTION MEASUREMENTS OF FUSED HAWAIIAN ROCKS

By D. B. Stewart, Washington, D.C.

The relation of the index of refraction of fused rock and rock composition has been clearly demonstrated by Mathews (1951) and Callaghan and Sun (1956). A similar study of 19 Hawaiian rocks was made to evaluate the fusion method for the rapid determination of their SiO_2 content and for possible use to distinguish the differentiates of the tholeiitic and alkali basalt magmatic series.

A uniform fusion procedure was developed from controlled experiments using different electrode configurations, arcing times, and arc current on differing amounts of sample of the same composition. Fig 29.1 is representative of these experiments. The arcing process and subsequent cooling of the sample cannot be considered controlled processes, so that a variation of index of refraction of 0.01 can occur in duplicate samples of homogeneous starting material because of incomplete fusion or partial recrystallization. Four samples were fused from each rock studied. The value given is the average of at least three determinations, and the range of the observations is given as the estimated error.

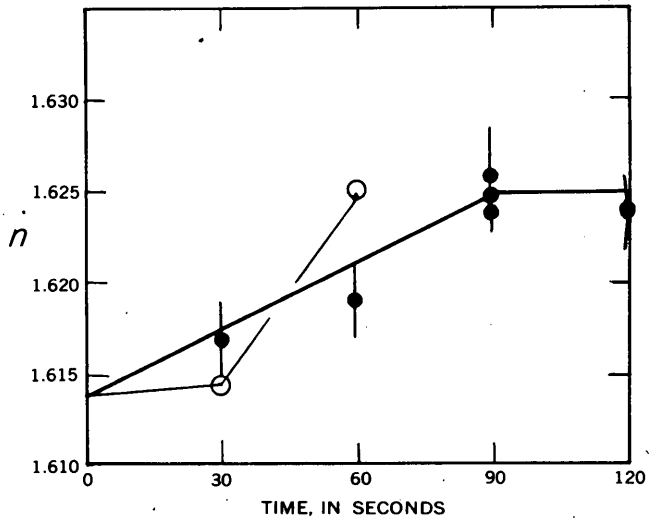

Figure 29.1.—Index of refraction (n) of homogeneous glass obtained by fusing 15-mg samples of powdered tholeiitic basalt for various times in air with a d–c arc current of 5 amp (black points) or 10 amp (circles). The starting material was glass (n=1.614) containing 10 percent magnesian olivine.

About a gram of representative rock was ground to −200 mesh, and a split of approximately 15 mg was placed in a cavity 0.140 inch deep and 0.140 inch wide, with walls 0.022 inch thick cut in the end of a 0.184 inch pedestal 0.3 inch long at the top of a 0.242 inch diameter carbon electrode. The sample was fused for 90 seconds in a 5-ampere 220-volt d-c arc with a gap of 0.1 inch. The water-cooled electrode holders resulted in cooling of the glass beads to room temperature in about 15 seconds. Index measurements were made to ±0.002 on the crushed beads, using white light and freshly calibrated immersion oils.

A suite representative of each of the Hawaiian differentiation series was selected by my colleague D. H. Richter, who discussed with me the conduct and significance of the investigation. The tholeiitic suite was from the 1959–60 eruption of Kilauea which is to be described petrographically by K. J. Murata and Richter at a later date. A sample believed identical to one described by Kuno, Yamasaki, Iida, and Nagashima (1957, p. 182) was studied, as was a sample with 52.04 percent SiO_2 described by Murata and Richter (1961). The samples of the alkali basalt magmatic suite were collected by G. A. Macdonald as close as possible to the localities described by Washington (1923a, 1923b) and Cross (1904). Possibly some of these samples are not chemically identical to the material analyzed, and this may contribute to the scatter of the data.

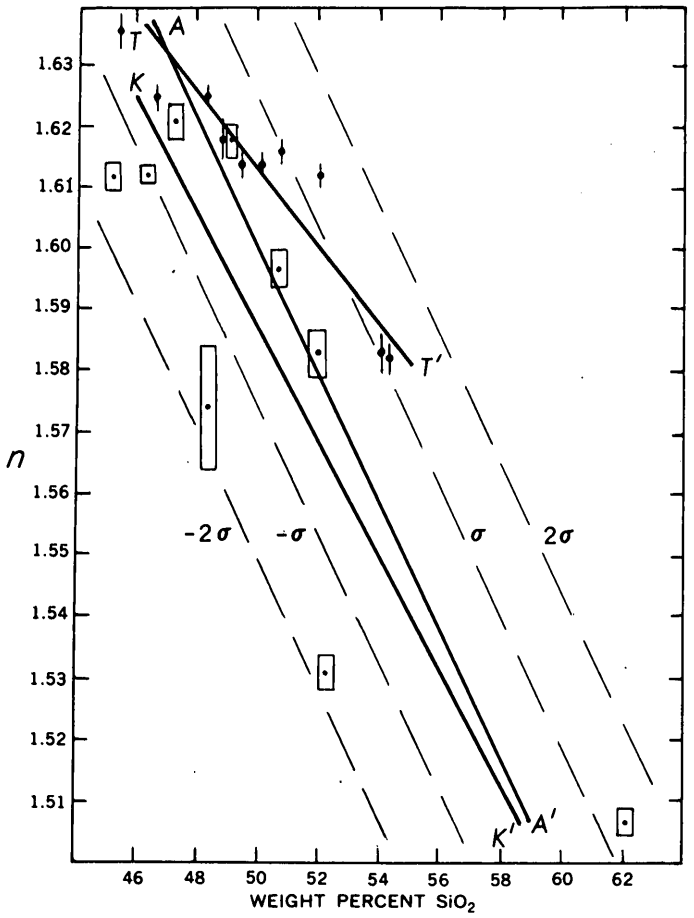

FIGURE 29.2.—Plot of index of refraction (n) against percent SiO_2 for fused Hawaiian rocks. Large dots, tholeiitic series; boxes, alkali basalt series; vertical dimension represents range of measurements. Line T–T' is the least-squares line for the tholeiitic series, K–K' for the alkali basalt series and A–A' for all the rocks studied. Dashed lines indicate standard deviations (σ) for line A–A'.

The results are shown graphically on figure 29.2 and are compared with similar investigations by others on figure 29.3. Straight lines computed by the least-squares method (computations by Ralph Eicher, U.S. Geological Survey, using a digital computer) for each magma series and for all the specimens are plotted on figure 29.2. The regression coefficients and standard deviations computed are

tholeiitic magma series:

Weight percent $SiO_2 = 202.15 - 95.019\ n$; standard deviation = 1.1

alkali basalt magma series:

Weight percent $SiO_2 = 301.69 - 156.06\ n$; standard deviation = 2.7

all specimens studied:

Weight percent $SiO_2 = 219.27 - 106.61\ n$; standard deviation = 2.4

The index of refraction measurement is denoted by n.

Yoder and Tilley (1957) determined the index of refraction of 3 tholeiites and 1 alkali basalt from Hawaii (analyzed by Tilley and Scoon, p. 63) after the samples were fused in sealed platinum capsules for 1 to 24 hours. The measurements reported by Yoder and Tilley are somewhat lower than those reported here, possibly because of the different fusion method used. However, the least-squares line using both their data and all of the present data differs from the present data only by a slightly smaller standard deviation.

There is a tendency for tholeiitic glasses to have a higher index of refraction than glasses with the same SiO_2 content from the alkali basalt series. The overlapping ranges of the two series preclude assignment of an unknown rock to either magmatic series. Moreover, the standard deviations are so great that even when the SiO_2 content is known independently, many Hawaiian rocks cannot be confidently assigned to either series. The general curve derived from all specimens studied shows that the fusion method can be used to estimate the silica content only to ± 4.8 percent within 95 percent confidence limits. However, the method may be useful for rough approximation of the composition of aphanitic or glassy rocks, such as groundmasses or some pumices.

The index of refraction of entirely fused tholeiitic rocks is 0.009 to 0.019 higher than that of the glass originally present, reflecting solution of olivine, pyroxene and ores, oxidation of iron, and volatilization of alkalies and H_2O.

The most siliceous tholeiite studied was fresh vitreous rock containing 54.08 percent SiO_2 and having an original index of refraction of 1.569. Washington (1923c, p. 341) found black glassy inclusions of lower index (n near 1.56) in blocks ejected from Kilauea, and Macdonald (1949, p. 65, 76) reported that where only 3 to 5 percent interstitial glass remained, its index of refraction was less than 1.54. Chapman (1947, p. 108) reported interstitial glass with $n = 1.555$ in blocks ejected during the 1924 phreatic explosions at Kilauea, and by reference to George (1924, p. 365) he estimated that this glass contained 53 percent SiO_2. Chapman's estimate of SiO_2 is lower than the present data would indicate. The generally low index of refraction of interstitial glass suggests that differentiation in the tholeiitic series can produce rocks considerably richer in SiO_2 than 54 percent.

Mathews (1951) proposed that a separate determinative curve be prepared for every magmatic suite, while Callaghan and Sun (1956, p. 765) believed a single curve would suffice for all igneous rocks. The difference in the curves for tholeiitic and alkali basalt differ-

entiates found here lends support to Mathews' hypothesis, even though the scatter and paucity of the data makes it advisable to use the single general curve for an unknown Hawaiian specimen. Furthermore, the general Hawaiian curve (fig. 29.3) is much steeper than Callaghan and Sun's general curve or the specific curves of Mathews. The Hawaiian tholeiitic series yields higher values, and the alkali basalt series lower, than any points reported by Callaghan and Sun or Mathews. This may be because the Hawaiian rocks are not contaminated by siliceous country rock, which is one of the unique advantages in the study of Hawaiian magmatism.

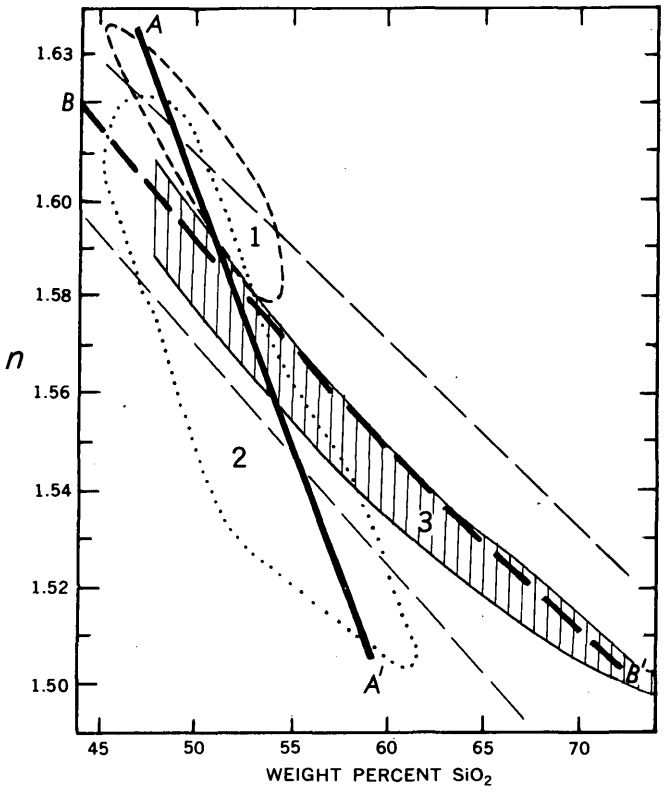

FIGURE 29.3.—Plot of index of refraction (n) against percent SiO_2 for various artificial and natural glasses. 1, Hawaiian tholeiitic series; 2, Hawaiian alkali basalt series; A–A' general determinative curve for Hawaiian artifical glasses; B–B', general determinative curve of Callaghan and Sun (1956) (sub-parallel dashed lines indicate the range of their observations); 3, area covered by determinative curves for three magma suites studied by Mathews (1951).

REFERENCES

Callaghan, Eugene, and Sun, Ming-Shan, 1956, Correlation of some igneous rocks of New Mexico by the fusion method: Am. Geophys. Union Trans., v. 37, p. 761–766.

Chapman, R. W. 1947, Crystallization phenomena in volcanic ejecta from Kilauea, Hawaii: Am. Mineralogist, v. 32, p. 105–110.

Cross, Whitman, 1904, An occurrence of trachyte on the island of Hawaii: Jour. Geology, v. 12, p. 510–523.

George, W. O., 1924, The relation of the physical properties of natural glasses to their chemical composition: Jour. Geology, v. 32, p. 353–372.

Kuno, H. Yamasaki, K., Iida, C., and Nagashima, K., 1957, Differentiation of Hawaiian magmas: Japanese Jour. Geology and Geography, v. 28, p. 179–218.

Macdonald, G. A., 1949, Petrography of the island of Hawaii: U.S. Geol. Survey Prof. Paper 214–D, p. 51–93.

Mathews, W. H., 1951, A useful method for determining approximate composition of fine grained igneous rocks: Am. Mineralogist, v. 36, p. 92–101.

Murata, K. J., and Richter, D. H., 1961, Magmatic differentiation in the Uwekahuna Laccolith, Kilauea Caldera, Hawaii: Jour. Petrology, v. 2, p. 424–437.

Tilley, C. E., and Scoon, J. H., 1961, Differentiation of Hawaiian basalts: Trends of Mauna Loa and Kilauea historic magma: Am. Jour. Science, v. 259, p, 60–68.

Washington, H. S., 1923a, Petrology of the Hawaiian Islands, pt. 1, Kohala and Mauna Kea: Am. Jour. Sci., 5th ser., v. 5, p. 465–502.

——— 1923b, Petrology of the Hawaiian Islands, pt. II, Hualalai and Mauna Loa: Am. Jour. Sci., 5th ser., v. 6, p. 100–126.

——— 1923c, Petrology of the Hawaiian Islands, pt. III, Kilauea and general petrology of Hawaii: Am. Jour. Sci., 5th ser., v. 6, p. 338–367.

Yoder, H. S., Jr., and Tilley, C. E., 1957, Basalt magmas: Carnegie Inst. Washington Year Book 56, p. 156–161.

30. DETERMINATION OF SILICA IN TEKTITES AND SIMILAR GLASSES BY VOLATILIZATION

By MAXWELL K. CARRON and FRANK CUTTITTA, Washington, D.C.

Work done in cooperation with National Aeronautical and Space Administration

As part of a systematic investigation of the chemistry of tektites, methods are being devised that will provide accurate analytical results, allow the study of smaller tektite samples, and conserve valuable museum specimens. This paper presents a volatilization method for the determination of silica that will furnish accurate analytical results comparable to those obtained by the conventional gravimetric (double HCl dehydration)

or the spectrophotometric (molybdenum-blue) methods, permit the determination of Al, Mg, Ca, Na, K, Ti, Fe, P, and Mn in the same sample taken for the silica determination, and be less time consuming than the conventional gravimetric procedure.

An accurately weighed portion of tektite is digested with HF in a weighed platinum crucible. Silicon is volatilized as SiF_4 at steam-bath temperature, and the resultant fluoride salts are converted to nitrates with concentrated HNO_3. The nitrates in the residue are decomposed with formaldehyde, evaporated to dryness on a steam bath, and ignited to constant weight at 750°C±15°C.

The decomposition of nitrates with formaldehyde is accomplished in two steps, as follows:

$$4NO_3^{-1}+2CH_2O \rightarrow 4NO_2^{-1}+2H_2O+2CO_2$$
$$4NO_2^{-1}+3CH_2O \rightarrow 2N_2+3CO_2+O_2+3H_2O$$

The residue contains the oxides of Al, Fe, Ca, Mg, Na, K, Ti, Mn, P, and the trace constituents. These oxides are brought into solution by digestion with a mixture of $HF \cdot HClO_4$ followed by heating to fumes of $HClO_4$. Except for the determination of ferrous iron, one sample can be used for the determination of all the major constituents of tektites.

The method appears to be especially suited to the determination of SiO_2 in tektites because of their low alkali content and almost complete absence of volatile constituents such as CO_2 and H_2O. A correction must be made for the oxidation of FeO to Fe_2O_3 after the final ignition to constant weight.

Procedure—To 0.2000 g of sample in a weighed platinum crucible, add 2 ml of water and 4–5 ml 49 percent HF. Cover with a platinum cover and digest on a steam bath for at least 2 hours. Uncover, evaporate the solution to about 2 ml, and add 5 ml conc HNO_3. Evaporate the solution to dryness. Repeat the evaporation twice with 5-ml additions of conc HNO_3. Add two 5-ml portions of formaldehyde, and evaporate to dryness each time to destroy nitrates. Allow the second evaporation to proceed overnight. Heat the partially covered crucible *gently* in an air bath, gradually raising the temperature to full heat of the burner. Continue heating for another 15 minutes. Transfer the crucible to a regulated muffle furnace. Heat at 750° C±15° C for 3 hours with the cover slightly aside to allow oxidation of iron to the ferric state. Weigh and repeat the heating for additional ½-hour periods until constant weight is obtained. The loss in weight after ignition to constant weight, corrected for the oxidation of the FeO originally present in the tektite to Fe_2O_3, represents the silica content of the sample.

The temperature of ignition of the residues is critical. Constant weights obtained at 750° C gave silica values comparable to those obtained by conventional gravimetric or spectrophotometric methods. Igniting at 700° C for 4 hours gave lower silica values, ranging from 1 to 2 percent absolute below acceptable values. At 800° C, results were high by nearly 0.5 percent absolute.

The possibility of loss by volatilization of the alkalies at the temperature (750° C) of ignition to constant weight was investigated. The alkali content (Na_2O and K_2O) of the ignited residues was determined by flame photometry. The results show no significant difference from those obtained for the original untreated tektite samples. The described procedure was devised primarily for use as an independent and accurate method for the determintion of silica in tektites and other similar glasses.

The table below presents a comparison of silica determinations by the volatilization-formaldehyde method with those by the conventional gravimetric or spectrophotometric methods. All results are well within 1 percent (relative) of each other. Our data also indicate that this procedure provides a better reproducibility of results than the conventional gravimetric or spectrophotometric methods.

Comparison of determinations of SiO_2 *in tektites by various methods*

Tektite [1]	Gravimetric [2]	Spectrophotometric [3]	Volatilization [4]
Bediasite B–6		76. 4	76. 26
Bediasite B–50		78. 4	78. 15
Bediasite B–85		75. 7	75. 77
Bediasite B–86		75. 4	75. 45
Synthetic bediasite [5] ST–1	76. 47, 76. 27		76. 41, 76. 35
Synthetic bediasite [5] ST–2	76. 19, 75. 90		76. 13
Synthetic australite [6] ST–3	75. 90, 75. 44	75. 6	75. 30, 75. 59
Synthetic australite [6] ST–4	75. 89. 75. 60	75. 8	75. 85, 75. 80
Synthetic australite [6] STG–2	74. 95	75. 2	74. 88

[1] Natural-bediasite samples are from Lee County, Tex.
[2] Double dehydration with HCl plus recovery of SiO_2 from the R_2O_3.
[3] Average of 6 determinations by the molybdenum-blue method.
[4] Volatilization-formaldehyde procedure described in this report.
[5] Prepared according to an average bediasite composition by Corning Glass Co.
[6] Prepared by Dr. Dean Chapman, Ames Research Center, Moffett Field, Calif.

31. USE OF La_2O_3 AS A HEAVY ABSORBER IN THE X-RAY FLUORESCENCE ANALYSIS OF SILICATE ROCKS

By HARRY J. ROSE, JR., ISIDORE ADLER, and FRANCIS J. FLANAGAN, Washington, D.C.

The major problem in the development of an X-ray fluorescence method of analysis applicable to a wide variety of silicate rock types has been the matrix of the sample for analysis. For a number of reasons the problem is particularly great for the light elements. The X-ray fluorescence yield is low and the absorption by the detector is high. Further, these intensities can be altered considerably because of the large absorption coefficients for the light elements. Problems of absorption can be minimized in various ways such as by dilution of the sample, by the use of internal standardization, and by the use of a heavy absorber as is described here.

To minimize interelement effects by the dilution method, a large diluent-to-sample ratio is required with a resultant loss in intensity that would interfere with the analysis of the light elements. Andermann (1961) and Claisse (1956) have discussed the heterogeneity of powdered samples even after long grinding periods and have indicated that one cannot reduce the particle size sufficiently to eliminate mineralogic differences from sample to sample. For the same reasons, the mechanical addition of a heavy absorber to the dilution mixture fails to improve either linearity or scatter, serving only to decrease counting rates.

The internal standardization method has been treated comprehensively by Adler and Axelrod (1955). The method requires the selection of an element as an internal standard that will be absorbed in the same way as the element to be analyzed. This technique works well when one element, or even several, is involved, but the method would prove cumbersome for the analysis of a large number of elements.

Of the several methods of sample preparation, that of smoothing the surface of a finely powdered sample (Chodos and Engel, 1961) has the advantage of speed and simplicity but requires the use of sets of standards whose composition approximates that of the rocks to be analyzed. Although both their unknowns and standards were amphibolites, these authors did not report SiO_2 and Al_2O_3, the main constituents of silicate rocks, because of the poor precision of these determinations. Two considerations are important to the success of this method: The standards must be mineralogically similar to the samples to be analyzed, and all preparations must be of uniform particle size.

Claisse (1956) made borax fusions to eliminate mineralogic and particle-size effects and analyzed molded, fused buttons. To avoid problems of absorption he used a large flux-to-sample ratio to analyze elements of intermediate atomic number where high intensities are available, but large dilutions cannot be tolerated for the light elements because of low intensities.

Andermann (1961) fused cement raw mixes with an equal weight of lithium tetraborate and demonstrated the improvement of analyses of fused samples over those using powdered, unfused materials. The method is described as eliminating standardization by type of material but requires extensive calculations to correct for differences in composition.

Claisse (1956) mentioned the addition of a heavy element to the fusion mixture to produce a more absorbing glass. The addition causes some loss in intensity for the lighter elements but should minimize differences due to absorption.

Since samples to be analyzed might contain varying amounts of strongly absorbing elements, the effect of these elements might be minimized by introducing into the sample melt a strong absorber, an element of high atomic number, in an amount such that the variation in concentration of absorbing elements in the unknown sample will not materially affect the overall absorption of the pellet for the elements being determined. Lanthanum is a strong absorber, is readily available at a moderate price in the form of the oxide, and offers the least interference to the elements to be analyzed.

Several methods of preparation have been tried in this study. A set of six analyzed materials covering a range of silica usually found in rock analysis was prepared by each of three methods: (1) One part of sample ground to 325 mesh is mechanically mixed with four parts of boric acid; (2) 0.250 g of sample is fused with 1.250 g of $Li_2B_4O_7$; and (3) 0.250 g of sample is fused with 0.250 g of La_2O_3 and 1.000 g of $Li_2B_4O_7$.

Fusions are made in graphite crucibles. After a preliminary heating at 750° C to remove CO_2 and H_2O, the samples are fused at 1,000° C for 8 to 10 minutes. The cooled bead is weighed to determine loss on ignition of the sample and sufficient boric acid is added to bring the weight to 1.600 g. The bead and boric acid are ground together in a mixer-grinder to pass a 325–mesh screen. The boric acid serves as a binder in pressing a pellet and obviates differences in ignition losses from sample to sample. The samples are double pelleted with a boric acid backing as described by Rose and Flanagan (Art. 32).

The counting-rate data for SiO_2, CaO and Fe_2O_3 for each of the three preparations and duplicate determinations are plotted against concentration (fig. 31.1).

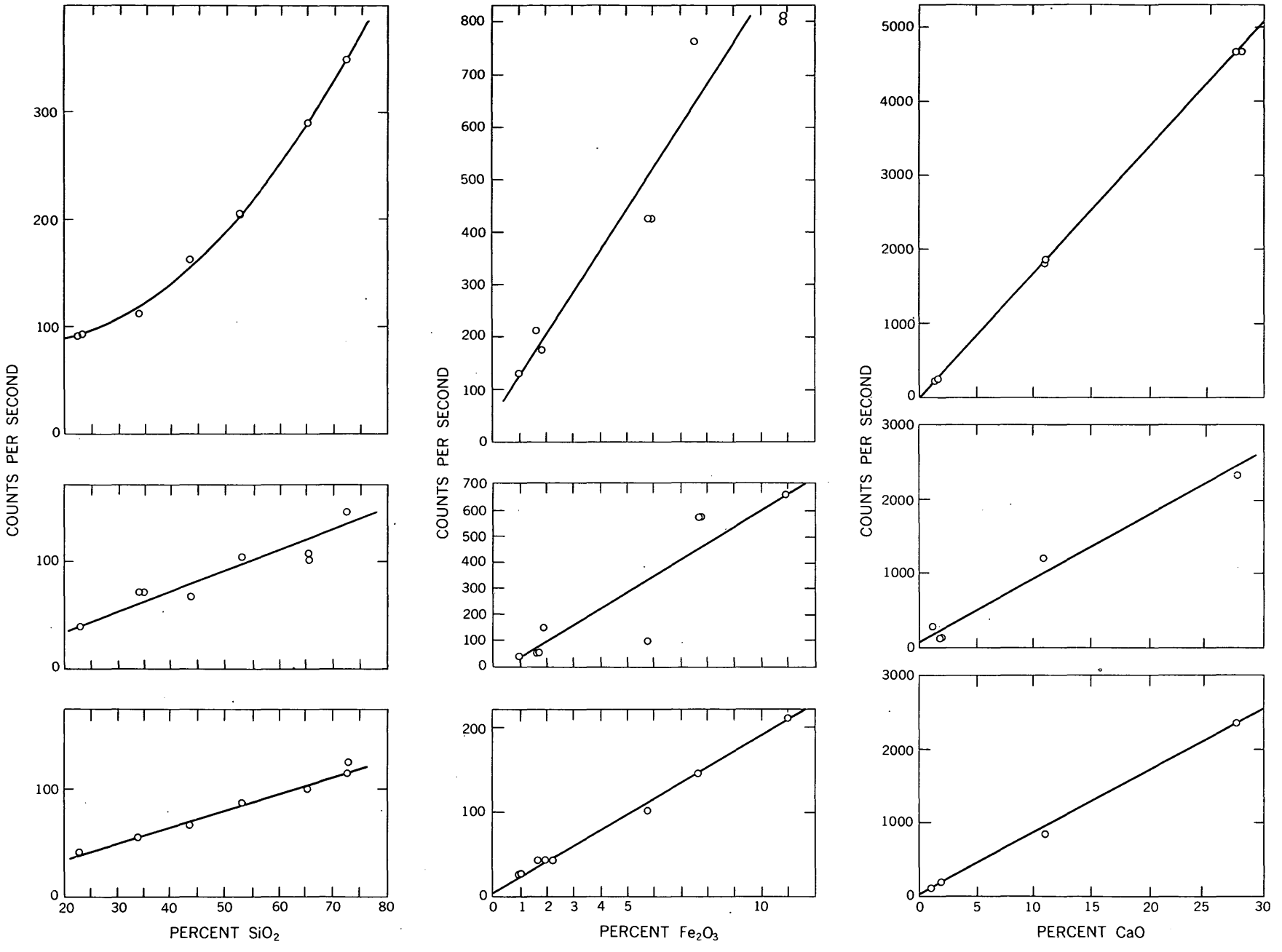

FIGURE 31.1.—SiO_2, Fe_2O_3, and CaO calibration curves for samples prepared by mechanical mixing (top), with $Li_2B_4O_7$ (middle), and fusion with La_2O_3 and $Li_2B_4O_7$ (bottom).

For samples mechanically mixed, the CaO data show excellent linearity over the range, the results for Fe_2O_3 are scattered widely, and the data for SiO_2 are curvilinear. Although a linear curve may be drawn for SiO_2, the scatter of points for samples simply fused with $Li_2B_4O_7$ indicates that the calibration curves are of little value. The problem encountered in both of these preparations is the large absorption differences among the samples chosen.

The decrease in scatter and the improvement in the calibration lines when a heavy absorber, La_2O_3, is present can be seen in the curves. Minor problems remain of determining the optimum ratio of La_2O^3 to $Li_2B_4O_7$ in the sample. The method, however, has been used to analyze successfully a variety of materials with results agreeing within 1 percent of the chemical determination.

REFERENCES

Adler, I. and Axelrod, J. M., 1955, Internal standards in fluorescent X-ray spectroscopy: Spectrochim. Acta, v. 7, p. 91–99.

Andermann, George, 1961, Improvements in the X-ray emission analysis of cement raw mix: Anal. Chemistry, v. 33, p. 1689–1695.

Chodos, A. A., and Engel, C. G., 1961, Fluorescent X-ray spectrographic analysis of amphibolite rocks: Am. Mineralogist, v. 46, p. 120–133.

Claisse, F., 1956, Accurate X-ray fluorescence analyses without internal standard: Department of Mines, Province of Quebec, Canada, P. R. 327, 16 p.

32. X-RAY FLUORESCENCE DETERMINATION OF THALLIUM IN MANGANESE ORES

By Harry J. Rose, Jr. and Francis J. Flanagan, Washington, D.C.

The X-ray spectrographic technique has been demonstrated as a useful tool for the determination of elements of geochemical interest (Adler and Axelrod, 1955, Axelrod and Adler, 1957). The determination of thallium is required occasionally, but the chemical procedure is frequently complicated by interference from geochemically related elements. A rapid X-ray spectrographic method for determining thallium in manganese ores has been developed that requires 100 mg (milligrams) of sample. While the method described will determine thallium down to 100 ppm (parts per million), the present study indicates that as little as 10 ppm can be detected. As in most X-ray fluorescent methods, the prepared samples and standards are not destroyed during the analysis and may be used for further study.

A set of synthetic standards is prepared by dilution of pure thallous nitrate with a mixture containing 90 percent manganese dioxide and 10 percent ferric oxide. By successive dilution of the thallous nitrate the composition of the standard approximates the major constituents of the sample to be analyzed. Each dilution mixture is ground in an agate mortar to pass a 325-mesh screen. The standards in this study cover a range from 0.01 to 1.00 percent thallium.

The sample is ground to pass a 325-mesh screen. One hundred milligrams of the sample or standard is mixed with 900 mg of H_3BO_3 in an agate mortar until homogeneous. The mixture is then pressed into a pellet 1 inch in diameter. For additional strength the pellet is prepared as a double layer by lightly pressing approximately 1 gram of H_3BO_3 in the mold and then adding the sample-boric acid mixture onto this pellet in the mold before final pressure is applied. Sample numbers and other data may be written in ink on the smooth face of the boric acid backing, and the pellets thus formed may be stored indefinitely in pill boxes for future use. Dilution at this level tends to minimize interelement effects.

The instrument consists of a two-channel fluorescent air-path X-ray spectrometer (Adler and Axelrod, 1953) with lithium fluoride analyzing crystals. Krypton-halogen filled Geiger counters are used with simultaneous counting by scalers operating in parallel. A tungsten target X-ray tube is operated at 50 kilovolts and 20 milliamperes. Two measurements are made: the time required to accumulate 10,000 counts for the Tl $L\alpha$ line, and the number of counts recorded for the background position during this interval.

The intensity of the background line at 33.30° 2θ is subtracted from the intensity of the Tl Lα line at 34.87° 2θ. A straight-line calibration curve is obtained over the range of 0.01 to 1.00 percent thallium. The table below gives the data obtained on five samples analyzed by this method and the chemical values obtained by Cuttitta (1961).

Sample	Thallium (percent)			
	X-ray	Chemical		
1	0. 23	0. 24	0. 20	0. 24
2	. 34	. 36	. 37	. 38
3	. 07	. 073	. 067	. 070
4	. 02	. 017	. 017	. 017
5	. 28	. 27	. 27	. 30

The X-ray results were obtained by counting each standard and sample twice in a random order. The standard deviation of a single observation calculated from the duplicate net-counting rates for samples and standards is 0.31 counts per second, equivalent to 0.005 percent Tl. The speed of the method may be demonstrated by the time necessary to prepare the pellets and count the set of five samples. Results on these samples were obtained within 4 hours, including the preparation of the standards.

For samples having a concentration of thallium an order of magnitude lower than the values given above, it is possible to extend the lower limit of detection by reducing the amount of boric acid to be added to the samples and standards. However, problems of absorption become more critical as the proportion of diluent is reduced. While the determination of thallium described herein was applied to manganese ores, the method can easily be adapted to other materials or elements of geochemical interest by preparing a set of standards whose matrix is similar to that of the material to be analyzed.

REFERENCES

Adler, Isidore, and Axelrod, J. M., 1953, A multi-wavelength fluorescence spectrometer: Opt. Soc. America Jour., v. 43, p. 769–772.

——— 1955, Determination of thorium by fluorescent X-ray spectrometry: Anal. Chemistry, v. 27, p. 1002–1003.

Axelrod, J. M., and Adler, Isidore, 1957, X-ray spectrographic determination of cesium and rubidium: Anal. Chemistry, v. 28, p. 1280–1281.

Cuttitta, Frank, 1961, Dithizone mixed-color method for determining small amounts of thallium in manganese ores: Art. 290 *in* U.S. Geol. Survey Prof. Paper 424–C, p. C384–C385.

OCEANOGRAPHY

33. ELECTRODE DETERMINATION OF THE CARBON DIOXIDE CONTENT OF SEA WATER AND DEEP-SEA SEDIMENT

By G. W. Moore, C. E. Roberson, and H. D. Nygren, Menlo Park, Calif., and U.S. Coast and Geodetic Survey, Washington, D.C.

Work done in cooperation with the U.S. Coast and Geodetic Survey

The P_{CO_2} (partial pressure of carbon dioxide) was determined in samples of water and sediment in the North Pacific using a P_{CO_2} electrode originally designed for medical studies of human blood. This work was done aboard the U.S. Coast and Geodetic Survey ship *Pioneer* in September and October 1961 as part of a general investigation of the geochemistry of deep-sea sediment. The determinations compare favorably with theoretical calculations and provide new data on the distribution of carbon dioxide in the North Pacific.

The Severinghaus P_{CO_2} electrode incorporates the glass-electrode principle (Severinghaus and Bradley, 1958). The instrument consists of a glass-calomel electrode pair mounted in a bicarbonate solution and separated from the sample to be measured by a thin Teflon membrane (fig. 33.1). The membrane permits passage of carbon dioxide molecules from the sample into the bicarbonate solution while excluding ions that might alter the pH of the solution. Carbon dioxide from the sample passes through the Teflon membrane

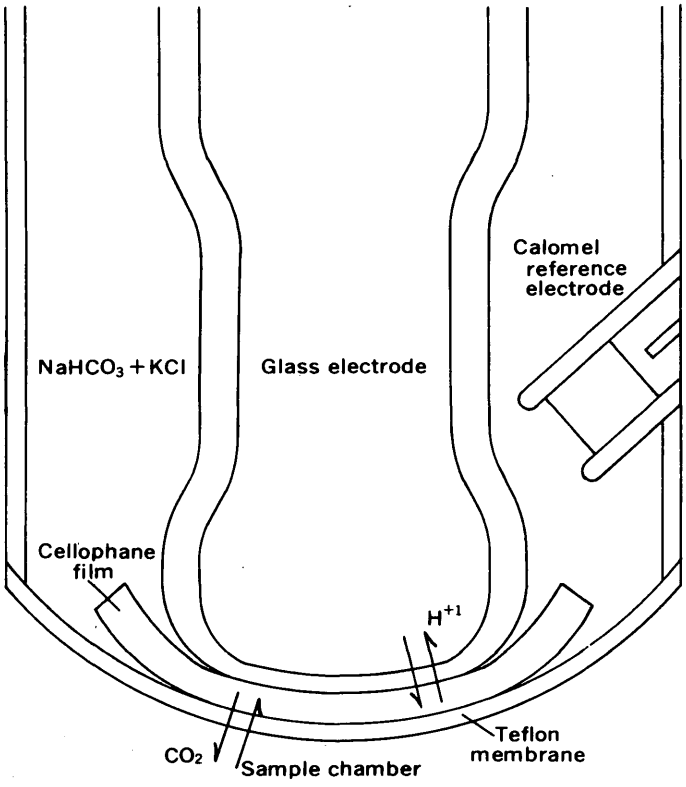

FIGURE 33.1.—Diagram of the Severinghaus P_{CO_2} electrode.

and equilibrates with a very thin layer of the bicarbonate solution carried by a cellophane film adjacent to the glass electrode. The electrode pair then records the pH of the bicarbonate solution which is a measure of the P_{CO_2} of the sample.

The carbon dioxide content of the samples from the North Pacific was determined as soon as possible after the samples were collected so as to minimize carbon dioxide loss. The samples of water and sediment were injected by means of a hypodermic syringe through a slender tube into the sample chamber of the electrode, which was sealed except for an overflow tube. The electrode was immersed in a constant-temperature bath, and the readings were made at a fixed elevated temperature of 40°C, which increased the sensitivity of the instrument. Readings are corrected to 25°C or to natural temperature in the ocean using the values of Henry's constant given by Harned and Davis (1943, p. 2033). Approximately 10 minutes was required to reach equilibrium with the water samples and 2 minutes with the sediment samples, which were richer in carbon dioxide. The lower limit of detection was 0.0006 atm (atmosphere) for analyses quoted at 25°C and 0.0003 atm at 1°C. The instrument could be used continuously for analyzing water samples, but it had to be disassembled and cleaned after each sediment analysis.

The sediment samples were taken in piston and Phleger coring devices, and the water samples were collected in Nansen bottles. Frank C. Rainwater, U.S. Geological Survey, and Theodore Ryan, U.S. Coast and Geodetic Survey, participated in the shipboard investigation.

The P_{CO_2} determinations on sea-water samples are shown on a profile along the 160th meridian from Alaska to Hawaii (fig. 33.2). Additional data are given in figure 33.3 for a typical station about 350 kilometers northwest of Honolulu. Pressure is not considered in the illustrations, to permit the surface and deep water to be compared. The actual P_{CO_2} at depth is higher than shown owing to the effect of pressure on Henry's constant.

The carbon dioxide content is low in the top few hundred meters of the sea where it approaches equilib-

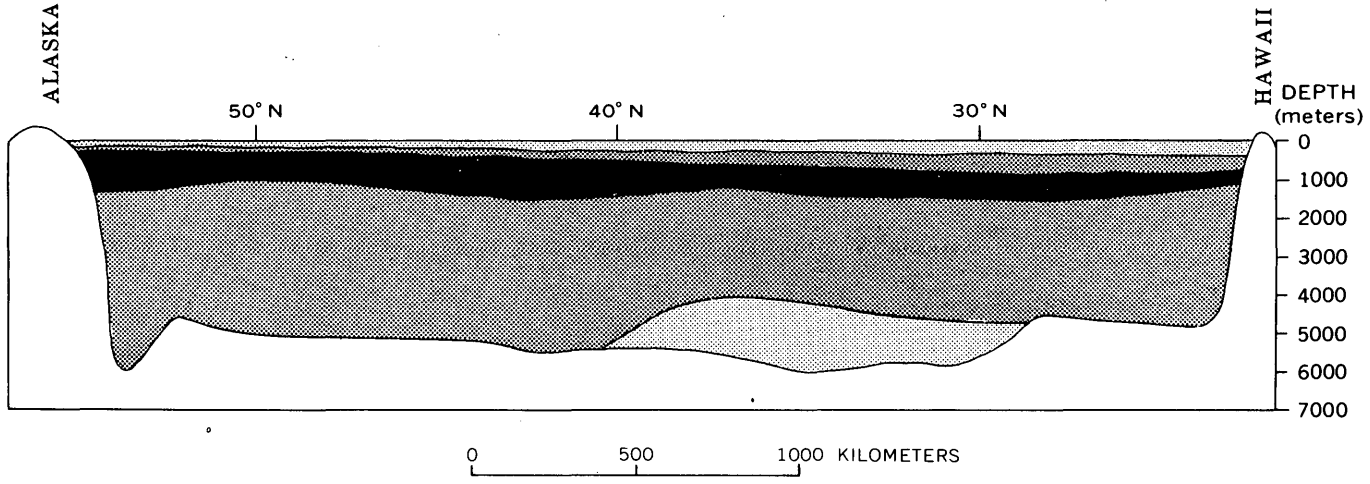

FIGURE 33.2.—P_{Co_2} at natural temperature in the ocean determined at oceanographic stations along the 160th meridian. The black zone indicates values greater than 0.0008 atm; the dark gray, values between 0.0004 and 0.0008 atm; and the light gray, values less than 0.0004 atm. Values for some near-surface samples were calculated from the alkalinity and the pH.

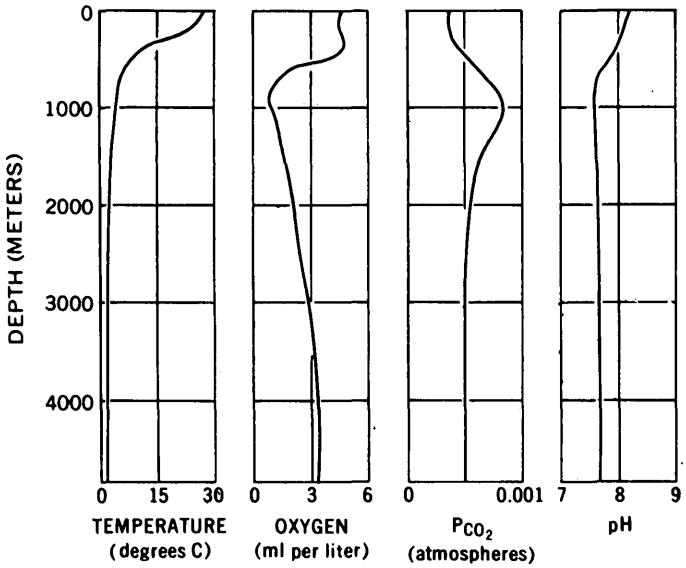

FIGURE 33.3.—P_{CO_2} at natural temperature and other properties of sea water from lat 23°30′ N., long 159°58′ W.

rium with the low content of the atmosphere. The carbon dioxide content reaches a maximum value at a depth of about a thousand meters, which is approximately the depth of minimum oxygen pressure. At this depth organic material sinking from the surface decays rapidly, but photosynthetic utilization of carbon dioxide cannot occur because light is almost absent.

The intermediate layers, which constitute the greatest part of the water of the North Pacific, have a carbon dioxide tension averaging 0.0006 atm, or about twice that of water in equilibrium with the atmosphere. This P_{CO_2} reflects a balance between the rate of overturn of this principal part of the water mass and the production of carbon dioxide by decay of sinking debris and by the respiration of the rare indigenous animals in this zone.

A tongue of water that has a carbon dioxide concentration only a little greater than that of the surface water occupies the floor of a broad trough north of Hawaii (fig. 33.2) and north of the station illustrated in figure 33.3. The tongue is probably made up of water that has most recently been added to the circulation system. Theoretical studies of oceanic circulation and observations of temperature, salinity, and dissolved oxygen content suggest that this cold dense water descended near Antarctica and moved northward along the floor of the ocean to its present position (Stommel and Arons, 1960).

In table 33.1 the measured values of P_{CO_2} at the station illustrated in figure 33.3 are compared with theoretical values derived from measurements of the pH and titration alkalinity. This method for calculating P_{CO_2} is based on the two following dissociation reactions (1 and 2) and a stoichiometric relation (3):

$$CO_2+H_2O=H^{+1}+HCO_3^{-1} \quad (1)$$

$$HCO_3^{-1}=H^{+1}+CO_3^{-2} \quad (2)$$

$$M_{HCO_3^{-1}}+2M_{CO_3^{-2}}=A \quad (3)$$

The equilibrium expressions for (1) and (2) are based on activity values, where the activity (a) is defined as the product of the molality (m) and the activity coefficient (γ) of an individual species. In (3) it is necessary to use molar concentrations (M), because the alkalinity (A) is expressed in equivalents per liter of acid used to titrate to pH 4.5. (The principal titratable constituents are assumed to be HCO_3^{-1} and CO_3^{-2}. At values below pH 8.0 the contribution to the alkalinity by borate is less than 2 percent and has been ignored.)

TABLE 33.1.—*Comparison between measured and calculated values of P_{CO_2} at 25° C in sea water from lat 23°30′ N., long 159°58′ W.*

Depth (meters)	Measured P_{CO_2} (atmospheres)	pH	Alkalinity (equivalents per liter)	Calculated P_{CO_2} (atmospheres)
1	<0.0006	8.20	0.00247	0.0003
191	<.0006	8.12	.00256	.0004
389	<.0006	7.95	.00243	.0006
588	.0011	7.79	.00254	.0009
716	.0013	7.62	.00251	.0014
895	.0014	7.62	.00256	.0014
1075	.0016	7.61	.00259	.0014
1343	.0014	7.58	.00256	.0015
1612	.0011	7.59	.00262	.0015
2726	.0010	7.65	.00259	.0013
3693	.0011	7.63	.00259	.0013
4380	.0011	7.63	.00262	.0013

The equilibrium constants K_1 and K_2 for (1) and (2) respectively at 25°C were calculated as $10^{-7.80}$ and $10^{-10.33}$ from free energy values given by Rossini and others (1952). The activity of water in sea water was taken as 0.98 (Harvey, 1955, p. 169), and $\gamma_{HCO_3^{-1}}$ and $\gamma_{CO_3^{-2}}$ were taken as 0.36 and 0.019 respectively (Sverdrup and others, 1942, p. 205).

In the equilibrium expressions (1) and (2), the concentrations expressed in molalities were calculated to molarities for use in (3). For sea water with an average salinity of 34.5 parts per thousand, the relation $m=1.010M$ applies. It is convenient to write (3) as

$$m_{HCO_3^{-1}}+2m_{CO_3^{-2}}=1.010A. \quad (4)$$

From (2), using the stipulated conditions,

$$m_{CO_3^{-2}}=\frac{10^{-9.05}m_{HCO_3^{-1}}}{a_{H^{+1}}}. \quad (5)$$

And from (1), assuming $a_{CO_2}=P_{CO_2}$,

$$P_{CO_2}=\frac{a_{H^{+1}}m_{HCO_3^{-1}}}{10^{-7.37}}. \quad (6)$$

Finally, by combining (4), (5), and (6), replacing a_{H^+} by pH, and collecting terms, the following relation between the P_{CO_2} in atmospheres, the alkalinity in equivalents per liter, and the pH is derived:

$$P_{CO_2}=\frac{10^{-2pH}A}{10^{-(pH+7.37)}+7.59\times10^{-17}}. \quad (7)$$

Comparison in table 33.1 between the calculated values of P_{CO_2} and those measured aboard the ship suggests that the values for the activity coefficients used in the calculations are reasonably accurate. Perhaps the electrode could be used to refine these values, however, in carefully controlled laboratory experiments.

The P_{CO_2} of the sediment in a layer 2 to 3 centimeters below the sediment-water interface is given in table 33.2 for 13 localities in the North Pacific. The values are remarkably uniform, averaging about 0.007 atm, and show no systematic variation with respect to either latitude or depth. The average value is about 20 times that of water in equilibrium with the atmosphere, and the carbon dioxide probably resulted from decay of organic material within the sediment. The relatively uniform carbon dioxide content is less surprising when considered together with the uniformity of the other aspects of the physical environment: The temperature of the bottom probably does not differ by more than 1°C; the pH ranges only 0.7 pH units; and the Eh ranges 0.20 volts. Romankevich (1961) states that the organic-carbon content of northwest Pacific sediment ranges between 0.2 and 0.8 percent. Variations within this range and differences in the rate of diffusion into the overlying sea water probably account for the observed differences in the P_{CO_2} of the sediment.

TABLE 33.2.—P_{CO_2} *at 25° C and other properties of deep-sea sediment in a layer 2 to 3 centimeters below the sediment-water interface.*

[Colors of the wet sediment follow the convention of Goddard and others (1948)]

Location		Depth (meters)	Sediment	Color	P_{CO_2} (atmospheres)	pH	Eh (volts)
Lat N	Long W						
51° 41′	161° 07′	4, 670	Silty clay	Dusky yellowish brown	0. 0058	7. 2	+0. 28
50° 24′	176° 30′	7, 260	Sandy clay	Dark yellowish brown	. 0077	7. 0	+. 42
45° 50′	176° 47′	5, 450	Clay	Moderate brown	. 0055	7. 5	+. 35
41° 31′	160° 31′	5, 490	do	Moderate yellowish brown	. 0090	7. 7	+. 34
39° 20′	160° 24′	5, 400	do	do	. 0058	7. 4	+. 38
36° 50′	177° 30′	5, 250	do	Dark yellowish brown	. 0056		
32° 42′	160° 12′	5, 820	do	Moderate brown	. 0075	7. 5	+. 43
30° 06′	177° 30′	5, 290	do	do	. 0052	7. 2	+. 38
25° 55′	177° 34′	5, 070	do	do	. 0059		
24° 42′	166° 24′	4, 690	do	do	. 0072	7. 3	+. 48
23° 30′	159° 58′	4, 820	do	do	. 0056	7. 3	+. 42
23° 29′	172° 23′	4, 630	Silty clay	Dark yellowish brown	. 0091	7. 3	
23° 22′	177° 54′	5, 120	Clay	Moderate brown	. 0063	7. 3	+. 43

REFERENCES

Goddard, E. N., chm., and others, 1948, Rock-color chart: Washington, Natl. Research Council, 11 p.

Harned, H. S., and Davis, R., Jr., 1943, The ionization constant of carbonic acid in water and the solubility of carbon dioxide in water and aqueous salt solutions from 0 to 50°C: Am. Chem. Soc. Jour., v. 65, p. 2030–2037.

Harvey, H. W., 1955, The chemistry and fertility of sea waters: Cambridge Univ. Press, 224 p.

Romankevich, E. A., 1961, Organic substance in the surface layer of bottom sediments in the western Pacific Ocean: Pacific Sci. Cong., 10th, Honolulu 1961, Abs., p. 384–385.

Rossini, F. D., Wagman, D. D., Evans, W. H., Levine, S., and Jaffe, I., 1952, Selected values of chemical thermodynamic properties: Natl. Bur. Standards Circ. 500, 1268 p.

Severinghaus, J. W., and Bradley, A. F., 1958, Electrodes for blood pO_2 and pCO_2 determination: Jour. Applied Physiology, v. 13, p. 515–520.

Stommel, H., and Arons, A. B., 1960, An idealized model of the circulation pattern and amplitude in oceanic basins, pt. 2 of On the abyssal circulation of the world ocean: Deep-sea Research, v. 6, p. 217–233.

Sverdrup, H. U., Johnson, M. W., and Fleming, R. H., 1942, The oceans: New York, Prentice-Hall, Inc., 1087 p.

HYDROLOGIC STUDIES

GROUND WATER

34. TRANSITORY MOVEMENTS OF THE SALT-WATER FRONT IN AN EXTENSIVE ARTESIAN AQUIFER

By HAROLD R. HENRY, Lansing, Mich.

The adjustment of the salt-water front in an extensive aquifer to a change in head in the salt water or the fresh water does not take place instantaneously. This article presents a mathematical demonstration that after a eustatic change in sea level many thousands of years may be required for the salt-water front to reach a new position of equilibrium in an extensive aquifer, such as the Floridan aquifer of the Southeastern States.

DERIVATION OF THE DIFFERENTIAL EQUATION

For the aquifer shown schematically in figure 34.1, the one-dimensional form of Darcy's law is

$$u=-\frac{k}{\mu}\left(\frac{\partial p}{\partial x}+\rho g\frac{\partial z}{\partial x}\right)$$

where u=velocity, k=specific permeability, μ=viscosity, p=pressure, x=distance along the aquifer from the water table in the recharge area, ρ=density of water, g=acceleration of gravity, and z=elevation above sea level. The values of velocity and pressure are continuous across the interface, whereas the density changes abruptly from ρ_0 on the fresh-water side to ρ_s on the salt-water side. It is assumed that the viscosity of salt water and fresh water are essentially equal and that the storage coefficient is 0. Integrating equation 1 and rearranging terms yields

$$H=\frac{ul}{\frac{k\rho_0 g}{\mu}}+y\frac{\rho_s-\rho_0}{\rho_0}$$

where H=height of water table above sea level, l=length of aquifer from water table to outcrop on the ocean floor and y=depth below sea level to the interface. The rate of the vertical component of movement of the interface or salt-water front is $dy/dt=u\sin\alpha/\theta$ where α is the angle of dip of the aquifer and θ is the porosity of the aquifer. For the sake of brevity the time parameter

$$T=\frac{\theta l}{\frac{k\rho_0 g}{\mu}\left(\frac{\rho_s-\rho_0}{\rho_0}\right)\sin\alpha}$$

is introduced. Equation 2 then takes the form

$$\frac{dy}{d\left(\frac{t}{T}\right)}+g=H\frac{\rho_0}{\rho_s-\rho_0}.$$

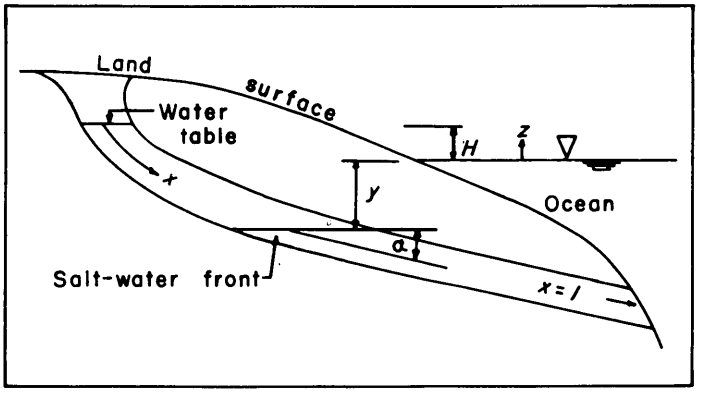

FIGURE 34.1.—Schematic sketch of an artesian aquifer with a salt-water front.

SOLUTION FOR A STEP CHANGE IN SEA LEVEL OR ARTESIAN HEAD

Let it be assumed that at a time $t=0$, H changes suddenly to a constant value which is maintained for all $t>0$. Such a change would be approximated in nature by a relatively rapid eustatic change in sea level. The variation of y is then given by the following solution of equation 3:

$$\frac{y-y_1}{H\left(\frac{\rho_0}{\rho_s-\rho_0}\right)-y_1}=1-e^{-t/T} \qquad (4)$$

where y_1 is the value of y at $t=0$. Equation 4, which is plotted in figure 34.2, indicates that the rate of the asymptotic approach of y to its equilibrium value $H\left(\frac{\rho_0}{\rho_s-\rho_0}\right)$ is governed by the parameter T.

A numerical example will clarify the relations involved. Consider an idealized artesian aquifer receiving recharge 100 miles inland, cropping out on the ocean floor 50 miles offshore, and having a seaward dip of 10 feet per mile. It is assumed that $\frac{\rho_0}{\rho_s-\rho_0}=40$, $\frac{k\rho_0 g}{\mu}=500$ feet per day, and $\theta=0.15$. These values are not unlike those applicable to the Floridan aquifer of Florida and adjacent States. For these assumed conditions $T=13{,}800$ years. It can be determined by

inspection of figure 34.2 that at $\frac{t}{T}=1$, or after a time lapse of 13,800 years, the salt front will have traveled only about 63 percent of the total distance to its new equilibrium position. If the sudden change which occurs at $t=0$ is, for example, a rise in sea level of 15 feet, then the total change to be expected in y is a decrease of 600 feet and the total distance that the salt-water front will move inland is 60 miles. After 13,800 years the front will have traveled only about 38 miles. The time necessary for the front to travel 90 percent of the total distance in this example is 31,000 years.

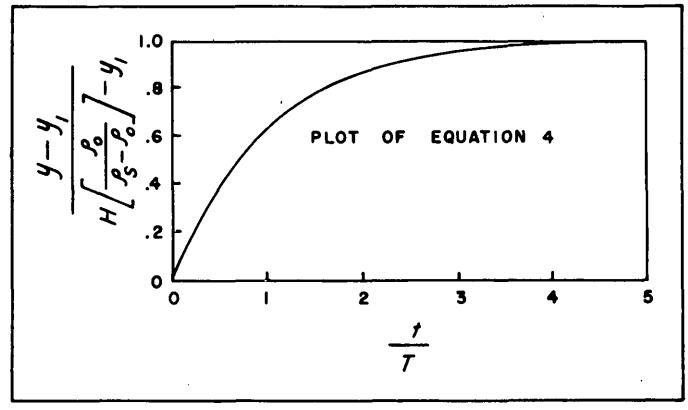

FIGURE 34.2.—The transitory movement of the salt-water front after a sudden change in sea level.

35. ESTIMATING THE EFFECTS OF STREAM IMPOUNDMENT ON GROUND-WATER LEVELS

By J. E. REED and M. S. BEDINGER, Little Rock, Ark.

Work done in cooperation with the U.S. Army, Corps of Engineers

The construction of reservoirs on streams that are hydraulically connected with aquifers results in a rise of the water table. This article describes an equation useful for estimating such changes in a semi-infinite or extensive aquifer.

At many reservoir sites the change in stream stage upstream from the dam due to the impoundment is very nearly linear with distance from the damsite. This linear change of head extends along the stream channel to the upper extreme of the pool. Upstream from this point, and at all points downstream from the dam, the change in surface-water stages due to impoundment can be considered negligible, or zero. These relations are shown graphically in figure 35.1.

The distribution of head change in the aquifer caused by such a change in stream stages can be found by using the Fourier integral. Slichter (1899, p. 336) has shown that the change of head (Δh) in a semi-infinite aquifer due to a change of head $F(y)$ along the stream boundary is given by

$$\Delta h=\frac{1}{\pi}\int_{-\infty}^{\infty}\frac{xF(z)dz}{x^2+(z-y)^2}$$

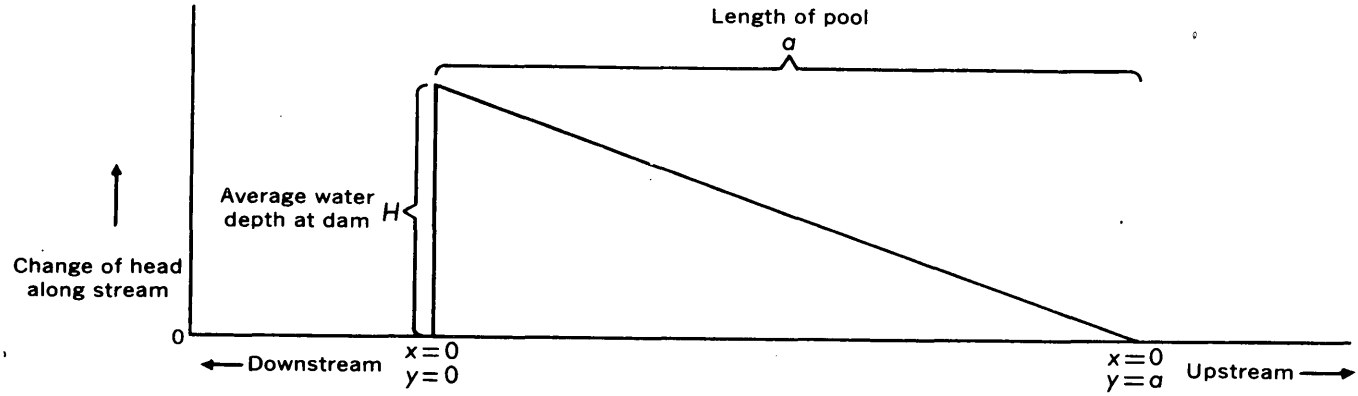

FIGURE 35.1.—Head change along stream due to impoundment.

where y represents distance along the stream, x represents distance normal to the stream, the dam is located at ($x=0$, $y=0$), and z represents a variable of integration. The boundary conditions along $x=0$ for the conditions indicated on figure 35.1 may be expressed as

$$F(y)=0,\ 0>y>a$$

and

$$F(y)=H-\frac{Hy}{a},\ 0<y<a.$$

Thus the integral becomes

$$\Delta h=\frac{1}{\pi}\int_0^a\left[H-\frac{Hz}{a}\right]\frac{x}{x^2+(z-y)^2}\,dz,$$

from which we find

$$h=\frac{1}{\pi}\left[\left(H-\frac{Hy}{a}\right)\left(\arctan\frac{a-y}{x}+\arctan\frac{y}{x}\right)+\frac{hx}{2a}\log_e\left|\frac{x^2+y^2}{x^2+(a-y)^2}\right|\right],\quad(1)$$

where Δh is the change in head in the aquifer at point (x,y), H is the change in stream stage at the dam, and a is the length of the upper pool. The head-change distribution in a part of an aquifer, determined from equation 1, is given below.

y \ x	0.0a	0.2a	0.4a	0.6a	0.8a	1.0a	1.2a	1.4a	1.6a	1.8a
1.2a	0.00H	0.05H	0.08H	0.09H	0.10H	0.09H	0.08H	0.08H	0.08H	0.07H
1.0a	.00H	.10H	.12H	.13H	.12H	.11H	.10H	.09H	.08H	.08H
0.8a	.20H	.22H	.19H	.17H	.16H	.12H	.11H	.11H	.09H	.08H
0.6a	.40H	.32H	.26H	.21H	.18H	.14H	.12H	.11H	.09H	.09H
0.4a	.60H	.43H	.31H	.23H	.18H	.15H	.13H	.11H	.10H	.09H
0.2a	.80H	.47H	.31H	.22H	.18H	.15H	.13H	.11H	.10H	.09H
0.0a	1.00H	.33H	.25H	.20H	.16H	.14H	.12H	.10H	.09H	.09H
−0.2a	.00H	.14H	.17H	.17H	.14H	.12H	.11H	.10H	.09H	.08H
−0.4a	.00H	.06H	.10H	.12H	.12H	.10H	.10H	.09H	.08H	.07H
−0.6a	.00H	.04H	.07H	.09H	.09H	.09H	.09H	.08H	.08H	.07H

Few stream channels are straight enough to fit exactly the idealized conditions indicated in figure 35.1. Thus, for example, estimates of head changes made as outlined will be in error if applied to the area near a meandering stream. At a great distance from the stream, however, irregularities in the stream path have a negligible effect on ground-water level. Equation 1 can be used in conjunction with an electrical model to determine change in head near the stream. The head change at relatively large distances from and along a line enclosing the affected portion of the stream is determined from equation 1. The head change along the stream is known. Thus, the boundary conditions are defined over the perimeter of a sensibly small part of the aquifer with its irregular configuration along the stream channel. The head change may be estimated conveniently for the limited area of irregular shape by an electrical-model study.

The method described above for estimating changes in the water table is based on the assumption that the flow system is in equilibrium. However, the water table is affected by several hydrologic agents that vary in time—a hydraulically connected stream, recharge from precipitation, discharge by evapotranspiration, and pumping from wells. The action of these hydrologic agents precludes the establishment of equilibrium in the aquifer. However, water-table fluctuations due to these agents may be averaged, and this average may be used to identify a quasi-equilibrium configuration of the water table that results from hydrologic conditions existing before construction of the dam. The average water-table configuration to be expected a long time after the reservoir is filled can be determined by simply adding the estimated change to the quasi-equilibrium configuration observed before construction. This addition is valid provided filling of the reservoir does not materially change such factors as the average stream stage above and below the pool, or the recharge and discharge rates through the area of the aquifer, and provided the flow through the aquifer may be defined by linear differential equations.

REFERENCE

Slichter, C. S., 1899, Theoretical investigation of the motion of ground waters, U.S. Geol. Survey, 19th Ann. Rept., 1897–98. pt. 2, p. 295–384.

36. MOVEMENT OF GROUND WATER BENEATH THE BED OF THE MULLICA RIVER IN THE WHARTON TRACT, SOUTHERN NEW JERSEY

By S. M. Lang and E. C. Rhodehamel, Trenton, N.J.

Work done in cooperation with the New Jersey Department of Conservation and Economic Development, Division of Water Policy and Supply

The Wharton Tract, which includes about 100,000 acres in the Pine Barrens region of southern New Jersey (fig. 36.1), was purchased by the State in 1954 as a water reserve to meet future requirements in the Camden and Atlantic City regions. An aquifer test was made by the Geological Survey at a site on the Mullica River, about 2½ miles northwest of the village of Batsto to determine the hydrologic characteristics of the water-bearing sands and the degree of hydraulic continuity between the sands and the Mullica River. The test results indicate the feasibility of developing the water resources of the tract by means of wells.

Water-level data from an extensive network of observation wells in the test site were evaluated and reported upon by Lang (1961). The evaluation indicated that ground water moves toward the river from the upland areas on either side and discharges to the river in two major areas.

In addition to the observation wells, a network of nine lines of piezometer tubes was installed in the streambed to detect ground-water movement immediately below the bottom of the river (fig. 36.2). Each piezometer tube was especially fabricated of a regular 1¼-inch well point with a ½-inch-long screen to allow for point determinations of pressure head. At each site, 2 piezometers were installed, 1 with the screen 1 foot below the streambed and 1 with the screen 2 feet below the streambed.

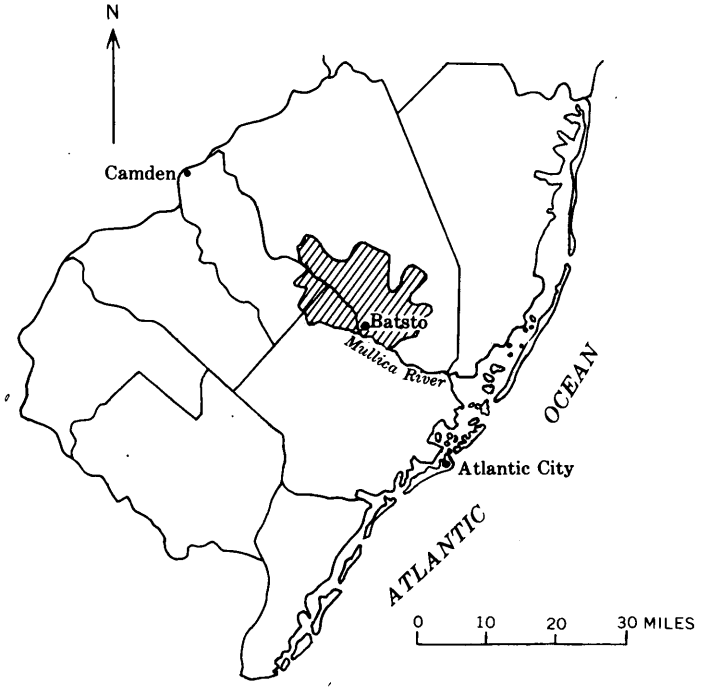

Figure 36.1.—Map of southern New Jersey showing location of Wharton Tract (crosshatched).

The discharge of ground water to the river in two major areas as indicated by the well data was corroborated by an analysis of data from the piezometer tubes. This is shown by an evaluation of the difference in the water levels (head differential) in the shallow and deep piezometers (fig. 36.2). The greater head differential in the vicinity of lines 5 and 9 results in a much larger vertical than lateral gradient, indicating that ground water discharges to the stream at these sites. Figure 36.3 shows the distribution of head as measured in the shallow piezometers. The pattern indicates movement of water in the direction in which the stream is flowing; however, because of the small head differential, the actual downstream gradient is very low compared to the gradient for lateral movement of water to the stream. Figure 36.4, showing the distribution of head in the deeper piezometers, shows centers of maximum piezometric pressure and indicates possible lateral movement in this lower level both upstream and downstream from these centers.

The piezometer levels were compared with the stream-gage height, a record of which was obtained from the stage recorder on the west bank south of line 6. This showed that the water level in both the shallow and deeper piezometer tubes stood higher than the stream level. This factor plus the pattern of head differentials shown in figure 36.2 indicates that the general pattern is one of upward movement of water from the deeper to the shallow piezometer horizon and thence to the river, with most of the discharge in the vicinity of lines 5 and 9.

The only area in which a downward gradient was observed is in the vicinity of the middle piezometer sites on line 9, where the head in the shallow piezometers is higher than that in the deeper ones. This is in part the result of turbulence in the stream produced by the backing up of water by protruding bed materials immediately north of line 9.

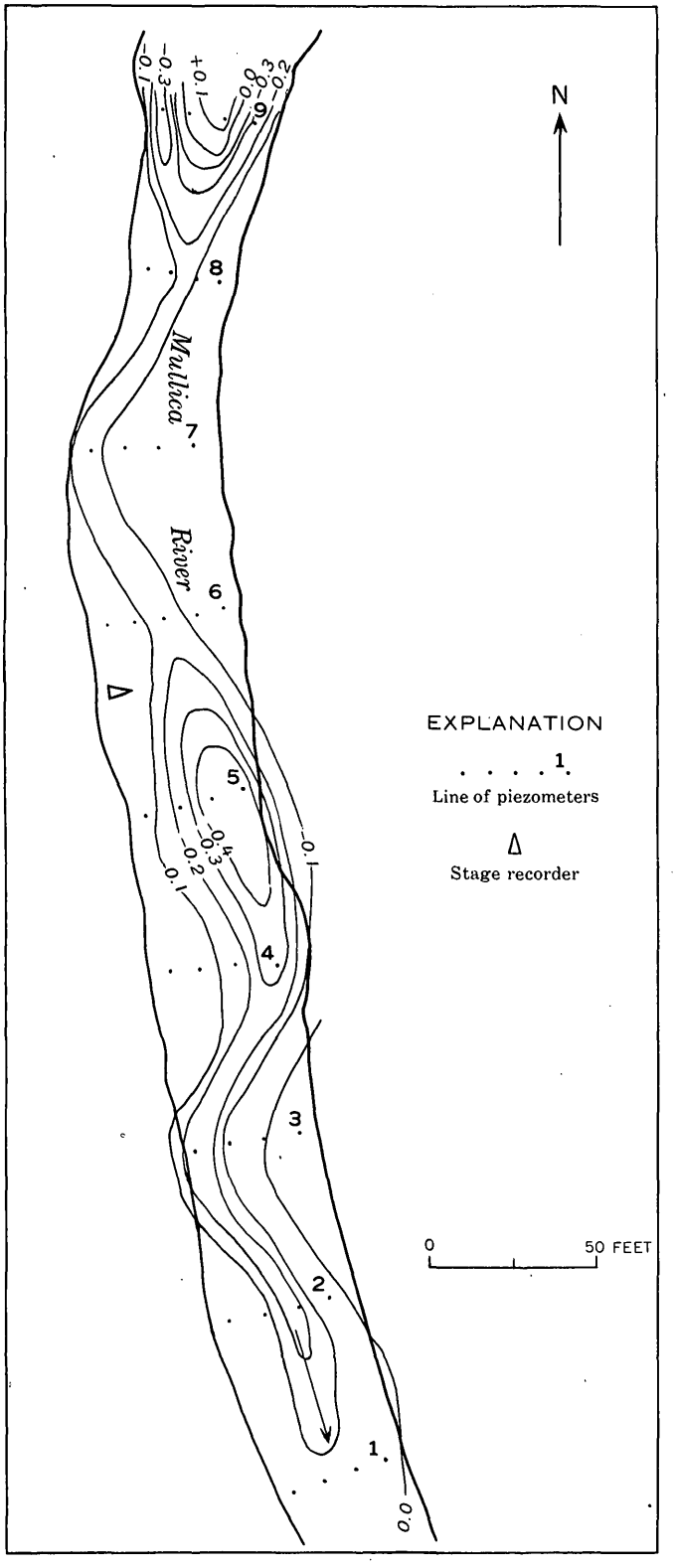

FIGURE 36.2.—Map of the Wharton Tract piezometer field showing lines of equal difference in water level (head differential) between shallow and deeper piezometer levels on June 9, 1960. Contour interval 0.1 foot. Numbers on lines of piezometers are referred to in text.

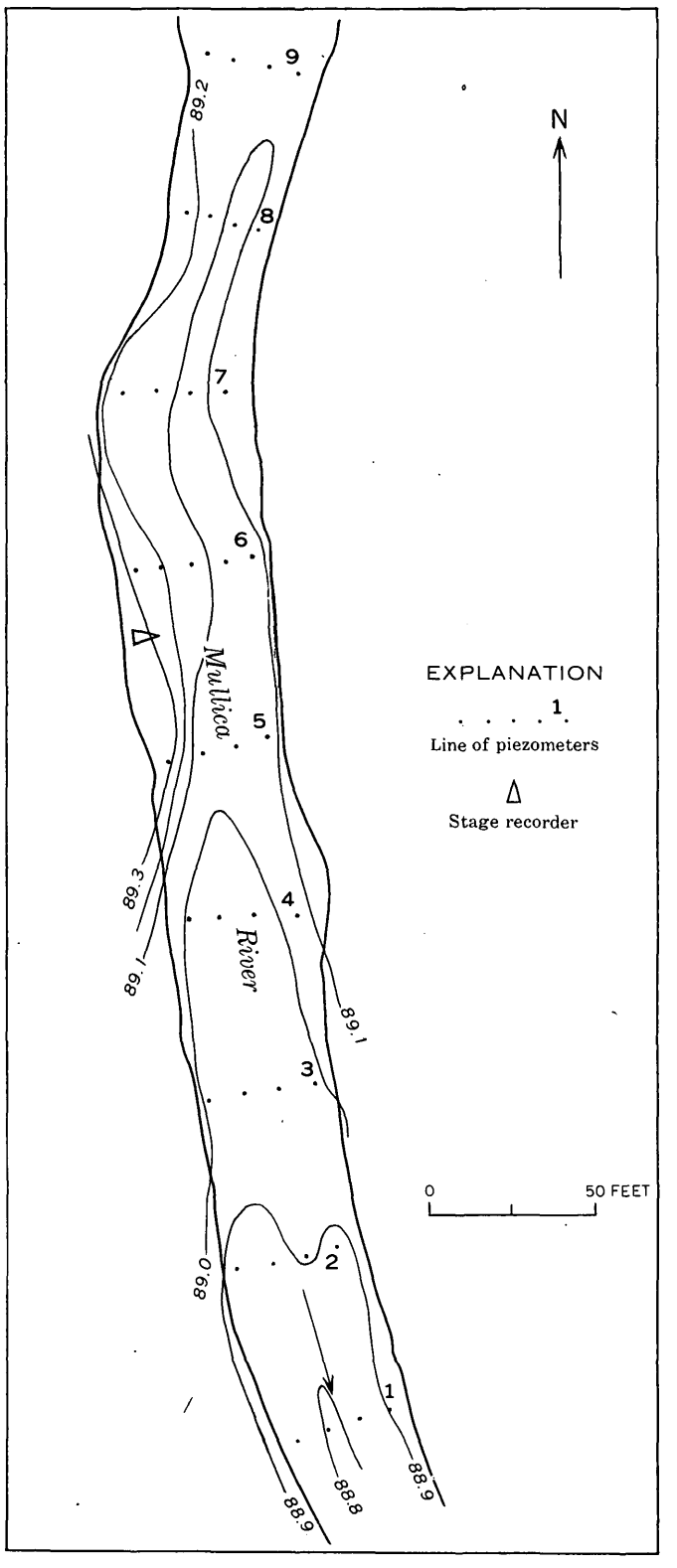

FIGURE 36.3.—Map of the Wharton Tract piezometer field showing contours of water level in piezometers 1 foot below the streambed on June 9, 1960. Contour interval 0.1 foot; datum assumed. Numbers on lines of piezometers are referred to in text.

620660—62——7

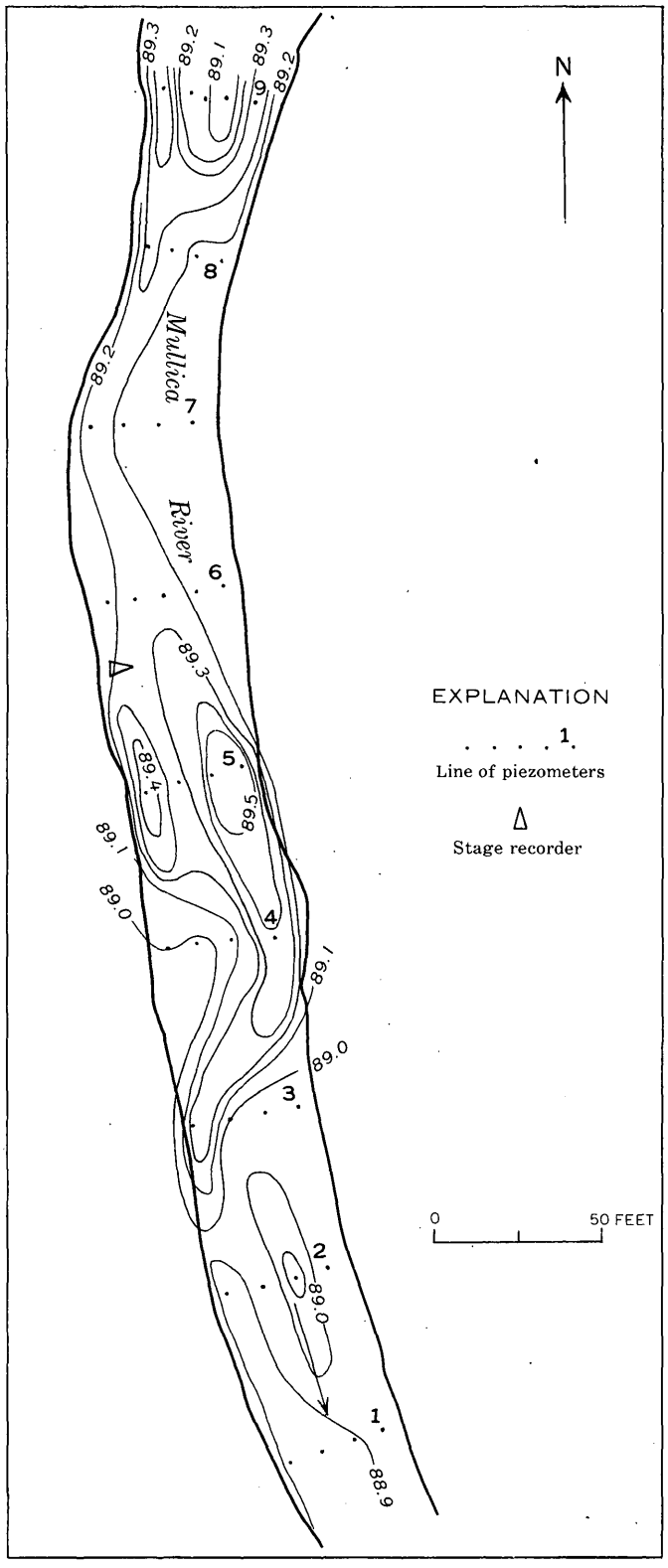

FIGURE 36.4.—Map of the Wharton Tract piezometer field showing contours of water-level in piezometers 2 feet below the streambed on June 9, 1960. Contour interval 0.1 foot; datum assumed. Numbers on lines of piezometers are referred to in text.

The sinuous pattern of head differential follows very closely the observed channel flow in the river. Much of the flow was along the west bank downstream from line 9 and crossed over toward the east bank just downstream from line 6. The natural scour that produced the channel flow also produced the major areas of discharge to the stream.

The principal conclusions from analysis of the piezometer data are: Locally there are marked differences in head between the 1-foot and 2-foot levels beneath the streambed, these head differences indicate important areas of upward movement of ground water to the stream, and the sinuous patterns of head differential and channel flow are the result of natural scour.

REFERENCE

Lang, S. M., 1961, Natural movement of ground water at a site on the Mullica River in the Wharton Tract, southern New Jersey: Art. 313 *in* U.S. Geol. Survey Prof. Paper 424–D. p. D52–D54.

37. MOVEMENT OF PERCHED GROUND WATER IN ALLUVIUM NEAR LOS ALAMOS, NEW MEXICO

By JOHN H. ABRAHAMS, JR., ELMER H. BALTZ, and WILLIAM D. PURTYMUN, Albuquerque, N. Mex.

Work done in cooperation with the U.S. Atomic Energy Commission

The infiltration and underground movement of snowmelt water in Mortandad Canyon near Los Alamos, N. Mex., were studied from March through June 1961. Mortandad Canyon is one of the deep, steep-walled easterly draining canyons that dissect the Pajarito Plateau. The part of the canyon studied has a drainage area of about 2 square miles and heads at an altitude of about 7,350 feet on the central part of the plateau, where the annual precipitation is about 17.5 inches.

The Bandelier Tuff of Pleistocene age caps the Pajarito Plateau and rests on the Santa Fe Group of middle(?) Miocene to Pleistocene(?) age. The principal ground-water body is in the Santa Fe Group about 960 feet beneath the canyon floor. However, a small body of perched ground water, which was the subject of investigation, occurs in alluvium resting on the Bandelier in the bottom of Mortandad Canyon. In the western part of the canyon the alluvium is 40 to 80 feet wide and 20 to 30 feet thick, whereas in the eastern part of the canyon the alluvium is 600 to 700 feet wide and may be as much as 100 feet thick.

The water in the alluvium was monitored by means of holes drilled in seven lines across Mortandad Canyon. At each line (fig. 37.1), 1 observation well and several 2-inch-diameter access tubes were constructed with plastic pipe. Water levels were measured periodically in the observation wells, and the moisture content of the alluvium and underlying tuff was determined by using a neutron-scattering moisture probe in the access tubes.

The source of recharge to the alluvium in Mortandad Canyon is local precipitation. In 1961 about one-fourth of the annual precipitation occurred in the winter, and a snowpack 1 to 2 feet deep accumulated in the deep, narrow western part of the canyon. Some diurnal melting occurred in January, February, and March, and the melt water infiltrated the soil and alluvium. As the length of the daily melting period increased in April, the thin alluvium in the upper part of the canyon became saturated to the level of the stream channel, and surface flow began because the alluvium was unable to absorb and transmit all the snowmelt water.

Infiltration occurred at the front of the surface stream and in the channel upstream from the front; however, the front of the stream advanced eastward more rapidly than did the front of the zone of complete saturation in the alluvium, as shown by the fact that the front of the stream passed test well 8a (fig. 37.2) almost 2 weeks before the water level in the well indicated that the alluvium was saturated to stream level.

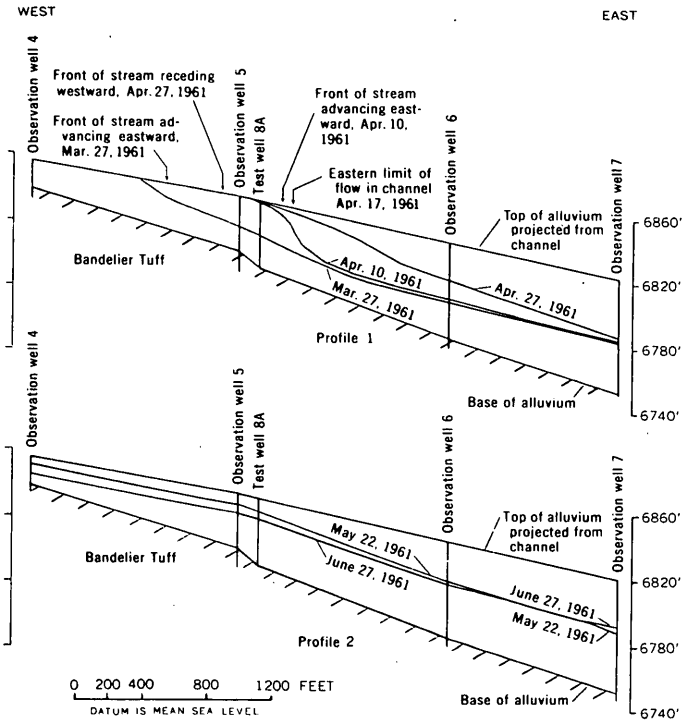

FIGURE 37.1.—Longitudinal profiles showing base and top of alluvium and water levels in alluvium in part of Mortandad Canyon.

Between observation wells 4 and 6, where the canyon widens, the alluvium thickens and consists of an upper unit of coarse, loose sand and an underlying unit of sandy clay. In this reach the part of the ground-water body in the coarse sand beneath the channel formed a mound with a steep eastward-sloping front. This happened because the coarse sand absorbed water from the stream and transmitted it downward at a faster rate than the sandy clay absorbed the water and transmitted it laterally. Water filtering downward in the coarse sand beneath the eastern part of the stream was accreted to the front of the ground-water mound, causing the front of the ground-water mound in the coarse sand to advance eastward faster than the movement of the ground-water body as a whole.

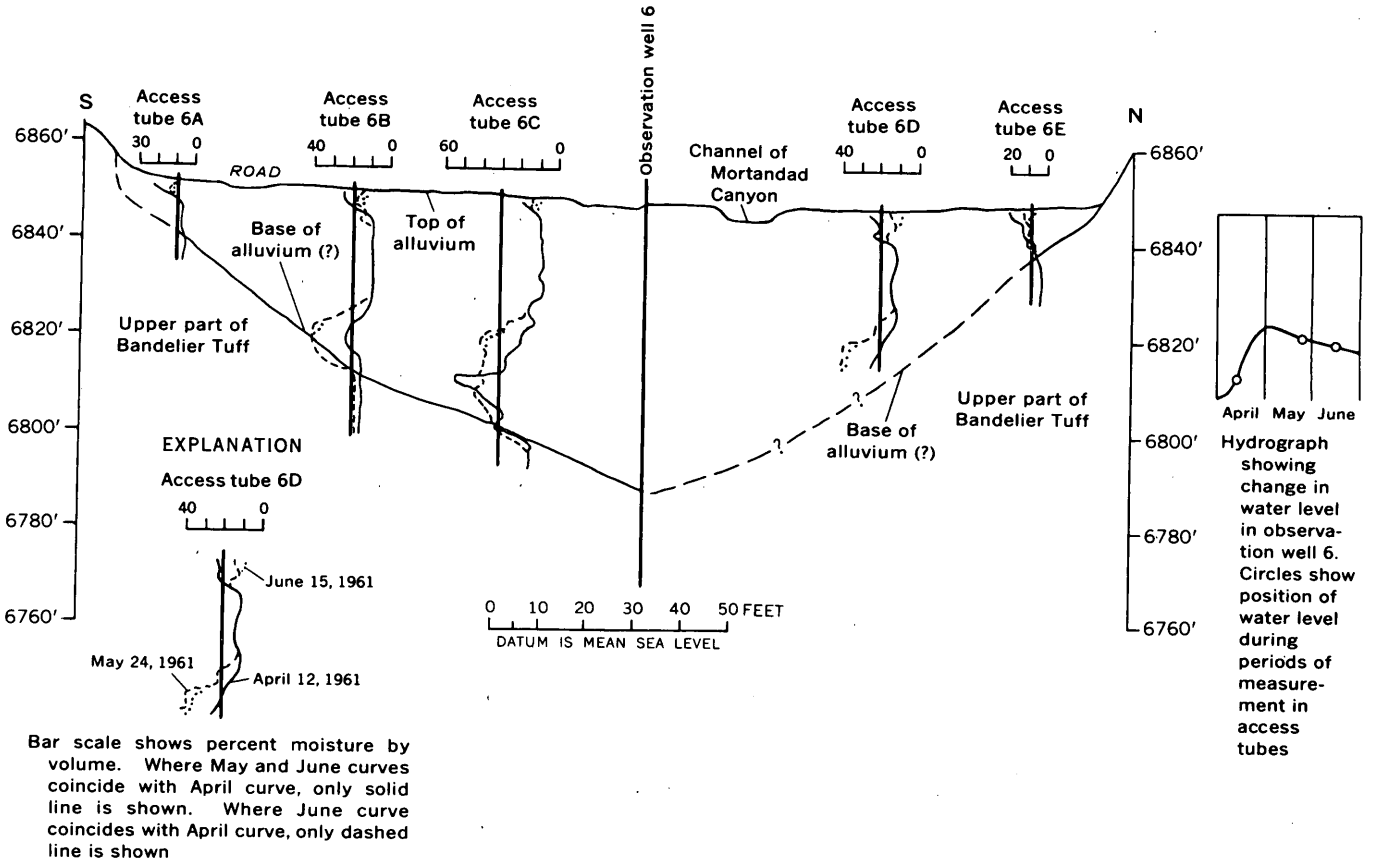

FIGURE 37.2.—Profile across Mortandad Canyon showing water levels and moisture content of alluvium and Bandelier Tuff in the spring of 1961.

Late in April the front of the stream receded upstream as the snowpack in the upper part of the canyon was depleted. The front of the ground-water mound began to decay and flatten because it no longer received recharge directly from the stream (water level for April 27, 1961, on profile 1, fig. 37.1). Subsequent changes of the water levels resulted from continued lateral subsurface drainage of ground water from the upper part of the canyon to the lower part (profile 2, fig. 37.1).

The moisture content of the Bandelier Tuff immediately beneath the alluvium increased slightly. The highest recorded moisture content was 19 percent by volume (access tube 6B, fig. 37.2); this is probably less than the minimum value necessary for significant amounts of water to be transmitted through the tuff. Perched water was not found in the Bandelier Tuff or in the Santa Fe Group above the principal zone of saturation at test well 8, indicating that little or no water is moving downward from the alluvium to the main aquifer in the part of the canyon studied.

The phenomenon of the building of a ground-water mound during infiltration and the different rates of movement of the resulting water strata probably occurs elsewhere. This possibility should be considered in other infiltration investigations, especially in the interpretation of rates of water movement, use of tracers, and studies of chemical quality of water.

38. SOURCE OF GROUND-WATER RUNOFF AT CHAMPLIN CREEK, LONG ISLAND, NEW YORK

By E. J. Pluhowski and I. H. Kantrowitz, Mineola, N.Y.

Work done in cooperation with Suffolk County Board of Supervisors and Suffolk County Water Authority

Streams on the south shore of Long Island flow in shallow valleys across a gently sloping, highly permeable glacial-outwash plain. The streams seldom overflow their banks and their sustained low flow indicates relatively small surface-water runoff and large ground-water runoff. More than 95 percent of all streamflow in southwestern Suffolk County originates as discharge from the ground-water reservoir.

The ground-water reservoir consists of about 1,500 feet of unconsolidated deposits of Cretaceous and Pleistocene age, which are subdivided hydraulically into a shallow unconfined aquifer and two confined aquifers. The shallow aquifer is recharged directly by precipitation. The confined aquifers are recharged from the overlying shallow aquifer by water that moves downward through the confining beds in the recharge area in the central part of Long Island. North and south of this recharge area, ground water at first moves roughly parallel to and then upward into the shallow aquifer.

Seventy percent of the discharge from the ground-water reservoir is ground-water runoff; the remainder leaves the area as ground-water outflow to the sea. Because the regional movement of ground water suggests discharge near the south shore of Long Island in the latitude of Champlin Creek, the increment of ground-water runoff per unit of channel length, defined as pickup, theoretically should increase uniformly from source to mouth. However, seepage investigations on several streams indicate that the pickup is greatest along their middle reaches and is substantially lower downstream. The purpose of this study was to determine the cause of the observed pattern of streamflow pickup.

Champlin Creek was selected for study because it has no tributaries, pondage, or major regulation above the gaging station at Islip. Discharge measurements made periodically at eight sites along the stream were correlated with the gaging-station records to estimate discharge for each site. Water levels were measured in shallow wells installed adjacent to, and in, the stream channel.

The pickup in mean annual discharge, computed for the reaches between stream-gaging sites and expressed in cubic feet per second per 1,000 feet of channel length, is shown in figure 38.1. The high pickup in the reach between Beech Street and Islip Boulevard may be attributed to increased lateral ground-water discharge, to upward movement of water from within the ground-water reservoir, or both.

To determine the relative amount of lateral ground-water discharge, shallow wells were driven along three lines oriented approximately at right angles to the stream. These lines, labeled *A*, *B*, and *C* on figure 38.2 cross the stream at the Poplar Street, Beech Street, and Islip Boulevard gaging sites (fig. 38.1); 4 wells are located along each line, 2 on each bank of the stream. Average water-table gradients, defined by the mean slope between pairs of outer and inner wells, were 0.7, 0.8, and 1.3 feet per 1,000 feet along lines *A*, *B* and *C*, respectively. Thus, the steeper water-table slope along line *C*, illustrated by the sharp reentrant of the 16-foot water-table contour (fig. 38.2), corresponds to the reach of greatest streamflow pickup. The uniform slope of Champlin Creek (fig. 38.1), in combination with the natural convex profile of the water table, results in an increase in hydraulic gradient between the aquifer and the middle reaches of the stream. Moreover, the relatively hilly land surface between lines *B* and *C* may result in a slightly higher water-table altitude and cause a further increase in the hydraulic gradient.

That steeper water-table gradients result in greater lateral ground-water discharge can be inferred from figure 38.3. Each plotted point represents the average altitude of the water table in 12 wells near the stream, plotted against concurrent discharge at the gaging station. The wells are on lines *A*, *B*, and *C* and are 400 to 1,600 feet from the stream. All measurements were made during periods of dry weather; thus the stream discharge is virtually all ground-water runoff. Because the altitude of the stream surface remains relatively constant, water-table fluctuations indicate changes in the hydraulic gradient toward the stream. Figure 38.3 shows that as the water-table altitude, and hence the hydraulic gradient, increases, ground-water runoff increases also. Therefore, part of the increase in streamflow pickup noted between lines *B* and *C* is caused by the steeper gradients of the water table, which result in a sharp rise in lateral ground-water discharge.

Wells driven directly into the streambed on lines

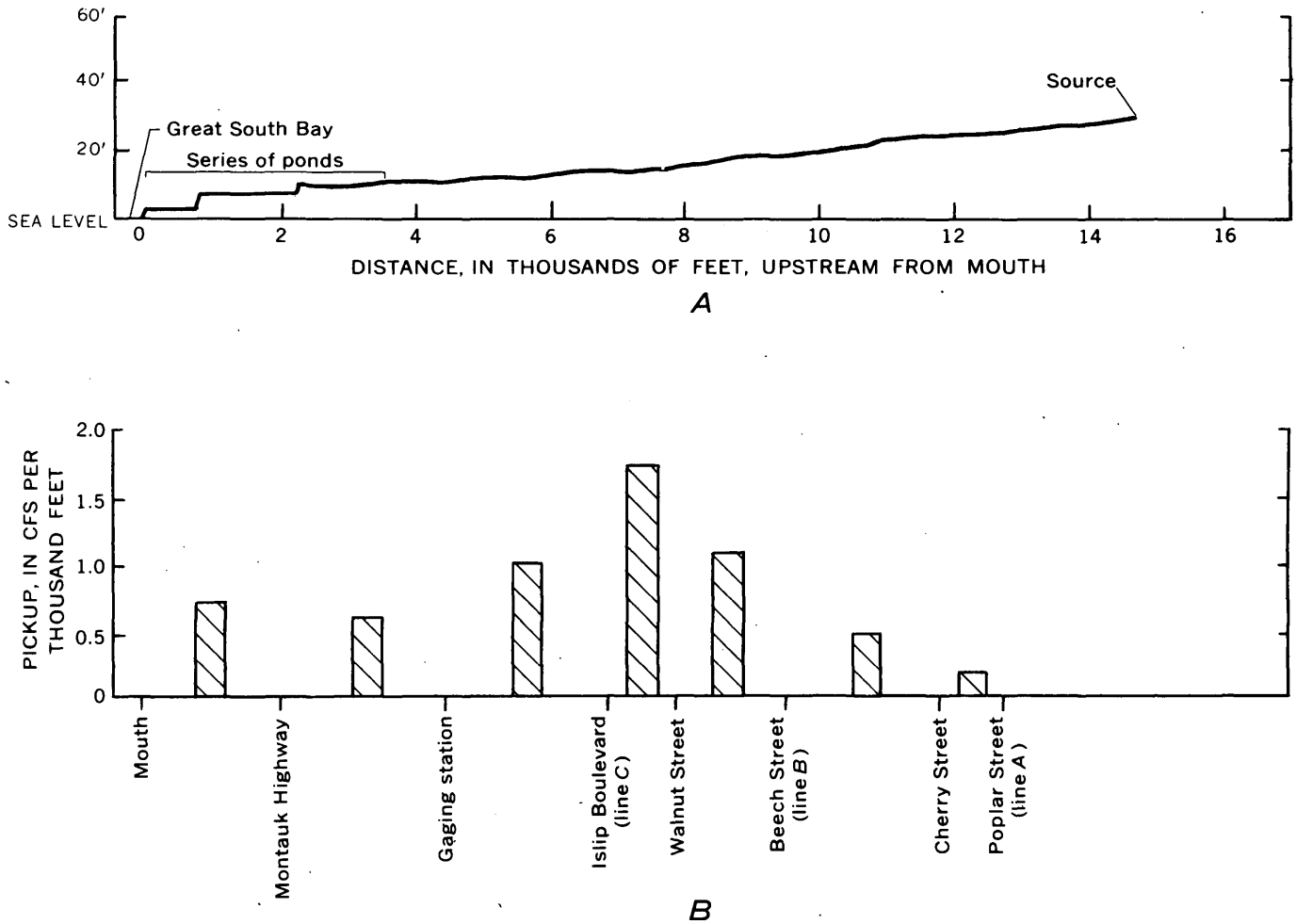

FIGURE 38.1.—Stream profile (*A*) and pickup in mean annual discharge (*B*) of Champlin Creek. Lines referred to in *B* are shown in figure 38.2.

A, *B*, and *C* were used to determine the relative amount of upward ground-water movement into the creek. All wells were screened in the uniform glacial-outwash deposits of the shallow unconfined aquifer. At each site, driving was stopped about every foot for the first 10 feet and about every 5 feet thereafter, the well was pumped, and observations of head were made after the water had returned to its static level. The head as indicated by water levels in the wells increased from about equal to the stream stage when the bottom of the well was just below the streambed, to half a foot higher than the stream stage at a depth of 5 feet. The head remained the same at depths between 5 feet and 60 feet, where driving was terminated.

These differences in head indicate that in the upper zone of the aquifer, ground water moves toward the stream both laterally and from below, but that below this upper zone the movement is predominantly horizontal under the regional hydraulic gradient.

The stream acts as a ground-water drain that causes a reduction in hydrostatic head adjacent to its channel. The hydraulic gradient thus established between the aquifer and the stream induces water to flow toward the stream. The limiting distance from which water moves toward the stream, both laterally and from below, is controlled by the interrelation of the hydraulic gradient between aquifer and stream, and the permeability of the aquifer. Because the stream is shallow, most ground water discharges through the streambed.

In summary, the rate of ground-water runoff is controlled largely by the height of the water table adjacent to the stream. Ground-water movement into the stream channel along the middle and upper reaches of Champlin Creek is principally lateral, with little or no upward flow reaching the stream from deep within the aquifer.

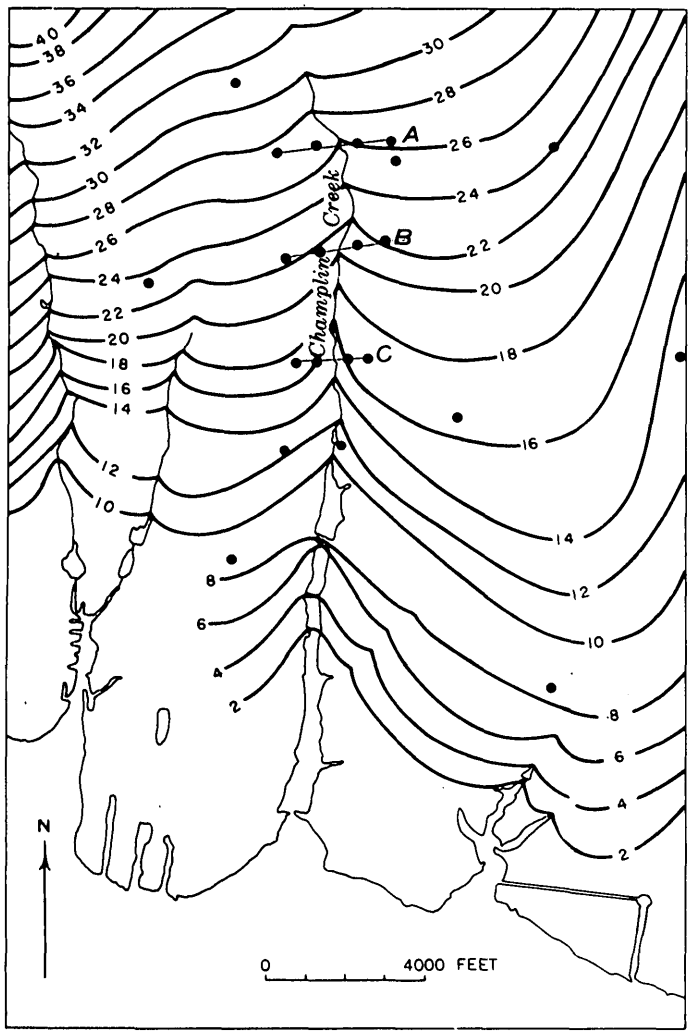

FIGURE 38.2.—Water-table contours, in feet above mean sea level, in the Champlin Creek area. Dots represent location of observation wells, lines *A*, *B*, and *C* are described in text.

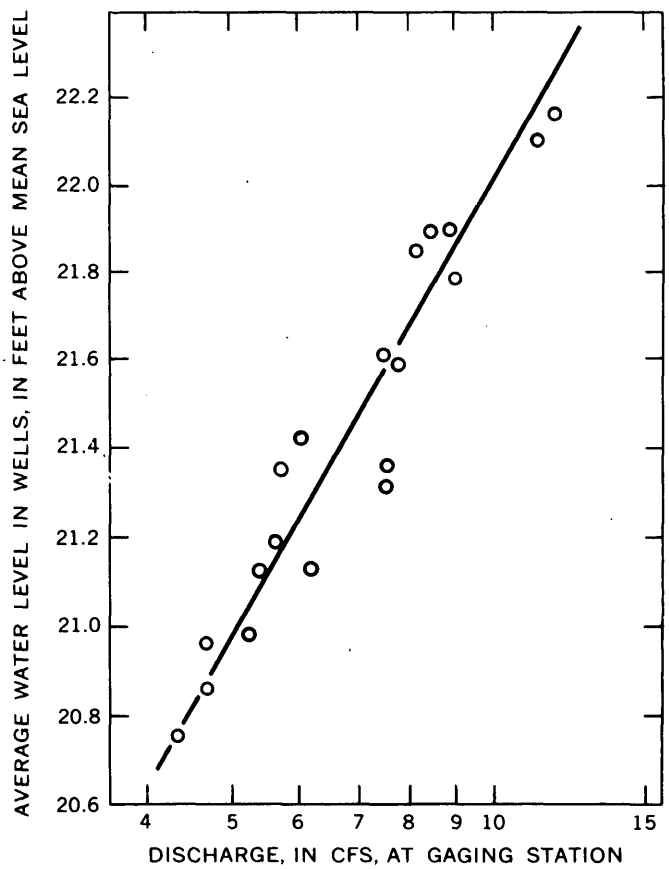

FIGURE 38.3.—Relation between average water level and discharge of Champlin Creek at Islip. Each point represents the average water level in 12 observation wells near the stream.

39. RELATION OF FAULTING TO THE OCCURRENCE OF GROUND WATER IN THE FLAGSTAFF AREA, ARIZONA

By J. P. AKERS, Tucson, Ariz.

Work done in cooperation with the city of Flagstaff

An investigation for additional water supplies for the city of Flagstaff indicated that highly fractured rocks in the vicinity of major faults transmit 10 to 50 times as much water as do the same rocks where unfractured; wells tapping these fractured rocks have proportionally large yields. As a result of the investigation, 5 wells were drilled along faults near Woody Mountain, 6 miles southwest of Flagstaff, and near Lake Mary, 6 miles southeast of Flagstaff.

A large part of the surface surrounding Flagstaff is underlain by lava flows and cinders of Tertiary and Quaternary age. The lava, ranging from 0 to at least

600 feet in thickness, is underlain, in descending order, by sedimentary formations that include the Moenkopi Formation of Triassic age, composed of 0 to 100 feet of red thin to thick beds of siltstone and sandstone; the Kaibab Limestone of Permian age, composed of about 250 to 350 feet of thick beds of yellowish-gray cherty, silty to sandy limestone; the Coconino Sandstone and Toroweap Formation, undifferentiated, of Permian age, composed of about 800 to 900 feet of very light orange to gray well-sorted very fine to fine-grained quartz sand; and the Supai Formation of Pennsylvanian and Permian age, composed of about 1,500 feet of brick-red to brown thin to thick beds of siltstone and sandstone. The Moenkopi Formation was removed by erosion in many places near Flagstaff before the lavas were erupted, but the other formations are continuous throughout the entire area. Sedimentary rocks older than the Supai underlie the Flagstaff area, but they are beyond the practical reach of water wells.

The Coconino Sandstone, sandstone strata in the upper 100 feet of the Supai Formation, and the lavas, where underlain by impermeable beds, are the principal aquifers in the Flagstaff area. The other formations are relatively impermeable or are above the regional water table.

The sedimentary rocks in the Flagstaff area were warped upward to form a broad, gentle arch before volcanism began. The Mormon Mountain anticline (written communication, M. E. Cooley, 1961) forms part of the arch and extends 30 miles southeast from a point about 5 miles south of Flagstaff (fig. 39.1). The lava and the sedimentary rocks are offset by several large and numerous small high-angle faults which trend mainly north or northwest.

Two of the large faults roughly bound the Mormon Mountain anticline in this area, and they and the anticline are the chief controls of the occurrence and movement of ground water in the area south of Flagstaff. The Oak Creek fault, west of the anticline, trends north, and its east side is downthrown as much as 500 feet. The Anderson Mesa fault, northeast of the anticline, trends northwest along the shore of Lake Mary, but swings to a north trend near the northwest end of the lake. It is downthrown on the west side about 400 feet. Impermeable beds in the Supai Formation in the upthrown blocks are juxtaposed with the permeable Coconino Sandstone in the downthrown block by both faults. A small fault trending northwest on the north flank of Woody Mountain cuts across the Oak Creek fault. This small transverse fault is downthrown on the southwest side.

The rocks near the faults are intensely fractured and in places pulverized. The fracturing greatly increases the effective permeability of the rocks and facilitates recharge of the Coconino Sandstone through the lava and Kaibab Limestone. Joints are particularly abundant in the Kaibab Limestone between the small transverse fault near Woody Mountain and the northwest-trending segment of the Anderson Mesa fault. Joints and faults in the limestone have been widened by solution, and several near the northwest end of Lake Mary had to be dammed off because large quantities of lake water were lost through them. The influence that these joints and the lake have on recharge is clearly shown by the ground-water mound indicated by the contours in figure 39.1. A similar mound near Woody Mountain suggests that a considerable amount of water from Rogers Lake enters the ground-water reservoir through the fractured zone paralleling the small transverse fault. A ground-water divide coincides with a line through these mounds.

The ground water moves north and northeast and south in the Coconino and Supai from the divide until it reaches impermeable beds in the Supai Formation on the upthrown sides of the Anderson Mesa and Oak Creek faults. The altitude of the impermeable beds in the Supai Formation on the crest of the Mormon Mountain anticline is lower than the altitude of the water table. Thus, water can move across the axis of the anticline. The water-table gradient is steeper northeast of the ground-water divide than it is southwest of the divide, mainly because the water moving northeast is in the Supai Formation, which is less permeable than the Coconino Sandstone through which most of the water moves southwest of the divide.

Flagstaff city well 1 was drilled near Woody Mountain on the downthrown side of the Oak Creek fault to take advantage of the high permeability of the fault zone. The well is about 1,500 feet east of the Oak Creek fault and a little more than 2,000 feet from the small transverse fault. The well bottomed in the top of the Supai Formation at a depth of 1,600 feet. Aquifer tests of this well indicate that the coefficient of transmissibility (expressed as the rate of flow of water in gallons per day through a vertical strip of aquifer 1 foot wide extending the full saturated height of the aquifer under a hydraulic gradient of 100 percent) of the Coconino at the well site is 5,000 gpd (gallons per day) per foot. The succeeding wells, 2, 3, and 4, were located nearer the fault and they bottomed in the Coconino Sandstone at depths between 1,516 and 1,746 feet. The coefficients of transmissibility obtained at these well sites—12,000, 20,000, and 50,000 gpd per foot, respectively—indicate that the fractur-

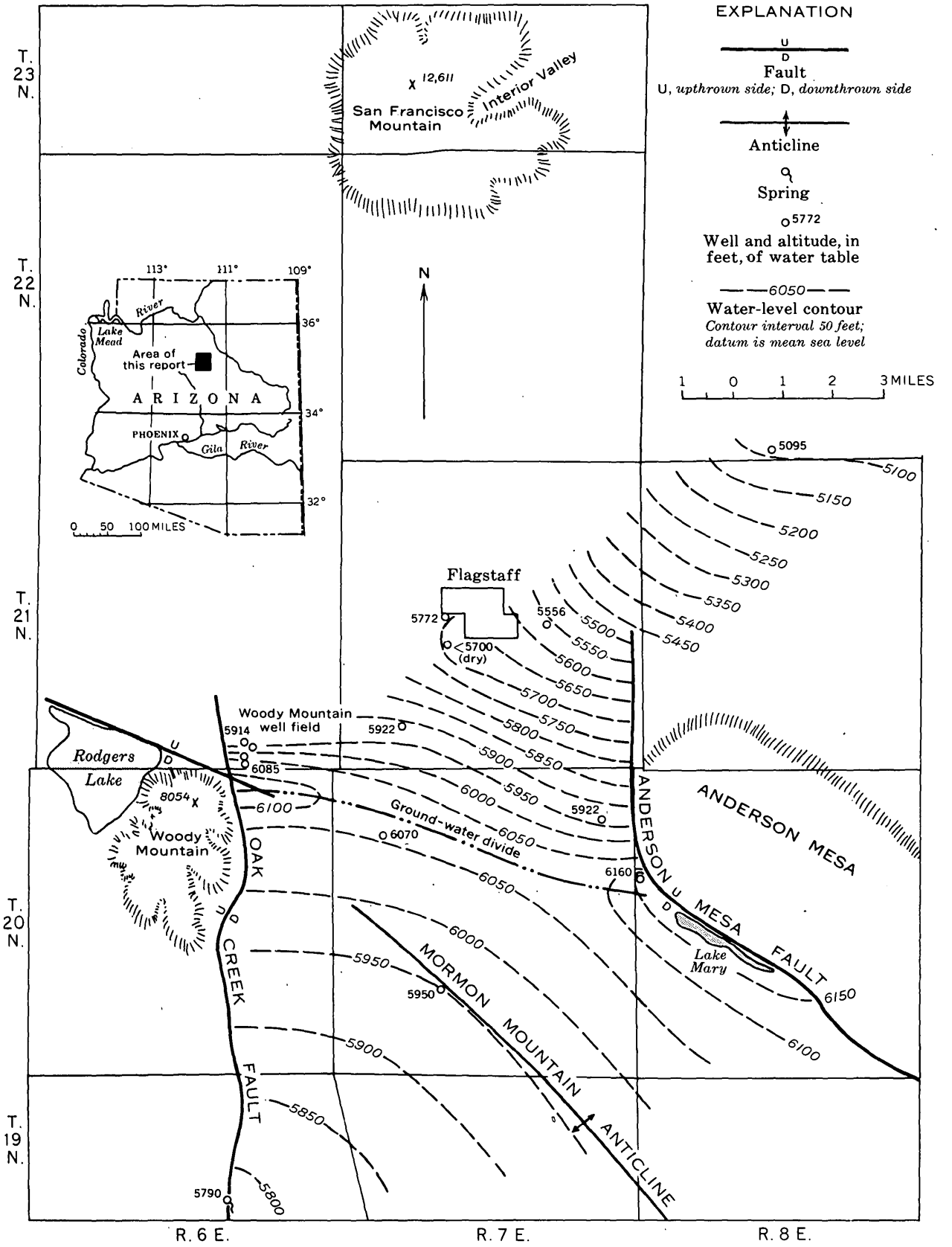

FIGURE 39.1.—Map showing main structural features and water-level contours in the Flagstaff area.

ing, and hence the transmissibility, increases toward the fault. Away from the fault zones transmissibilities generally are less than 1,000 gpd per foot. Similarly, the specific capacity of wells completed in undisturbed Coconino ranges from a fraction to 1 gpm (gallon per minute) per foot of drawdown, whereas the specific capacity of the wells in the fractured fault zone near Woody Mountain ranges from 2.5 to 8.6 gpm per foot of drawdown.

Hydrologic conditions along the Anderson Mesa fault are similar to those along the Oak Creek fault, and the city of Flagstaff in November 1961 was drilling a well near Lake Mary to ascertain whether similar high yields could be obtained from wells in that area.

40. METHOD FOR MEASURING UPWARD LEAKAGE FROM ARTESIAN AQUIFERS USING RATE OF SALT-CRUST ACCUMULATION

By J. H. Feth and R. J. Brown, Menlo Park, Calif., and Ogden, Utah

Work done in cooperation with the U.S. Bureau of Reclamation

Nearly 60,000 acres of wet salt-encrusted barren land was exposed along the east shore of Great Salt Lake, Utah, during the period 1953–56 in an area underlain by aquifers that contain water under artesian pressure. A method was sought to measure the rate of upward leakage of the artesian water through the sodium-saturated clays that form the surface of the salt-encrusted barrens.

The mudflats west of the Ogden Bay Bird Refuge were selected in 1954 as being representative of the area. The crust was removed from 3 plots, each having an area of 5 square feet, so that a new layer of salt could accumulate. Then the new crust was removed, separated from the clay adhering to it, dried, and weighed, thus showing the amount of salt that had been deposited by evaporation of rising brine during a given period of time. Five determinations of rate of accumulation were made during the study (see table below).

The salt content of the brine was determined by digging a shallow well near the test plots and analyzing the water for its salt content. The brine was found to contain 93,000 parts per million of dissolved solids, mostly sodium chloride, or 126.5 tons per acre-foot. From this information was calculated the amount of water evaporated to produce the accumulations of salt that were collected and weighed. The rate of evaporation, in acre-feet per acre, was calculated on the basis of the evaporation during the frost-free season of 160 days (Brown, 1960), inasmuch as the salt crust does not form during the cold season.

Evaporation pans were used to compare the normal rate of evaporation of fresh water and the rate of evaporation from the salt crust.

The average evaporation from the salt crust during the frost-free season was 0.04 acre-feet per acre (see table). This factor applied to the 60,000 acres of bar-

Rates of evaporation at and near the Ogden Bay Bird Refuge during the frost-free season of 1954

Plot	Period [1]	Number of days	Salt-crust tests		Evaporation-pan tests			Comparison of salt-crust evaporation to pan evaporation (percent)
			Amount of salt accumulated (grams)	Calculated potential evaporation during 160 days (acre-feet per acre)	Depth of water evaporated		Calculated potential evaporation during 160 days (acre-feet per acre)	
					Inches	Feet		
A	June 30–July 13	13	92	0.09	5.70	0.48	5.90	1.5
B	June 30–Aug. 2	33	70	.03	13.37	1.11	5.38	.6
A	July 13–Aug. 2	20	85	.05	7.67	.64	5.12	1.0
C	June 30–Aug. 24	55	73	.02	21.43	1.79	5.21	.4
B	Aug. 2–Aug. 24	22	41	.02	8.06	.67	4.87	.4
Average				.04			5.30	

[1] Rainfall during the period June 30 to August 24 at rain gage adjacent to evaporation pan totaled 0.25 inches (July, 0.16; Aug., 0.09), and fell during several periods, none having an intensity of as much as 0.1 inches in 24 hours, and is considered negligible in its effect upon the experiments.

ren land yields a total evaporation discharge of about 2,500 acre-feet of water.

Aquifer leakage presumably continues during the cold season, although the salt crust does not form. The brine flows gradually lakeward or is mixed with lake water on occasions when a strong west wind causes the lake water to move 1 or 2 miles eastward across the nearly level mudflats, a phenomenon the writers have observed several times. Annual upward leakage, therefore, may be 365/160 of that calculated for the growing season, or nearly 6,000 acre-feet per year.

As the data obtained during the experiments of 1954 showed very low rates of upward leakage, additional studies were made in 1955. A tank was filled with saline clay and a bottom-feed system installed. Brine from a shallow brine well was introduced into the feed system under a few feet of head. The amount of brine moving upward through the clay in the tank during a period of more than a month was too small to measure. Still later, laboratory tests on saline-mud cores from deposits of Great Salt Lake yielded rates of movement of water in the range of 0.001 to 0.003 foot per day. The authors believe, therefore, that the average rate determined during the 1954 tests is probably in the proper order of magnitude and that disturbance and puddling of the clay during its introduction into the experimental tank in the 1955 tests account for the fact that no movement was detected.

Landward from the barrens, and at least locally lakeward under the brine-saturated clay, the aquifers of the area contain potable water. The location of the interface between fresh and saline waters is not known in the area of the experiments. It is assumed, however, that fresh water moving lakeward from the mountains furnishes the hydrostatic head that causes upward leakage and the resultant deposition of salt on the barrens. The mineral content is residual and is derived from bottom sediments laid down when Great Salt Lake was at a higher level.

So far as is known, the results here reported represent the first attempt to measure rates of upward movement of water through brine-saturated clay in the environment of an artesian system underlying a saline mudflat. The results indicate that the movement is slow and the total loss by evaporation measurable but small. The method probably could be applied to various "wet playa" areas in arid and semiarid regions where artesian systems underlie mudflats on which measurable deposits of salt are accumulating.

REFERENCE

Brown, Merle, 1960, Climates of the States—Utah: U.S. Weather Bur. Climatography of the United States, no. 60–42, 15 p.

41. SEASONAL TEMPERATURE CHANGES IN WELLS AS INDICATORS OF SEMICONFINING BEDS IN VALLEY-TRAIN AQUIFERS

By Stanley E. Norris and Andrew M. Spieker, Columbus, Ohio

Work done in cooperation with Ohio Department of Natural Resources, Division of Water, the Miami Conservancy District, and the Commissioners of Hamilton County, Ohio

The most productive aquifers in Ohio are valley-train deposits of sand and gravel in the principal river valleys. In many areas, the sand and gravel deposits are interbedded with wide-spread sheets of relatively impermeable till that retard recharge to the deeper wells and thus set practical limits on the quantity of water available from induced infiltration.

A technique for determining the presence of interbedded till layers, based on temperature logs of wells, is described in Article 42. Another method of determining from water-temperature data the presence or absence of semiconfining beds is based on annual temperature fluctuations in wells. If two wells drilled in a homogeneous and isotropic aquifer, and located at equal distances from a source stream, receive replenishment principally from the stream, the temperature of the water pumped from the wells will vary with seasonal changes in stream temperature. Temperature-versus-time graphs of the well water and stream water will have the same general shape. The amplitude of the fluctuations of the ground-water temperature will not be as great as that of stream temperature, and the sea-

sonal high and low temperatures of the ground water will lag behind those of the stream. If the two wells are of unequal depth, differences in amplitude of the temperature fluctuations and in the time of arrival of seasonal highs and lows from the source stream will be apparent, but the curves will have the same general shape unless the inequalities of depth are very large.

The presence in the water-bearing deposits of a semiconfining bed through which the water must leak, or around which water must flow to reach the wells, will change the shape of the ground-water temperature graph. If at the site of one well the flow of ground water is impeded by a semiconfining bed, the annual temperature graph for that well will be different from the annual temperature graph for another well where there is no semiconfining bed. The semiconfining bed will, in general, dampen the seasonal temperature fluctuations and produce a relatively flat graph.

Figure 41.1 shows an example of the effect of a semiconfining bed on the seasonal temperature fluctuations in a well at the Tait Station of the Dayton Power and Light Co. in southern Dayton. Pumpage from the well field, chiefly replenished by infiltration from the Miami River is about 5 million gallons per day. The graph of the water temperature in well 521, which is about 65 feet deep and screened above a semiconfining till bed, reveals seasonal fluctations much like those of the Miami River. In contrast, the temperature graph of water from well 524, which is 155 feet deep and screened below the till, is nearly flat. That the semiconfining bed dampens the seasonal temperature fluctuations in well 524 is readily apparent. The effect is even more significant in view of the fact that well 524 is only 195 feet from the Miami River whereas well 521 is 320 feet from the river.

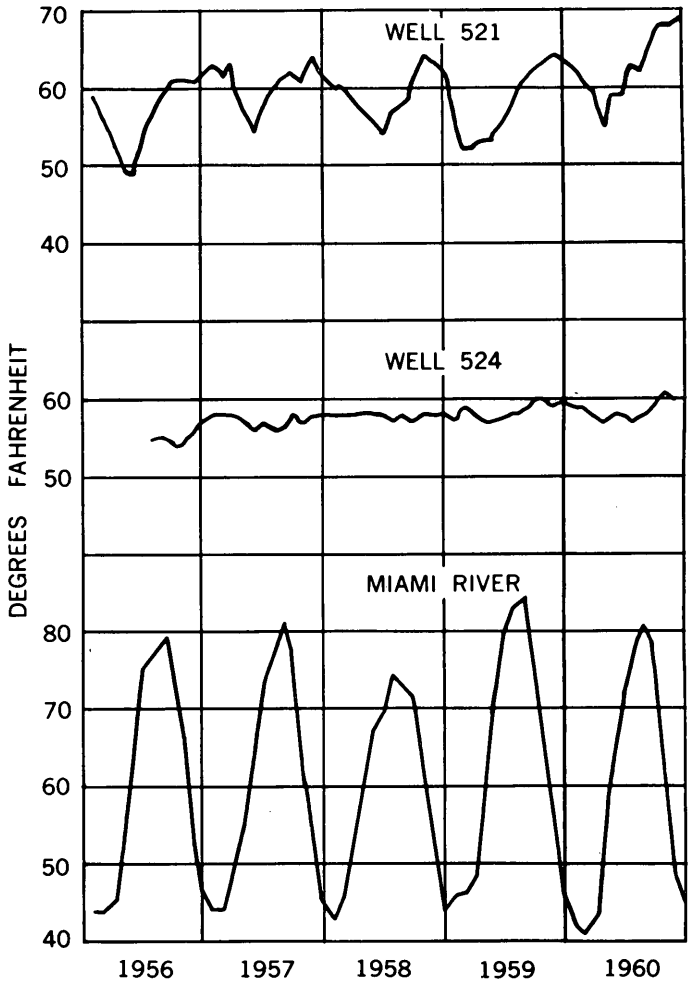

FIGURE 41.1.—Temperature graphs of water in wells at the Tait Station of the Dayton Power and Light Co., compared to that of the Miami River. Well 521 taps an unconfined upper zone; well 524 taps a semiconfined lower zone.

42. TEMPERATURE-DEPTH RELATIONS IN WELLS AS INDICATORS OF SEMICONFINING BEDS IN VALLEY-TRAIN AQUIFERS

By Stanley E. Norris and Andrew M. Spieker, Columbus, Ohio

Work done in cooperation with Ohio Department of Natural Resources, Division of Water, the Miami Conservancy District, and the Commissioners of Hamilton County, Ohio

Widespread sheets of relatively impermeable till, interbedded with valley-train deposits of sand and gravel in the Miami River valley at Dayton, Ohio, retard recharge to many of the deeper wells and limit the quantity of water available from the induced infiltration of streamflow. A technique for determining the presence of these till layers, based on temperature-depth relations in wells, was developed by the authors during a water-resources investigation of the Dayton area. Another method for determining the presence of interbedded till layers, based on seasonal temperature fluctuations in wells screened above the till compared to those screened below, is presented in Article 41.

If the circulation of ground water is relatively rapid near centers of pumping or sources of recharge, differences in temperature of water in aquifers separated by till of relatively low permeability may be large enough to be detected by sensitive thermistor-type thermometers. The method is most easily explained by considering temperature gradients in wells drilled where each of three hypothetical flow systems prevails. The explanation is simplified by specifying that the temperature of the water infiltrating from a source stream is higher than the temperature of the water in the aquifer. In Ohio this condition commonly occurs in late spring and summer.

The simplest of the three hypothetical flow systems is that of a homogeneous and heavily pumped sand and gravel aquifer traversed by an infiltrating stream. The water temperature will decrease linearly with depth in an observation well that penetrates the aquifer between the stream and the discharging well (fig. 42.1*A*).

Consider next an otherwise homogeneous aquifer in which a horizontal layer of till of small lateral extent (fig. 42.1*B*) is situated so that some water that enters the discharging well passes downward through the till, while the remainder flows around the till layer. The temperature gradient in the observation well will be approximately linear above and below the till, but the part of the graph representing temperatures below the till will be displaced relative to that above the till, in the direction of lower temperature. The position of the till layer is indicated by a pronounced "blip" on the temperature-gradient line, caused by the colder water in the till.

The third hypothetical flow system consists of two aquifers hydraulically separated by a laterally extensive till layer, through which all recharge to the deeper aquifer must pass (fig. 42.1*C*). Under these conditions that part of the graph depicting temperatures beneath the till will be displaced relative to that above the till by colder water in the till and in the lower aquifer. However, unlike conditions shown in the second example (fig. 42.1*B*), the temperature of the water beneath the completely separating till layer will be no higher than that of the water in the till. Thus the temperature in the observation well will decline with depth, but the rate of decline will increase significantly in the till.

On figure 42.2 are shown drillers' logs of wells 530 and 531, at the Frank M. Tait station of the Dayton Power and Light Co., beside which are plotted the respective temperature gradients. The wells are in the south part of Dayton about 700 feet from the Miami River in a well field yielding about 5 million gallons per day. The measurements were made in June 1957, when the water in the Miami River was appreciably warmer than the ground water, similar to the condition specified in the discussion of the hypothetical flow systems.

Except for the somewhat anamolous lower part of the temperature gradient curve for well 531, which suggests the presence of an unlogged till deposit, zones of colder water closely correspond in depth to deposits of till as logged by the driller, while warmer water is associated with the intervening or underlying sand and gravel. Had all the water entered the deeper aquifer by leakage through the till it would have been no warmer than the water in the till itself. The zones of warmer water in well 530 reach nearly the same maximum temperatures, whereas the lower warm zone in well 531 is much cooler than the upper warm zone. This indicates that the movement of water from the shallower to the deeper aquifer was taking place more rapidly in the vicinity of well 530, where the till is absent locally, than in the vicinity of well 531, where the flow was chiefly by leakage through the till.

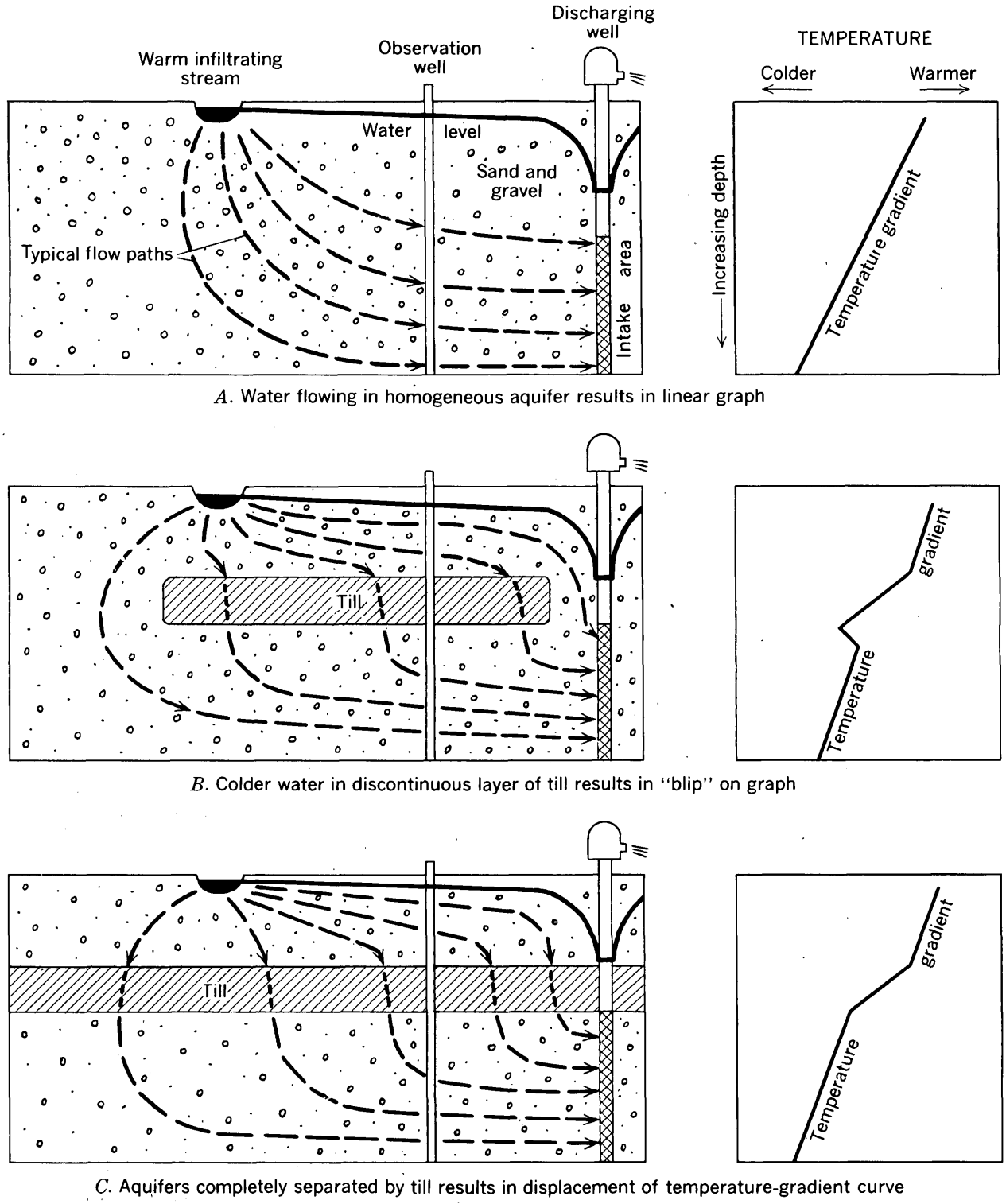

FIGURE 42.1.—Idealized ground-water circulatory systems, showing characteristic temperature gradients resulting from infiltration of warm water into a relatively cool aquifer.

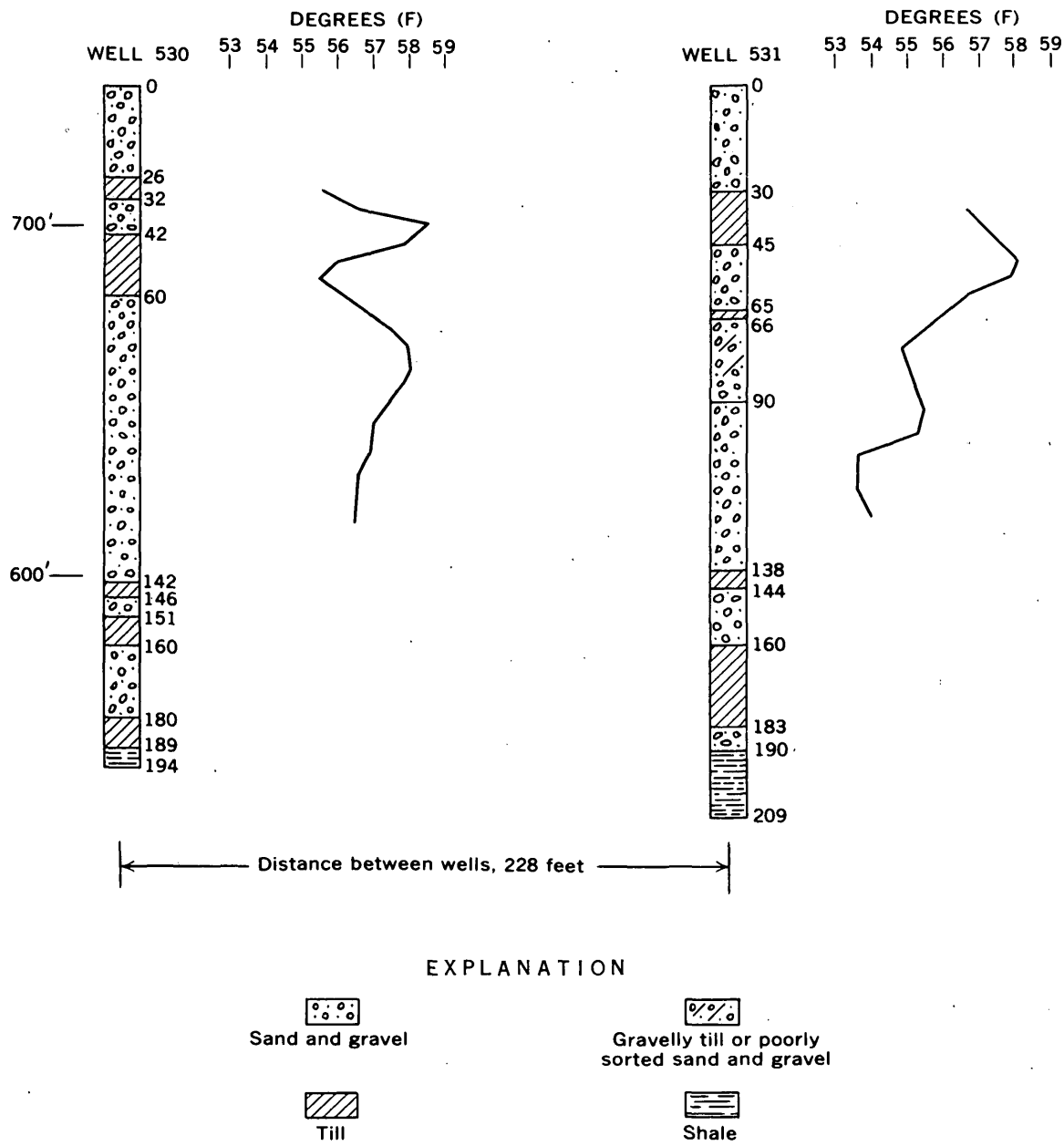

FIGURE 42.2.—Drillers' logs of two wells near the Miami River and temperature graphs of the wells for June 11, 1957. Temperature anomalies show that the ground water partly flows around discontinuous deposits of till in moving from shallow to deeper aquifers.

43. WATER-YIELDING POTENTIAL OF WEATHERED CRYSTALLINE ROCKS AT THE GEORGIA NUCLEAR LABORATORY

By J. W. Stewart, Atlanta, Ga.

Work done in cooperation with the U.S. Atomic Energy Commission and the U.S. Air Force

Metamorphic crystalline rocks underlie the Georgia Nuclear Laboratory in the Piedmont physiographic province of Georgia, about 45 miles north-northeast of Atlanta. The area is capped by a mantle derived from deep weathering of quartz-mica schist, biotite schist, quartz-mica gneiss, and amphibolite gneiss. The mantle consists of a soil zone 1 to 2 feet thick, a zone of highly weathered rock called saprolite that retains the structure of the parent rock, and a transitional zone between the saprolite and the unweathered rock. The saprolite consists almost entirely of alteration products derived from the weathering of minerals similar to those now found in the underlying rock, and its composition and thickness vary from one rock type to another.

The direction and rate of ground-water movement in the saprolite are influenced by the degree of weathering to which the material has been subjected, by the mineral composition of the parent rock, by the orientation of the mineral grains, and by the presence of shear zones, quartz veins, and joints. Bedding and foliation in the laboratory area dip about 50° to 70° SE. except in the northern part, where they dip 20° to 30° SE. The parallel arrangement of the mica crystals impedes the movement of water across the schistosity but favors movement parallel to it.

The permeability of samples taken parallel to the schistosity from the upper part of the saprolite is 25 to 100 times greater than that of samples taken normal to or at an angle to the schistosity. Consequently most ground-water movement is along the plane of schistosity.

In the upper part of the saprolite, below the soil zone, the grain-size distribution at 2 sites is 45 and 49 percent sand and rock fragments, 35 and 40 percent silt, and 20 and 11 percent clay, respectively. The change in grain-size distribution between the saprolite and the soil is abrupt.

The clay-size fraction of the saprolite consists mainly of kaolinite, biotite-vermiculite, muscovite, and gibbsite; the silt-size fraction mainly of kaolinite, quartz, muscovite, biotite-vermiculite, and garnet; and the sand and rock fragments largely of quartz, biotite, and feldspar.

Figure 43.1*A* shows the results of laboratory tests for porosity and specific yield of core samples collected at

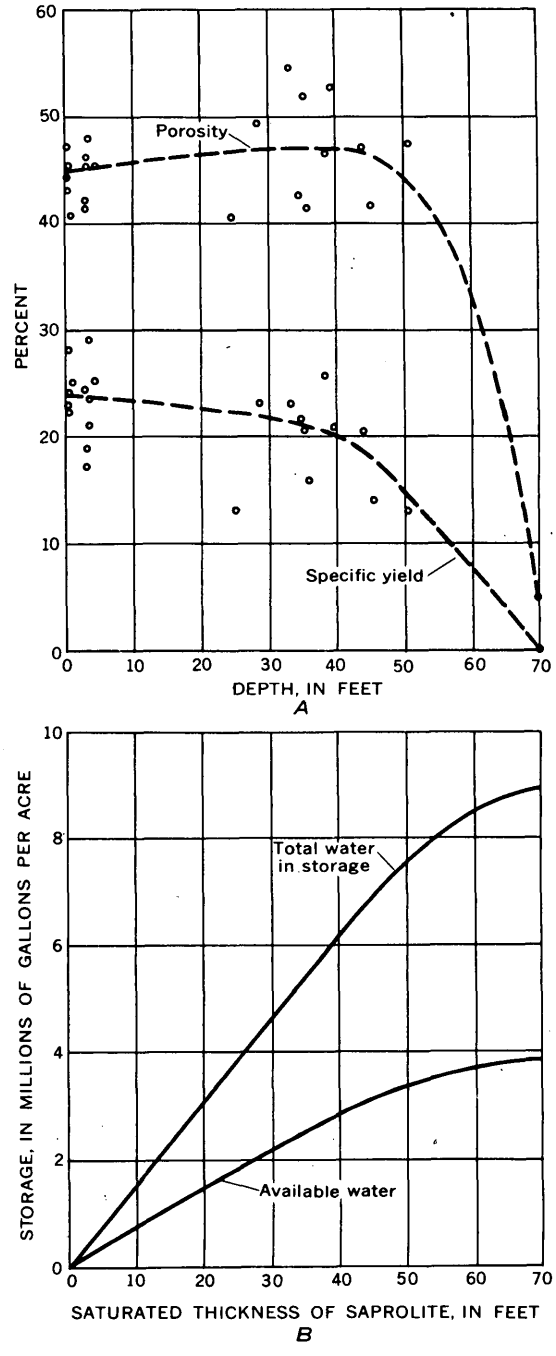

Figure 43.1.—Results of laboratory tests on core samples of saprolite from the Georgia Nuclear Laboratory area. *A*, Porosity and specific yield; *B*, total water in storage and water potentially available to wells.

different depths below the land surface. The porosity of the saprolite is greatest—as much as 54 percent—at depths of 30 to 40 feet, but decreases with depth as saprolite grades into unweathered rock. The porosity of the unweathered rock is about 5 percent, or about one-ninth the average porosity of the saprolite. The specific yield determined from the same samples decreases with increasing depth, and the amount of water in storage below about 40 feet decreases markedly. The average specific yield of the saprolite is about 21 percent and ranges from about 28 percent in the upper part of the saprolite to 0 in unweathered rock.

Figure 43.1*B* compares the total water in storage in a 70-foot saturated thickness of the saprolite and the water that is available by gravity drainage based on laboratory values of porosity and specific yield.

The quantity of water stored in the upper 35 feet of a water-saturated saprolite 1 acre in area is about 5.4 million gallons, of which about 2.5 million gallons, or 46 percent, could be recovered by wells. The amount of water between the depths of 35 and 70 feet is 3.5 million gallons, of which about 1.1 million gallons or 31 percent is available to wells. The quantity of water stored in the lower zone is 35 percent less than that in the upper zone, and the water available to wells is 56 percent less.

For all practical purposes the specific yield of the unweathered rock is zero. The rock is compact and the pore spaces are so minute that capillary forces virtually prevent movement of water. As a result, very little if any water stored in interstitial pores in fresh rock is available to wells. Most of the water available to wells in hard rock occurs in joints, bedding planes, cleavage planes, and other openings.

629660—62——8

44. USE OF INFLATABLE PACKERS IN MULTIPLE-ZONE TESTING OF WATER WELLS

By F. C. Koopman, J. H. Irwin, and E. D. Jenkins, Denver, Colo.

Packers have been used for many years in testing and completing oil wells, but have not been used extensively in testing water wells. Recent developments in design now make the use of inflatable straddle packers feasible for testing sandstone and siltstone aquifers. One such test of aquifers of Permian to Cretaceous age near Las Animas, Colo., is described here.

A test hole approximately 8 inches in diameter was drilled to a depth of 1,014 feet through beds of Cretaceous to Permian age (table 44.1). Five zones, isolated by means of the packer assembly, were found to yield water. These zones included the Dakota Sandstone, the Cheyenne Sandstone Member of the Purgatoire Formation, part of the Morrison Formation, the Entrada Sandstone, and siltstones and sandstones of Triassic and Permian age.

The packer assembly consists of an upper valve housing and two heavy-duty steel-reinforced rubber packer elements (fig. 44.1, *A*), separated by a "straddle pipe" (fig. 44.1, *C*) 8 feet or more in length. A variety of packer elements are commercially available to fit test holes of various diameters. The spacing between the packer elements and the depth of setting are determined after evaluation of such geologic and geophysical information as electric, gamma-ray, hole-diameter, lithologic, and drillers' logs of the test hole.

The packer assembly is lowered into the test hole on a suspension pipe (fig. 44.1, *B*). Four-inch standard steel pipe was used at Las Animas. The packer elements are inflated against the wall of the test hole by water under a pressure of about 850 to 1,250 pounds per square inch. Valve ports above, below, or between the packer elements are opened or closed by raising or lowering the suspension pipe. This permits water-level measurements, sampling, or pumping of the isolated zone between the two packer elements or of the composite zone above the top element or below the bottom element. When testing is complete, the packers may be deflated by turning the pipe. The assembly must be removed from the hole and fitted with a new blowout plug if it is to be set at a different level. The packer assembly can be reset and reused many times or can be installed permanently in a well.

Drilling fluid and free sediment are removed by the "air lift" method from the zones to be tested. In the tests at Las Animas, yield and transmissibility of each aquifer were determined, and water samples were collected for chemical analysis (table 44.2). A sub-

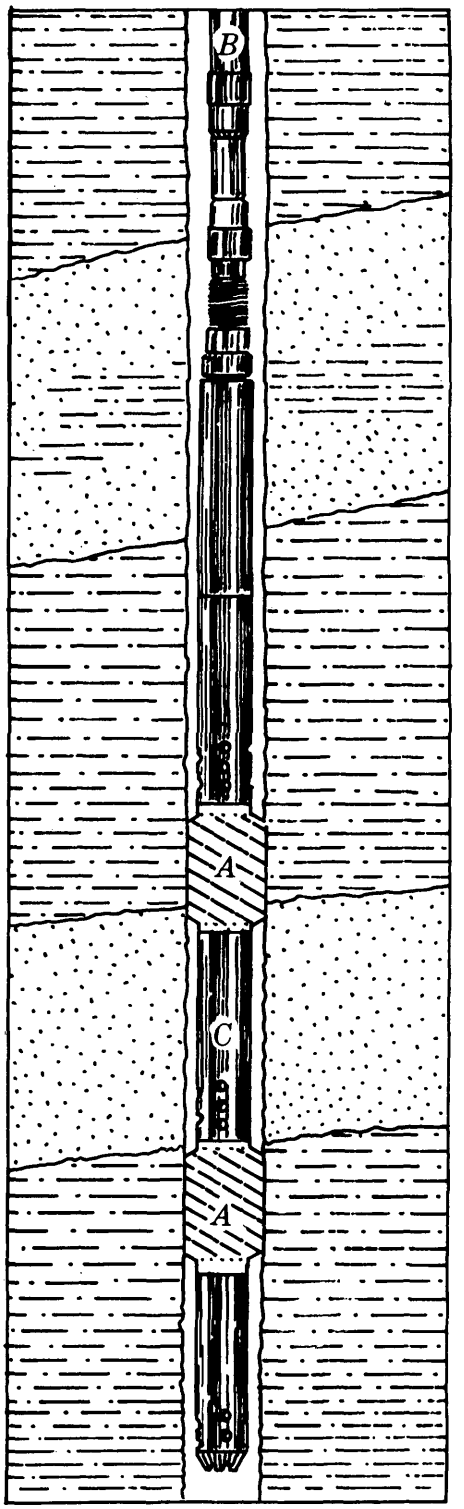

FIGURE 44.1.—Straddle-packer assembly. *A*, packer elements; *B*, suspension pipe; *C*, straddle pipe.

TABLE 44.1.—*Generalized section of the stratigraphic units penetrated in test hole near Las Animas, Colo.*

System	Geologic unit	Thickness (feet)	Physical character	Depth intervals of water bearing zones (feet)
Cretaceous	Graneros Shale	79	Dark-gray to black gypsiferous shale with thin layers of bentonite.	Not water bearing.
	Dakota Sandstone	133	White to brown fine-grained sandstone, thin- to massive-bedded; contains beds of clayey to sandy shale.	79–212
	Kiowa Shale Member of the Purgatoire Formation.	48	Gray to black calcareous shale, thin-bedded; contains some thin-bedded sandstone beds.	Not water bearing.
	Cheyenne Sandstone Member of the Purgatoire Formation.	137	White to buff fine-grained sandstone.	260–397
Jurassic	Morrison Formation	132	Green, red, and reddish-brown mudstone, siltstone, and sandstone; contains some thin limestone beds.	447–452
	Middle unit of Jurassic age	135	Red, orange-red to brown siltstone and very fine grained sandstone; orange chert beds at top; contains some limestone and gypsum.	Not water bearing.
	Entrada Sandstone	86	Buff to reddish-brown very fine grained sandstone.	644–750
Triassic	Triassic beds (Dockum Group)	180	Orange-red to red siltstone, mudstone, and very fine grained sandstone.	750–930
Permian	Permian beds	84+	Red to reddish-brown siltstone and fine-grained sandstone.	930–1,014

mersible pump capable of pumping 20 gallons per minute at a lift of 500 feet was used to pump from each aquifer while it was isolated by the straddle packer. Depths of water were measured before, during, and after pumping from each aquifer. The effects of interaquifer leakage were observed by means of measurements of water level in a small-diameter tube lowered past the packer elements prior to their inflation. Measurements were made in the tube simultaneously with measurements made in the zone isolated by the packer assembly.

The aquifer-test data were analyzed by the nonequilibrium method and are summarized in table 44.2. The test near Las Animas proved that only the aquifers in the Dakota and in the Cheyenne Sandstone Member of the Purgatoire Formation were suitable for development, because deeper zones had very low transmissibility and contained water of very poor quality.

TABLE 44.2.—*Summary of aquifer tests in test hole near Las Animas, Colo.*

Aquifer	Interval tested (feet)	Saturated thickness of permeable beds (feet)	Depth to water below land surface (feet)	Average pumping rate (gpm)	Drawdown (feet)	Specific capacity (gpm per ft of drawdown)	Duration of pumping (hours)	Coefficient of transmissibility (gpd per ft)	Coefficient of permeability (gpd per ft²)	Water temperature (°F)	Specific conductance (micromhos at 25° C)
Dakota Sandstone	79–212	133	60. 0	27	73	0. 37	72	1, 200	9	65	1, 630
Cheyenne Sandstone Member of the Purgatoire Formation 0°	260–397	114	61. 2	27	82	. 33	89	900	8	65	1, 660
Part of Morrison Formation and part of Entrada Sandstone	397–700	----	(1)	2. 5	270	. 01	2	5	----	66	7, 260
Basal part of Entrada Sandstone and Triassic sandstone	724–930	206	308. 4	7	48	. 15	6	100	. 5	75	6, 700
Permian sandstone	930–1, 014	84	296. 6	10	153	. 07	5	40	. 5	75	7, 160

[1] Artesian flow.

SURFACE WATER

45. ESTIMATING DAYS OF CONTINUOUSLY DEFICIENT DISCHARGE

By C. H. Hardison and J. R. Crippen, Washington, D.C., and Los Angeles, Calif.

The number of days the flow of a stream remains less than a given discharge (days of continuously deficient discharge), which is sometimes a factor in selecting an industrial site, can be estimated from frequency curves of annual low flow in States along the eastern seaboard. Data for preparing low-flow frequency curves are obtained as part of a routine program of analyzing records of streamflow by electronic computer and are more readily available than are similar data for days of continuously deficient discharge.

The procedure for estimating days of continuously deficient discharge uses the low-flow frequency data in the following manner. The ratio of the 120-day annual low flow to the 30-day annual low flow at the 2-year recurrence interval is taken from curves for specific stations, such as are shown in figure 45.1, and used as an index to enter the curves shown in figure 45.2. The ratio of deficiency discharge to annual low flow obtained from the ordinate of figure 45.2 is then applied to other low-flow frequency data taken from figure 45.1 to obtain the results plotted in figure 45.3.

The deficiency discharge shown as the ordinate in figures 45.2 and 45.3 is the discharge below which the flow remains continuously for the number of days indicated. The annual low flow is the lowest average flow each year for the indicated number of consecutive days. Thus, by definition, the deficiency discharge of a given unregulated station at a given recurrence interval is almost invariably higher than the annual low flow for the same number of days.

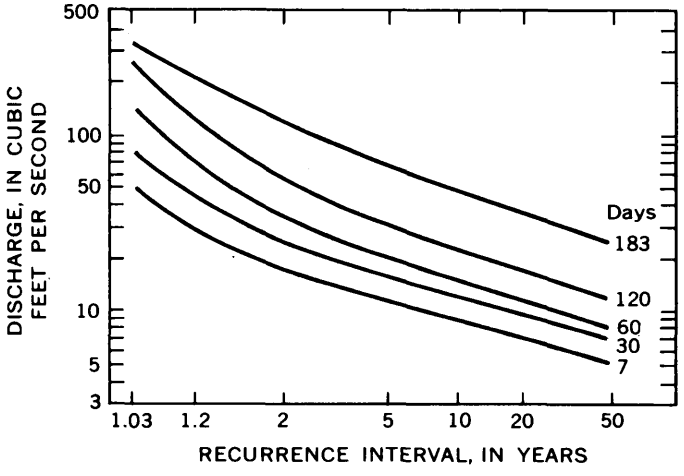

FIGURE 45.1.—Magnitude and frequency of annual low flow, French Creek at Carters Corners, Pa., 1913–52. Index ratio (120-day to 30-day annual low flow at 2-year recurrence interval) is 2.3.

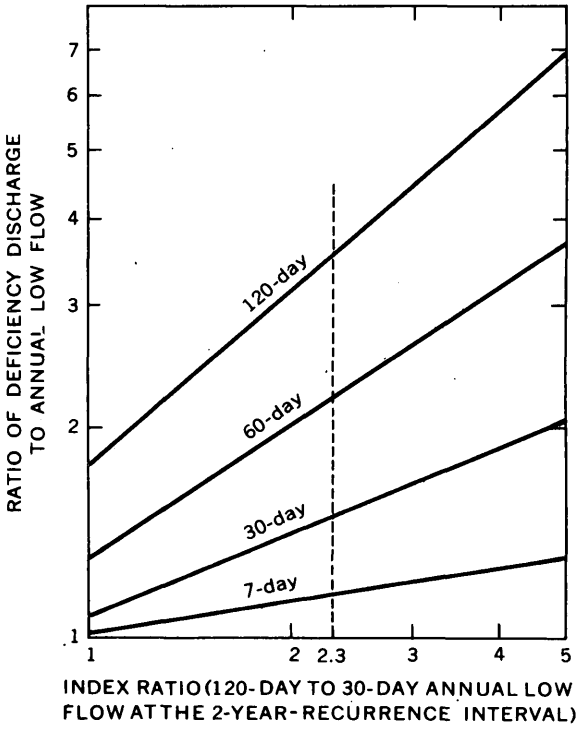

FIGURE 45.2.—Ratio of deficiency discharge to annual low flow for 7- , 30- , 60- , and 120-day periods at 10-year recurrence interval as function of index ratio for 32 stream-gaging stations in Eastern United States. Dotted line represents index ratio for French Creek at Carters Corner (fig. 45.1).

The curves in figure 45.2 are from least-square relations based on records at 32 long-term stream-gaging stations distributed as follows:

Alabama	2	New York	3
Georgia	3	North Carolina	5
Indiana	5	Pennsylvania	4
Maryland	2	Virginia	5
New Jersey	1	West Virginia	2

Relation lines, between the lowest deficiency discharge for selected numbers of consecutive days each year and the corresponding annual low flow, were established from the observed record at each of these stations and used to obtain the ratios used in the ordinate in figure

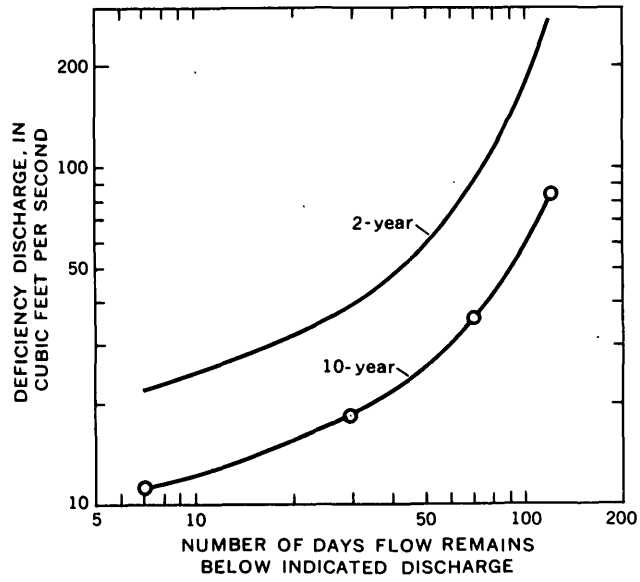

FIGURE 45.3.—Days of deficient discharge at the 2-year and 10-year recurrence intervals, French Creek at Carters Corners, Pa. Circles represent discharge computed from figures 45.1 and 45.2.

45.2. The ratios used in the abscissa were obtained from low-flow frequency curves for each station such as are shown in figure 45.1.

The computations for obtaining the curve for the 10-year recurrence interval in figure 45.3 are shown in the table below.

	7 days	*30 days*	*60 days*	*120 days*
10-year annual low flow from fig. 45.1, in cfs	9.4	12	16	23
Ratio of deficiency discharge to annual low flow from fig. 45.2 for an abscissa of 2.3	1.16	1.52	2.27	3.63
10-year deficiency discharge, in cfs, by multiplication	10.9	18.2	36.3	83.5

The curve for the 2-year recurrence interval in figure 45.3 was computed in the same manner using a set of curves for the 2-year recurrence interval similar to those shown in figure 45.2. The equations for the 10-year curves in figure 45.2 and the equations for the 2-year curves, which are not shown, are as follows:

Length of period (days)	*Recurrence interval*	
	2-year	*10-year*
7	$Y=1.027X^{0.158}$	$Y=1.02X^{0.154}$
30	$Y=1.159X^{0.413}$	$Y=1.096X^{0.384}$
60	$Y=1.432X^{0.730}$	$Y=1.30X^{0.660}$
120	$Y=2.20X^{0.958}$	$Y=1.76X^{0.854}$

In these equations, Y is the ratio of deficiency discharge to annual low flow at the indicated recurrence interval, and X is the ratio of the 120-day to the 30-day annual low flow at the 2-year recurrence interval which is used as an index ratio. The standard error of estimate by these equations ranges from about 5 percent for the 7-day periods to about 20 percent for the 120-day periods.

Comparison of the standard errors of estimate of the results by the equations presented here and the standard error of the previously mentioned relation lines between observed deficiency discharge and observed annual low flow for each station shows that the results obtained by using the equations are more accurate than those obtained by using the relation lines when the relation lines are based on less than 15 years of record. For observed records longer than 15 years, the relations based on observed record give a more accurate estimate.

The method presented here for estimating the number of days the flow of a stream can be expected to remain less than a given amount should be applicable to stream-gaging stations in the States along the Atlantic seaboard from New York to Georgia. Data for 2 stations in Alabama and 5 in Indiana indicate that the equations may be applicable as far west as the Mississippi River.

46. DETERMINATION OF TIDE-AFFECTED DISCHARGE OF THE SACRAMENTO RIVER AT SACRAMENTO, CALIFORNIA

By S. E. RANTZ, Menlo Park, Calif.

Work done in cooperation with California Department of Water Resources

The computation of momentary discharge of a tide-affected stream has been greatly simplified by the use of electronic computors (Baltzer and Shen, 1961), but the need still remains for a simple method for making reasonably accurate "on-the-spot" determinations of streamflow. A method of this kind is required, for

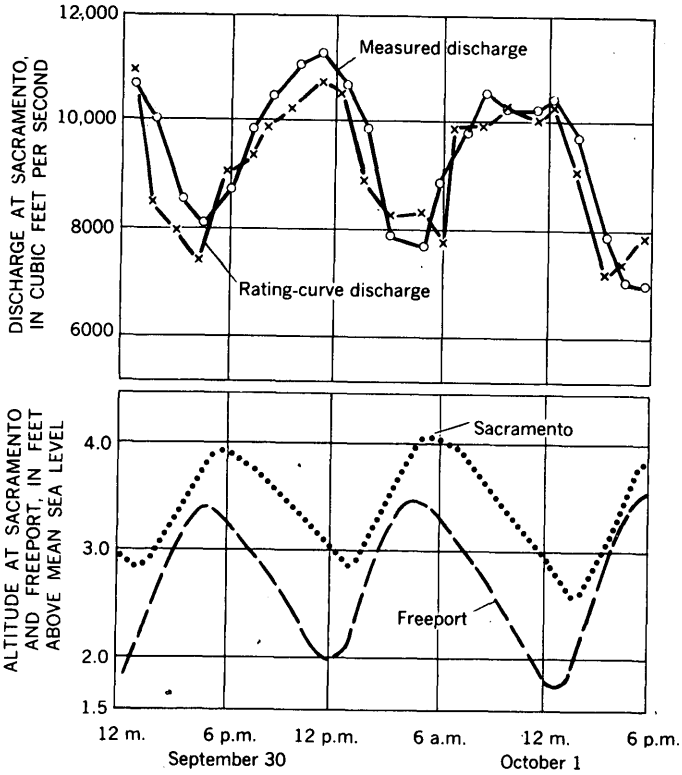

FIGURE 46.1.—Stage and discharge of the Sacramento River, Sept. 30 to Oct. 1, 1959.

example, in the operation of a sewage plant discharging its effluent into a tide-affected stream. The coaxial correlation method described in this article fills this need in that readings from a pair of stage gages can be used to determine momentary discharge directly from a set of curves.

The coaxial rating curves that were developed are based on 302 measurements of discharge of the Sacramento River at Sacramento, Calif. To obtain these data, a series of about 25 measurements was made during the course of each of 12 daily tidal cycles in the years 1957 to 1960. Measured discharges ranged from 4,060 cfs (cubic feet per second) to 19,300 cfs.

The streamflow measuring section is at the site of the stage recorder in the city of Sacramento; the auxiliary stage recorder is 10.8 miles downstream near the town of Freeport. Local inflow into the 10.8-mile reach of channel is negligible. The reach itself is located far enough upstream on the Sacramento River estuary so that no reversal of flow occurs. When upland flow (streamflow) into the estuary is less than about 30,000 cfs, however, the discharge is affected by tidal action, and the flow in the reach is unsteady. The relative magnitude of the tidal effect in the reach increases with decrease in the upland flow and with increase in the range of elevation between high and low tides. The stages at Sacramento and Freeport during a 36-hour period and the fluctuation of discharge at Sacramento illustrate a typical low-flow condition (fig. 46.1). The upland flow above Sacramento was 9,300 cfs. As a result of tidal effect the discharge at Sacramento varied from 6,800 cfs to 11,300 cfs.

The differential equations of unsteady flow were used to devise a graphical technique for determining discharge. The following parameters serve as indices of the terms that appear in these differential equations:

Dependent variable.—Measured discharge at Sacramento.

Independent variables.—(1) Stage at Sacramento, (2) fall in the reach between Sacramento and Freeport, and (3) the algebraic average of the change in stage observed at Sacramento and Freeport during a 15-minute interval.

Because of the differential form of the equations of unsteady flow, there is no statistical model on which to base the relationship of these variables. A further complication arises from the fact that joint functions are involved, for interrelations among the independent variables affect the flow at Sacramento. The versatile statistical technique known as the coaxial method of graphical multiple correlation (Linsley, Kohler and Paulhus, 1949, p. 650–659) was adopted for developing the rating curves for the Sacramento River.

The coaxial graphical correlation that was the end product of this study is shown in figure 46.2. In the interest of simplicity only a few lines are shown in each family of curves. To use the graph, first, the curves in the upper left-hand group are entered with the stage at Sacramento and the fall in the reach; next, the curves in the lower left-hand group are entered with the average rate of change of stage in the reach; finally, the adjustment graph to the right is entered and the discharge is read. The adjustment graph was added to the correlation to introduce a necessary curvilinearity to the relationship. This curve may also serve another purpose—if the relationship should change, as a result of channel dredging, for example, only the adjustment graph need be revised, thereby eliminating the laborious task of revising the two families of curves.

A graphical correlation of the type developed in this study, or a modification, should be useful for determining the momentary discharge for many streams, tidal or otherwise, that are subject to unsteady flow.

REFERENCES

Baltzer, R. A., and Shen, John, 1961, Computation of homogeneous flows in tidal reaches by finite difference method: Art. 162 *in* U.S. Geol. Survey Prof. Paper 424–C, p. C39–C41.

Linsley, R. K., Kohler, M. A., and Paulhus, J. J. H., 1949, Applied hydrology; New York, McGraw-Hill.

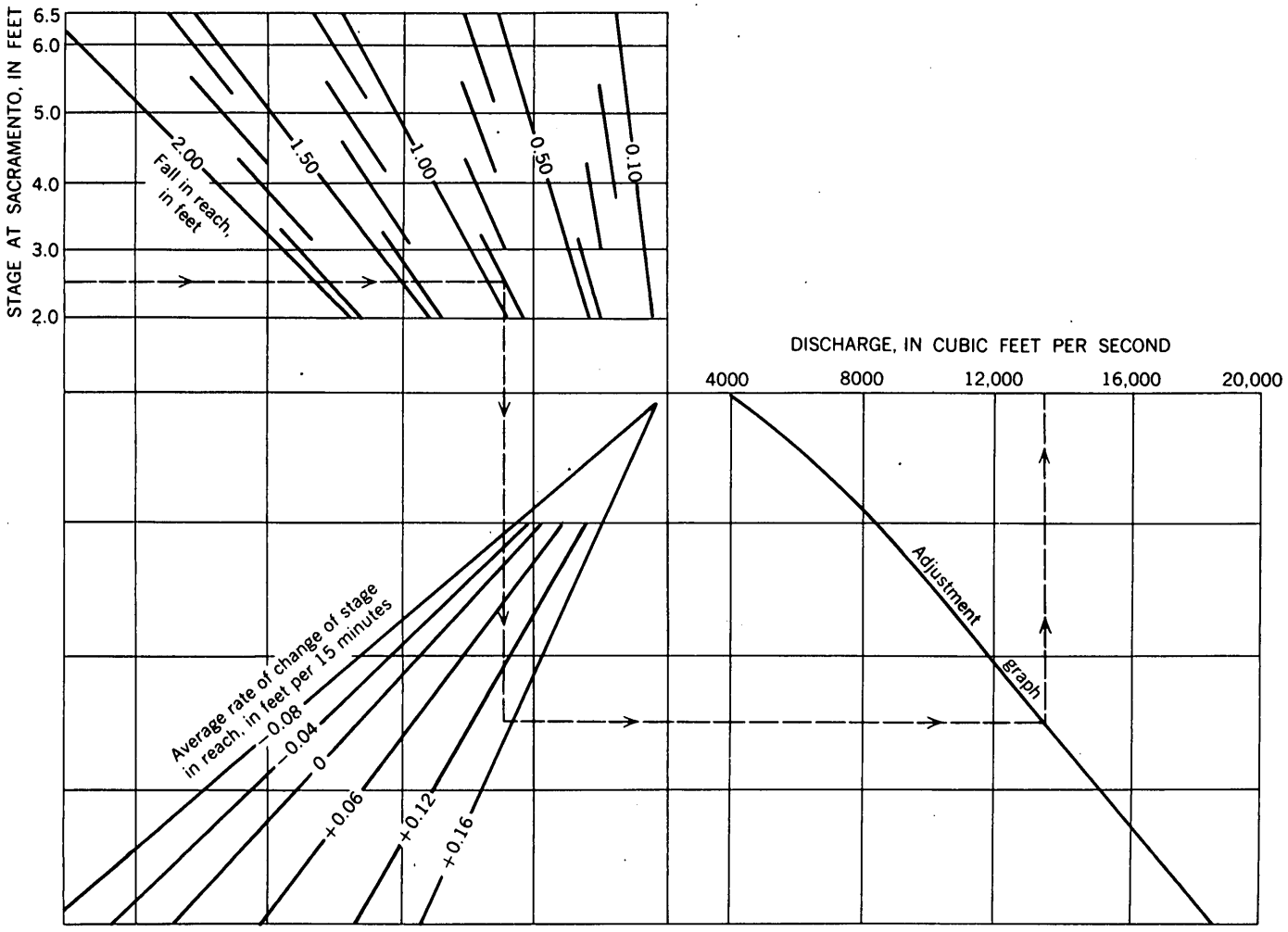

FIGURE 46.2.—Coaxial rating curves for the Sacramento River at Sacramento. Dashed lines and arrow illustrate use of the curves. the curves.

47. POINTS OF ORIGIN OF PERENNIAL FLOW IN GEORGIA

By WILLIAM J. SCHNEIDER, Washington, D.C.

The Yellow River basin near Snellville, Ga., which drains 134 square miles in the Piedmont province northeast of Atlanta, and the Tired Creek basin near Cairo, Ga., which drains 55 square miles in the Tifton Upland of the Coastal Plain province, are representative of a large part of the State. The hydrology and physical characteristics of these two areas in Georgia are being studied to establish criteria for accurate classification of stream channels on topographic maps as ephemeral or perennial.

Field investigations of more than 200 small headwater stream valleys in both basins indicate that streamflow becomes perennial at sharply defined points, and 112 such points were identified in the field. These points of origin of perennial flow are characterized by abrupt beginnings of incised stream channels. The channels have semicircular heads with vertical walls. The depths of incision at the wall range from about 1 to 8 feet. The valleys just upstream from the channel heads are rather broad, flat flood plains that are covered with

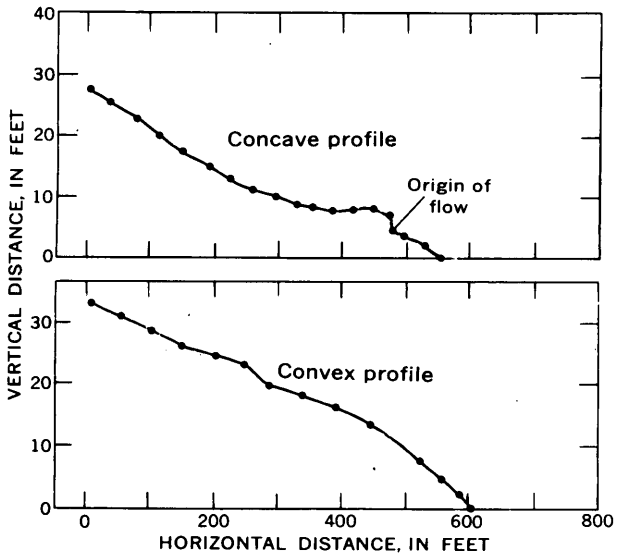

FIGURE 47.1.—Types of stream profiles in Yellow River basin.

vegetation, generally woodland, and are areas of deposition of recent sediments. The geologic significance of these points of origin has not as yet been investigated. Estimated flows up to 4 to 5 gallons per minute were observed issuing from small pools at the bases of the vertical channel heads. Because observations of flow were made at selected sites at several times during the low-flow season, it is reasonable to assume that streamflow below the sharply defined points of origin is perennial.

Not all first- or second-order headwater streams become perennial, however; some remain ephemeral throughout their length. These ephemeral streams can be identified by the shape of their longitudinal profile. Measured longitudinal profiles of 16 headwater streams in the Yellow River basin can be grouped according to upward concavity or convexity. A typical profile for each group is shown in figure 47.1. Streams that are ephemeral throughout their length to their junction with a perennial stream have generally convex profiles; streams that become perennial at a spring issuing from a well-defined seepage face at the head of an incised channel have generally concave profiles in their ephemeral reaches. Ordinarily, except in densely wooded areas, the type of longitudinal stream profile can be determined from stereoscopic viewing of aerial photographs, thus giving a practical method of delineating these points of origin of perennial streamflow.

QUALITY OF WATER

48. DETERMINATION OF BORON IN WATERS CONTAINING FLUORIDE

By JACK J. ROWE, Washington, D.C.

Many investigators have reported that fluorine interferes in colorimetric determinations of boron. Gaestel and Huré (1949) found it necessary to complex fluorine with $AlCl_3$ during the methyl borate distillation prior to the determination of boron colorimetrically with curcumin, and Ryabchikov and Danilova (1950) used a resin to separate boron from fluorine for the determination of boron with carmine. Sher (1957) also reported that fluorine concentrations of as little as 2.5 ppm interfere in the quinalizarin or alizarin S. methods for the determination of boron in waters; Cogbill and Yoe (1957) reported that fluorine must be absent for the colorimetric determination of boron using anthrarufin, quinizarin, or diaminochrysazin. Ellis and others (1949) reported that fluorine in concentrations greater than those usually found in plants will cause low results in the dianthtrimide determination of boron. Later, Powell and Poindexter (1957) and Langmyhr and Skaar (1961) also reported that fluorine will interfere in the determination of boron with dianthrimide. Rainwater and Thatcher (1960), in their modification of the dianthrimide method, did not study the effect of fluorine. The present study was made to determine the fluorine tolerance of this method.

Apparatus and reagents

Oven, 90° C. Uniformity and stability of temperature control are critical.

Absorption cells, 25-mm diameter. Boron-free glassware with glass stoppers was used for digestions and development of the colors.

Spectrophotometer, Beckman Model B. Blue-sensitive phototube, sensitivity setting 2, slit width approx. 0.6 mm, wavelength setting 620μ.

Sodium tetraborate standard solution, 0.200 B_2O_3 mg per ml. Dissolve 0.5477 g $Na_2B_4O_7 \cdot 10\ H_2O$ in distilled water and dilute to 1 liter.

Sodium tetraborate solution, 0.002 mg B_2O_3 per ml. Dilute 10 ml standard solution 0.200 mg B_2O_3 per ml to 1 liter.

1,1′ dianthrimide stock reagent. Dissolve 200 mg dianthrimide in 50 ml conc H_2SO_4. Store in refrigerator in polyethylene bottle.

1,1′ dianthrimide working reagent. Dilute 1 volume of stock reagent to 20 volumes with conc H_2SO_4. Store in tightly closed polyethylene bottles in the dark. Reagent is stable for long periods.

Sulfuric acid, 95.5–96.5 percent, (sp gr 1.84) (Danielsson, 1959).

Sodium fluoride, 1.000 mg F per ml. Dissolve 2.21 g NaF in distilled water, dilute to 1 liter.

Sodium fluoride, 0.10 mg F per ml. Dilute 10 ml 1.000 mg F per ml to 1 liter.

Procedure

1. Pipet a volume of the sample containing less than 0.012 mg B_2O_3 into the absorption cell.
2. Prepare a blank of distilled water and sufficient standards. Adjust volumes to about 5 ml.
3. Add 1.0 ml conc H_2SO_4. Mix by swirling.
4. Evaporate overnight in an oven at 90° C. At end of evaporation the volume should be about 1.0 ml.
5. Add 5.0 ml dianthrimide working reagent and mix by swirling.
6. Incubate for 4.0 hr at 90° C.
7. Cool and dilute with 10.0 ml conc H_2SO_4.
8. Stopper and mix by swirling.
9. Clean the exterior surfaces of the tube.
10. Determine the absorbancy of the sample and standards against the blank at 620m μ.

EFFECT OF FLUORINE ON THE DETERMINATION OF BORON

Standards.—The effect of fluorine on the determination of boron was studied by adding 0.010- to 1.000-mg quantities of fluorine to standards containing 0 to 0.010 mg of B_2O_3 at step 2 of the above boron procedure. The procedure was then followed through step 10; optical densities are shown in table 48.1. The optical densities were determined in the absorption tubes used for the digestion, hence optical densities are reported to only two decimal places. The addition of up to 1.000 mg of fluorine does not affect the dianthrimide-boron color, as can be seen from table 48.1.

Natural waters.—A study was also made of the effect of adding 0.010 mg of fluorine to samples of water from Yellowstone National Park. Water samples were first analyzed for boron using the above procedure. To equivalent samples of the water, 0.010 mg of fluorine and 0.002 mg of B_2O_3 were then added, and boron again determined. It was found that the originally determined boron, plus the added amount, was recovered in each case, as shown in table 48.2.

TABLE 48.1.—*Effect of fluorine on dianthrimide determination of boron*

Mg B_2O_3	*Mg F added*	*Optical density*	*Mg B_2O_3*	*Mg F added*	*Optical density*
0	0	0		0.030	0.96
	.010	0		.040	.95
	.050	0		.050	.97
	.100	0		.075	.95
0.004	0	.47		.100	.97
	.010	.47		.150	.97
	.020	.47		.200	.97
	.030	.475		.500	.96
	.040	.48		1.000	.95
	.050	.47	0.010	0	1.18
0.008	0	.95		.020	1.19
	.010	.96		.030	1.18
	.020	.95		.050	1.18

TABLE 48.2.—*Effect of adding fluorine and boron to water samples from Yellowstone National Park*

Sample No.	Description	Mg B_2O_3		Mg F		Total Mg B_2O_3
		Originally in sample	Added	Originally in sample	Added	
4	Cinder Pool	0.0073	0.002	0.005		0.0095
5	Echinus Geyser	.0053	.002	.006		.0073
10	Porcelain Terrace	.0055		.002	0.010	.0054
11	Pork Chop Pool	.0062	.002	.006		.0083
18	Excelsior Geyser	.0066		.024	.010	.0067
19	Artemisia Geyser	.0134	.002	.022	.010	.0152
20	Daisy Geyser	.0215	.002	.028	.010	.0235
21	Pool near Daisy	.0245	.002	.002	.010	.0265

BEHAVIOR OF FLUORINE

A study was made of the behavior of fluorine in the concentrated sulfuric acid medium employed for the dianthrimide determination of boron. Standards were prepared containing 0 to 0.500 mg of B_2O_3 and 0.500 to 1.000 mg of fluorine and carried through steps 1, 2, 3, and 4 of the boron procedure. Fluorine analyses were made to determine whether any fluorine was still present in the sample after the sulfuric acid evaporation at 90° C and before the addition of the dianthrimide (step 5). The sulfuric acid concentrate was diluted and transferred to a distilling flask. The procedure of Grimaldi and others (1955) was used for the distillation and determination of fluorine with thoron. To check the method used for the determination of fluorine in the presence of boron, a control sample, containing 0.400 mg of B_2O_3, 1.000 mg of fluorine, and 1 ml of concentrated sulfuric acid was placed in the distilling flask, and the procedure of Grimaldi and others (1955) used for the determination of fluorine was followed. All the fluorine present in the control sample was recovered in the distillate. The results of this study are shown in table 48.3.

TABLE 48.3.—*Fluorine remaining after evaporation at 90°C with concentrated sulfuric acid*

	Mg B_2O_3	*Mg* F *added*	*Mg* F *after overnight evaporation*
1	0	0. 500	0
2	0	1. 000	0
3	. 010	. 500	0
4	. 020	. 500	0
5	. 050	. 500	0
6	. 100	. 500	0
7	. 200	1. 000	0
8	. 400	1. 000	0
9	. 500	1. 000	0
Control	. 400	1. 000	1. 000 (not evaporated)

DISCUSSION

The study of the fluorine tolerance of the dianthrimide method of Rainwater and Thatcher showed that the suggested method could be applied to the determination of boron in waters from Yellowstone National Park, some of which contain up to 30 ppm of fluorine. It can be seen from the data of tables 48.1 and 48.2 that the presence of as much as 1.000 mg of fluorine will not interfere with the determination of boron using this procedure. Although these data may seem to contradict the observations of Powell and Poindexter, who reported interference from fluorine caused by the complexing of boron with the fluorine, investigation of the behavior of fluorine during evaporation of the concentrated sufuric acid solution used for the boron-dianthrimide determination reconciled the apparent inconsistency. Powell and Poindexter and Langmyhr and Skaar measured the effect of adding fluorine to a solution containing boron and dianthrimide but did not include an evaporation step. From the data of table 48.3, it can be seen that the fluorine is volatilized during the sulfuric acid evaporation at 90° C, thereby separating fluorine from the boron prior to the addition of the dianthrimide. Cogbill and Yoe, in their study of the determination of boron with diaminochrysazin, and other isomeric dihydroxy anthraquinones, found some indication of this behavior of fluorine. It would seem, then, that under the conditions of the proposed procedure involving evaporation with sulfuric acid in glass tubes, the fluorine is selectively eliminated, probably as silicon tetrafluoride as evidenced by the etching of the glass near the bottom of the absorption tubes used for the digestion. For the analysis of waters containing more than 10 ppm of fluorine, it is recommended that old tubes be used for the digestion and development of colors. Solutions should be transferred to clean tubes or cells for the final readings of the absorption.

REFERENCES

Cogbill, E. C. and Yoe, J. H., 1957, Spectrophotometric determination of boron with diaminochrysazin, diaminoanthrarufin and tribromoanthrarufin: Anal. Chemistry, v. 29, p. 1251–1258.

Danielsson, L., 1959, A study of the conditions for the determination of boron with dianthrimide: Talanta, v. 3, p. 138–146.

Ellis, G. H., Zook, E. G., and Baudisch, O., 1949, Colorimetric determination of boron using 1,1′ -dianthrimide: Anal. Chemistry, v. 21, p. 1345–1348.

Gaestel, Ch., Huré, J., 1949, Colorimetric determination of microgram amounts of borates in presence of fluorides: Soc. chim. France Bull., p. 830.

Grimaldi, F. S., Ingram B., and Cuttitta, F., 1955, Determination of small and large amounts of fluorine in rocks: Anal. Chemistry, v. 27, p. 918–921.

Langmyhr, F. J., and Skaar, O. B., 1961, The effect of foreign ions on the spectrophotometric determination of boron with 1,1′ -dianthrimide: Anal. Chim. Acta, v. 25, p. 262–270.

Powell, W. A., and Poindexter, E. H., 1957, 1,1′ -dianthrimide for spectrophotometric determination of boron: U.S. Atomic Energy Comm. Report CCC–1024–TR–229.

Rainwater, F. H., and Thatcher, L. L., 1960, Methods for collection and analysis of water samples: U.S. Geol. Survey Water-Supply Paper 1454, p. 113–115.

Ryabchikov, D. I., and Danilova, V. V., 1950, Determination of boron and fluorine when present together: Zhur. Anal. Khim., v. 5, p. 28–31.

Scher, A., 1957, Rapid colorimetric determination of the boric acid content of water by means of quinalizarin and alizarin S.: Hidrol. Kozlony, v. 37, p. 168–170.

49. LIMITATIONS OF THE METHYLENE BLUE METHOD FOR ABS DETERMINATIONS

By Cooper H. Wayman, Denver, Colo.

Work done in cooperation with Federal Housing Administration

The anionic surface-active agent alkylbenzenesulfonate (ABS) is the most abundant detergent found in ground- and surface-water supplies. The ABS anion is represented by

$$[C_{12}H_{25}-C_6H_4-SO_3]^{-1}.$$

In water, the anion is extremely stable to both chemical and biochemical degradation. Walton (1960) recently reported ranges in ABS concentrations from 0.00 to 1.8 ppm (parts per million) for surface-water supplies and from 0.00 to 10.0 ppm for ground-water supplies.

Although the physiological implications of ABS to human beings is unknown, prolonged ingestion of this material by rats is believed to be nontoxic (Paynter, 1960). Laboratory studies suggest that bacteria do not travel great distances in water-saturated sands containing ABS (Robeck, 1961). Nichols and Koepp (1961) found that Wisconsin ground water became more bacteriologically unsafe with increase in concentration of detergent. Miller (1961) indicated that certain ingredients in detergents cause pathogenic bacteria to flourish. The relationship between detergent pollution and bacteriological pollution of ground water, if any, has not been well established, but ABS can be used as an excellent indicator of pollution.

Because of the importance of ABS as an indicator of pollution, the limitations, precision, and accuracy of present methods available for its determination should be known. Most analysts prefer to use the methylene blue method (American Public Health Association and others, 1960, p. 246–248) because of its simplicity. However, some laboratories use an infrared technique (Sallee and others, 1956) as a referee method.

Both organic and inorganic materials interfere with the methylene blue method, which is nonspecific for the sulfonated benzene ring. Organic sulfates, sulfonates, carboxylates, phosphates, and phenols form complexes with methylene blue, and inorganic cyanates, chlorides, nitrates, and thiocyanates form ion pairs with this compound; other organics, such as amines, offer additional interference through competition with methylene blue for a reaction. Because of these interferences and because some constituents might be present in surface- or ground-water supplies in amounts exceeding ABS concentrations, determinations of ABS in natural water by the methylene blue method requires some reservations.

Our experience with this method suggests that experimental technique can contribute additional error. Therefore, deionized water containing a solid composed of 99.0 percent ABS was studied to determine the influence of the following variables on the method: (1) Time-of absorbancy measurement after extraction, (2) type of methylene blue used, and (3) temperature. The colored complex that is formed decays with time. Figure 49.1 shows the change in absorbancy (A) with time (t). At 10 ppm and 1.0 ppm, $-dA/dt$ is 7×10^{-4} and 2×10^{-4} absorbancy units per minute respectively. The complex is more stable at low ABS concentrations. Little error is introduced if the complex is measured within 60 minutes after extraction. Many laboratories frequently extract 6 to 8 samples in an 8-hour day, however, and measure the absorbancy at the end of this period; obviously, poor precision would be attained with such a technique. The type of dye used is extremely important. A dye that displays maximum absorbancy at the wavelength of interest should be used. Figure 49.2 shows the change of absorbency for a variety of dyes in solutions containing 0.5 ppm and 1.0 ppm of ABS. Of these dyes, Eastman P–573 or Fisher NA–652 give maximum absorbency and should be preferred with this method. Organic dyes may deteriorate with time, and the impurities contained from batch to batch may vary; these factors also should be considered in the choice of a dye. Temperature in the range from 10° to 35°C has no apparent influence on the stability of the complex.

The precision of the method seems to depend on the concentration of ABS. The table below shows that the standard error of estimate increases with concentration. Standard errors of estimate of 0.75±0.13

Standard error of estimate of ABS at various concentrations

ABS concentration (ppm)	Standard error of estimate				Report
	Field samples		Laboratory samples		
	Source	Ppm	Type of water	Ppm	
0.40			Distilled	0.05	Am. Public Health Service and others (1960).
.75			do	.13	B. B. Ewing (written communication, 1961).
2.22			Tap	.18	Am. Public Health Service and others (1960).
2.50			Deionized	.30	Wayman (this article).
.35		0.04			Cohen (1961).
1.00		.12			Do.
1.25		.19			Do.
1.31	River water.	.25			Am. Public Health Service and others (1960).

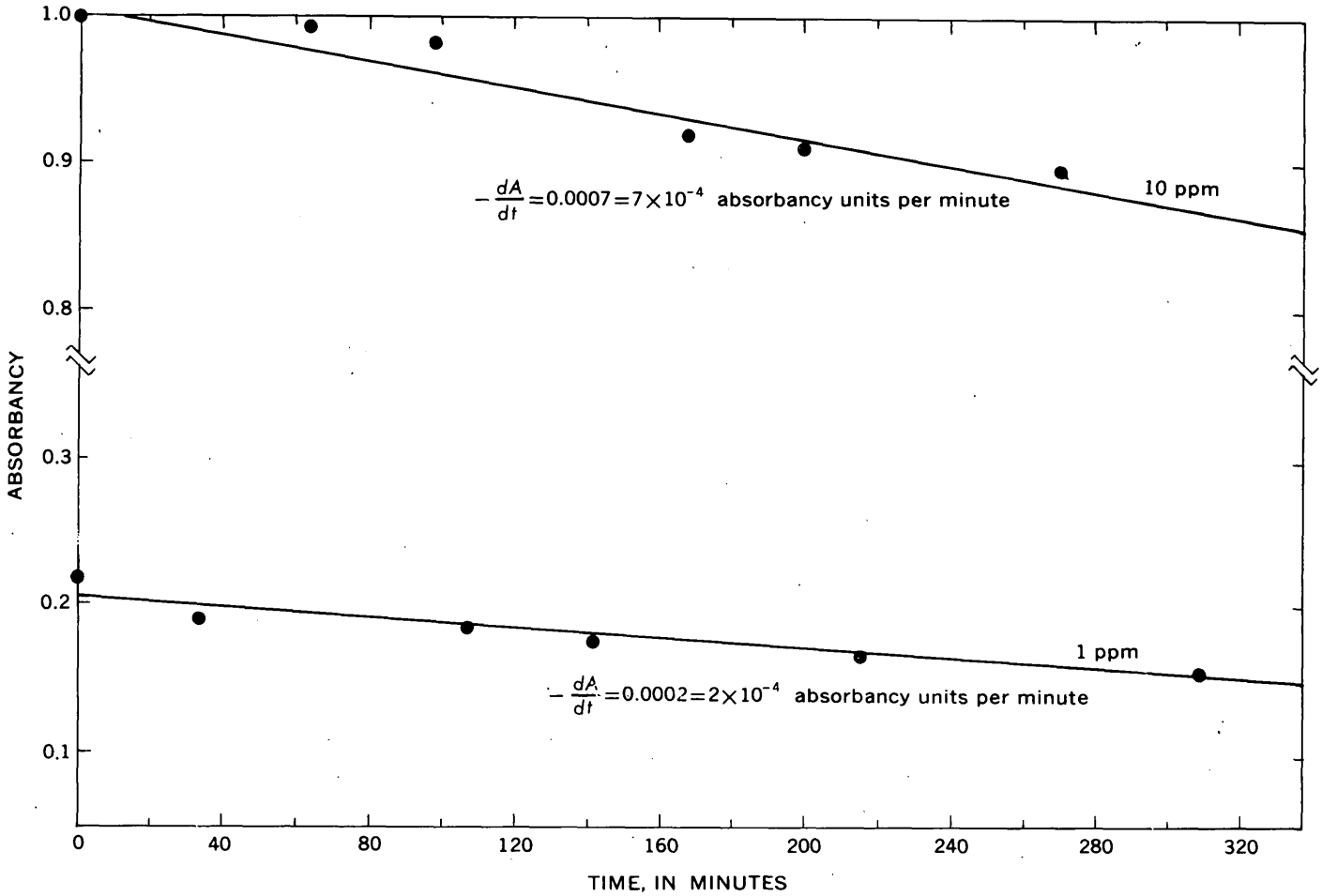

FIGURE 49.1.—Influence of time of measurement on ABS absorbancy determination.

ppm of ABS (B. B. Ewing, written communication, 1961) and 2.50±0.30 ppm (from the subject study) can be cited. These data represent about 60 samples for each value reported. A detection limit of 0.025 ppm is reported for ABS (American Public Health Association and others, 1960). Our studies of deionized water containing a solid composed of 99.0 percent ABS indicate that the detection limit is about 0.1 ppm of ABS. In a study of drinking-water supplies of 32 cities throughout the United States, the Association of American Soap and Glycerine Producers Committee (1961) reports that the average ABS content of the supplies was 0.024 ppm and that 98 percent of the supplies contained ABS in the range of 0.00 to 0.10 ppm. If the detection limit is 0.1 ppm of ABS in deionized water, of what significance are ABS concentrations of less than 0.1 ppm that are reported for natural water? For the methylene blue method, most analysts prepare calibration curves from solutions containing a solid that is equivalent to 60 to 70 percent ABS. If the remaining 30 to 40 percent of this solid contains ingredients that react with methylene blue, additional error is possible; a standard containing 99.0 percent ABS (prepared by the California Research Corp.) was used in the study described in this report. A calibration curve prepared from the purest standard available appears to be the most accurate.

How accurate are ABS determinations made by the methylene blue method? This procedure depends on the formation of a blue-colored salt when methylene blue reacts with ABS. Because the method is nonspecific with regard to ABS, other organic or inorganic ions in solution can influence the accuracy of a determination. Because ABS is resistant to chemical oxidation, recent investigators (Hill, Shapiro, and Kobayashi, 1961) have utilized chrome sulfuric acid as an oxidant to remove surfactants other than ABS and other ions from solution before use of the methylene blue method. When this oxidation step is used, the methylene blue method is less subject to interferences from inorganic ions and certain surfactants and it appears to be more accurate than the standard meth-

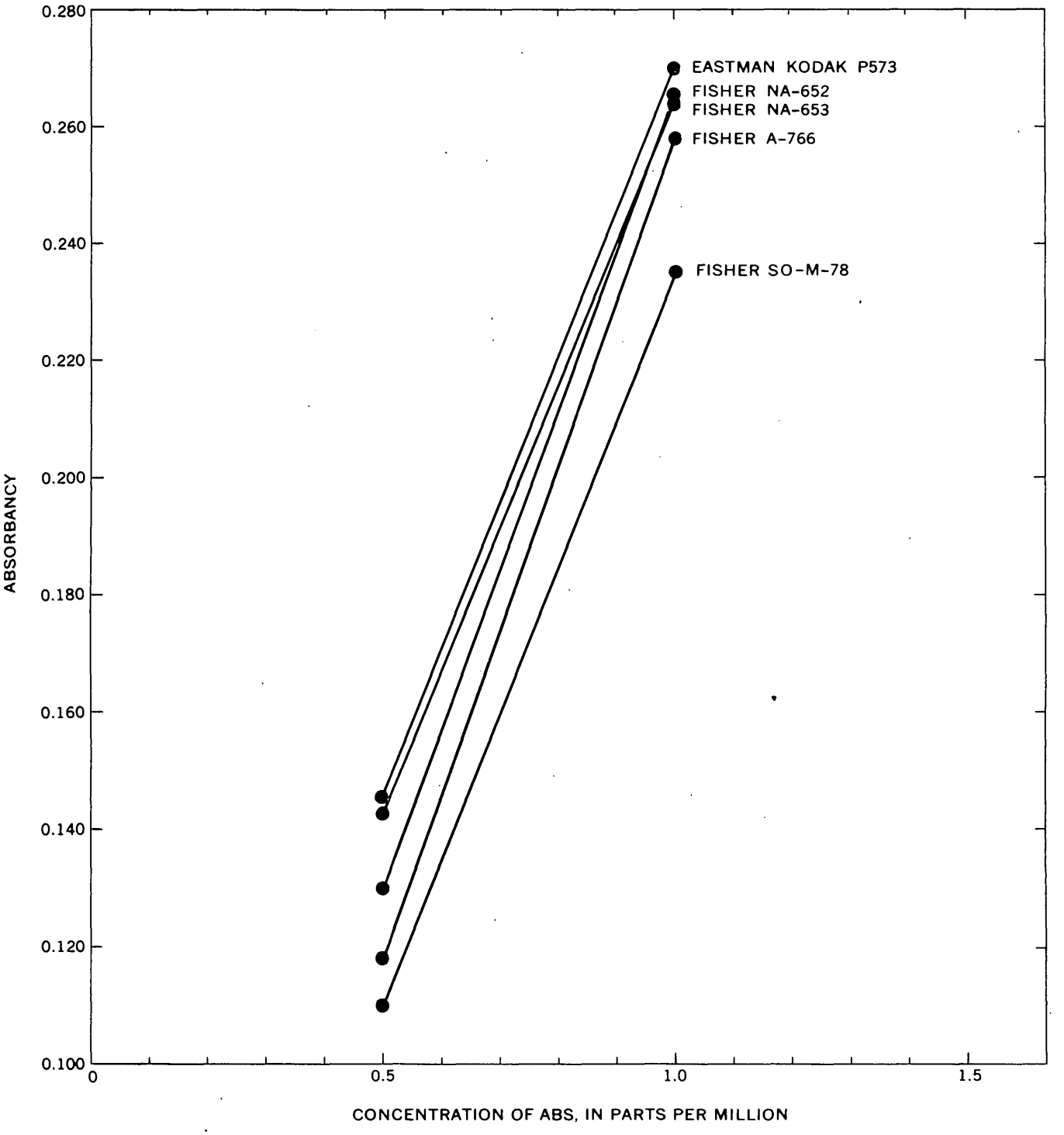

FIGURE 49.2.—Effect of dye type on absorbency determination.

ylene blue method. Another modification of the standard method (Webster and Halliday, 1959) is reported to give results comparable to those for infrared for river water and sewage. Because of the purported improved accuracy of the two modified methylene blue methods, these methods should be investigated further or perhaps combined into a single method.

Certain limitations regarding the precision, accuracy, and experimental technique in use of the standard methylene blue method are indicated. For those analysts making ABS determinations on surface-water, ground-water, and public-water supplies, concentrations of less than 0.1 ppm should be reported with some reservation.

REFERENCES

American Public Health Association and others, 1960, Standard methods for the examination of water and wastewater: 11th ed., New York, Am. Public Health Assoc., Inc., 626 p.

Association of American Soap and Glycerine Producers, 1961, ABS in drinking water in the United States: Am. Water Works Assoc. Jour., v. 53, p. 297–300.

Cohen, J. M., 1961, Detergent detection: The Sanitarian, v. 23, no. 4, p. 194–197.

Hill, H. H., Shapiro, M. A., and Kobayashi, Y., 1961, Determination of alkylbenzenesulfonate in water: Am. Chem. Soc. Natl. Mtg., 140th, Chicago, 1961, Div. of Water and Waste Chemistry, Paper 5, 16 p. (presented Sept. 4)

Miller, B. W., 1961, Syndets and pathogens: Am. Water Works Assoc. Ann. Mtg., Detroit, 1961 (paper presented June 6); Detroit Free Press, June 7, 1961.

Nicholas, M. S., and Koepp, E., 1961, Synthetic detergents as a criterion of Wisconsin ground-water pollution: Am. Water Works Assoc. Jour., v. 53, p. 303–306.

Paynter, O. E., 1960, The chronic toxicity of dodecylbenzene sodium sulfonate: U.S. Public Health Service Conference on Physiological Aspects of Water Quality Proc., Washington, D.C., Sept. 8–9, 1960, p. 175–179.

Robeck, G. G., 1961, Ground water contamination studies at the Sanitary Engineering Center: U.S. Public Health Service Symposium on Ground-Water Contamination, Robert A. Taft Sanitary Engineering Center, Cincinnatti, 1961. (paper presented at meeting)

Sallee, E. M., Fairing, J. D., Hess, R. W., and others, 1956, Determination of trace amounts of alkylbenzenesulfonate in water: Anal. Chemistry, v. 28, p. 1822–1826.

Walton, G., 1960, ABS contamination: Am. Water Works Assoc. Jour., v. 52, p. 1354–1362.

Webster, H. L., and Halliday, J., 1959, Determination of alkylbenzenesulfonate in river waters and sewage: The Analyst, v. 84, p. 552–559.

50. HYDROCHEMICAL FACIES IN THE "400-FOOT" AND "600-FOOT" SANDS OF THE BATON ROUGE AREA, LOUISIANA

By C. O. Morgan and M. D. Winner, Jr., Baton Rouge, La.

Work done in cooperation with the Louisiana Department of Public Works and the Department of Conservation, Louisiana Geological Survey

The "400-foot" and "600-foot" sands, two major aquifers of the Baton Rouge area, Louisiana, crop out and are recharged in East Feliciana and West Feliciana Parishes north of Baton Rouge (Morgan, 1961). The principal artificial discharge area of these artesian aquifers is in the industrial district of East Baton Rouge Parish.

The "400-foot" and "600-foot" aquifers in the recharge area have been considered early Pleistocene by a number of writers (Doering, 1958; Rollo, 1960, pl. 2; Morgan, 1961), whereas others have correlated equivalents of these sediments with the Citronelle Formation of Pliocene age (Stringfield and LaMoreaux, 1957).

The water-analysis diagram in figure 50.1 is modified after Back (1961, p. D–381), who described the ground waters of the Atlantic Coastal Plain in terms of hydrochemical facies (Back, 1960). In the investigation described herein, chemical analyses were made of water from selected wells in an area extending from the recharge area in East Feliciana and West Feliciana Parishes to beyond the salt-water interface in East Baton Rouge Parish (fig. 50.2). The chemical constituents are plotted in percent of total equivalents per million on the water-analysis diagram (fig. 50.3).

Analyses of water from the recharge area show the cation facies in the ground water to be Na,Ca and the anion facies to be $Cl+SO_4$,HCO_3. The pH of the ground water in this area usually is less than 6.0; the lowest was 5.2 (fig. 50.2, sample 5). This low pH is attributed to solution of CO_2 from abundant decaying vegetation in the soil zone. Dissolved solids range from a low of 27 ppm (parts per million) in sample 4 to 83

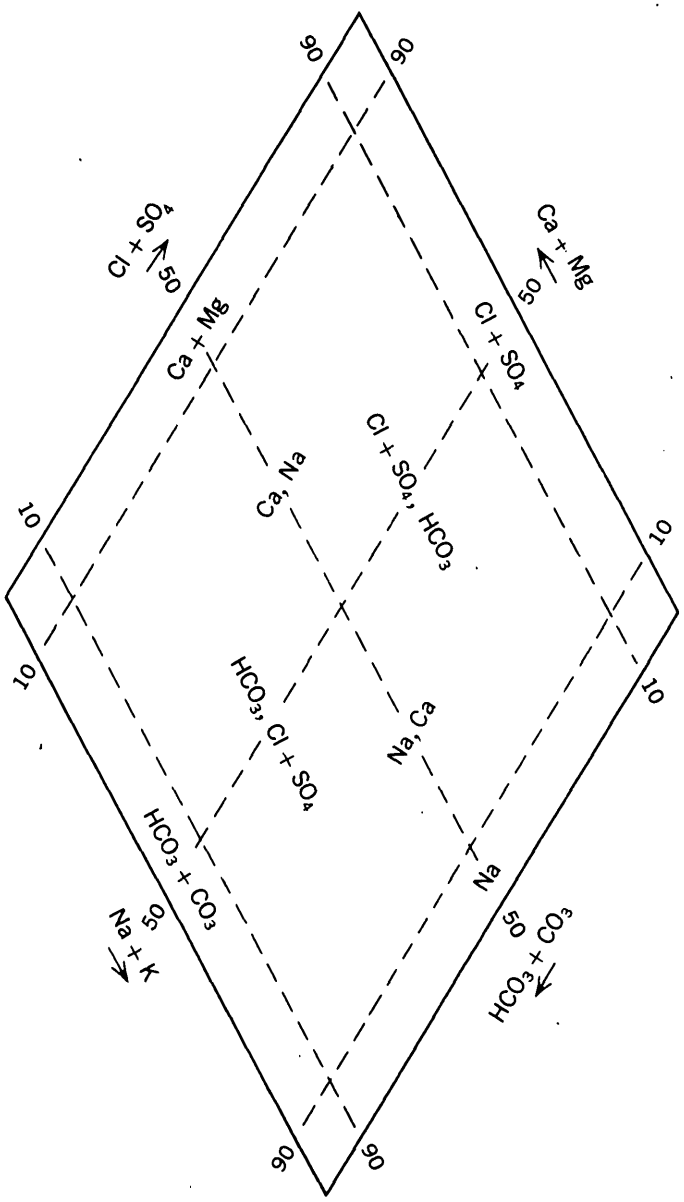

FIGURE 50.1.—Water-analysis diagram showing hydrochemical facies, in percent of total equivalents per million (after Back, 1961).

ppm in sample 3. Presence of ground water of a low pH in combination with a low dissolved-solids content indicates that the recharge area is a highly leached zone (Back, 1960, p. 94). Accordingly, ground water in this area is of Na,Ca facies rather than Ca+Mg or Ca,Na facies as in recharge areas of the Atlantic Coastal Plain.

As the CO_2-charged water moves downdip in the aquifer, Ca and Mg are dissolved in the extent that the water approaches a Ca,Na facies (fig. 50.3, sample 7), but this action is countered by cation exchange, which replaces the Ca and Mg ions in the water with Na ions. The Na facies is reached near the area of the fresh water–salt water interface.

The anion facies in the ground water progressively changes downdip from a $Cl+SO_4$, HCO_3 facies through HCO_3, $Cl+SO_4$ to a HCO_3 facies near the fresh water–salt water interface (fig. 50.2). Ground water in this part of the system is characterized by a pH between 7.0 and 8.0 and a dissolved-solids content of 175 to 225 ppm.

At the fresh water–salt water interface, mixing is caused by pumping. The mixture is represented as a gradual cation change from the Na facies to the Na, Ca facies, and as a sharp anion change from the HCO_3 facies to the $Cl+SO_4$, HCO_3 facies (fig. 50.3). The change in facies over a period of time as the interface moves northward is illustrated by samples 15A, 15B, and 17A, 17B, and 17C, which represent replicate samples from wells 15 and 17.

In summary, the recharge area of the "400-foot" and "600-foot" sands of the Baton Rouge area is a highly leached zone identified by ground water of an Na,Ca facies, low pH, and low dissolved-solids content. As the water moves slowly downdip its chemical character is altered—the dissolved-solids content increases and the water is softened by cation exchange. Mixing of salt water and fresh water at the interface causes a sharp change in the anion facies from HCO_3 to $Cl+SO_4$, HCO_3. However, the cation facies change from Na to Na,Ca is less pronounced.

REFERENCES

Back, William, 1960, Origin of hydrochemical facies of ground water in the Atlantic Coastal Plain: Internat. Geol. Cong., 21st, Copenhagen 1960, proc., pt. 1, p. 87–95.

———1961, Techniques for mapping hydrochemical facies: U.S. Geol. Survey Prof. Paper 424–D, p. D380–D382.

Doering, J. A., 1958, Citronelle age problem: Am. Assoc. Petroleum Geologists Bull., v. 42, no. 4, p. 764–786.

Morgan, C. O., 1961, Ground-water conditions in the Baton Rouge area, 1954–59, with special reference to increased pumpage; Louisiana Dept. Conserv., Geol. Survey and Louisiana Dept. Pub. Works, Water Resources Bull. 2, 78 p.

Rollo, J. R., 1960, Ground water in Louisiana: Louisiana Dept. Conserv., Geol. Survey and Louisiana Dept. Public Works, Water Resources Bull. 1, 84 p.

Stringfield, V. T., and LaMoreaux, P. E., 1957, Age of Citronelle Formation in Gulf Coastal Plain: Am. Assoc. Petroleum Geologists Bull., v. 41, no. 4, p. 742–746.

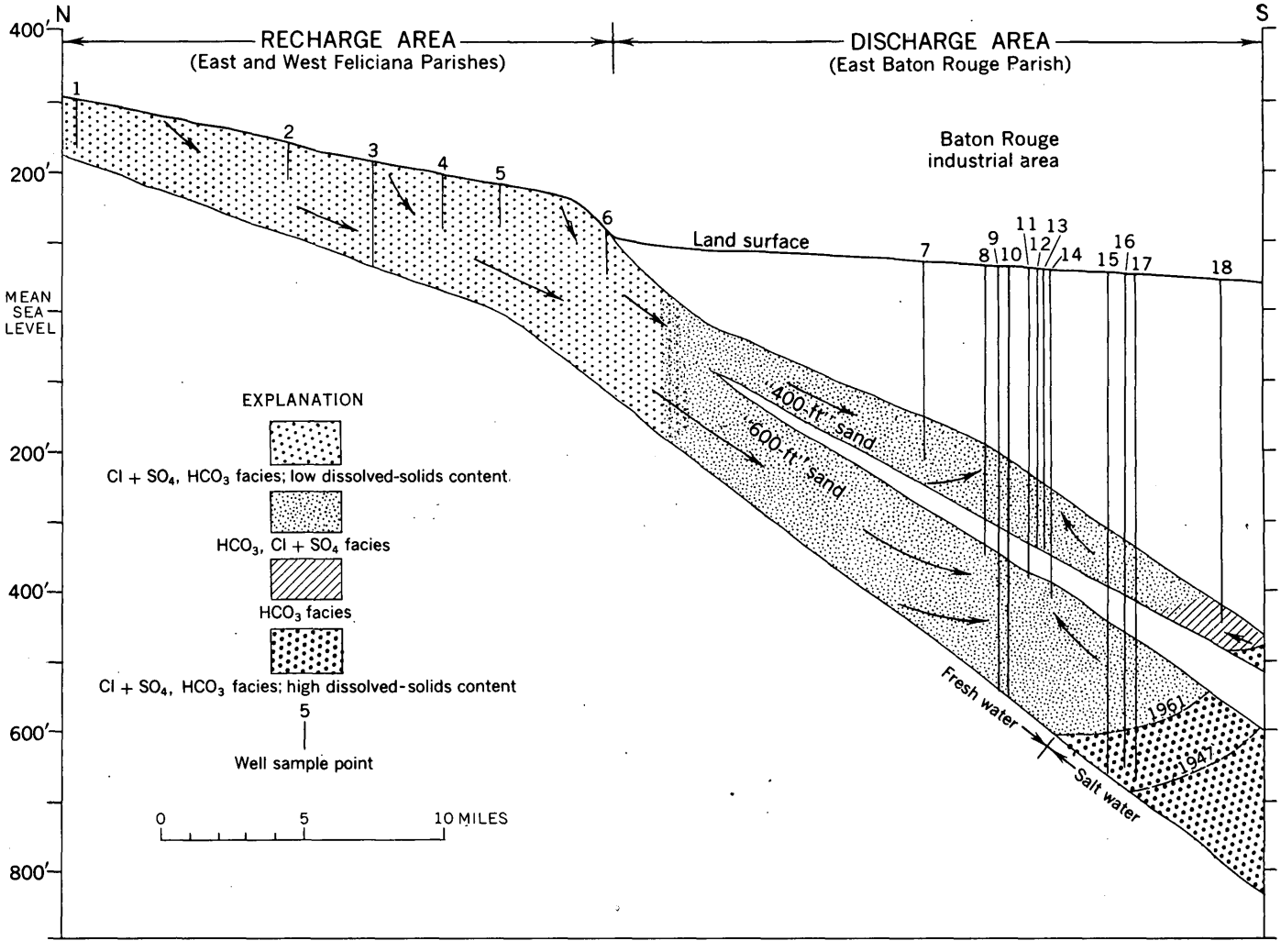

FIGURE 50.2.—Generalized north-south geologic section showing movement of ground water, areas sampled, and distribution of anion hydrochemical facies in the "400-foot" and "600-foot sands of the Baton Rouge area. Dashed lines show migration of the fresh water–salt water interface.

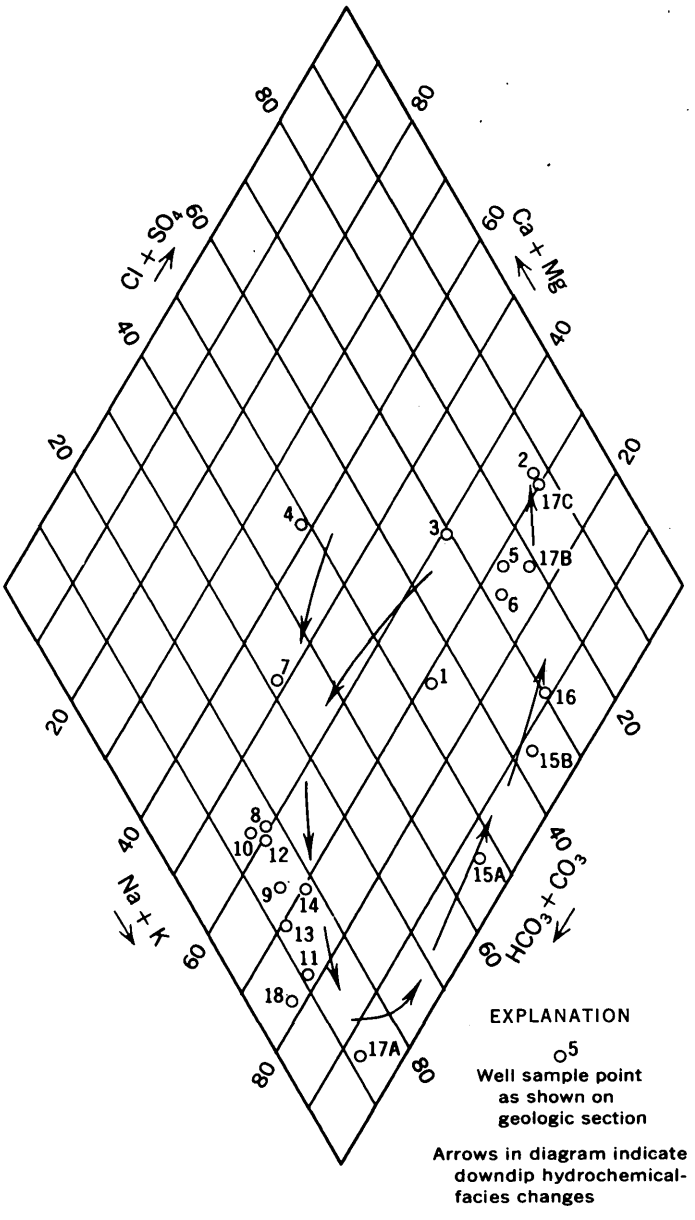

FIGURE 50.3.—Water-analysis diagram showing hydrochemical facies, in percent of total equivalents per million, in the "400-foot" and "600-foot" sands of the Baton Rouge area.

629660—62——9

51. CATION HYDROCHEMICAL FACIES OF GROUND WATER IN THE ENGLISHTOWN FORMATION, NEW JERSEY

By PAUL R. SEABER, Trenton, N.J.

Work done in cooperation with the New Jersey Division of Water Policy and Supply

The sandy part of the Englishtown Formation of Late Cretaceous age has been utilized as an aquifer throughout approximately 1,100 square miles of the Atlantic Coastal Plain of New Jersey. The greatest ground-water development from this aquifer is in the shore communities of Monmouth and Ocean Counties.

The chemical character of the water in the Englishtown Formation indicates a relation between topography of the coastal plain, the lithology, and ground-water movement (fig. 51.1). The concept of hydrochemical facies has been used by Back (1960) to demonstrate a regional relation between these same factors in the Atlantic Coastal Plain.

A hydrochemical facies may be thought of as a diagnostic chemical aspect of ground water indicative of the relative proportions of the anions or cations. Variations in the relative proportions of Ca, Mg, Na, and K reflect environmental effects and can be used as diagnostic indicators of hydrochemical relations. Concentrations of K and Mg do not vary significantly in the Englishtown, but they are included to conform to the terminology previously used by Back (1961). HCO_3 is the predominant anion of the ground water in the Englishtown Formation; even in the coastal area there is no indication of a high Cl content. The dissolved-solids content (residue on evaporation) of the ground water ranges from 14 to 243 ppm.

The topographic highs of the coastal plain lie 5 to 10 miles southeast of the outcrop of the Englishtown Formation (fig. 51.1*A*). The northern and southern topographic highs are separated by a topographic low.

The Englishtown Formation, where exposed in the northeast part of the area, is a conspicuous unit of dominantly light-colored well-sorted medium-grained sand that is slightly micaceous and sparingly glauconitic and lignitic. The unit contains a few laminae and discontinuous lenses of clay and silt and some fine gravel. The formation thins southwestward along the strike, but appears to thicken downdip. Minard and Owens (1960) suggest that most of the pre-Quaternary formations in the coastal plain of New Jersey have similar depositional characteristics. The sandy part of the formation forms a wedge that thins southwestward (fig. 51.1*B*). The sandy unit becomes increasingly clayey and silty and the sand becomes finer grained southwestward along the strike as well as southeastward downdip. In the southern part of the Atlantic Coastal Plain of New Jersey, the Englishtown Formation is composed entirely of clay and silt.

The formation appears to be of continental and deltaic origin in the northeastern part of the outcrop area, and of marine origin in the south. Groot and Glass (1960) reported that kaolinite is the predominant clay mineral in the nonmarine sediments and that montmorillonite is predominant in the marine deposits of the coastal plain.

Recharge to the Englishtown occurs mostly by leakage from overlying sediments. The piezometric highs correspond to topographic highs (fig. 51.1*C*), which are separated by a piezometric low that corresponds to the topographic low in the same area. The outcrop functions as a natural-discharge area throughout its extent. Increased pumpage along the Atlantic coast has resulted in interception of most of the flow that formerly discharged through the submarine outcrop northeast of Sandy Hook Bay. A discharge area in the southern part of the system has not been defined, but ground water may move upward into the overlying formations.

The cation hydrochemical facies characterized by water of more than 90 percent Ca+Mg (in equivalents per million) forms a belt that corresponds to the topographic highs and the piezometric highs (fig. 51.1*D*). This facies results from solution of calcareous materials in the overlying formations by ground water, which enters the Englishtown Formation in the areas of the piezometric highs. Both updip and downdip from this belt the Ca content is lower, updip the Na content is about the same. This presumably is due chiefly to infiltration of water that contains less Ca and about an equal amount of Na. Downdip to the southeast, the water contains more than 90 percent Na+K. This cation hydrochemical facies results from ion exchange in which Ca of the water is absorbed by montmorillonite, and Na of the montmorillonite is taken into solution. The water contains more Na than could be released by exchange with the amount of Ca in solution in waters coming from areas of higher head. This indicates another source of Ca, presumably from solution of calcareous fossils at depth in the formation. The high proportion of Na in the ground water downdip from the recharge area suggests the presence of sodium mont-

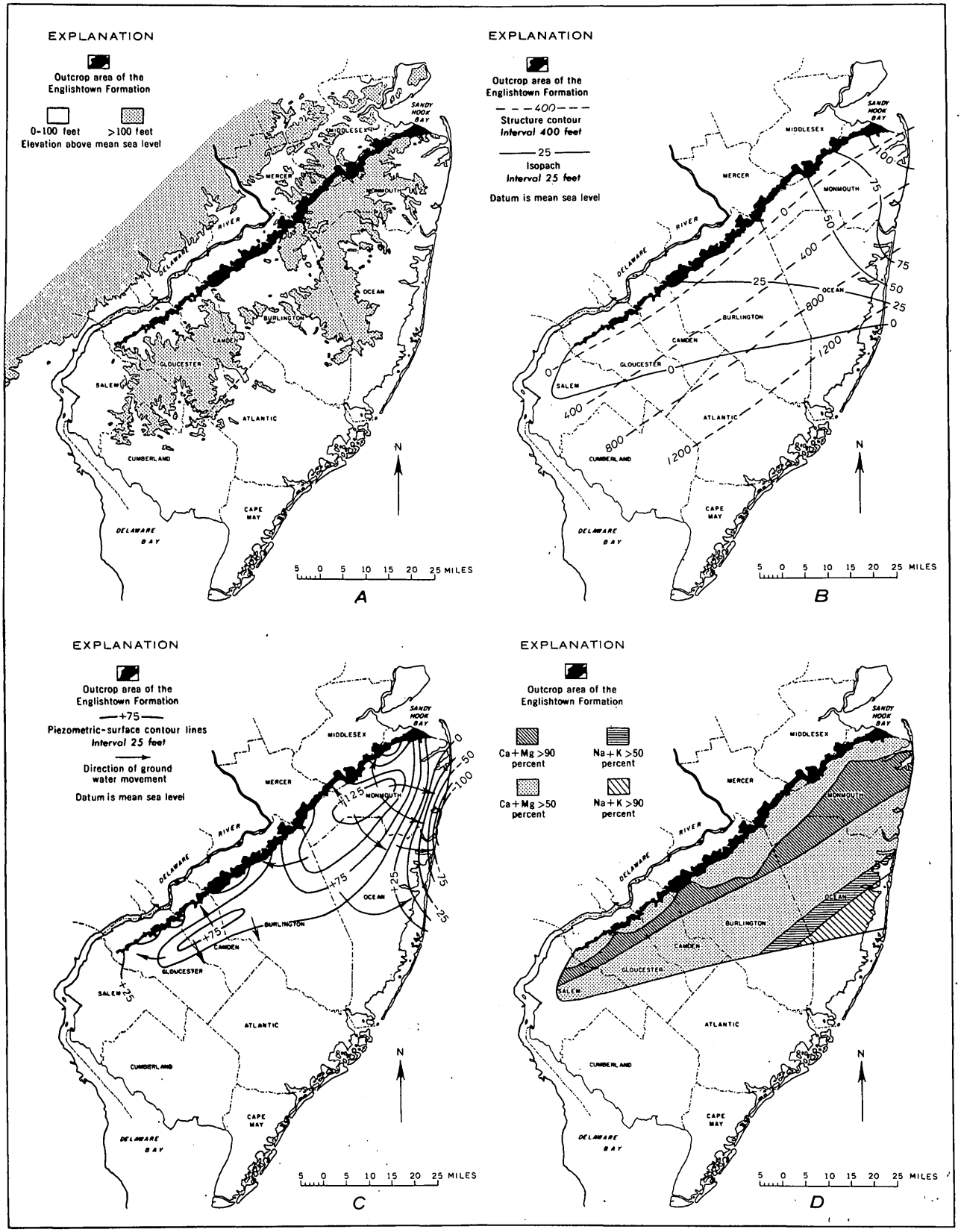

FIGURE 51.1.—Maps showing the relation between topography, geology, ground-water movement, and cation hydrochemical facies in the Englishtown Formation. *A*, Generalized topography of the coastal plain of New Jersey. *B*, Structure contours of the top of the Englishtown Formation and isopachs of the sandy part of the formation. *C*, Generalized ground-water movement in the sandy part of the formation in December 1958. *D*, Hydrochemical facies showing relative proportions of cations in the ground water of the sandy part of the formation.

morillonitic clay in the subsurface, which in turn substantiates the supposed marine origin of the Englishtown Formation in that area.

The zone separating the cation facies containing more than 50 percent Ca+Mg from that containing more than 50 percent Na+K is considered to be an "ion-exchange front." This front is presumably moving slowly east-southeastward at an indefinite rate in the direction of the movement of the water within the formation. The present alinement and position of the front is governed more by the piezometric surface that existed prior to pumping from the Englishtown Formation than by the present piezometric surface.

REFERENCES

Back, William, 1960, Origin of hydrochemical facies of groundwater in the Atlantic Coastal Plain: Internat. Geol. Cong., 21st, Copenhagen, 1960, Proc., pt. 1, p. 87–95.

———1961, Techniques for mapping hydrochemical facies; Art. 423 *in* U.S. Geol. Survey Prof. Paper 424–D, p. D380–D382.

Groot, J. J., and Glass, H. D., 1960, Some aspects of the mineralogy of the Atlantic Coastal Plain, *in* Clay Conf., 7th, Washington, D.C., 1958: New York, Pergamon Press, p. 271–284.

Minard, J. P., and Owens, J. P., 1960, Differential subsidence of the southern part of New Jersey coastal plain since early Late Cretaceous time: Art. 82 *in* U.S. Geol. Survey Prof. Paper 400–B, p. B184–B186.

52. USE OF Na/Cl RATIOS TO DISTINGUISH OIL-FIELD FROM SALT-SPRING BRINES IN WESTERN OKLAHOMA

By A. R. Leonard and P. E. Ward, Oklahoma City, Okla.

Work done in cooperation with the U.S. Public Health Service

At several places in western Oklahoma and nearby Kansas and Texas highly mineralized ground water issues from natural salt springs. The chloride content of water from individual springs is as much as 190,000 ppm (parts per million) and in nearby streams at times reaches several thousand parts per million. Some brine pumped from oil wells in the area also may find its way into surface streams. The oil-field brines have concentrations of chloride and dissolved solids in the same ranges as the natural brines. Neither chloride nor dissolved solids content can be used to distinguish brine from the two sources nor to identify the source of mineralized water at many places in surface streams in concentrations of only a few thousand parts per million.

During a recent study, it was found that the two types of brines could be distinguished on the basis of their Na/Cl ratios. The procedure was suggested to the junior author by chemists of the Quality of Water Branch, U.S. Geological Survey. On figure 52.1 the ratio of sodium to chloride (both in parts per million) has been plotted against the concentration of chloride for selected oil-field and salt-spring brines. Brines from several natural salt springs are remarkably similar in chemical quality, although they range in chloride concentration from a few thousand to nearly 200,000 ppm. The Na/Cl ratio for these waters is uniformly within 1 or 2 percent of 64/100. This suggests a nearly pure halite source for the sodium and chloride because the combining ratio of sodium and chloride in parts per million is 65/100, and halite is virtually pure sodium chloride.

In the same area, oil-field brines consistently have Na/Cl ratios of less than 60/100, but the ratio decreases as the chloride content increases (fig. 52.1). The average ratio for about 30 oil-field brines plotted was about 50/100. In the oil-field brines the excess of chloride over sodium evidently results from other compounds of chloride, for example, calcium or magnesium chloride, which are not present in either the halite deposits or the water from the natural salt springs.

On figure 52.1 analyses of water from several rivers in Oklahoma have been plotted to demonstrate use of the ratio for identifying the source of chloride in the water. Analyses are from published reports of the Geological Survey (Dover, 1959; Pate and others, 1961). Analyses 1 to 4 are of water samples collected from the Little River, near Sasakwa, Seminole County, Okla. Samples were collected during 1956 when the flow was low and the mineral content was high. The Na/Cl ratio ranged from about 47/100 to 50/100, indicating

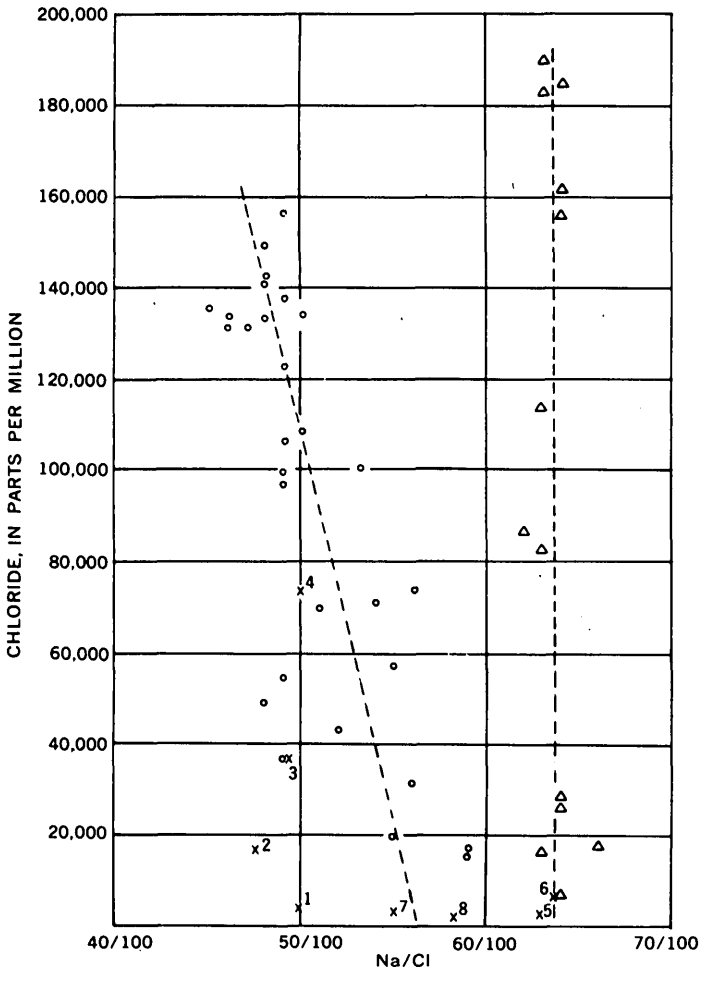

FIGURE 52.1.—Comparison of Na/Cl ratios for oil-field and natural-spring brines in western Oklahoma and southwestern Kansas. Analyses of oil-field brines (Wright, 1957) are represented by circles, natural-spring waters by triangles, and analyses of river water by ×'s. Superscripts are explained in text.

that the source of chloride in the water was oil-field brine. Large quantities of brine are discharged into this stream as it passes through oil fields a short distance upstream from the sampling station.

Analyses 5 and 6 are of water collected from the Cimarron River at the Perkins sampling station in Payne County, Okla., in December 1955 and February 1956, respectively. Both samples represent low flow having a high mineral content. The Na/Cl ratios are higher than 60/100 because the source of most of the chloride is natural brine emerging from salt springs and salt plains upstream.

Analyses 7 and 8 are of water samples collected from the Arkansas River near Tulsa, Okla., in October 1955 and September 1956. They were collected at low flow when the mineral content was high for this station. The chloride in the water is from both oil-field and natural sources; accordingly the analyses plot between numbers 1 and 5 on figure 52.1.

The Na/Cl ratio is a useful tool for identifying the source of chloride in stream waters in the western Oklahoma area. If the ratio is greater than 60/100, the chloride is most likely derived from natural halite deposits through water emerging from salt springs. If the ratio is near or less than 50/100, the chloride source is most likely connate water pumped from oil wells.

REFERENCES

Dover, T. B., 1959, Chemical character of surface waters of Oklahoma 1955–56: Oklahoma Water Resources Board Bull. 16, 144 p.

Pate, C. O., Murphy, J. J., and Orth, R. P., 1961, Chemical character of the surface waters of Oklahoma, 1956–57: Oklahoma Water Resources Board Bull. 18, 140 p.

Wright, Jack, and others, 1957, Analyses of brines from oil-productive formations in Oklahoma: U.S. Bur. Mines Rept. Inv. 5326, 71 p.

53. RELATION BETWEEN ALUMINUM CONTENT AND pH OF WATER, BEAVER CREEK STRIP-MINING AREA, KENTUCKY

By GEORGE W. WHETSTONE and JOHN J. MUSSER, Columbus, Ohio

Prepared in cooperation with the Kentucky Geological Survey

Water-quality studies in the Beaver Creek basin, Kentucky, indicate that acid mine water is especially significant in transporting aluminum in solution.

Aluminum is one of the most abundant metallic elements in the earth's crust, occurring principally as a silicate in clays and feldspars and as the commercial

ore bauxite, an impure hydrate oxide. The element is amphoteric in behavior and can be in solution either as a cation or as a part of a complex anion, as illustrated in the following equation:

$$Al^{+3}+3OH^{-1}\rightleftharpoons\left\{\begin{matrix}Al(OH)_3\\H_3AlO_3\end{matrix}\right\}AlO_2^{-1}+H^{+1}+H_2O$$

Aluminum hydroxide is only slightly dissociated and is nearly insoluble in natural water, for which the pH generally ranges from 5.5 to slightly more than 8. The aluminum concentrations of natural water usually are less than 1 or 2 ppm (parts per million) and much of this probably is colloidal and undissociated. Dissociated aluminum as Al^{+3} occurs in amounts of more than 2 or 3 ppm only in solutions in which the pH is less than about 4. Aluminate ions (AlO_2^{-1}) are rarely found in natural water because, theoretically, they can be in solution in measurable amounts only at pH values of more than 9.

Natural surface water in the Beaver Creek basin is poorly buffered. A marked reduction in the pH of the water is caused by small amounts of sulfuric acid derived from the oxidation of pyrite and from hydrolysis involving sulfate, in the spoil banks of strip mines.

Median values of pH and the range of aluminum concentrations are shown in the table below for two nonpolluted streams in the Beaver Creek basin—Helton Branch and West Fork Cane Branch—and for Cane Branch, which was polluted by acid mine waters.

In the Beaver Creek basin, surface water free of acid mine water generally has a pH ranging from 5.0 to 7.3 and an aluminum concentration of 0.4 ppm or less. Water in Cane Branch from January to June 1956, before the spoil bank was leveled, had a pH ranging from 4.0 to 6.8 and an aluminum concentration less than 5.0 ppm.

Median values of pH *and range of aluminum concentration in surface water in Beaver Creek Basin, Kentucky, January 1956 to September 1958*

Stream	pH	Aluminum (in parts per million)		
	Median	Maximum	Median	Minimum
West Fork Cane Branch	6.0	0.2	0.1	0.0
Helton Branch	6.7	.4	.1	.0
Cane Branch	3.2	85	5.5	.0

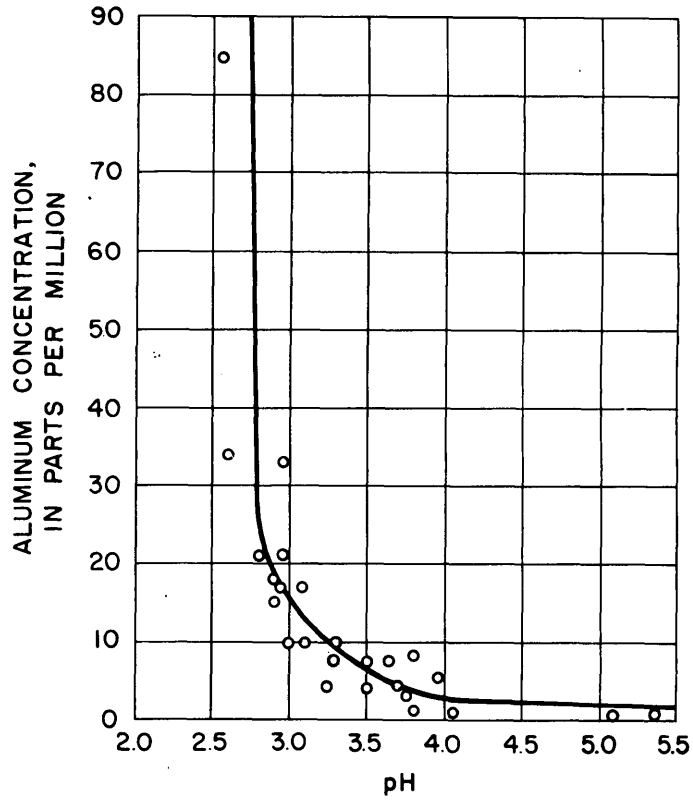

FIGURE 53.1—Solubility of aluminum as a function of pH in Cane Branch, 1956–58.

From June 1956 to September 1958, the pH of Cane Branch water generally was less than 4.15, and the aluminum concentration was greater than 5.0 ppm (fig. 53.1). The maximum aluminum concentration was 85 ppm. Aluminum concentrations were highest for pH values less than 3.0.

Aluminum concentrations in the ground water in the Beaver Creek area followed a pattern similar to that of the surface water. Water from coal test holes and springs had pH values greater than 5.0 and contained less than 0.2 ppm of aluminum. Water within the spoil bank frequently had pH values less than 2.8 and had as much as 46 ppm of aluminum. Water from pools on the spoil bank had a pH less than 3 and an aluminum concentration up to 50 ppm.

54. CHEMICAL QUALITY OF SURFACE WATERS IN THE BRAZOS RIVER BASIN, TEXAS

By Burdge Irelan and H. B. Mendieta, Austin, Tex.

Prepared in cooperation with the Brazos River Authority and the Texas Water Commission

The Brazos River basin (fig. 54.1) occupies 15 percent of the land area of Texas and extends from the High Plains, where altitudes reach a maximum of 4,200 feet and precipitation ranges from 15 to 20 inches a year, to the Gulf coast, where the annual precipitation ranges from 45 to 50 inches. The average annual water discharge of the Brazos River at Richmond is 5,288,000 acre-feet for 39 years of record and represents the discharge of about 99 percent of the Brazos River basin.

The Brazos River has not been as greatly developed for municipal and industrial use as the Trinity River to the north and the Colorado River to the south. Major upstream reservoirs on both the Trinity and Colorado Rivers store water of good quality. In contrast, the large reservoirs on the upper Brazos River were designed primarily for power production and flood control, and they store water that is too saline for municipal and most industrial uses. However, reservoirs on a number of upstream tributaries provide water that is suitable for municipal use.

A study of quality-of-water data for the Brazos River basin shows that salinity was a problem as early as 1906 (Clarke, 1924, p. 126). The quality of the

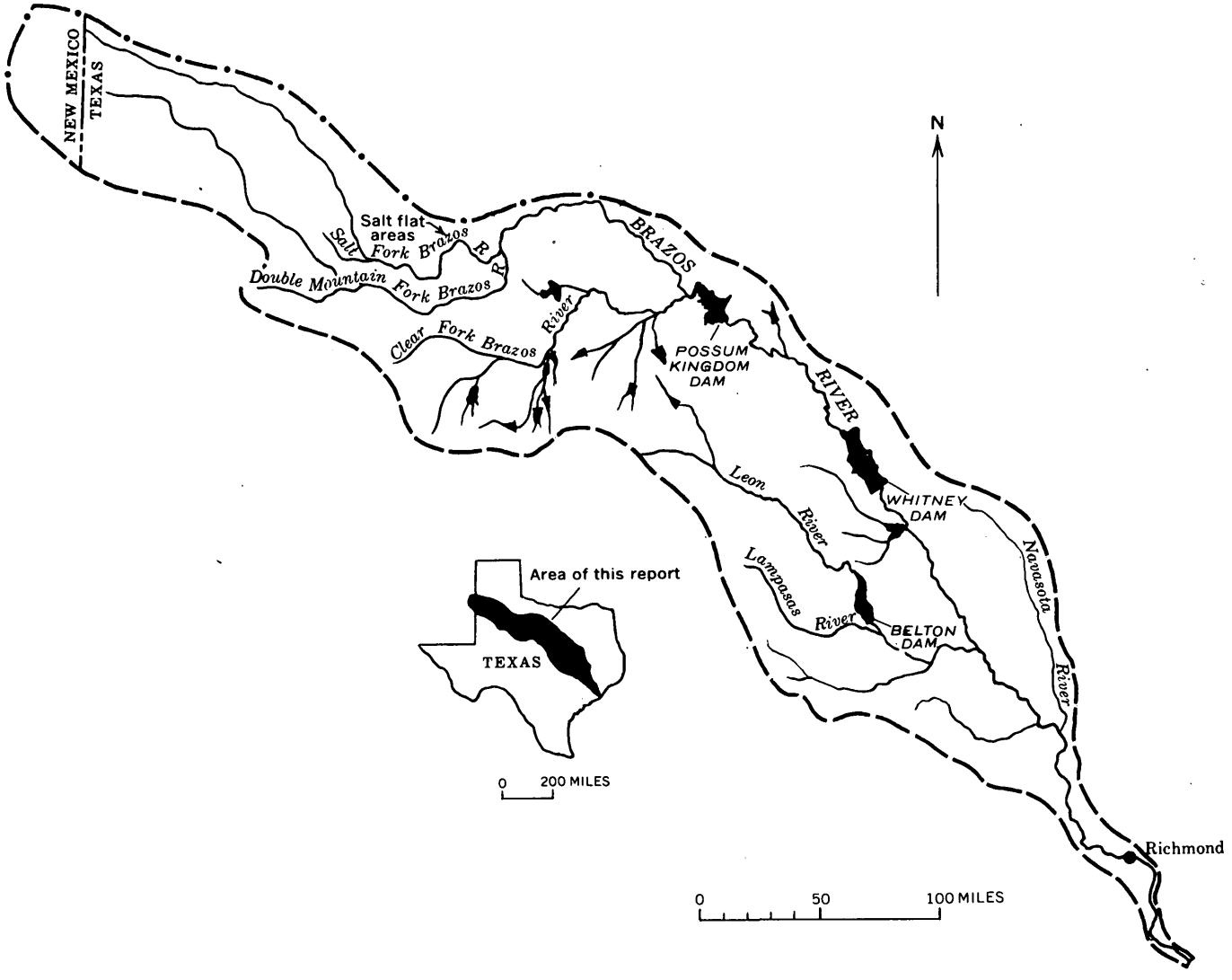

FIGURE 54.1.—Map of the Brazos River basin showing principal tributaries and hydrologic features.

surface waters of most of the tributaries of the Brazos River ranges from excellent to good, in the general range from 250 to 500 ppm (parts per million) of dissolved solids, but most of the water in the main stem and two of its principal tributaries, the Salt Fork and the Double Mountain Fork Brazos Rivers, is saline (more than 1,000 ppm of dissolved solids) (Winslow and Kister, 1956, p. 45, 93–94).

The salt load of the Brazos River is derived from basin-wide solution of the products of rock weathering and decomposition, undetermined but apparently large amounts of oil-field brines, and natural brines and seeps. The flow from springs and seeps, although relatively small, contributes large quantities of salts to the stream system, for saturated brines have as much as 300,000 ppm of dissolved solids. About 50 percent of the annual salt load of the Brazos River is caused by inflow of brines from springs and seeps in the area above Possum Kingdom Dam, which forms about 52 percent of the total drainage area of the basin but contributes only about 17 percent of the water discharge.

Water of the Salt Fork Brazos River is too saline for most uses. Much of the runoff of the Salt Fork is from areas underlain by rocks of Permian age. The surface runoff from these areas contains large amounts of dissolved solids, and even larger amounts are contributed by the salt springs that rise in the barren salt flats of the drainage basins of Croton and Salt Croton Creeks. The average load of chloride in the base flow from the springs in the Salt Croton Creek basin was computed to be about 400 tons per day, about 40 percent of the average daily chloride load of the Brazos River at Possum Kingdom Dam.

The water of the Double Mountain Fork is less saline than that of the Salt Fork and probably could be used as an irrigation supply but not as a municipal or industrial supply. The quality of water of the Clear Fork Brazos River generally is good but would be better if brine pollution from oil fields were prevented. Records for the Lampasas, the Leon, and the Navasota Rivers indicate that the water of these streams is of excellent quality, but more data are needed to determine the variations in chemical quality. The quality of the water in other tributaries in the lower basin is inferred to be good from the results of miscellaneous sampling and form the types of rocks that underlie the basins.

The difference in density of inflow into Possum Kingdom and Whitney Reservoirs tends to cause density stratification. Samples collected in 1956 at Whitney Reservoir show that the chloride concentration at the bottom of the reservoir was about twice that at the surface. In June 1957 the dissolved-solids content of the water at the bottom of Possum Kingdom Reservoir was almost double that of the water released through the spillway. The water on the bottom remained saline even though the flood discharge during the previous month was more than twice the reservoir capacity.

Water passing the sampling station on the Brazos River at Richmond is a constantly changing mixture of water from the entire basin. In some years, releases from Possum Kingdom and Whitney Reservoirs are a large part of the flow at Richmond. In other years, more than half the flow enters the river downstream from Whitney. The different sources of flow result in a marked variability of annual weighted-average and mean daily dissolved-solids loads. Although the mean daily loads generally are greater in years of high flow than in years of low flow, the relation between salt-load discharge is irregular because of the release of saline water from Possum Kingdom and Whitney Reservoirs. A comparison of the concentrations in the Brazos River at Richmond and at Whitney Reservoir indicates that inflow below Whitney Reservoir dilutes the water of the Brazos River.

For 12 of the 14 years of record, the weighted-average dissolved-solids content of the Brazos River at Richmond was less than the recommended maximum (500 ppm) of the U.S. Public Health Service (1961), and was never more than 1,000 ppm.

If pollution from oil fields is controlled, the water of the major tributaries of the Brazos River, except the Double Mountain Fork and the Salt Fork, may be used by municipalities and industries. Water of the Double Mountain Fork may be used for irrigation, but the water of the Salt Fork cannot be used for any purpose, except perhaps for oil-field injection, until the brine discharge from springs and seeps is prevented from entering the stream. Injection of water from salt springs into deep rock strata or impoundment and evaporation are possible remedial measures.

The quality of water during low flows in the lower main stem can be improved even if the saline contributions from upstream continue. Increased conservation storage in the lower basin would permit the retention of the better quality waters for dilution of the saline water from the upper reaches.

REFERENCES

Ambursen Engineering Corp., 1956, Combined report on investigations directed toward the improvement of the Brazos River water: Brazos River Authority.

Clarke, F. W., 1924, The composition of the river and lake waters of the United States: U.S. Geol. Survey Prof. Paper 135, 199 p.

U.S. Public Health Service, 1961, Report on the Advisory Committee on revisions of U.S. Public Health Service 1946 Drinking Water Standards: Am. Water Works Assoc. Jour., v. 53, no. 8, p. 935–945.

Winslow, A. G., and Kister, L. R., 1956, Saline-water resources of Texas: U.S. Geol. Survey Water-Supply Paper 1365, 105 p.

55. CHEMICAL QUALITY OF GROUND WATER IN ST. THOMAS, VIRGIN ISLANDS

By I. G. Grossman, San Juan, Puerto Rico

Work done in cooperation with the Government of the Virgin Islands

The Virgin Islands of the United States consist of about 80 small islands approximately 50 miles east of Puerto Rico and about 1,000 miles southeast of Florida (fig. 55.1). St. Thomas, the second largest of the islands, is only about 1 to 3 miles wide and 13 miles long. Because of its excellent harbor, St. Thomas early assumed military and commercial importance, becoming the most populous island and the site of the capital, Charlotte Amalie, but its full potentialities have never been realized because of a chronic water shortage.

The island is very hilly and has a central ridge that parallels its long axis and rises to a maximum altitude of 1,556 feet. The hills are rocky and the colluvial and other unconsolidated materials are generally thin. A small but significant deposit of alluvium extends along Turpentine Run, the only stream having a perennial reach, in the eastern part of the island. The annual precipitation is comparatively high, averaging about 46 inches, but the tropical oceanic climate, with a mean annual temperature of about 80°F, and the small range in mean monthly temperature permit a year-round growing season which, coupled with the steady blowing of the northeasterly trade winds, results in high evapotranspiration losses. Moreover, the steep, rocky slopes facilitate rapid runoff at the expense of ground-water recharge.

The traditional source of potable water has been rain caught on "catchments," consisting of paved hillsides leading to storage tanks. Supplemental water supplies that are more highly mineralized are obtained from shallow dug wells and from a very few springs. Charlotte Amalie employs a dual water supply, as salt water is used for firefighting and flushing of streets. In recent years, the spiraling demand for water sparked by the influx of tourists and new residents resulted in a critical situation that was met only by shipping in additional water by barge from Puerto Rico at a rate that exceeded 1 million gallons per week in 1960. A distillation unit to convert sea water to fresh water, having a capacity of 250,000 gallons per day, was under construction in 1961.

Complete chemical analyses of water from 31 wells, including 20 sampled in an earlier study (Vaughan and Kidwell, 1920) and 11 sampled recently (Grossman, 1959), permit a delineation of the chemical quality of ground water from the shallow deposits. The wells were dug to depths ranging from 9 to 50 feet and averaging about 18 feet. The only drilled well on St. Thomas is situated northeast of the hospital in the northern part of Charlotte Amalie. It is 216 feet deep, but all of its very small supply was reportedly obtained

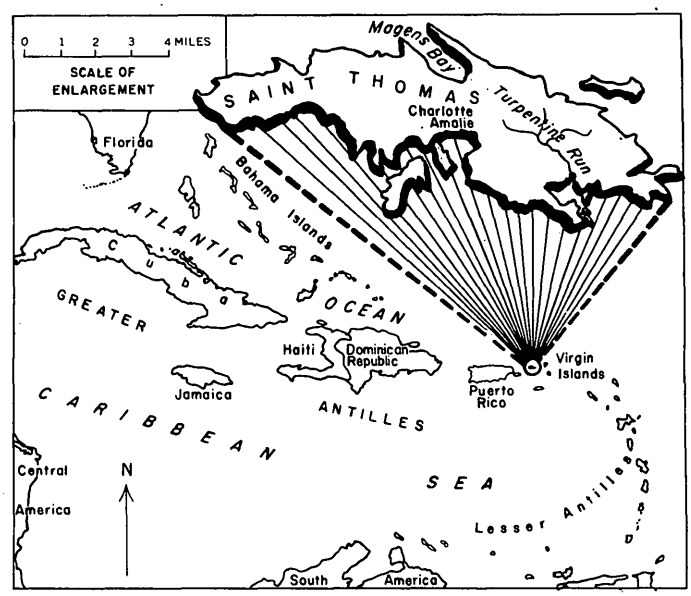

FIGURE 55.1.—Map of St. Thomas, V.I., and its geographic setting.

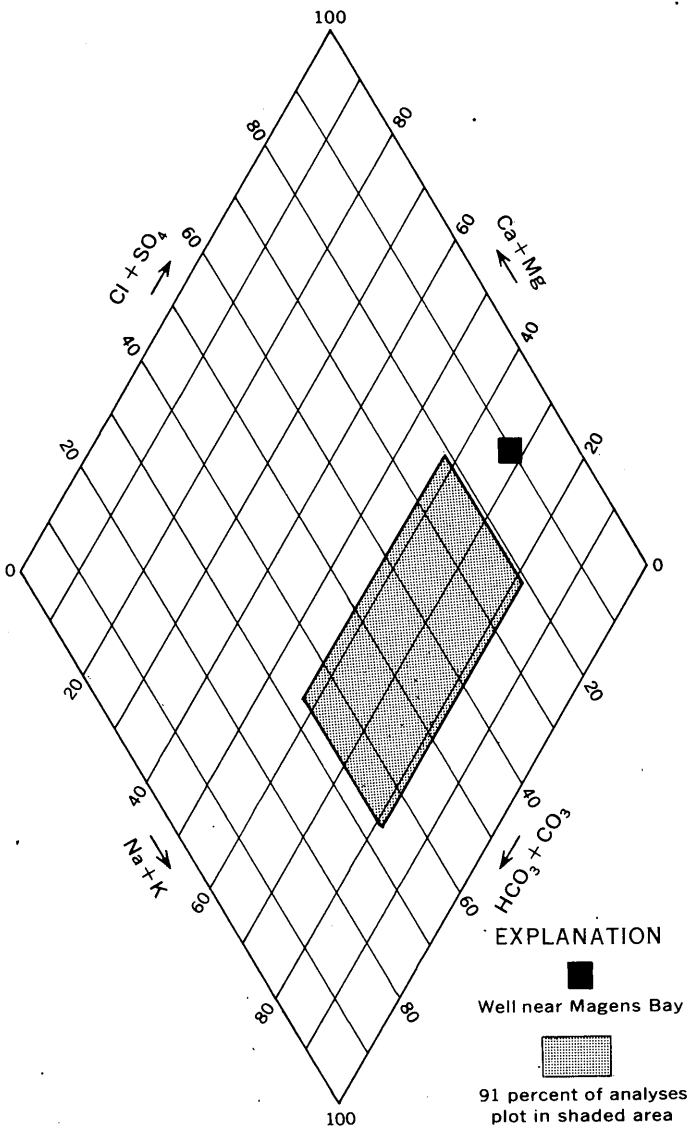

FIGURE 55.2.—Chemical classification of water from shallow wells in St. Thomas, in percent of total equivalents per million.

at a depth of 30 feet from clayey "detritus" overlying the bedrock. Hence its chemical quality is more likely to reflect that of water from the unconsolidated deposits than from the bedrock. This well was completely covered over when revisited in 1958.

Ground water from the unconsolidated deposits commonly had a high mineral content; the average dissolved-solids content in 33 samples was 1,650 ppm (parts per million). The lowest dissolved-solids content was 838 ppm; only 3 samples of the 33 contained less than 1,000 ppm of dissolved solids. Two of the wells sampled by Vaughan were resampled in 1958. After a lapse of about 40 years, the dissolved-solids content in one remained about the same but that in the second had declined from 1,320 to 989 ppm.

The proportions of the dissolved constituents in local ground water are influenced significantly by the geology, the degree of mixing with salt water, and the lingering urban pollution. The island is made up largely of volcanic rocks of probable Cretaceous age, although there are some relatively thin beds of limestone in the northeast. The overall poverty of potash in all the bedrock is striking (Donnelly, 1959). The potassium content of local water likewise was low; the average in water from 10 wells for which separate determinations are available was only 6.5 ppm, with a range of from 4.0 to 10 ppm. By contrast, the sodium content in these 10 samples averaged 409 ppm and ranged from 275 to 915 ppm. Although some of this high sodium content reflected the relatively high sodium content of the volcanic bedrock from which most of the colluvial and alluvial cover is derived, some of it probably resulted from mixing with airborne salt and with sea water in shoreline areas.

The maximum sodium concentration recorded in the study was that in brackish water in a well on the north coast about 2,000 feet southeast of Magens Bay at an altitude of about 15 feet (fig. 55.1). Water from this well had a dissolved-solids content of 5,800 ppm and a chloride concentration of 2,500 ppm (fig. 55.2). The chloride content of the 32 other samples ranged from 118 to 979 ppm and averaged 400 ppm. Some wells produced salty or brackish water as a result of salt-water intrusion induced by overpumping. In and near Charlotte Amalie, ground water had been contaminated locally by salt water that had leaked from fire mains and hydrants. Field tests made in 1945 on water from 16 publicly owned wells in Charlotte Amalie showed an average chloride content of about 1,100 ppm (McGuinness, 1946, p. 24–26).

As indicated on the geochemical graph (fig. 55.2) sodium is the predominant cation in the ground water. In some water, chloride is the predominant anion, and in other, bicarbonate or nitrate predominates.

In Charlotte Amalie, chloride was not the only objectionable anion. The nitrate content in 16 publicly owned wells sampled in 1919 averaged 217 ppm and ranged from 9.5 to 419 ppm. By contrast, the nitrate content of 3 rural wells sampled at the same time averaged only 14 ppm. Ten rural wells sampled in 1958 showed an average nitrate concentration of only 11 ppm, with a range of 0 to 44 ppm. Moreover, 8 of the 10 samples contained less than 5.0 ppm of nitrate. Sanitary facilities were primitive in 1919, the year in which appropriations for sanitary sewers were first passed, and the high nitrate content of water from the public wells was attributed to human pollution (Vaughan and Kidwell, 1920, p. 25). As late as 1943, 247 open-pit

privies were still being used, most of them in Charlotte Amalie. Most of the wells in the city had been sealed or were not in use when revisited in 1957.

Although improved sanitation might result in improvement of the quality of water from wells in the city, the possibility of substantial additional recharge is limited by the small size of the tributary drainage basin and the widespread use of rainfall from roofs and other catchments. The most promising source of ground water of acceptable chemical quality appears to be in Turpentine Run basin, where 1 well of 9 yielded water containing less than 1,000 ppm of dissolved solids. Of the remaining 8, 6 had water containing less than 1,300 ppm. Water from these six wells could be mixed with rainwater or other relatively fresh water for use without additional treatment, but the preference of Virgin Islanders for the relatively pure rainwater they are accustomed to might necessitate additional treatment.

REFERENCES

Donnelly, T. W., 1959, The geology of St. Thomas and St. John, V. I.: Caribbean Geol. Conf., 2d, Puerto Rico, 1959, Trans., p. 153. [1960]

Grossman, I. G., 1959, Ground-water data from St. Thomas, V.I.: U.S. Geol. Survey open-file report, 35 p.

McGuinness, C. L., 1946, Ground-water reconnaissance of St. John, Virgin Islands, with a supplement on St. Thomas: U.S. Geol. Survey open-file report, 27 p.

Vaughan, T. W., and Kidwell, C. H., 1920, The ground-water resources of the West Indian Islands, St. John, St. Thomas, Culebra, Vieques, and the eastern end of Puerto Rico: U.S. Geol. Survey open-file report, 53 p.

TOPOGRAPHIC STUDIES

PHOTOGRAMMETRY

56. A TEST OF THE DIRECT GEODETIC RESTRAINT METHOD OF ANALYTICAL AEROTRIANGULATION

By Robert C. Eller and Morris L. McKenzie, Washington, D.C.

The direct geodetic restraint method of analytical aerotriangulation was first presented by Dodge in 1957 [1] and, after revisions in the geometrical approach, by Dodge, Handwerker, and Eller.[2] Briefly, it is a simultaneous block solution for horizontal and vertical positions based on a method developed by Herget (1956). Input data for the method consist of (1) photographic coordinates for ground control and model pass points, (2) geographic coordinates and elevations for ground control, and (3) estimates of camera position and orientation for each exposure station. The six parameters for each exposure station are improved through iterative solutions of linear equations involving adjustments by least squares. When stable conditions have been reached, geographic coordinates and elevations for all points are computed.

A prototype computer program for investigative use has been prepared with a problem-solving capability limited to nine photographs. Tests both with fictitious data by Dodge [3] and actual photographic and ground-control data demonstrate that the method has potential for producing ground-point positions to a degree of accuracy that satisfies standard mapping needs.

A recent actual-data test involved nine aerial photographs of the Dale, Ind., quadrangle (fig. 56.1). The flight height for the photography was 9,000 feet above mean ground and the camera's nominal focal length was 6 inches. The horizontal control consisted of 5 first- and second-order triangulation stations and 1 transit traverse station. All vertical control was established by standard U.S. Geological Survey supplemental control procedures.

The photocoordinates of the ground control and model pass points were measured on a Nistri TA–3 stereocomparator by the U.S. Army Engineer Geodesy,

[1] Dodge, H. F., 1957, Geometry of aerotriangulation: Cornell Univ., unpublished M.S. thesis.

[2] Dodge, H. F., Handwerker, D. S., and Eller, R. C., 1959, A geometrical foundation for aerotriangulation, Progress report 3, Analytical aerotriangulation research: U.S. Geological Survey, Topographic Division. (duplicated)

[3] Dodge, H. F., 1958, Results of initial tests of analytical aerotriangulation in the Geological Survey, Progress report 1, Analytical aerotriangulation research: U.S. Geological Survey, Topographic Division. (duplicated)

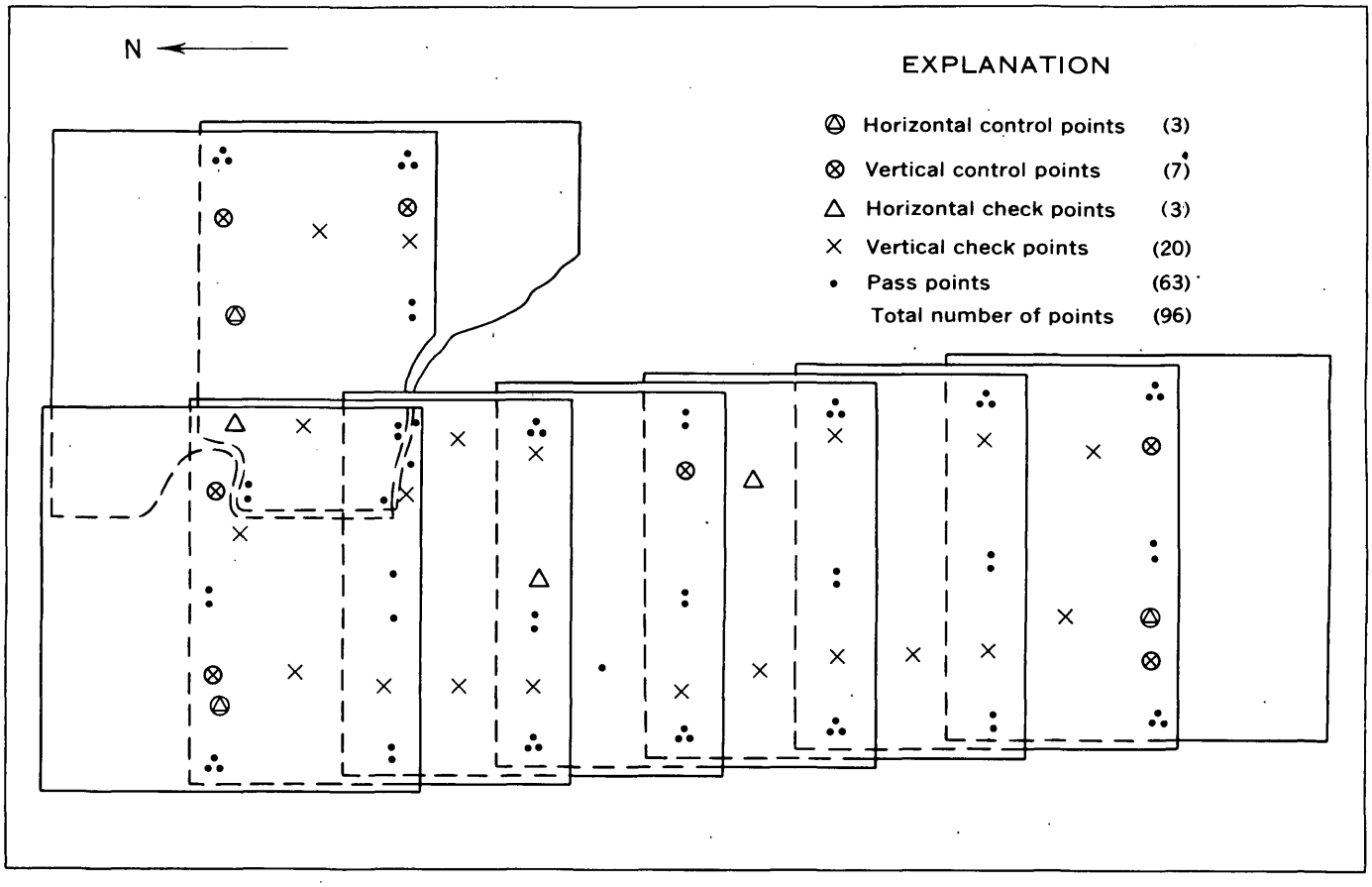

FIGURE 56.1.—Analytical aerotriangulation test, Dale, Ind.

Intelligence and Mapping Research and Development Agency. Three readings were made for each point and the average was accepted as the most probable value. Corrections for the systematic components of lens and film distortion and film flatness were computed manually and applied to all photocoordinates before starting the computer solution. None of the horizontal ground-control stations could be identified on the photographs, but ground detail near each station was tied to the station by transit-stadia methods. By measuring the photocoordinates on this ground-detail imagery, it was possible to compute the photocoordinates for the stations.

In the preliminary computer runs, a minimum control distribution was used in order to eliminate the influence of control on relative orientation and thus permit the detection and rejection of poorly transferred points. All control points except the minimum number used were treated as pass points. As a result of preliminary runs made first for individual strips and then for the combined strips, 3 pass points and 1 vertical control point were discarded. In addition, 4 pass points shown to be poorly transferred between strips were rejected as tie points but retained for model control on 1 strip.

To make the final run, it was not necessary to repeat the entire computer solution. Advantage was taken of the partial solution provided by the two-strip preliminary run. Control in the pattern shown in figure 56.1 was inserted and the computations were continued for two additional iterations. The final results are shown in the table below. It should be noted that the use of the term "root mean square error" in the table is not strictly valid in theory because of the small number of points considered; it is used here only to give an indication of the magnitude of the discrepancies. The vertical and horizontal errors are based both on the control points used in the solution and on the control points reserved as check points.

Summary of results, analytical aerotriangulation test, Dale, Ind.

	Root mean square(feet)	Maximum (feet)
Horizontal error	7. 93	11. 83
Vertical error	4. 53	11. 90
Within-model parallax	1. 54	10. 96
Model-to-model parallax	2. 66	7. 16
Strip-to-strip parallax	3. 37	4. 26

The photography used for this test was intended for the preparation of 1 : 24,000-scale standard topographic quadrangle maps. The accuracy standards for such maps require that 90 percent of all discrete points tested fall within 40 feet of true horizontal position and that 90 percent of all elevations tested be correct within one-half a contour interval (5 feet in this case). The attainment of these standard accuracies in the finished map requires that the photogrammetric control established by aerotriangulation be considerably more accurate than the finished map. The horizontal accuracy of the network of points determined in the test is considered to meet this requirement, but vertical accuracy needs improvement. More accuracy should result from the use of polyester base or similar aerial film, targeted horizontal and vertical control, and vertical control of greater accuracy.

REFERENCE

Herget, P. P., 1956, Computational extension of control along a photographed strip: Ohio State Univ. Research Found., Mapping and Charting Research Lab., Tech. Paper 201.

57. RESEARCH ACTIVITY WITH THE U–60 ORTHOPHOTOSCOPE

By Marvin B. Scher, Washington, D.C.

The function of an orthophotoscope is to convert conventional perspective photographs into uniform-scale photographs that portray all images in their correct orthographic positions. The value of a photograph upon which precise horizontal-distance measurements can be made without applying corrections for image displacements due to tilt and relief has long been appreciated. Such photographs simplify the problem faced by the geologist or engineer when he needs to record his scientific field observations in their correct orthographic positions. The orthophotomosaic is an accurate assembly of orthophotographs which can be substituted for a planimetric map. A mosaic of this sort often permits scientific field activity to proceed without the delay otherwise imposed by inadequate map coverage in an area of interest.

An orthophotoscope may be described as a photogrammetric restituting enlarger that magnifies the different images on a perspective photograph inversely as their scale. Fabrication of the U–60 orthophotoscope, the third in a series of such instruments developed during the past decade in the research laboratory of the Topographic Division, U.S. Geological Survey, was completed by the Property Maintenance Shop in Silver Spring, Md., early in 1960.

The design of the U–60 benefited from the experience gained in the development and use of the preceding orthophotoscopes. The structural design has been altered to accommodate the supporting bar for Kelsh-type projectors as well as the ellipsoidal-reflector type shown in figure 57.1. The flat film-supporting platform of the earlier instruments has been replaced with a 12-inch-diameter cylinder around which the blue-sensitive film is attached. The cylinder and its concentric light-tight outer envelope are alined with their longitudinal axis horizontal and parallel to the x direction of the instrument. The platen carriage containing the scanning aperture is mounted on a track that extends the entire 32-inch length of the outer drum. The entire assembly of the drums, platen carriage, and track can be raised or lowered as a unit by manual control. The emulsion of the film is exposed through the scanning aperture to small differential areas of the stereoscopic-model surface as the platen carriage moves along its track. Although the film is exposed to both the red and blue projected rays which create the anaglyphic model, only the blue rays have an actinic effect on the blue-sensitive film.

The direction of travel of the platen carriage is reversed upon completion of each successive scan. Two automatic, synchronized motions occur when the end of a scanning path is reached: The inner cylinder is rotated about its longitudinal axis and the assembly of the drums and platen carriage is translated in the y direction. The amount of cylinder rotation must be precisely controlled to place the unexposed section of film bordering upon the film area previously exposed into correct position under the path of the scanning aperture. The assembly translation must be such that the scanned area across the stereoscopic model will be contiguous with that of the previous scan. This modification permits the operator to have an improved view

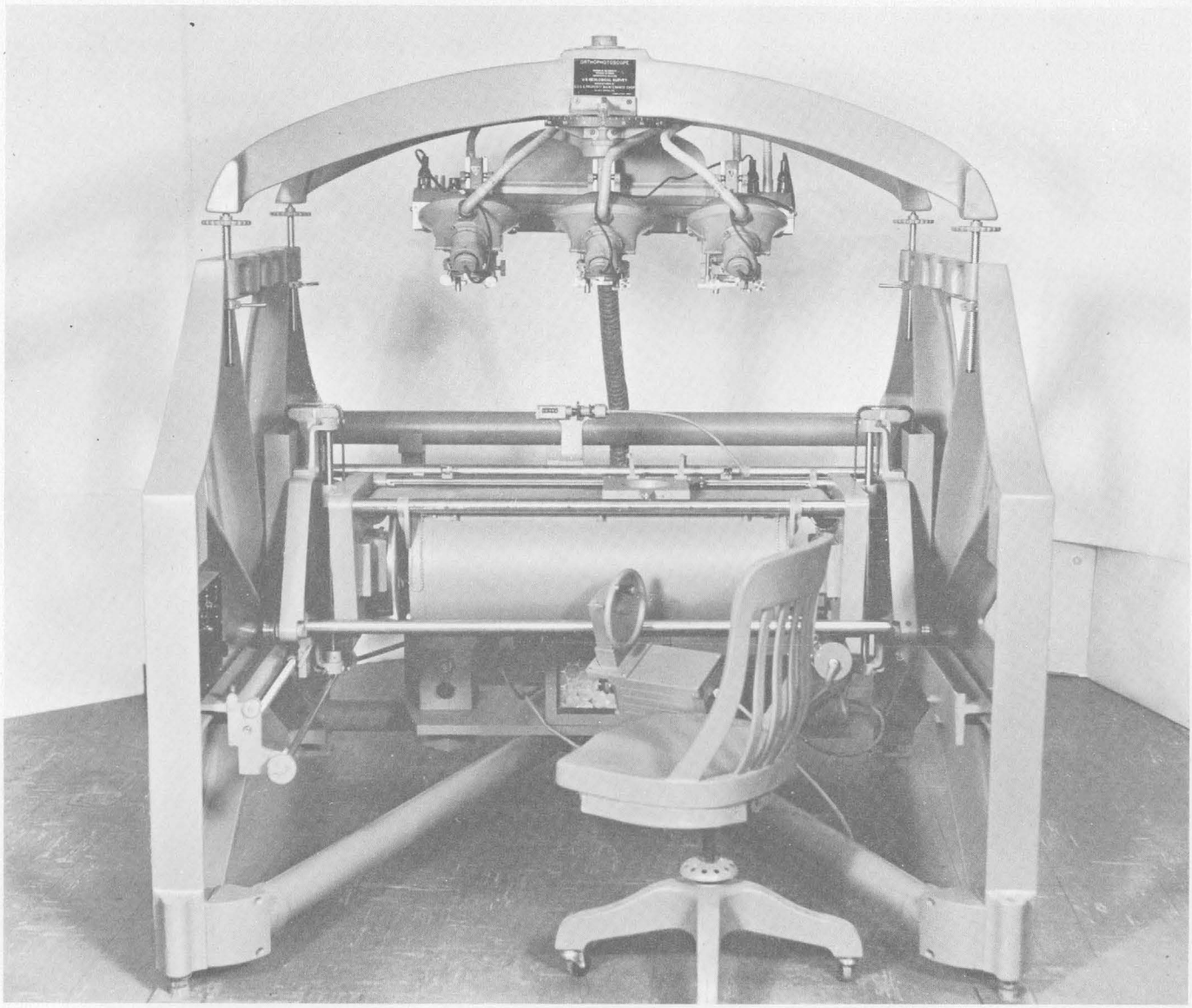

FIGURE 57.1.—U–60 orthophotoscope.

of the scanning platen, thereby enhancing the accuracy of scanning. Since the geometric faithfulness of orthophotographs depends directly upon scanning accuracy, a better product should result.

The insertion of self-synchronizing mechanisms in the transmission of manual and automatic commands to the scanning assembly is another significant innovation of the 1960 instrument. A constant-speed electric motor rotates a generator selsyn that drives the scanning carriage in the x direction on the cylinder assembly. The z motion of the cylinder assembly is manually controlled through a handwheel mounted on the operator's chair. This handwheel rotates a generator selsyn that transmits the mechanical rotation of the handwheel electrically, through a flexible cable, to a motor selsyn mounted on the instrument. This selsyn in turn controls a lead-screw rotation that imparts z motion to the cylinder assembly. The response of the x and z motions to the commands issued through the servomechanisms is positive and smooth and represents a considerable improvement over that achieved by the mechanical-linkage transmissions used on the earlier instruments. Because each generator selsyn can function as a master for more than one motor selsyn, additional remotely located motors can be made to respond to the electric currents induced by the generator selsyn on the orthophotoscope. Means have thus been provided for reproducing and (or) recording the three coordinate motions of the scanning carriage by other remote instrumentation.

Performance testing of the U–60 model began in March 1960 at the Topographic Division's Branch of Research and Design, in Arlington, Va. Tests designed to determine the geometric faithfulness of the produced orthonegatives led to further investigation into: (1) the geometric relationship between the rotation of the film-carrying drum and the translation of the scanning carriage in the y direction, (2) the relationship between the width of the scanning aperture and the translation of the scanning carriage, (3) the parallelism of successive scanning paths, and (4) the perpendicularity of the z motion of the scanning carriage to the plane defined by the x and y axes of the instrument. Appropriate adjustments were made to improve these features.

Efforts to enhance the photographic quality of the orthonegatives included the checking, adjusting, and (or) correction of: (1) the shape of the scanning aperture to reduce to insignificance, if not eliminate, scan lines; (2) excessive instrument vibration; and (3) light leaks that would cause unintentional exposure of the orthonegative. During these testing activities it was determined that the original platen lacked the stability needed to insure a constant width of exposure for successively scanned strips. When a platen of sturdier design was machined and installed on the instrument, this difficulty was overcome.

Studies were made to determine the effect on image definition in the orthonegative caused by varying the dimension of the scanning aperture parallel to the direction of scan. A reduction in this dimension has the effect of a shorter exposure time for each segment of the orthonegative. When this dimension had been reduced to a value of 0.3 mm, it was noted that harmonics in the horizontal motion of the scanning carriage were registering photographically on the orthonegative. A value of 0.4 mm was then determined to be optimum for the present scanning speed of the instrument.

Several minor features were added to the instrument to facilitate operational procedure. A scale was added to indicate the y setting of the scanning carriage. Safelights were installed in appropriate locations. Clamps were added to the x and y motions of the center projector of the three-projector group so that the center projector can be locked in position directly above the center of the area traversed by the scanning carriage. A mercury switch was installed on the carriage to illuminate automatically either the right-end or the left-end projector, depending on the position of the scanning carriage along the scanning track. This provision makes feasible the continuous scanning of two adjacent stereomodels in the x direction.

The first production assignment of the U–60 orthophotoscope involved the preparation of 1:20,000-scale orthophotomosaics of three standard 7½-minute quadrangles in Idaho. Seventeen orthonegatives were required to cover the area; nine of these negatives were exposed with the U–60 and the remainder with an earlier orthophotoscope. Comparison of the products of the two instruments demonstrated the superior appearance of the orthophotographs prepared with the newer instrument.

FIELD CONTROL

58. RESEARCH ON TARGET DESIGN FOR PHOTOIDENTIFICATION OF CONTROL

By David Landen, Washington, D.C.

A research project to improve the design of targets used for photoidentification was carried out by the U.S. Geological Survey in 1960 and 1961. A large tract of land in the Dulles International Airport property at Chantilly, Va., was made available through the cooperation of the Federal Aviation Agency for use as a testing range. Targets of various sizes, patterns, and materials were laid out, then standard vertical aerial photographs of the area were made. In addition, supplemental black-and-white and color photographs were taken with a short-focal-length 35-mm camera. The targets were evaluated by observation in a stereomodel to determine the best target configurations, minimum sizes, and most suitable materials.

Two 1,000-foot base lines were laid out at right angles to each other, and the terminal points were marked with cloth panels. Six parallel north-south lines were laid out at 100-foot intervals; these are marked 1 to 6 (fig. 58.1) and are referred to as columns in the following discussion. Nine parallel east-west lines were laid out at 100-foot intervals; they are marked A to I and are referred to as rows. Individual targets are identified by their row letter and column figure, as C–4, D–3, and so forth.

In order to arrive at a formula for minimum target sizes, initial target sizes were first selected. If these proved to be incorrect, the correct size could be easily obtained from the stereomodel tests. The determination of the initial target sizes to be photographed at altitudes varying from 1,000 to 23,500 feet was based on the fact that an image measuring 0.02 inch can usually be recognized on mapping photography. (In the Kelsh plotter model such an image will measure approximately 0.1 inch.) The overall size of an object on the ground corresponding to 0.02 inch at 1:24,000 scale is 40 feet. If single target panels are arranged in cross-shaped configuration and are spaced about 6 feet from the center, the panel length required would be about 12 feet. The initial reference panel was 3 feet wide because most cloth is available in this width. Other panel sizes were computed proportionately as simple fractions of the flight altitude H when length $L=H/1{,}000$ and width $W=L/4$.

A characteristic and unique target pattern is needed to provide positive recognition against a complex background that may contain other patterns. Tests were made for comparison between 3-legged radial targets, which are most widely used, and 4-legged or cross-shaped targets. The configuration of a square, circle, or rectangle was not selected because such a pattern does not always provide positive identification unless its location is known in advance. Right-angle or other two-legged targets also were eliminated because experience showed that the apex of such a target bleeds beyond its proper boundaries and introduces a significant error.

Because such factors as a variable background affect the recognizability of a target, some targets having an uncontrasted center were compared with similar targets having the center paneled in black, which provides a sharp contrast. A black center also permits better centering of the floating mark in the stereomodel tests. A record of seasonal variation of the background was obtained by photographing the targets 3 times during a 1-year period. The six columns of targets shown on figure 58.1 are described below.

Column 1 consists of 9 open-centered 3-legged targets. The panel length is 1/1,000 of the flight height; the width is 1/4,000. The panels extend radially and are spaced from the center a distance equal to twice the width of the panel. Material is white cotton sheeting or muslin. Minimum panel sizes for the indicated flight heights are given in table 58.1.

Column 2 consists of 9 black-centered 3-legged targets the same size and configuration as those in column 1 but with black cloth centers to provide increased contrast.

Column 3 consists of 9 black-centered 4-legged targets. The white panels are the same size as those in columns 1 and 2. The centers are black panels the same size as the white panels.

Column 4 was used to test a principle in visual optics that, for a given area, detectability is influenced to a large extent by the perimeter of an observed object. The column consists of 7 open-centered 3-legged targets having panels of white cotton sheeting. Each panel is 36 square feet in area, but for each target the perimeter of the panels increases as the ratio of panel length to panel width increases, as follows:

	Panel size (feet)	
Target	*Width*	*Length*
A–4	6	6
B–4	3	12
C–4	2.5	14
D–4	2	18
E–4	1.5	24
F–4	1	36
G–4	.5	72

The shorter targets A–4 to C–4 are easier to see than the longer ones. The possible advantage of increased perimeter of the longer targets was reduced by weeds, grass, and shadows that masked the edges.

Column 5 consists of 9 miscellaneous 4-legged targets made of material that included white freezer paper, white polyethylene film, black polyethylene film, aluminum foil, and fluorescent color materials that have special characteristics.

Column 6 consists of panels used to appraise the durability of various typical, easily procured materials over a period of approximately 1 year. The panels are spaced 50 feet apart. Each panel is 3×12 feet and is made of unbleached muslin in both 4.6- and 2-ounce weights, white cotton sheeting, white jean, white bunting (flagging), denim, butcher paper, rosin building paper, white paint (on road), lime, both white and black polyethylene film, black tar paper, and black muslin.

Seven targets were placed in the nearby wooded areas to study the relations between percentage of woods cover and detectibility, seasonal variations in detecta-

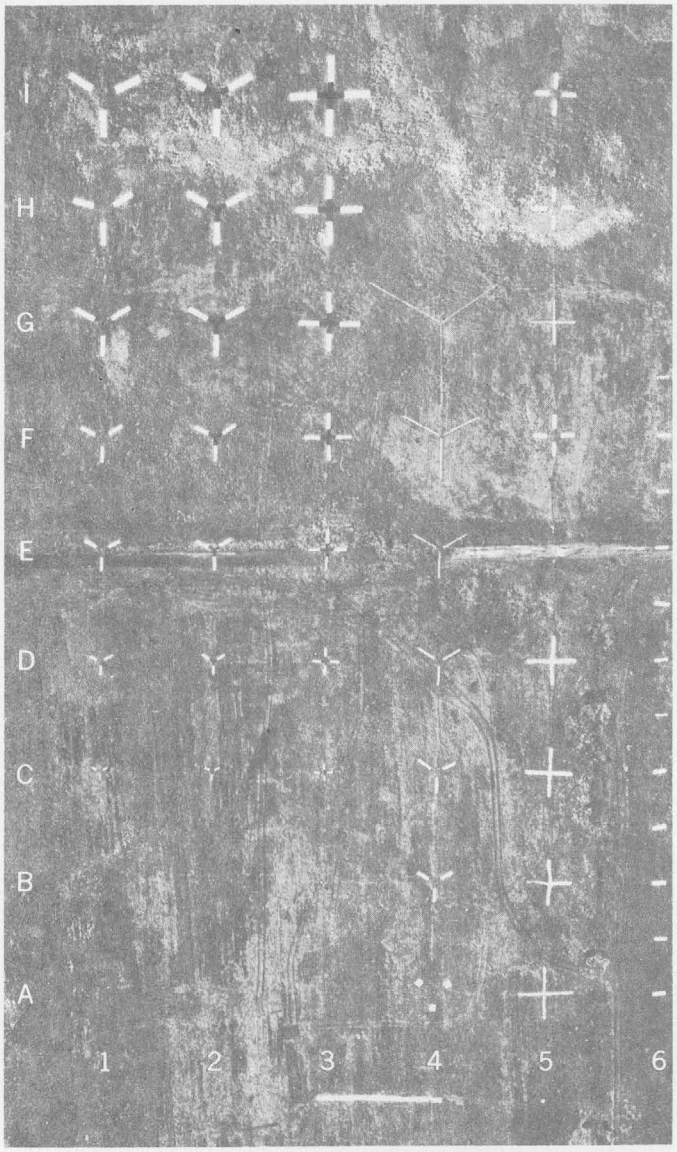

bility, and the use of large or intermittently spaced materials alternating between open and closed patches in overhead cover.

Standard mapping photography was flown over the target area from flight heights of 1,000, 2,000, 5,000, 8,500, 11,500, 14,000, 18,700, 20,000 and 23,500 feet. A Fairchild cartographic camera equipped with a 6-inch Planigon lens was used to obtain compilation-type photography. The targets were completed in July 1960 and aerial photography was flown during three seasonal periods: (1) September 14 and October 7, 1960; (2) November 7 and December 2, 1960; and (3) March 26 and April 14, 1961. During the third and final run, the trees were bare and the targets in the wooded areas could be readily identified. In the open testing range, however, the ground was light colored because of the relative absence of vegetation, and target detection was more difficult because of the reduced contrast.

TABLE 58.1—*Minimum panel sizes for indicated flight heights*

Target	Flight height (feet)	Panel size (feet)	
		Length	Width
A–1	1, 000	1. 0	0. 25
B–1	2, 000	2. 0	. 50
C–1	5, 000	5. 0	1. 25
D–1	8, 500	8. 5	2. 0
E–1	11, 500	12. 0	3. 0
F–1	14, 000	14. 0	3. 5
G–1	18, 700	19. 0	4. 5
H–1	20, 000	20. 0	5. 0
I–1	23, 500	23. 5	6. 0

FIGURE 58.1.—U.S. Geological Survey target-testing range at Chantilly, Va. Flight height 1,000 feet. (White line at bottom of photograph is a panel, 40 inches wide and 108 feet long, that identifies the test range.)

TABLE 58.2.—*Results of stereomodel evaluation tests of targets photographed during March and April 1961 from heights of 1,000 to 20,000 feet (D, detectable; N, nonvisible; R, recognizable)*

Model / Row / H (ft)	30–32	18–20	36–37	11–12	9–10	7–8	5–6	3–4	Model / H (ft) / Row
	1,000	2,000	5,000	8,500	11,500	14,000	18,700	20,000	
I	R R R R	R R R R	R R R R	R R R R	R R R R	R R R R	R R R N	R R R N	I
H	R R R R	R R R R	R R R R	R R R R	R R R R	R R R R	R R R N	R R R N	H
G	R R R R R	R R R R R	R R R R R	R R R N R	R R R N D	R R R N D	R R R N N	D D D N N	G
F	R R R R R	R R R R R	R R R R R	R R R N N	R R R N N	R R R N N	D D D N N	N N N N N	F
E	R R R R R	R R R R R	R R R R N	R R R D N	R R R N N	D D D N N	N N N N N	N N N N N	E
D	R R R R R	R R R R R	R R R R R	R R R R R	N N D D R	N N N N R	N N N N R	N N N N D	D
C	R R R R R	R R R R R	R R R R R	N N N R N	N N N R N	N N N D N	N N N N N	N N N N N	C
B	R R R R R	D D D R R	N N N R R	N N N R N	N N N R N	N N N D N	N N N N N	N N N N N	B
A	N N N R R	N N N R R	N N N R R	N N N R R	N N N R R	N N N D N	N N N N N	N N N N N	A
Row / Column	1 2 3 4 5	1 2 3 4 5	1 2 3 4 5	1 2 3 4 5	1 2 3 4 5	1 2 3 4 5	1 2 3 4 5	1 2 3 4 5	Row / Column

629660—62——10

A 35-mm hand-held camera was used for black-and-white photography in the low-altitude 1,000- and 2,000-foot flights. Using the 35-mm supplemental photographs, the most effective target patterns, minimum sizes, and material were evaluated. The three flights also carried a separate 35-mm camera with 50-mm focal length equipped for color photography. The color photography was needed to appraise the fluorescent materials used and to compare the color photography with black-and-white photography.

By visual inspection of the aerial photographs and the stereomodel, a four-man evaluation group selected (a) the most effective pattern of the target; (b) minimum sizes of target panels for various flight altitudes; and (c) the most suitable material.

When the appraisal of the stereomodel was not unanimous, the test was reexamined by the four observers without reference to previous tests. Final decisions on individual targets were unanimous. Targets evaluated in the stereoscopic model formed by ER–55 projectors were then classified as:

Nonvisible (N).—The target could not be determined even when its approximate location was known.

Detectable (D).—The target could be seen but its shape could not be recognized.

Recognizable (R).—The configuration of the target could be positively identified.

Table 58.2 is an example of such a steromodel test of the targets photographed during the third and final flight.

Minimum recognition criteria obtained from stereomodel testing of 4-legged targets that were exposed during the 9-month period are shown in figure 58.2.

The tests indicate that the area of a target, or panel, should be proportional to the square of the flight height, and that 4-legged targets are more recognizable than 3-legged targets. Targets with legs separated radially from the centers are more recognizable than those which are not separated. Targets placed on low-contrast backgrounds can be made more recognizable by providing a black center. Four-legged targets having 3-×12-foot panels should be adequate for standard compilation photography flown at heights up to 12,000 feet. At higher altitudes the panel sizes should be proportionally longer and wider. The minimum length and width for the higher altitudes should be equal to the flight height divided by 1,000 and 4,000 respectively. The tests suggest that panel sizes of 3×12, 4×16, 5×20, and 6×24 feet could have been used for the entire range of photographic heights up to 24,000 feet.

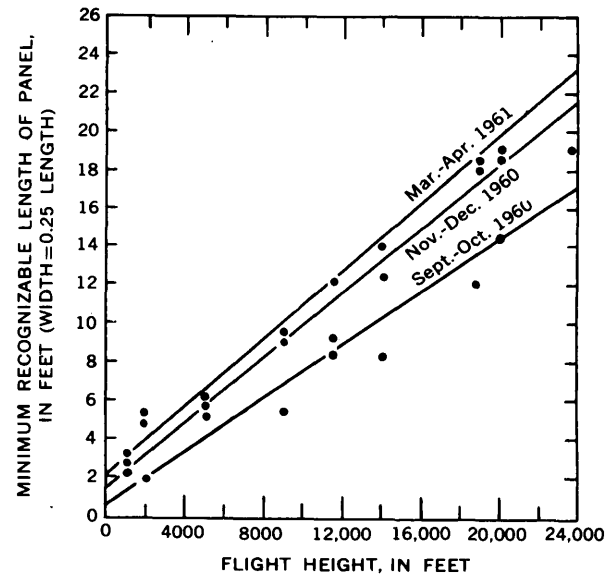

FIGURE 58.2.—Recognizability of targets in relation to flight height. Only 1 flight at 23,500 feet.

Targets for supplemental photography may be either 3 legged or 4 legged. A wide-angle 35-mm-focal-length hand-held camera should provide adequate coverage at 1,000- and 2,000-foot altitudes if enough nearby details are available for transferring the point. Transfer of points to the mapping photography should be made under a stereoscope. The usefulness of supplemental photography is greatly increased if it can be flown at an altitude which results in approximately the same scale as the compilation photography, but the height should not exceed 5,000 feet.

White polyethylene film (target D–5), either 0.004 or 0.006 inch thick, is recommended: the heavier material should be used where the target is liable to be damaged by wind and sun. Other white materials such as unbleached muslin (4.6 oz.), cotton sheeting (4.6 oz.), and mercerized flagging material or bunting are satisfactory. Black cloth or black tar paper may be used to provide contrast.

SELECTED REFERENCES

Aschenbrenner, C. M., 1954, Problems of getting information in and out of air photographs: Photogramm. Eng., v. 20, no. 3, p. 398–401.

Pryor, W. T., 1958, Photographic targets for markers of survey control: Highway Research Board Bull. 199, p. 49–67.

Traenkle, C. A., 1954, Resection in space by projective transformation: Photogramm. Eng., v. 20, no. 1, p. 157.

Van Zandt, F. K., 1961, Sheep Mountain cadastral survey: The Military Engineer, v. 53, no. 353, May-June, p. 194–197.

59. NEW ELEVATION METER FOR TOPOGRAPHIC SURVEYS

By JULIUS L. SPEERT, Washington, D.C.

In April 1961 the Topographic Division of the Geological Survey acquired two new elevation meters for determining the elevations of supplemental control stations for stereotopographic mapping. The new, radically improved elevation meters were built by the Sperry-Sun Well Surveying Co., based on specifications developed jointly with engineers of the Topographic Division.

Basically, the elevation meter is a vehicle-borne electromechanical device for measuring differences of elevation along a traversed route (fig. 59.1). It contains a very sensitive electronic pendulum for continuously measuring the instantaneous slope of the road. Distance traveled is measured by a calibrated small fifth wheel near the pendulum. The product of slope distance times the sine of the inclination angle is integrated continuously by a built-in electronic computer to yield the desired elevation difference. To maintain the desired accuracy, precise calibration and adjustment are necessary for many of the mechanical and electronic features of the equipment.

The pendulum is supported on a bar between the front and rear axles, near the left wheels. To assure the measurement of true slope, uniform air pressure must be maintained in the tires on these wheels at all times. These tires are therefore connected to a common regulated-pressure manifold to maintain their pressure regardless of temperature, speed, or other variables. To avoid changes in load distribution on the tires because of fuel consumption during operation, a special gasoline tank is provided as near as possible to the center of gravity of the vehicle.

FIGURE 59.1.—Elevation meter, 1961 model.

To avoid false slope measurements on crowned roads and on curves, it is essential that the rear wheels traverse exactly the same path as the front wheels. This is accomplished by steering with all four wheels when the meter is in operation. The rear axle is therefore a duplicate of the front axle. Four-wheel drive is also available for use on soft roads.

All the electronic circuits are transistorized and are printed on pluggable boards, to reduce power requirements and field maintenance problems and to improve reliability. In many cases, troubleshooting in the field consists merely of replacing circuit boards, in turn, until the faulty one is located.

Precise adjustment of the pendulum is, of course, essential to accurate measurement of elevation. The pendulum base is first alined with the line connecting the axles. The pendulum itself is then calibrated on a special tilting stand for various slope angles between $-15°$ and $+15°$. After these mechanical adjustments, the meter is driven around a closed loop and a further electronic adjustment is made, if necessary, to bring the loop closure to zero.

Precision of elevation determination is a direct function of precision of distance measurement. The fifth wheel is therefore calibrated periodically to compensate for wear, and its tire pressure is maintained constant by connection with the regulated-pressure tank. Effects of centrifugal force on the wheel circumference are compensated electronically. This compensation is calibrated both at very slow speeds and at higher, operating speeds.

The danger of inaccurate recording is overcome in the new elevation meter by an automatic printing recorder. The vehicle is stopped for each elevation reading, to avoid dynamic effects on the pendulum, and the following information is automatically printed on adding-machine tape at the push of a button: The station designation (preset manually at each station), the elevation of the starting point on the line (preset manually at the beginning of the run), the increment in elevation, the elevation of the new point, and the distance from the starting point. This distance is compared visually with that on a mechanical counter, as a check on the electronic measurement of distance and elevation.

A small builders' level and a level rod are used to tie to bench marks and other off-road points. The level is supported on a special bracket so that the operator may take a rod reading on a side point without leaving his seat.

The cab of the vehicle is air conditioned to assure dust-free operation of the delicate equipment. Numerous other features are included for comfort, convenience, and efficiency. A number of safety devices are included to reduce traffic hazards. The vehicle is equipped with a full set of replaceable spare parts, necessary handtools, calibration and test equipment, and other survey equipment that might be needed on an assignment. A special electrical-analog adjuster is included so that a least-squares adjustment may be applied to survey networks in the field if desired.

In normal operations over good roads, the elevation meter may be driven at speeds up to 25 miles per hour. On soft or rough roads it is necessary to reduce the speed to protect the equipment, to maintain accuracy, and to avoid driver strain. Average survey mileage ranges from 30 to 50 miles per day, with a maximum of 102 miles recorded in a single day over good roads. Adjusted elevations accurate within 1 or 2 feet are readily attainable with proper controls on planning and execution of the work. Lines may be double run for greater accuracy. The elevation meter is used most effectively on large projects with a fairly dense network of passable roads. It is not economical on small projects or where good roads are sparse.

SUBJECT INDEX

[For major topic headings, such as "Economic Geology," "Stratigraphy," "Ground Water," see under State names or refer to "Table of Contents"]

AUTHOR INDEX

U.S. GOVERNMENT PRINTING OFFICE : 1962 O—629660